Diffraction, Radiation and Propagation of Elastic Waves in Isotropic and Anisotropic Bodies

Alexander Kleshchev

Diffraction, Radiation and Propagation of Elastic Waves in Isotropic and Anisotropic Bodies

Diffraction, Radiation and Propagation of Elastic Waves in Isotropic and Anisotropic Bodies

By
Alexander Kleshchev

Cambridge
Scholars
Publishing

Diffraction, Radiation and Propagation of Elastic Waves in Isotropic and Anisotropic Bodies

By Alexander Kleshchev

This book first published 2019

Cambridge Scholars Publishing

Lady Stephenson Library, Newcastle upon Tyne, NE6 2PA, UK

British Library Cataloguing in Publication Data
A catalogue record for this book is available from the British Library

ISBN (10): 1-5275-3993-8
ISBN (13): 978-1-5275-3993-8

The monograph presents the main results of the author's published research on the diffraction, radiation, and propagation of elastic waves.

1. *Hydroacoustic scatterers*. St. Petersburg: Sudostroenie, 1992 (1st ed.); Prima, 2012 (2nd ed.).
2. *The diffraction and propagation of waves on elastic media and bodies*. St. Petersburg: Vlas, 2002.
3. *The diffraction, radiation, and propagation of elastic waves*. St. Petersburg: Profprint, 2006.

In this book, the author's main ideas and results have been developed from his previous monographs.

CONTENTS

PREFACE

In recent years, there has been an increase in interest in problems in the field of the diffraction, radiation, and propagation of elastic waves that are associated with the interaction of bodies both with each other and with media interfaces. In addition, a great deal of attention has recently been paid to solutions to three-dimensional wave problems (with the help of Debye potentials) for elastic isotropic and anisotropic bodies of analytical and non-analytical forms.

The seventh chapter of this monograph provides the characteristics of the sound scattering (scattering cross-sections and angular diagram) of prolate and oblate spheroids, as well as theWatson transformation for ideal spheroids. The same chapter investigates an acoustic model of the agitated sea surface. In the eighth chapter, we will study the use of equations and diffraction theory methods for problems related to the synthesis of hydroacoustic antennas. In chapter nine, we will investigate the scattering of sound by elastic and viscoelastic bodies in the form of an infinite circular cylinder. The author has tried to consider all of these tendencies and trends when writing this monograph.

The research into the characteristics of sound scattering by spheroidal bodies was performed by S. A. Bespalova, E. Sedola, and A. P. Eglaya, under the direction of the Doctor of Physical and Mathematical Sciences, Yu. A. Klokov.

The calculations for the phase velocities in cylindrical bodies were carried out by S. L. Il'menkov and K. A. Klyubina. E. I. Kuznetsova performed the calculations for diffracted and radiated pulses. The author is also grateful V. Yu. Chizhov, G. K. Evstatiev, V. M. Kuz'kin, F. F. Legusha, and S. A. Peresyolkov for their helpful comments on the research results.

B. Ivanov and M. Moshchuk actively participated in the experiment to find the amplitude-phase characteristics of the scattering field of models in the Fresnel zone.

The author thanks V. I. Gromova, S. M. Kleshchev, A. S. Klimenkov, and M. M. Pavlov. I would also like to thank the CSP team, including Helen Edwards, Joanne Parsons, and Ivan Veller, for editing, proofreading, and publishing my manuscript.

CHAPTER 1

THE RESONANCES OF ELASTIC SPHEROIDAL BODIES

1.1. Solution to the Problem of the Diffraction of Sound from an Elastic Spheroidal Body using Debye's Potentials

In this section, the resonances of prolate and oblate spheroidal bodies (in their entirety and in the form of shells), which are impacted by three-dimensional and axisymmetric angles of irradiation, will be investigated. Debye's potentials have been used to calculate the three-dimensional pattern of irradiation in order to solve the diffraction problem. Various publications are devoted to the resonances of elastic spheroidal bodies [1–9].

Debye first proposed expanding the vector potential $\vec{A}$ and the scalar potentials $U$and Vin his publication [10], which is devoted to studying the behavior of light waves near the local point or line. Later, this approach was used to solve the diffraction problems in the electromagnetic wave diffraction of a sphere, a circular disk, and a paraboloid revolution [11–16], as well as for the diffraction by spheroidal bodies in longitudinal and transverse waves [7, 17]. When Debye's potentials are applied to problems based on the theory of dynamic elasticity, it occurs as follows: the displacement vector $\vec{u}$ of an elastic isotropic medium obeys the Lame equation

$$(\lambda+\mu)graddiv\vec{u}-\mu curlcurl\vec{u}=-\rho\omega^2\vec{u}, (1.1)$$

where λ and μ are Lame constants, ρ is the density of the isotropic medium, and ω is the circular frequency of harmonic vibrations. According to the Helmholtz theorem, the displacement vector $\vec{u}$ is expressed through scalar Φ and vector $\vec{\Psi}$ potentials as follows:

$$\vec{u}=-grad\Phi+curl\vec{\Psi} (1.2)$$

Substituting E. (1.2) in E. (1.1), we obtain two Helmholtz equations, which include one scalar equation for Φ and one vector equation for$\vec{\Psi}$:

$$\Delta\Phi+h^2\Phi=0, (1.3)$$
$$\Delta\vec{\Psi}+k_2^2\vec{\Psi}=0. (1.4)$$

Here $h=\omega/c_1$ is the wavenumber of the longitudinal elastic wave; c_1 is the velocity of this wave; $k_2=\omega/c_2$ is the wavenumber of the transverse elastic wave; and c_2 is the velocity of the transverse wave. In the three-dimensional case, the variables involved in scalar equation (1.3) can be separated into 11 coordinate systems. As for equation (1.4), in the three-dimensional problem, it yields three independent equations for each of components of the vector function $\vec{\Psi}$ in the Cartesian coordinate system alone. To overcome this difficulty, one can use Debye's potentials U and V, which obeys the Helmholtz scalar equation as follows:

$$\Delta V+k_2^2V=0;\Delta U+k_2^2U=0. (1.5)$$

The vector potential $\vec{\Psi}$ (according to Debye) is expanded in potentials V and U as follows:

$$\vec{\Psi}=curlcurl(\vec{R}U)+ik_2curl(\vec{R}V), (1.6)$$

where $\vec{R}$ is the radius vector of a point of the elastic body or the elastic medium.

Let us demonstrate the efficiency of using Debye's potentials to solve the three-dimensional diffraction problems in the acoustical diffraction of an elastic spheroidal shell. The advantage of the representation (6) becomes evident, if we take into account that potentials V and U obey the Helmholtz scalar equation. It is convenient to represent components of $\vec{\Psi}$ in the spherical coordinate system by expressing them through U, V, and $\vec{R}$ and then, using vector analysis formulas, to change to spheroidal components. The expressions for spherical components of the vector function $\vec{\Psi}(\Psi_R, \Psi_\theta, \Psi_\varphi)$ in terms of Debye's potentials take the following form [7]:

$$\Psi_R = (\partial\xi/\partial R)^2(\partial^2 B/\partial\xi^2) + 2(\partial\xi/\partial R)(\partial\eta/\partial R)(\partial^2 B/\partial\xi\partial\eta) + (\partial\eta/\partial R)^2(\partial^2 B/\partial\eta^2) + (\partial^2\xi/\partial R^2)(\partial B/\partial\xi) + (\partial^2\eta/\partial R^2)(\partial B/\partial\eta) + k_2^2 B, \quad (1.7)$$

$$\Psi_\theta = [h_0(\xi^2 - 1 + \eta^2)]^{-1}[(\partial\xi/\partial\theta)(\partial\xi/\partial R)(\partial^2 B/\partial\xi^2) + (\partial\xi/\partial\theta)(\partial\eta/\partial R)(\partial^2 B/\partial\xi\partial\eta) + (\partial\xi/\partial R)(\partial\eta/\partial\theta)(\partial^2 B/\partial\xi\partial\eta) + (\partial\eta/\partial R)(\partial\eta/\partial\theta)(\partial^2 B/\partial\eta^2) + (\partial B/\partial\xi)(\partial^2\xi/\partial R\partial\theta) + (\partial B/\partial\eta)(\partial^2\eta/\partial R\partial\theta)] + ik_2(\sin\theta)^{-1}(\partial V/\partial\varphi), \quad (1.8)$$

$$\Psi_\varphi = [h_0(\xi^2 - 1 + \eta^2)^{1/2}\sin\theta]^{-1}[\partial\xi/\partial R)(\partial^2 B/\partial\xi\partial\varphi) + (\partial\eta/\partial R)(\partial^2 B/\partial\eta\partial\varphi) - ik_2 \times [(\partial\xi/\partial\theta)(\partial V/\partial\xi) + (\partial\eta/\partial\theta)(\partial V/\partial\eta)], \quad (1.9)$$

$$B = h_0(\xi^2 - 1 + \eta^2)^{1/2}U; -1 \le \eta \le +1; 1 \le \xi \le +\infty.$$

Spheroidal components of the function $\vec{\Psi}(\Psi_\xi, \Psi_\eta, \Psi_\varphi)$ are expressed as follows [7]:

$$\Psi_\xi = \Psi_R(h_0/h_\xi)\xi(\xi^2 - 1 + \eta^2)^{-1/2} + \Psi_\theta(h_0/h_\xi)(\xi^2 - 1 + \eta^2)^{1/2}(\partial\theta/\partial\xi), \quad (1.10)$$

$$\Psi_\eta = \Psi_R(h_0/h_\eta)\eta(\xi^2 - 1 + \eta^2)^{-1/2} + \Psi_\theta(h_0/h_\eta)(\xi^2 - 1 + \eta^2)^{1/2}(\partial\theta/\partial\eta), \quad (1.11)$$

$$\Psi_\varphi \equiv \Psi_\varphi, \quad (1.12)$$

$$h_\xi = h_0(\xi^2 - \eta^2)^{1/2}(\xi^2 - 1)^{1/2}; h_\eta = (\xi^2 - \eta^2)^{1/2}(1 - \eta^2)^{1/2}.$$

Let us consider a scatterer in the form of an isotropic elastic spheroidal shell (Fig. 1-1). All potentials, including the plane wave potential Φ_0, the scattered wave potential Φ_1, the scalar shell potential Φ_2, Debye's potentials U and V, and the potential Φ_3 of the gas filling the shell can be expanded in spheroidal functions:

$$\Phi_0 = 2\sum_{m=0}^{\infty}\sum_{n\ge m}^{\infty} i^{-n}\varepsilon_m \overline{S}_{m,n}(C_1,\eta_0)\overline{S}_{m,n}(C_1,\eta)R_{m,n}^{(1)}(C_1,\xi)\cos m\varphi, \quad (1.13)$$

$$\Phi_1 = 2\sum_{m=0}^{\infty}\sum_{n\ge m}^{\infty} B_{m,n}\overline{S}_{m,n}(C_1,\eta)R_{m,n}^{(3)}(C_1,\xi)\cos m\varphi; \quad (1.14)$$

$$\Phi_2 = 2\sum_{m=0}^{\infty}\sum_{n\ge m}^{\infty}[C_{m,n}R_{m,n}^{(1)}(C_l,\xi) + D_{m,n}R_{m,n}^{(2)}(C_l,\xi)]\overline{S}_{m,n}(C_l,\xi)\cos m\varphi; \quad (1.15)$$

$$\Phi_3 = 2\sum_{m=0}^{\infty}\sum_{n\ge m}^{\infty} E_{m,n}R_{m,n}^{(1)}(C_2,\xi)\overline{S}_{m,n}(C_2,\eta)\cos m\varphi; \quad (1.16)$$

$$U = 2\sum_{m=1}^{\infty}\sum_{n\ge m}^{\infty}[F_{m,n}R_{m,n}^{(1)}(C_t,\xi) + G_{m,n}R_{m,n}^{(2)}(C_t,\xi)]\overline{S}_{m,n}(C_t,\eta)\sin m\varphi; \quad (1.17)$$

$$V = 2\sum_{m=0}^{\infty}\sum_{n\ge m}^{\infty}[H_{m,n}R_{m,n}^{(1)}(C_t,\xi) + I_{m,n}R_{m,n}^{(2)}(C_t,\xi)]\overline{S}_{m,n}(C_t,\eta)\cos m\varphi, \quad (1.18)$$

$\bar{S}_{m,n}(C_1,\eta)$represents the angular spheroidal function; $R_{m,n}^{(1)}(C_1,\xi)$, $R_{m,n}^{(2)}(C_1,\xi)$, and $R_{m,n}^{(3)}(C_1,\xi)$ represents the radial spheroidal functions of the first, second, and third kinds $C_l = hh_0$; $C_t = k_2h_0$; $C_1 = kh_0, k$ is the wavenumber of the sound wave in the liquid; $C_2 = k_1h_0$, k_1 is the wavenumber of the sound wave in the gas filling the shell; h_0 represents the half-focal distance; $B_{m,n}, C_{m,n}, D_{m,n}, E_{m,n}, F_{m,n}, G_{m,n}, H_{m,n}$and $I_{m,n}$ are unknown expansion coefficients.

Expansion coefficients are determined from the physical boundary conditions present at two surfaces of the shell (ξ_0 and ξ_1; see Fig. 1-1) [7]:

(i) The continuity of the normal displacement component at both of the boundaries ξ_0 and ξ_1;

(ii) The normal stress on the outside boundary of the elastic shell is equal to the sound pressure in the liquid (ξ_0) and the normal stress on the inner boundary of the shell is equal to the sound pressure in the gas (ξ_1);

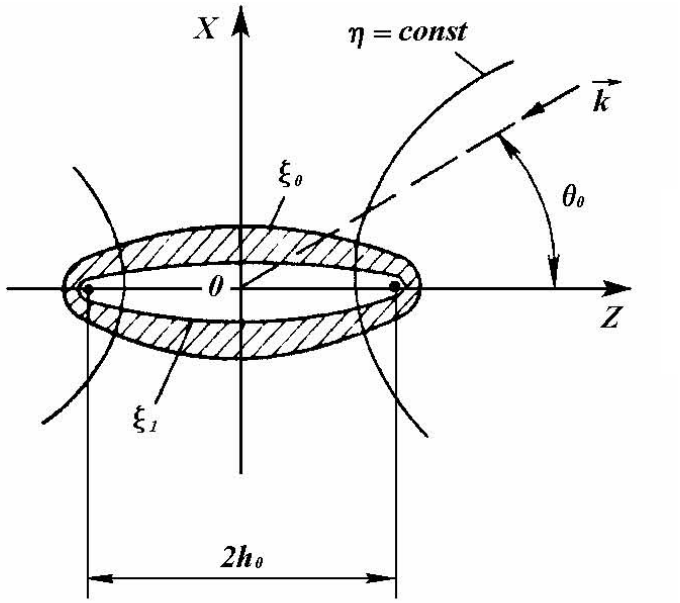

Figure 1-1: The elastic spheroidal shell in a harmonic plane wave field

(iii) The absence of tangential stresses at both of the shell boundaries, ξ_0 and ξ_1.

The corresponding expressions for boundary conditions take the following form [7]:

$$(h_\xi)^{-1}(\partial/\partial\xi)(\Phi_0+\Phi_1)=(h_\xi)^{-1}(\partial\Phi_2/\partial\xi)+(h_\eta h_\varphi)^{-1}[(\partial/\partial\eta)(h_\varphi\Psi_\varphi)-(\partial/\partial\varphi)(h_\eta\Psi_\eta)]_{\xi=\xi_0};\ (1.19)$$

$$(h_\xi)^{-1}(\partial\Phi_1/\partial\xi)=(h_\xi)^{-1}(\partial\Phi_2/\partial\xi)+(h_\eta h_\varphi)^{-1}[(\partial/\partial\eta)(h_\varphi\Psi_\varphi)-(\partial/\partial\varphi)(h_\eta\Psi_\eta)]_{\xi=\xi_1};\ (1.20)$$

$$-\lambda_0 k^2(\Phi_0+\Phi_1)=-\lambda h^2\Phi_2+2\mu[(h_\xi h_\eta)^{-1}(\partial h_\xi/\partial\eta)u_\eta+(h_\xi)^{-1}(\partial u_\xi/\partial\xi)]_{\xi=\xi_0};\ (1.21)$$

$$-\lambda_1 k_1^2\Phi_3=-\lambda h^2\Phi_2+2\mu[(h_\xi h_\eta)^{-1}(\partial h_\xi/\partial\eta)u_\eta+(h_\xi)^{-1}(\partial u_\xi/\partial\xi)]_{\xi=\xi_1};\ (1.22)$$

$$0=(h_\eta/h_\xi)(\partial/\partial\xi)(u_\eta/h_\eta)+(h_\xi/h_\eta)(\partial/\partial\eta)(u_\xi/h_\xi)_{\xi=\xi_0;\xi=\xi_1};\ (1.23)$$

$$0=(h_\varphi/h_\xi)(\partial/\partial\xi)(u_\varphi/h_\varphi)+(h_\xi/h_\varphi)(\partial/\partial\varphi)(u_\xi/h_\xi)_{\xi=\xi_0;\xi=\xi_1},\ (1.24)$$

where$h_\varphi=h_0(\xi^2-1)^{1/2}(1-\eta^2)^{1/2}$; $\lambda_0$is the bulk compression coefficient of the liquid and $\lambda_1$is the bulk compression coefficient of the gas filling the shell,

$$u_\xi=(h_\xi)^{-1}(\partial\Phi_2/\partial\xi)+(h_\eta h_\varphi)^{-1}[(\partial/\partial\eta)(h_\varphi\Psi_\varphi)-(\partial/\partial\varphi)(h_\eta\Psi_\eta)];$$
$$u_\eta=(h_\eta)^{-1}(\partial\Phi_2/\partial\eta)+(h_\xi h_\varphi)^{-1}[(\partial/\partial\varphi)(h_\xi\Psi_\xi)-(\partial/\partial\xi)(h_\varphi\Psi_\varphi)];\ u_\varphi=(h_\varphi)^{-1}(\partial\Phi_2/\partial\varphi)+$$
$$(h_\xi h_\eta)^{-1}[(\partial/\partial\xi)(h_\eta\Psi_\eta)-(\partial/\partial\eta)(h_\xi\Psi_\xi)].$$

The substitution of series (1.13)–(1.18) in boundary conditions (1.19)–(1.24) yields an infinite system of equations to determine the desired coefficients. Due to the orthogonality of the trigonometric functions, $\cos m\varphi$ and $\sin m\varphi$, the infinite system of equations breaks into infinite subsystems with fixed numbers, m. Each of the subsystems is solved using the truncation method. The number of retained terms of expansions (1.13)–(1.18) is increased with a greater wave size for the given potential.

The solution to the axisymmetric problem of sound waves diffraction from elastic spheroidal bodies has been presented in [1], [2], and [7–9].

1.2. Results of the Numerical Experiment to Determine the Low-Frequency Resonances from Elastic Spheroidal Bodies

The characteristics of the prolate gas-filled shell were calculated for two angles of irradiation: $\theta_0 = 0^0$ and $\theta_0 = 90^0$. In a different scale, Figure 1-2 presents the modules of the angular characteristics of the $|D(\theta)|$ scattering of a steel prolate gas-filled spheroidal shell (curve 1), a soft prolate spheroid (curve 2), and a hard spheroid (curve 3) impacted by the sound wave at an angle of $\theta_0 = 0^0$, where $C_1 = 1{,}0$.

Figures 1-3 and 1-4 present the same angular distributions, but (C_1 is the wave size) $C_1 = 3{,}1$ (for the elastic shell), $C_1 = 3{,}0$ (for the ideal spheroid), and $C_1 = 10{,}0$ (for the ideal spheroid). The notations of the curves for all three figures are identical. An analysis of the results shows that for an angle of $\theta_0 = 0^0$ and a wave dimension of $C_1 = 1{,}0$ (see Fig. 1-2), the angular characteristic of the elastic shell is similar to the characteristic of the hard spheroid. When $C_1 = 3{,}1$ and the irradiation angle of the impact is equal to $\theta_0 = 0^0$, the situation becomes indeterminate. The angular characteristic of the shell has a dipole character at the hard spheroid (see Fig. 1-3). In parallel with the increase of the wave dimension C_1, the character of the sound scattering from the shell remains complicated (see Fig. 1-4). In the lit region, the characteristic is $|D(\theta)|$ in the hard spheroid but, in the shaded region, it is nearer to the shade lobe of the soft spheroid than the shadow lobe of a hard spheroid. From known angular characteristics of $D(\theta, \varphi)$, the relative backscattering of the cross-sections (σ_0) from the elastic spheroidal bodies can be calculated [7]. Fig. 1-5 presents the mathematical term for the relative backscattering of cross-sections σ_0 of prolate spheroids with a semi axes correlation of 1:10 ($\xi_0 = 1{,}005$), which are impacted by the sound wave at an axially symmetric angle of irradiation ($\theta_0 = 0^0$). The behavior of the solid elastic spheroid is very similar to that of the ideal hard scatterer. This is seen through a comparison of the angular characteristics $D(\theta, \varphi)$ in steel and ideal spheroids. This is a coincidence and can be observed everywhere, with the exception of the resonance point, $C = 7{,}4$. This resonance is called a Rayleigh surface wave [5]. At a wave dimension of $C = 7{,}4$, the surface contour of the continuous steel prolate spheroid is $2{,}5\lambda_R$, where λ_R is the length of a Rayleigh-type wave. The velocity of the wave c_R is equal to 2889 m/s; however, on the planar boundary of the steel-vacuum, the velocity of the Rayleigh wave is equal to 2980 m/s.

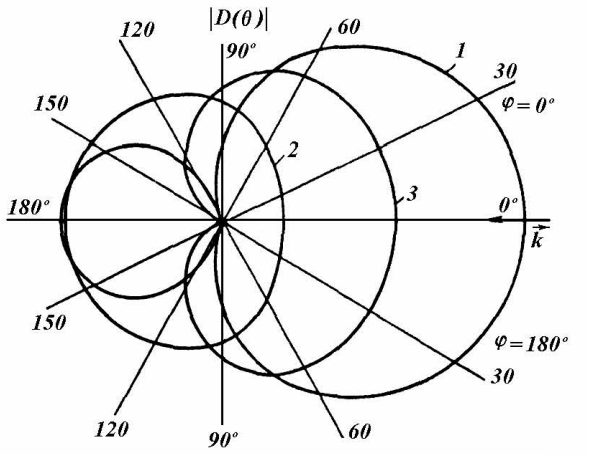

Figure 1-2: Modules of angular characteristics for spheroidal scatterers

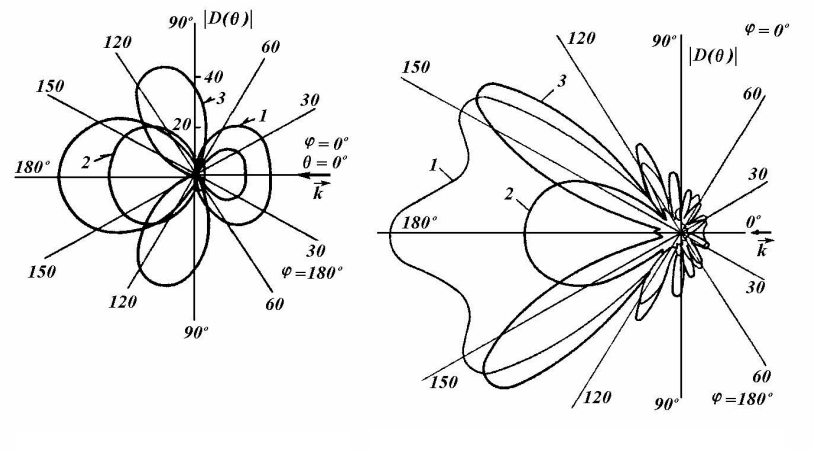

Figure 1-3 (left): Modules of the angular characteristics of spheroidal scatterers

Figure 1-4 (right): Modules of the angular characteristics of spheroidal scatterers

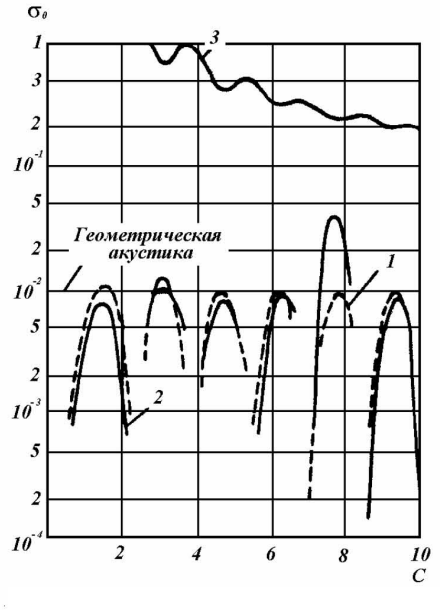

Figure 1-5: The relative backscattering of prolate spheroid cross-sections

Figure 1-6 presents the relative backscattering in the cross-sections σ_0 of oblate spheroids with a semi-axes correlation of 1:10 ($\xi_0 = 0{,}1005$) when, through an axially symmetric angle of irradiation $\theta_0 = 0^0$, the notations coincide with Figure 1-5. This will occur until the resonance of the zeroth antisymmetrical-flexural wave ($C \approx 5{,}3$) σ_0 of the steel oblate spheroid is closer to the σ_0 of the soft spheroid. Whereas for $C > 5{,}3$, it approaches the σ_0 of the hard spheroid, although the angular characteristic $D(\theta)$ obtained for the elastic spheroid at $\theta_0 = 0^0$ is for any wave size C close to the angular characteristic $D(\theta)$ of the hard spheroid.

Figure 1-7 presents sections σ_0 of prolate spheroidal scatterers. The steel prolate spheroid irradiated by the sound wave at an angle of $\theta_0 = 90^0$ has the resonance of the surface wave with the same meaning $C = 7{,}4$ (see curve 2, Fig. 1-5) [7]. The same section of the scattering σ_0 of the steel continuous spheroid (curve 3), which is irradiated by the sound wave at an angle of $\theta_0 = 90^0$, is visibly closer to the σ_0 of the hard spheroid (curve 4) in comparison with the σ_0 of the soft spheroid (curve 5). This similarity in the scattering properties of continuous elastic and hard spheroids was also shown in the angular characteristic $D(\theta, \varphi)$. The frequency dependence of the relative section σ_0 in the prolate spheroidal shell (curve 1) irradiated by the sound wave at an angle of $\theta_0 = 0^0$ shows the presence of considerable resonance by $C = 6{,}75$ [1, 7–9]. Figure 1-8 shows the modular uses of angular characteristics $|D(\theta)|$ in prolate spheroidal scatterers. Curve 1 is the steel, gas-filled shell with a wave dimension $C = 6{,}75$ that corresponds to its resonance. Curve 2 is a soft spheroid, while curve 3 is a hard spheroid. For all ideal spheroids, the wave size C is equal to 10,0.

From the comparison of the three curves, we can see that the shaded lobe of shell's angular characteristic is shown as the "soft background", but the lobe of the backscattering is shown as the "hard background".

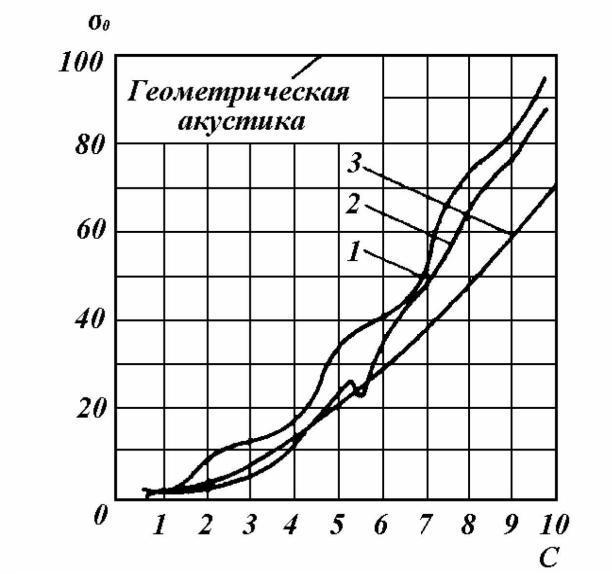

Figure 1-6: The relative backscattering in the cross-sections of oblate spheroids

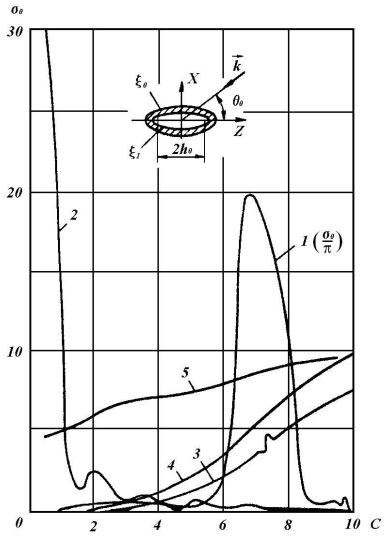

Figure 1-7: The relative backscattering in cross-sections of the prolate spheroidal scatterers

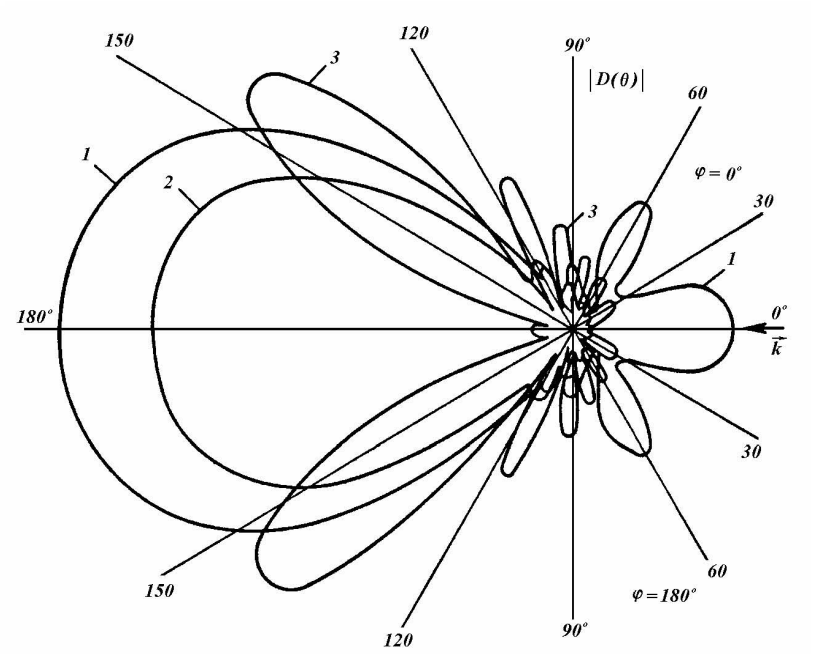

Figure 1-8: Modules with the angular characteristics of prolate spheroidal bodies

Table 1-1

Wave size C	σ_0 at an angle of $\theta_0 = 90°$		
	Spheroidal gas-filled shell $\xi_0 = 1{,}005075$; $\xi_1 = 1{,}005$	Hard spheroid $\xi_0 = 1{,}005$	Soft spheroid $\xi_0 = 1{,}005$
0,5	$0{,}3012 \cdot 10^{-3}$	$0{,}2452 \cdot 10^{-3}$	4,506
1,0	$0{,}4748 \cdot 10^{-2}$	$0{,}3908 \cdot 10^{-2}$	4,760
1,5	$0{,}2365 \cdot 10^{-1}$	$0{,}1965 \cdot 10^{-1}$	5,194
2,0	$0{,}7354 \cdot 10^{-1}$	$0{,}6147 \cdot 10^{-1}$	5,748
2,5	0,1751	0,1479	6,300
3,0	0,3470	0,3006	6,754
3,5	0,6068	0,5418	7,094
4,0	0,9736	0,8911	7,358
4,5	1,447	1,362	7,592
5,0	2,014	1,960	7,815
5,5	2,599	2,680	8,029

The relative backscattering of the cross-section σ_0 of a spheroidal shell irradiated by a sound wave at an angle of $\theta_0 = 90^0$ was calculated for a wave size ranging from C=0,5 to $C = 5{,}5$. The meanings of the σ_0 in a shell is very similar to the σ_0 in a hard spheroid; it is worthwhile to compare these sections in tabular form. As can be seen from Table 1-1, the angle of the shell's irradiation with wave sizes ranging from C=0,5 to $C = 5{,}5$ indicates a "hard background" to the scattering. This is what we can see from a comparison of the angular characteristics of the scattering $D(\theta, \varphi)$. A full scattering of the cross-section σ [7] is determined through the square of a modulus via the angular characteristic of the sound scattering $D(\theta, \varphi)$:

$$\sigma = \int_0^{\pi} \int_0^{2\pi} |D(\theta, \varphi)|^2 \sin\theta \, d\theta d\varphi.$$

The relative scattering of the cross-section σ_r is equal to the following:

$$\sigma_r = \sigma / 2A_0,$$

where A_0 is depicted by the shaded geometrical region of the scatterer.

With the help of an optical theorem, a scattering cross-section σcan be found through the imaginary part of an angular characteristic in the direction of an incident wave (a forward scattering) $Im\, D\,(180^0 - \theta_0; 180^0)$ [7]:

$\sigma = (4\pi/k)\, Im\, D\,(180^0 - \theta_0; 180^0)$,

where θ_0 is the angle of the fall, $\varphi_0 = 0^0$.

Following the analogy with the scattering of a cross-section σ, it is possible to introduce the radiation cross-section σ_{rad} of an elastic or liquid body under the point source [7]:

$\sigma_{rad} = \int_0^{\pi} \int_0^{2\pi} |F(\theta, \varphi)|^2 \sin\theta \, d\theta d\varphi$,

where $F(\theta, \varphi)$ is an angular characteristic of the sound radiation of a body subjected to the action of a point source.

On the basis of formulas presented, a full account was made of the total scattering cross-section σ and the relative cross-section σ_r. The radiation σ_{rad} should be moved off the cross-section σ_{rad} in the spheroidal prolate and oblate bodies. Figure 1-9 presents the sections of the scattering cross-section σ_r of an ideal hard oblate spheroid (curve 1), a steel oblate spheroid (curve 2), and an ideal soft oblate spheroid (curve 3). In all three cases, there is a relation between the semi-axes $a/b = 1{:}\,10 (\xi_0 = 0{,}1005)$, but this has an irradiation angle of $\theta_0 = 0^0$. A relative section σ_r of an elastic spheroid shows the resonance of a coincidence, as in the case of the backscattering of σ_0 (see Fig. 1-6), but the maximum is displaced: for $\sigma_0$the maximum is observed at $C = 5{,}25$ but for σ_r it is $C - 5{,}35$. With an increase of C, curve 2 approaches $\sigma_r = 1{,}0$, thereby corresponding to the geometric acoustics calculations performed for an elastic oblate spheroid. This shows that at$C = 15{,}0$ section $\sigma_r = 0{,}866$, while at $C = 20{,}0 \rightarrow \sigma_r = 0{,}941$. Figure 1-10 presents the relative cross-sections of the scattering σ_r (curves 1 and 2) and the radiation σ_{rad} (curve 3) from prolate spheroidal bodies. Curve 1 shows the frequency dependence $\sigma_r(C)$ of an ideal soft prolate spheroid. Curve 2 corresponds $\sigma_r(C)$ to a steel gas-filled prolate spheroidal shell ($\xi_0 = 1{,}005075; \xi_1 = 1{,}005$). Both curves correspond to $\theta_0 = 0^0$ (an axially symmetric problem). Curve 2, for an elastic shell's relative backscattering section (curve 1 in Fig. 1-7) has two maximums (two resonances). The first maximum is observed at $C = 6{,}7$ (unlike from $C = 6{,}75$ for σ_0), while a second resonance is $C \approx 8{,}25$ and corresponds with $L = 1{,}5\Lambda$, where L is a length of a contour of the neutral surface of a shell, and Λ is the length of a longitudinal wave (a zeroth symmetrical Lamb's wave) that spreads with a velocity of $c_1 \approx 5420\ m/s$. Curve 1, for the ideal soft spheroid, asymptotically tends to the following geometric acoustical value:

$\sigma_r = 1{,}0)$: $\sigma_r(15{,}0) = 4{,}16; \sigma_r(65{,}0) = 2{,}23; \sigma_r(100) = 1{,}93.$

Curve 3 characterizes the radiating faculty of the same shell, if it is exited from the outside by a point source at an angle of $\theta_0 = 0^0 (h_0 = 50m)$. A section of the radiation σ_{rad} is at its most extreme point, and there is a relative section of σ_r. A comparison of curve 1 (in Fig. 1-7) with curves 2 and 3 (presented in Fig. 1-10) shows the relative backscattering cross-section when it does not provide sufficient information about resonant properties of elastic scatterers.

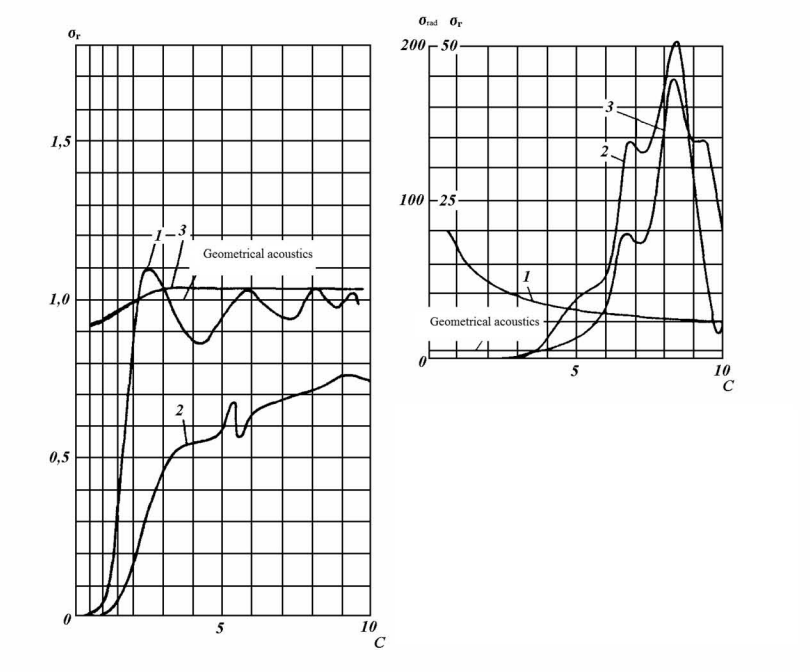

Figure 1-9 (left): The relative scattering of oblate spheroids cross-sections

Figure 1-10 (right): The relative scattering and radiating of prolate spheroidal bodies cross-sections

The results of the numerical calculations presented above make it possible to analyze the experimental amplitude-phase characteristics of the pulsed-sound signal scattering in the Fresnel and Fraunhofer zones [18, 19].

A series of recent publications [20–23] has demonstrated the efficiency of high-frequency asymptotes when calculating the diffraction fields of spheroids without using wave functions. It is remarkable that this approach is also valid for relatively low frequencies.

Resonances of elastic spheroidal shells (under axisymmetric excitation) have been studied in [24, 25]. In these publications, the authors considered steel and aluminum shells with different eccentricities and different thicknesses. For an aluminum shell with an axis ratio of 1:6 (an eccentricity of 0,995), the values of the normal velocity component were calculated. These revealed the presence of shell resonance at a wave size of C = 11,4 (recalculated according to the sound velocity in the liquid). In our steel shell with an axis ratio of 1:10 (an eccentricity 0,995), two resonances within the wave size interval 0,5–10,0 were observed for C=6,75 and C=8,25.

In [3], [5-6], [26–27], the resonances of elastic spheroidal shells were determined by the T-matrix method by applying the modified procedure to the extended Waterman method [26]. The function of the backscattering (scattering pattern) was calculated using the formulas proposed in [5]. Since the authors of these publications used spherical wavefunctions, the application of the T-matrices of dynamic elasticity theory in this method was limited to spheroidal axis ratios of 1:3. Our method of separating variables is free from this drawback.

CHAPTER 2

THE DIFFRACTION OF SOUND STATIONARY AND NON-STATIONARY IDEAL AND ELASTIC BODIES PLACED NEAR THE INTERFACE OF MEDIA IN AN UNDERWATER SOUND CHANNEL AND IN A PLANAR WAVEGUIDE

2.1. An Elastic Scatterer Near the Interface of Media

In the series of problems on the study of the influence of media interfaces on the characteristics of sound scattering by various bodies, the following variants are usually investigated:

a) The interaction of a scatterer with a single interface between media;
b) The scatterer in the field of interacting modes of the underwater sound channel; and
c) The finding of the total scattered field of the system of real and imaginary sources and scatterers of the planar waveguide.

The interaction of the scatterer with the interface between media is considered in the example of the scattering of sound by an elastic spheroidal body located at the interface between a liquid and an elastic medium [28]. Let the elastic gas-filled prolate spheroidal shell be placed near the boundary, a liquid, or an elastic medium (Fig. 2-1). The axis of rotation of the shell is parallel to the planar boundary. We introduced two systems of spheroidal coordinates ξ_s, η_s, φ_s ($s=1,2$): the first ($s=1$) is associated with the scatterer and the second ($s=2$) with the interface plane. The beginning of the Cartesian coordinate system O_2 and the foci of the second spheroidal coordinate system are defined as projections: O_1 and the foci of the first coordinate system on the plane of the boundary Z_2Y_2. The interfocus distance, $2h_0$, is common for both coordinate systems. The interface plane is two coordinate halves planes, $\phi_2' = \pi/2$ and $\phi_2'' = -\pi/2$, of the second coordinate system. In order to relate this solution to the solution of the problem of diffraction off of the elastic spheroidal shell, we simplify the formulation of the problem and assume that the wave vector $\vec{k}$ of the incident wave is in the X_1Z_1 plane and, correspondingly, in the X_2Z_2 plane as well: $\phi_{os} = 0°$ (see Fig. 2-1). Now, along with potential $\Phi_1^{(1)}$ of the wave and scattered by the shell, the potential $\Phi_1^{(2)}$ from the elastic half-space will appear as follows:

$$\Phi_1^{(2)} = 2\sum_{m=0}^{\infty}\sum_{n\geq m}^{\infty} K_{m,n}\bar{S}_{m,n}(C_1,\eta_2)R_{m,n}^{(1)}(C_1,\xi_2)\cos m\,\phi_2 \ . \quad (2.1)$$

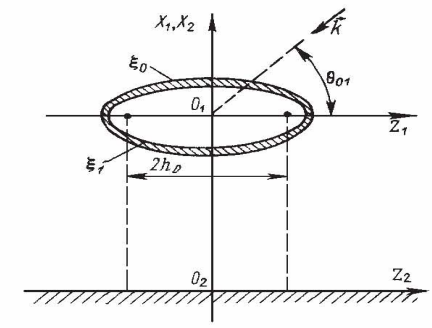

Figure 2-1: Elastic spheroidal shell near the liquid-elastic isotropic media interface

The potential $\Phi_1^{(2)}$ expands radial functions of the first kind. This is due to the fact that the foci of the second coordinate system lie in the plane of the interface. Physically, this means that the fields of pressure from two plane waves—an incident and when it is reflected by an interface—distort the scatters' interactions. Expansions in the shell's potentials are accompanied by expansions in the elastic half-space's potentials:

$$U_2^{(2)} = 2\sum_{m=1}^{\infty}\sum_{n\geq m}^{\infty} M_{m,n}\bar{S}_{m,n}(C_{t_2},\eta_2)R_{m,n}^{(1)}(C_{t_2},\xi_2)\sin m\,\phi_2 \ ; \quad (2.2)$$

$$W_2^{(2)} = 2\sum_{m=0}^{\infty}\sum_{n\geq m}^{\infty} N_{m,n}\bar{S}_{m,n}(C_{t_2},\eta_2)R_{m,n}^{(1)}(C_{t_2},\xi_2)\cos m\,\phi_2 \ ; (2.3)$$

$$\Phi_2^{(2)} = 2\sum_{m=0}^{\infty}\sum_{n\geq m}^{\infty} L_{m,n}\bar{S}_{m,n}(C_{l_2},\eta_2)R_{m,n}^{(1)}(C_{l_2},\xi_2)\cos m\,\phi_2 \ , (2.4)$$

where C_{l_2} and C_{t_2} are wave dimensions of longitudinal and transverse waves, respectively.

The potential of the incident wave Φ_0 in two coordinate systems has the following form [29, 30]:

$$\Phi_0 = 2\sum_{m=0}^{\infty}\sum_{n\geq m}^{\infty} i^{-n}\varepsilon_m\bar{S}_{m,n}(C_1,\eta_0)\bar{S}_{m,n}(C_1,\eta_s)R_{m,n}^{(1)}(C_1,\xi_s)\cos m\,\phi_s \ , (s=1,2) \ . (2.5)$$

The potential of a diffracted field $\Phi_\Sigma = \Phi_0 + \Phi_1^{(1)} + \Phi_2^{(2)}$ simultaneously meets the boundary conditions on both the surface of a shell and the planar interface between a liquid and an elastic medium. The boundary conditions on a surface of a shell are supplemented by the conditions of an interface on a liquid elastic medium:

$$\lambda_0 k^2\left(\Phi_0 + \Phi_1^{(1)} + \Phi_1^{(2)}\right) = \lambda_2 k_{l_2}^2\Phi_2^{(2)} + 2\mu_2 u_{\phi\phi}^{(2)}\Big|_{\phi=\pi/2;-\pi/2} \ ; (2.6)$$

$$\left(h_\phi^{(2)}/h_\xi^{(2)}\right)(\partial/\partial\xi)\left(u_\phi^{(2)}/h_\phi^{(2)}\right) + \left(h_\xi^{(2)}/h_\phi^{(2)}\right)(\partial/\partial\phi)\left(u_\xi^{(2)}/h_\xi^{(2)}\right)\Big|_{\phi=\pi/2;-\pi/2} = 0 \ ; (2.7)$$

$$\left(h_\phi^{(2)}/h_\xi^{(2)}\right)(\partial/\partial\xi)\left(u_\phi^{(2)}/h_\phi^{(2)}\right) + \left(h_\xi^{(2)}/h_\phi^{(2)}\right)(\partial/\partial\phi)\left(u_\xi^{(2)}/h_\xi^{(2)}\right)\Big|_{\phi=\pi/2;-\pi/2} = 0 \ ; (2.8)$$

$$-(h_\phi)^{-1}(\partial/\partial\phi)\left(\Phi_0 + \Phi_1^{(1)} + \Phi_1^{(2)}\right) =$$
$$= \left(h_\phi^{(2)}\right)^{-1}(\partial\Phi_2/\partial\phi) + \left(h_\xi^{(2)}h_\eta^{(2)}\right)^{-1}\left[(\partial/\partial\xi)\left(h_\eta^{(2)}\psi_\eta^{(2)}\right) - (\partial/\partial\eta)\left(h_\xi^{(2)}\psi_\xi^{(2)}\right)\right]\Big|_{\phi=\pi/2;-\pi/2} \ , (2.9)$$

where λ_2 and μ_2 represent Lame coefficients of an elastic half-space and $k_l^{(2)}$ represents the wave number of the longitudinal wave an elastic half-space.

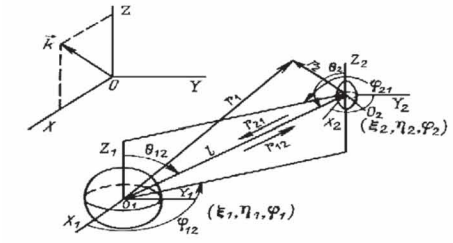

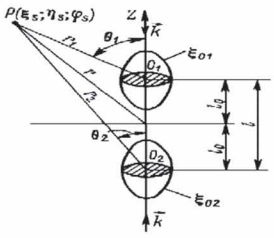

Figure 2-2 (left): Systems of spheroidal coordinates

Figure 2-3 (right): An ideal spheroid at associated with two interacting scatterers and a media interface

In our formulation, the evenness of the solution, with respect to the *XZ* planar boundary conditions for $\phi = -\pi/2$, completely repels the conditions for $\phi = +\pi/2$. Additionally, given the similarity between $\phi = -\pi/2$ and $\phi = +\pi/2$, there is no need to repeat the same kind of calculation for the other half of the scatterer, which is located on other side of the axis of symmetry, because doing so does not provide any additional information. When substituting potential expansions into boundary conditions for a shell and a planar interface when expansion coefficients are used an additional theorem for wave spheroidal functions [30] is as follows:

$$R_{p,q}^{(1),(3)}(C_j,\xi_j)\bar{S}_{p,q}(C_j,\eta_j)\,exp(ip\phi_j) = \sum_{n=0}^{\infty}\sum_{m=-n}^{n} R_{m,n}^{(1)}(C_s,\xi_s)\times$$
$$\times\,\bar{Q}_{m,n,p,q}^{(1),(3)}(C_j,C_s;l;\theta_{js})\bar{S}_{m,n}(C_s,\eta_s)\,exp(ip\phi_s) \ , (2.10)$$

where $\overline{Q}^{(1),(3)}_{m,n,p,q} = 2(-i)^{n-q}\sum_{r=0,1}^{\infty}{}'\sum_{t=0,1}^{\infty}{}' d_r^{pq}(C_j)d_t^{mn}(C_s)\sum_{\sigma=|r+p-t-m|}^{r+p+t+m}(-i)^{\sigma}\times$

$\times \tilde{b}_{\sigma}^{(r+p,p,t+m,m)} Z_{\sigma}^{(1),(3)}(kl)\tilde{P}_{\sigma}^{p-m}(\theta_{js})exp[i(p-m)\varphi_{js}]$;

θ_{js} represents the polar angle of a point O_s which is the beginning of an s-th coordinate system in an i-th system (Fig. 2-2); l represents the distance between O_j and O_s; $d_r^{pq}(C_j)$ and $d_t^{mn}(C_s)$ represent the coefficients of the expansion of functions $\bar{S}_{p,q}(C_j,\eta_j)$ and $\bar{S}_{m,n}(C_s,\eta_s)$ by $\tilde{P}_r^p(\eta_j)$ and $\tilde{P}_t^m(\eta_s)$, which (up to a constant factor) coincide with normalized joined Legendre functions; $Z_{\sigma}^{(1)} = j_{\sigma}(kl)$ represents spherical Bessel functions; $Z_{\sigma}^{(3)} = h_{\sigma}^{(1)}(kl)$ represents spherical Hankel functions of the first kind coefficients $\tilde{b}_{\sigma}^{(r+p,p,t+m,m)}$ are obtained from coefficients $b_{\sigma}^{(r+p,p,t+m,m)}$ [30], taking into account a relationship $\tilde{P}_t^m(\eta_s)$and associated Legendre functions; a prime for signs Σ means that a summation of r and t is carried out on an even mean basis if, corresponding, g - p and n - m is even and a summation of r and t is carried of on an odd basis if g - p and n - m is odd.

A strict solution can be obtained for another orientation of a spheroidal shell with respect to the planar boundary—namely, due to the perpendicularity of the rotational axis of a shell in relation to the planar interface between liquid and elastic media (Fig. 2-3). We will consider this orientation in more detail by replacing a spheroidal shell with an ideal prolate soft spheroid and by replacing the elastic half-space with an ideal medium (hard or soft) [31]. We will map a scatterer and a source mirror-wise with respect to a boundary and so reduce the problem to one the diffraction of the fields of two sources (both real and imaginary) by two spheroidal scatterers (both real and imaginary). Potentials Φ_s ($S=1,2$) of waves scattered by spheroids are chosen in the form of expansions (taking axial symmetry into account) [31]:

$$\Phi_s(\xi_s,\eta_s) = \sum_{n=0}^{\infty} B_{0,n}^s \bar{S}_{0,n}(C_s,\eta_s)R_{0,n}^{(3)}(C_s,\xi_s) \ . (2.11)$$

Since spheroids (both real and imaginary ones) are ideally soft then, for their surfaces ($\xi_0=\xi_{01}=\xi_{02}$), the key requirement of a homogeneous Dirichlet is satisfied:

$$\Phi_0 + \sum_{s=1}^{2}\Phi_s = 0|_{\xi=\xi_0;s=1,2} \ . (2.12)$$

The potential of a falling plane wave is given by the following expansion:

$$\Phi_0(\xi_s,\eta_s) = 2\sum_{n=0}^{\infty} i^{-n}\bar{S}_{0,n}(C_s,\eta_s)R_{0,n}^{(1)}(C_s,\xi_s)\bar{S}_{0,n}(C_s,1) \quad s=1,2 \ . (2.13)$$

Unknown coefficients $B_{0,n}^s$of expansions (2.11) are sought from an infinite system of equations and boundary conditions (2.12) [31]:

$$B_{0,n}^s + \sum_{q=0}^{\infty} B_{0,q}^t R_{0,n}^{(1)}(C_s,\xi_{0s})\left[R_{0,n}^{(3)}(C_s,\xi_{0s})\right]^{-1}\bar{Q}_{0n0q}^{(3)}(C_t,C_s;l;\theta_{ts}) =$$
$$= -2i^{-n}\bar{S}_{0n}(C_s,1)R_{0,n}^{(1)}(C_s,\xi_{0s})\left[R_{0,n}^{(3)}(C_s,\xi_{0s})\right]^{-1}, \quad s=1,2; \quad t=1,2; \quad s\neq t \ , (2.14)$$

where l represents the distance between centers of coordinate systems O_1 and O_2 (Fig. 2-3), in the given case

$$\theta_{12} = 0 \ \theta_{21} = \pi$$

$$\bar{Q}_{0n0q}^{(3)}(C_t,C_s;l;\theta_{ts}) = 2i^{-n+q}\sum_{r=0,1}^{\infty}{}'\sum_{j=0,1}^{\infty}{}' d_r^{0q}(C_t)d_j^{0n}(C_s)\sum_{\sigma=|r-j|}^{r+j} i^{-\sigma}b_{\sigma}^{(r,0,j,0)}h_0^{(1)}(kl)P_{\sigma}(\cos\theta_{ts}) \ ;$$

$$.b_{\sigma}^{(r,0,j,0)} = (rj00|\sigma O)^2.$$

For the regularization of a system (2.14) with respect to unknown coefficients $B_{0,n}^s$ we introduce a new unknown $X_{0,n}^s$ [31]:

$$B_{0,n}^s = R_{0,n}^{(1)}(C_s,\xi_{0s})X_{0,n}^s \ . (2.15)$$

As a result, an infinite system (2.14) for unknown $B_{0,n}^s$is reduced to another infinite system of a relatively new unknown $X_{0,n}^s$ [31]:

$$X_{0,n}^{s} + \sum_{q=0}^{\infty} X_{0,q}^{t} R_{0,q}^{(1)}(C_t, \xi_{0t}) \left[R_{0,n}^{(3)}(C_s, \xi_{0s})\right]^{-1} \bar{Q}_{0n0q}^{(3)}(C_t, C_s; l; \theta_{ts}) =$$
$$= -2i^{-n} \bar{S}_{0,n}(C_s, 1) \left[R_{0,n}^{(3)}(C_s, \xi_{0s})\right]^{-1} . \quad (2.16)$$

Furthermore, by means of a truncation method, we find the solution of a regular system (2.16). Initially, we calculated the angular scattering functions $D_s(\theta_s)$ of two interacting spheroids, which distorted the monochromatic plane wave field. Fig. 2-4 shows the modules of angular characteristics $|D_s(\theta_s)|$ in interacting spheroids (curve 1 refers to the first spheroid, and curve 2 refers to the second spheroid). Curve 3 depicts another scale, $|D(\theta)|$, for a single soft spheroid in an infinite medium. The scale had to be changed so that curve 3 did not merge with curves 1 and 2. Curve 4 is characterized by the modulus $|D_\Sigma(\theta_1)|$ of a total angular characteristic in coordinates of a first spheroid (Fig. 2-1):

$$|D_\Sigma(\theta_1)| = |D_1(\theta_1) + D_2(\theta_1)\, exp(ikl \cos\theta_1)| .$$

Calculations were carried out for $C_1=C_2=10,0$, $\xi_{01}=\xi_{02}=\xi_0=1,005$, with a half-focus distance of $h_{01}=h_{02}=1$м, $l=8h_0$. An analysis of the curves presented in Fig. 2-4 shows that when selected parameters were (C_1, C_2, l), the interaction of scatterers turned out to be small and, because of this, the curves 1, 2, 3 are close to each other. The main role is played by the interference effects (especially in the shadow region); therefore, curve 4 stands out sharply (again in the shadow region) against the background of the other curves. In a second stage (based on a calculation of the scattered field of two spheroids), the angular characteristics $D_\Sigma(\theta)$ of a soft spheroid ($\xi_0=1,005$; $C=10$) located at a distance ($l_0=4h_0=4$ m) from an interface between the liquid and an ideal medium, were calculated. The results of the calculations $|D_\Sigma(\theta)|$ are shown in Fig. 2-5. Curve 1 corresponds to the interface between liquid and soft media.

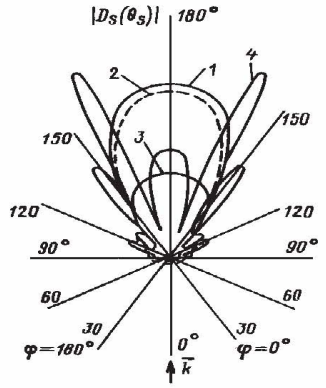

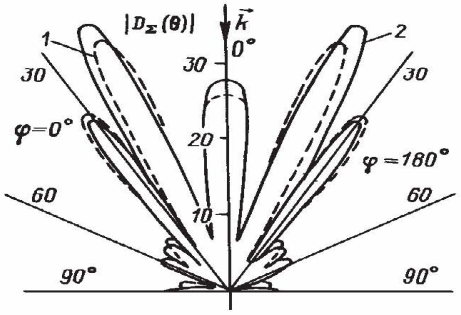

Figure 2-4 (left): Modules of the angular characteristics of single and interacting spheroids

Figure 2-5 (right): Modules of angular characteristics of a soft spheroid placed at the interface media

A certain contribution to $D_\Sigma(\theta)$ is made by an imaginary source and interference is associated with it along the fringes of both spheroids, including physically intense scattering in an illuminated region. This arises due to the reflection of the waves scattered by spheroids in the planar interface between media. We must not forget that, in this case, we are not talking about the distortion of a plane-traveling wave (as if it were an boundless medium) but we are, instead, talking about the distortion of a standing wave field that makes real and imaginary sources.

There is only one strict solution to the problem of the scattering of sound by a spheroidal half-body placed on the interface between a liquid and an ideal medium. Using the mirror image of a scatterer and a source connected to the planar boundary, we receive a spheroidal scatterer located in a field two sources (real and imaginary). A phase of a wave potential, from an imaginary source on a planar interface, coincides with a phase of a potential of an incident wave in a liquid, which borders on an ideally rigid medium. The phases of these waves differ from this boundary by 180° if the liquid borders on an ideally soft medium. Fig. 2-6 shows the modules of the angular characteristics $|D(\theta)|$ (in different scales) of spheroidal half-bodies located on the boundary between a liquid and an ideal medium. Curve 1 corresponds to half of a hollow steel oblate spheroidal shell placed on the boundary between a liquid and an ideally soft media. The outer radial coordinate of a shell is $\xi_0=0,1005$ and the internal is – $\xi_1=0,07669$. It has a wave size of $C=7,1$, and an irradiation angle of $\theta_0=0°$ (an axisymmetric problem). Two other curves (see Figure 2-6) relate to the modulus

of angular characteristics of a soft oblate hemispheroid bordering on a soft media (curve 2) and a hard media (curve 3) at the same angle of irradiation $\theta_0=0^\circ$ and the wave size of a body of $C=10,0$, with a radial coordinate of a soft oblate spheroid $\xi_0=0,1005$.

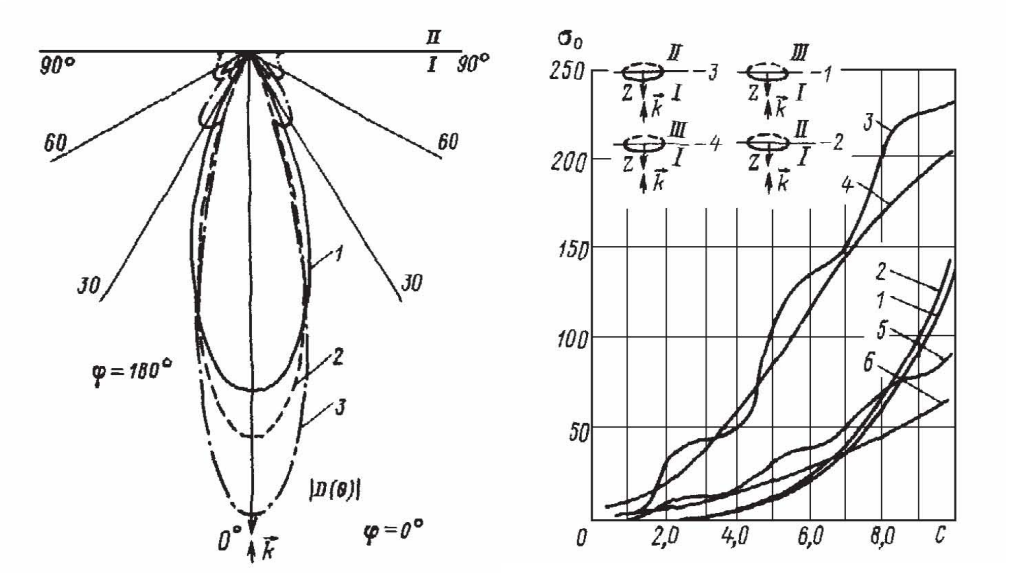

Figure 2-6 (left): Modules of angular characteristics of spheroidal semi-bodies located at an interface between the media

Figure 2-7 (right): Relative cross sections for the backscattering of oblate spheroids

Fig. 2-7 shows the relative cross-sections for the backscattering σ_0 of oblate ideal hemispheroids located at the interface between the two media, where by $D(\theta;\phi)$ we mean the total angular characteristics (from real and imaginary sources). Curves in Fig. 2-7 correspond to the axial radiation ($\theta_0=0^\circ$) of an oblate hemispheroid (soft or hard) with a radial coordinate of $\xi_0=0,1005$. Curves 1 and 3 refer to a hard hemispheroid placed at a boundary with (1) a hard media and (3) a soft media (we have designated the liquid as number "I", the soft media as number "II", and the hard media as number "III"). Curves 3 and 4 correspond to a soft hemispheroid located at a boundary between soft media ("2") and hard media ("4"). Curves 5 and 6 give an idea of the variation σ_0 between hard ("5") and soft ("6") oblate spheroids ($\xi_0=0,1005$) in an infinite liquid medium. It is easy to see that if a hemispheroid and an ideal semi-bounded medium (whether hard or soft; see curves 1 and 2) or a hemispheroid represents a distortion in the shape of a boundary, which hides this unevenness. If σ_0 grows slowly at small wave dimensions close to zero, then the hemispheroid and semi-bounded ideal medium cross-sections σ_0 will have much larger curves 3 and 4) across an entire investigated range of wave dimensions. While curves 5 and 6 tend asymptotically towards a value geometric acoustics, the remaining curves increase indefinitely. The mathematical and physical explanations for this phenomenon are given in the comments related to Fig. 2-5.

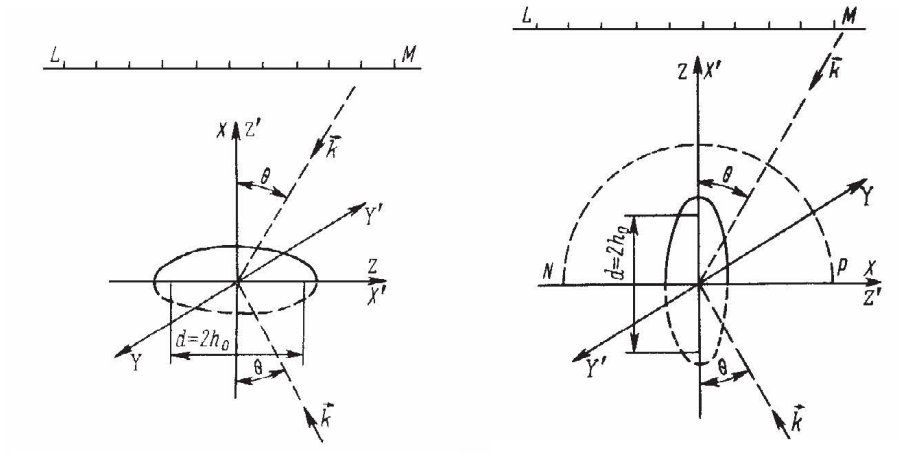

Figure 2-8 (left): The mutual orientation of a combined system and a hemispheroid (1st variant)

Figure 2-9 (right): The mutual orientation of a combined system and a hemispheroid (2nd variant)

Let us now turn to passive characteristics in a scattering indicatrix from hemispheroids located on an interface between a liquid and an ideal medium. We imagine that, for a fairly large distance from a boundary across, there is a combined system (source-receiver) which moves along a line *LM*. However, we are interested in a reflected signal to the point of the disposition in the combined system. The movement of the system is so slow that a Doppler effect can be ignored. Two admittedly possible orientations for the two half-bodies are depicted in Figs. 2-8 and 2-9. Fig. 2-10 presents (in different scales) modules $\left|D_{\Sigma}^{0}(\theta)\right|$for a prolate soft hemispheroid on the boundary of a liquid with an ideal hard medium (as depicted by curve 1, where the scale is to the left of the vertical axis, $\xi_0=1{,}005$, $C=10$) and for an oblate hard hemispheroid on the boundary of a liquid with an ideal l soft medium (as depicted by curve 2, the scale is to the right of the vertical axis, $\xi_0=0{,}1005$; $C=10$). A layout orientation of the two hemi-bodies corresponds to Fig. 2-8, and the directions of the rays meet the oblate coordinate system. Fig. 2-11 shows modules $\left|D_{\Sigma}^{0}(\theta)\right|$for a prolate hard hemispheroid at the boundary of a liquid with an ideally soft medium (a curve 1, $\xi_0=1{,}005$, $C=10$) and for an oblate hard hemispheroid on the boundary of a liquid with an ideally soft medium (a curve 2, $\xi_0=0{,}1005$; $C=10$). The orientation of the hemi-bodies corresponds to Fig. 2-9, and the directions of the rays meet the prolate coordinate system. The analysis presents a scattering indicatrix and shows the advantages of a second-type orientation (see Fig. 2-9; this is because it appears that an intense non-mirror component is associated with the sound reflective nature of the interface. With regard to an orientation of the first type (see Fig. 2-8), an intensive back-reflection at $\theta=0^{o}$ will be masked by the reflection from the planar interface.

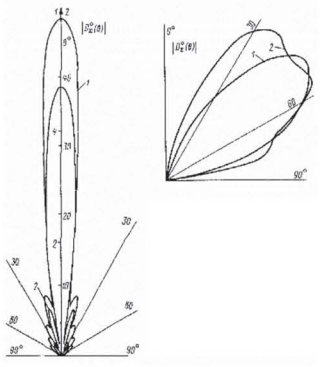

Figure 2-10 (left): Modules of scattering indicatrics of soft hemispheroids

Figure 2-11 (right): Modules of scattering indicatrics of hard hemispheroids

We will now move from examining stationary (harmonic) irradiation to non-stationary radiation in the form of sound pulses with a rectangular envelope and monochromatic filling. As before, we will consider media interfaces of three types: the boundary between a liquid and an elastic bottom; the boundary between a liquid and an ideally soft medium (the Dirichlet condition); and the boundary between a liquid and an ideally hard medium (the Neumann condition).

If a scatterer (an oblate hard spheroid) is placed at the interface between media (the boundary between a liquid and an elastic bottom) at an observation point, it will first accept the pulse of a mirror reflection from a scatterer.

Fig. 2-12a shows a mirror reflection pulse $r_1 \cdot \Psi_S(t)$ for a hard oblate spheroid when it is irradiated at an angle of $\theta_1 = 30°$; a normalized modulus of the spectrum of a pulse $r_1 \cdot \Psi_S(t)$ can be seen in Fig. 2-12b. After a while, the pulse $\Psi_{\Sigma}(t')$ will reach observation point *P*, which is reflected from an elastic bottom and diffracted on a spheroid.

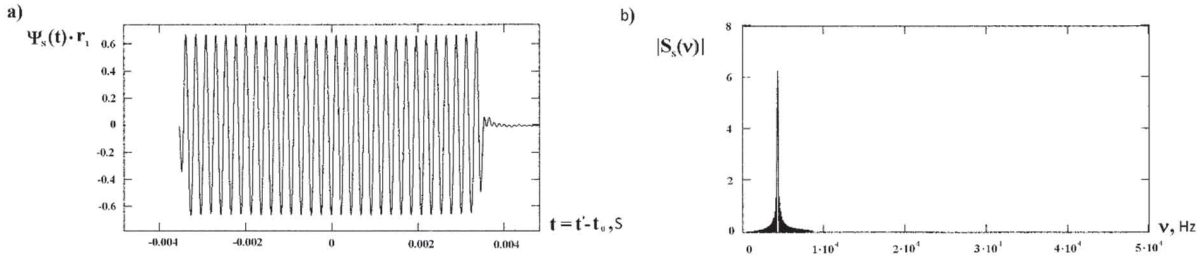

Figure 2-12a (left): A mirror reflection pulse $r_1 \cdot \Psi_S(t)$

Figure 2-12b (right): The normalized modulus of the spectrum $|S_S(\nu)|$ of a pulse $r_1 \cdot \Psi_S(t')$

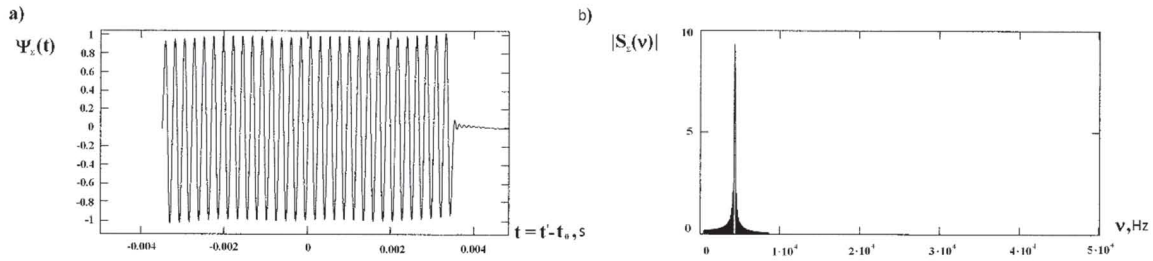

Fig. 2-13a (left) shows a pulse $\Psi_\Sigma(t)$. The normalized modulus spectrum $|S_\Sigma(\nu)|$ of a pulse $\Psi_\Sigma(t')$ is presented in Fig. 2-13b.

Figure 2-13b (right): The normalized modulus of the spectrum $|S_\Sigma(\nu)|$ of a pulse$\Psi_\Sigma(t')$

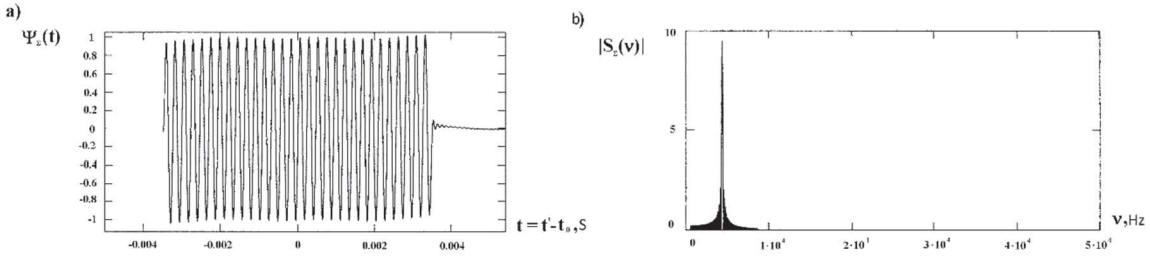

Figure 2-14a (left): A mirror image of the reflection pulse $\Psi_\Sigma(t)$ for a hard prolate hemispheroid on a boundary with a hard medium

Figure 2.14b (right): The normalized modulus of a spectrum $|S_\Sigma(\nu)|$

We orient a hard prolate hemispheroid in such a way that its major semi-axis will be in the plane of an interface between the media. We calculate mirror-reflected pulses $\Psi_\Sigma(t')$, which occur at an angle of incidence $\theta_1 = 60°$, for two variants: 1) a hard prolate hemispheroid on a boundary with a hard medium and 2) a hard prolate hemispheroid on a boundary with a soft medium. Fig. 2-14a presents a pulse $\Psi_\Sigma(t)$ and a normalized modulus of a spectrum $|S_\Sigma(\nu)|$ for the first variant.

Fig. 2-15 shows the same characteristics for a second variant.

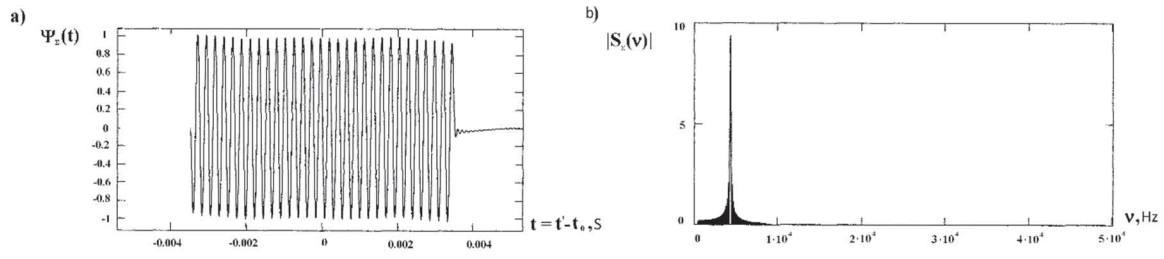

Figure 2-15a (left): A mirror reflection pulse $\Psi_\Sigma(t)$ for a hard prolate hemispheroid on a boundary with a soft medium

Figure 2.15b (right): The normalized modulus of a spectrum $|S_\Sigma(\nu)|$

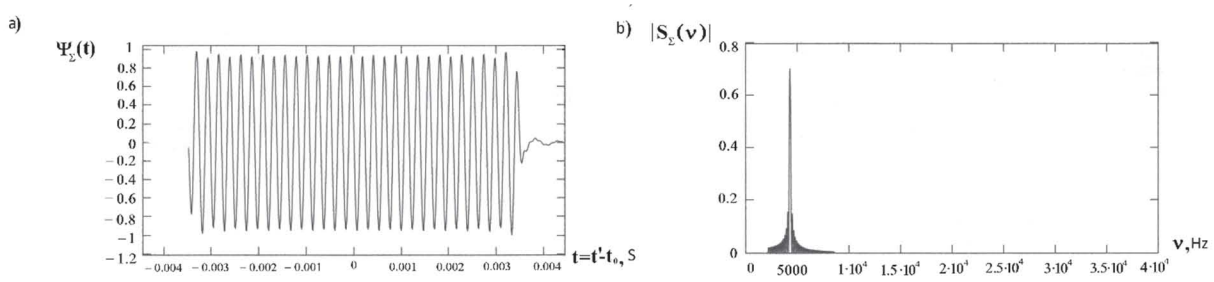

Figure 2-16a (left): A mirror reflection pulse$\Psi_\Sigma(t)$ for a hard oblate hemispheroid

Figure 2-16b (right): The normalized modulus of a spectrum $|S_\Sigma(\nu)|$ of a pulse $\Psi_\Sigma(t)$

We see in Fig. 2-16 a diffracted pulse $\Psi_\Sigma(t)$ and a modulus of its spectrum $|S_\Sigma(\nu)|$ in the direction of a mirror component for a hard oblate hemispheroid, which is located on the border between a liquid and an ideally soft medium in such a way that its major axis lies in a planar boundary. The angle of irradiation remains the same at$\theta_1 = 30°$.

Fig. 2-17 shows a diffracted pulse $\Psi_\Sigma(t)$ in the direction of a mirror component and a modulus of its spectrum $|S_\Sigma(\nu)|$ for a soft prolate hemispheroid placed on the border between a liquid and an ideally hard medium. The dimensions, the orientation of the hemispheroid, and the ratio of the semi-axis are the same as in Fig. 2-16. We note that for oblate and prolate hemispheroids located on an interface between the media, a diffracted pulse $\Psi_\Sigma(t)$ in the direction of a mirror component is obtained as a result of the interference between two reflected signals: the hemispheroid and the boundary. Therefore, it is designated as a diffracted pulse /.$\Psi_\Sigma(t)$.

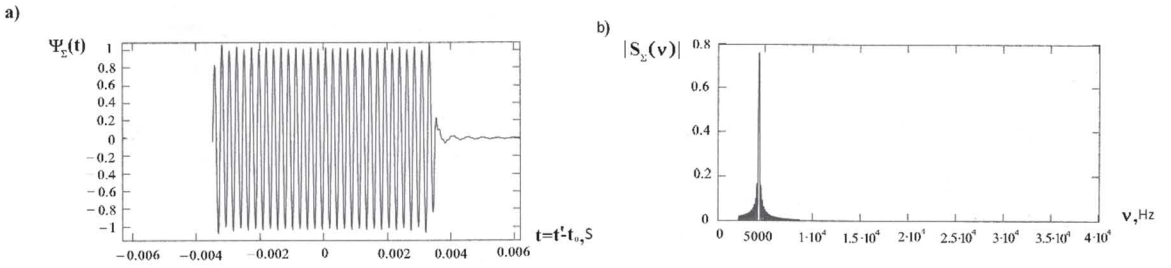

Figure 2-17a (left): The mirror reflection pulse$\Psi_\Sigma(t)$ for a soft prolate hemispheroid

Figure 2-17b (right): The normalized modulus of a spectrum $|S_\Sigma(\nu)|$ of a pulse $\Psi_\Sigma(t)$

Figure 2-17 depicts the sound's reflection by a spheroidal body located at the boundary between the liquid and an elastic bottom. We supplement these results with angular scattering characteristics $R(\theta, \phi)$ for a stationary sound signal with a fixed frequency.

2.2. An Ideal Spheroid in an Underwater Sound Channel

A study into the influence of two boundaries of the waveguide on the scattered field of a spheroidal scatterer will begin with an ideal spheroid placed in an underwater sound channel. The sound channel has non-reflective boundaries [32] and is irradiated with a pulsed signal with monochromatic filling [33]. At a depth z_0 of such a waveguide, we place a point source of an impulse signal and, at a horizontal distance r from that sound source, a spheroidal scatterer is placed at a depth of z_2 (Fig. 2-19a). A velocity profile of sound in a symmetrical underwater sound channel is shown in Fig. 2-19b. A receiver of a scattered signal is compatible with the sound source and so we will consider a combined system to find the spectrum of a scattered signal. Since, the velocity of sound depends only on vertical coordinate z, the rays in a horizontal plane are not bent. In each vertical half-plane, which passing through the center of a scatterer, a sound field will be independent of the adjacent half-planes and, at each half-plane, there will be complex coefficients from the excitation the modes of a sound channel. As a result, in each of these half-planes, one observes an interference pattern of modes independent of neighbouring half-planes. We are interested in a field in one vertical half-plane P, which contains the coincident point of a source-receiver and the center of a scatterer. Since a scattered field in this half-plane does not depend on the behavior of this field in all other half-planes, we shall take it to be the same in all vertical half-planes and equal to a field in half-plane P. The spectrum of a scattered signal at

the location of a source will be approximately (without taking into account the effect of the medium on an angular scattering characteristic) equal to [6]

$$S_2(\omega) = \rho_0^2(r_1)^{-1} \sum_{m=1}^{M} \sum_{n=1}^{N_m} P_m P_{n,m} D_{nm}(\omega)\, exp[-i(\kappa_m r_1 + \kappa_{nm} r_1 - \pi/2)] \text{ , (2.17)}$$

where $P_m = p_m(\rho_0)^{-1}\phi_m(z_2)\phi_m(z_0)$; p_m represents a mode excitation coefficient m; $\phi_m(z_2)$ represents an intrinsic waveguide function determined by boundary conditions; ρ_0 represents the density at the depth of the source and the receiver; $P_{nm} = (1/\rho_2)\phi_n(z_2)\phi_n(z_0)$; ρ_2- represents density at the depth of the centre of a scatterer; $D_{nm}(\omega)$ represents the space-transfer function of the scattering for an m-th mode of a source and an n-th mode of a scatterer; κ_m and κ_{nm} represent horizontal components of the wave numbers of modes of an incident and scattered waves, respectively; M represents the largest admissible source mode; and N represents the largest admissible scatterer mode for the m-th mode of a source.

The dependence of a sound velocity on a coordinate z for a symmetric waveguide (see Fig. 2-18 b) has the following form [32]:

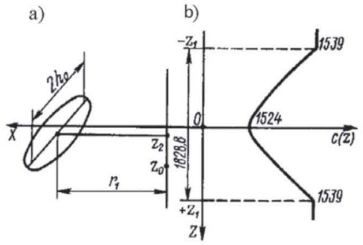

Figure 2-18 a (left): The mutual arrangement of a spheroidal scatterer and a source in a sound channel

Figure 2-18b Right): The profile of the velocity of sound in a sound channel with non-reflective boundaries

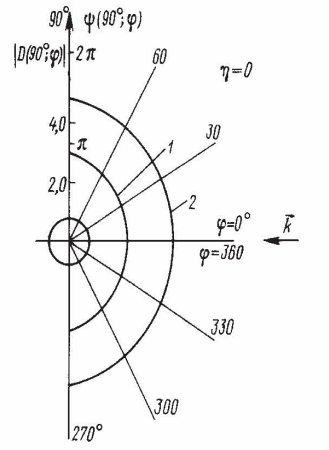

Figure 2-19: The amplitude-phase characteristic of sound scattering by a soft spheroid

We will find spectrum $S_2(\omega)$ located at the combined point of a source and the receiver for an ideal soft scatterer in the form of a prolate spheroid with a coordinate of an outer surface $\xi_0=1{,}005$. We place the combined system (source and receiver) on the axis of a symmetric waveguide ($z_2=z_0=0$), which is a major axis of the spheroid that is perpendicular to the Z-axis. An inter-focus spheroid distance (between the foci) $2h_0$ is assumed to be equal to 9,7 m. A source generates a pulse signal with a duration $\tau_0=0{,}05$ s at a frequency $f_0= 400$ Hz ($C=8{,}0$). The space-transfer function $D_{nm}(\omega)$ is determined by a picked frequency and, in an XOZ plane, the angular characteristics of a sound-scattering spheroid. With the chosen velocity profile of a sound (see Fig. 2-18b), one of the largest angles between wave vectors in the incident and scattered waves is approximately 16^o. Referring to the amplitude-phase angular characteristic of the scattering $D(\theta;\phi)$ from a sound wave reflected off a soft spheroid in an XOZ plane ($\theta = 90°$, $\eta = 0$) (see Fig. 2-19), we note that, even with a maximum wave size of ($C=10{,}0$), the angular characteristic $D(90°;\phi) = |D(90°;\phi)|\, exp[i\psi(90°;\phi)]$ is practically non-directional within angles $\phi = 0 \div 16°$ (see Fig. 2-19). Such an approach, in which modes of an underwater sound channel are considered in the form of plane waves

irradiating our spheroidal scatterer, is also approximate. Curve *1*, in Fig. 2-19, refers to $|D(90°;\phi)|$, while curve *2* characterizes a phase $\psi(90°;\phi)$ which is increased by π for all angles φ. At lower wave dimensions, its characteristics will be even closer to the circular form. Therefore, taking into account our assumption about a uniform scattering in a horizontal plane, we can assume that each incident wave from a set of admissible modes will uniformly scatter in all directions (as a non-directional scatterer) with an angular constant excitation coefficient $D(\omega)$, which then transfers the function $D_{nm}(\omega)$. As a result, the spectrum of a scattered signal will be calculated by means of the following formula [33]:

$$S_2(\omega) = D(\omega)\rho_0^2(r_1)^{-1}\sum_{m=1}^{M}\sum_{n=1}^{M} P_m P_{nm}\, exp[-i(\kappa_m r + \kappa_{nm} r - \pi/2)] \; . \quad (2.18)$$

2.3. The Diffraction of a Pulse Sound Signal on a Soft Prolate Spheroid Placed in a Planar Waveguide with a Hard Elastic Bottom

We turn to the familiar problem of the diffraction of pulses on spheroidal bodies in the planar waveguide [34–40]. These preserve the ideal soft upper boundary (the Dirichlet condition), waveguide dimensions, and scatterer with respect to the boundaries; they only replace the ideal hard lower boundary on the elastic isotropic bottom. Physical parameters of the lower medium will correspond to the isotropic elastic bottom but their values will be very close to the parameters of a transversely isotropic rock (a large slab of grey siltstone) [41]. The longitudinal wave velocity in this material is 4750 m/s, while the transverse wave velocity is 2811 m/s. Therefore, the method of imaginary sources needs the reflection of the coefficient V to be entered for each source [40] when displaying sources relative to the upper border sources. This [34–37, 41, 42] will change the sign of the source on the opposite side, which corresponds to a change of phase byπ.

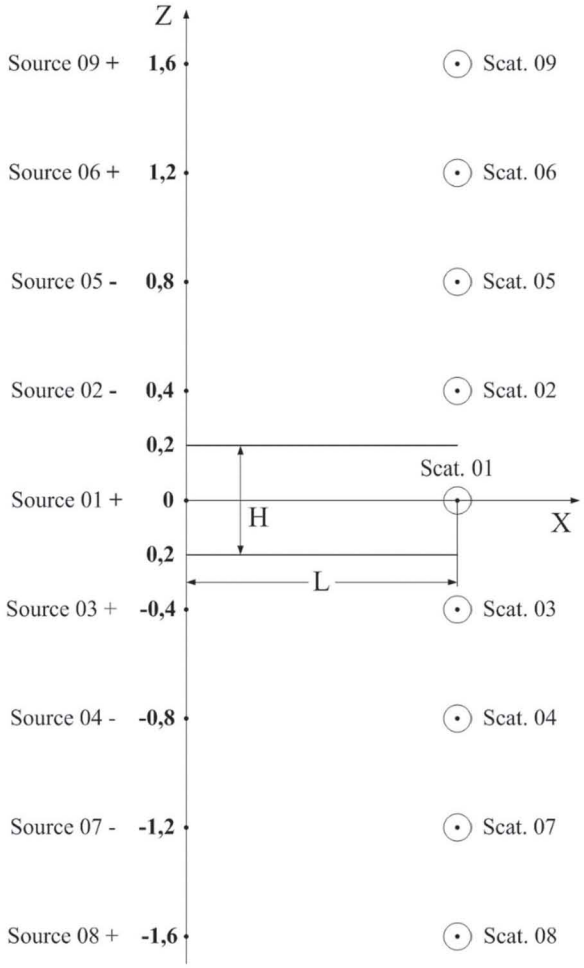

Figure 2-20: The mutual disposition of the pulse point sources and scatterers in the planar waveguide

It is known [40] that the imaginary sources method, used to calculate the boundary conditions, is not strictly fulfilled for any of the borders of the waveguide, even in the case of ideal Dirichlet and Neumann boundary conditions. For the better fulfillment of these conditions in diffraction problems [7, 34–37, 41, 42], imaginary

scatterers were introduced by mirroring their relative waveguide boundaries. Likewise, we introduce imaginary scatterers to compare with the reflection of such pulses [7, 34, 35] in the ideal borders and in the presence of a hard elastic bottom in the waveguide. [40] shows that the method of imaginary sources is applicable in the case where the reflection coefficient V will be a function of the angle in the wave, which is from a source relative to the normal (perpendicular) boundary. In our case, this angle will be determined by the mutual position of the source (whether real or imaginary) and the scatterers (real or imaginary), where the wave falls from the source. Since the receiver is combined with a real source Q, the sequence of the reflected pulses will be determined by the quantity and the amplitudes of the reflected signals (from different scatterers), which have the same propagation time as the waves that travel from sources to scatterers and from scatterers to point Q. The parameters of the waveguide, the position of the real source Q (combined with the receiver), and the position of the real scatterer remain unchanged as in [7, 34, 35]: L = 1000 m. and H = 400 m. The real source Q and the real scatterer are each located at a depth of 200 m. The scatterer is an ideal soft prolate spheroid with a semi-axes ratio of a/b = 10 (a = 0,279 m.). Its axis of rotation is perpendicular to the plane of the figure (see Fig. 2-20). The formula for the reflection coefficient V_{0N}, where N represents the number of a source, is given in [40]. For the calculation of the first four reflected pulses, the following reflection coefficients are needed: V_{03}, in the direction of the first (real) scatterer 01; V_{05}, in the direction of the second (imaginary) scatterer 02. As a result of simple calculations made with the help of [10], we obtain: V_{03}= 0,8423 + i 0,5390; V_{05}=0,8423 + i 0,5390.

Coefficients have become complex. This means that the total internal reflection is at the boundary between the liquid and the hard elastic bottom. Therefore, modules of reflection coefficients are equal to 1,0 and the real parts of the coefficients are close to +1,0, which is typical for the boundary between a liquid and an absolutely hard bottom. The resulting sequence of calculations of first four reflected pulses is shown in Fig. 2-21.

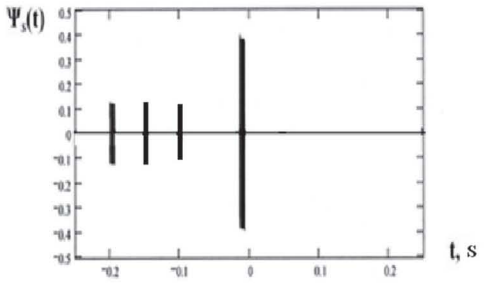

Figure 2-21: The normalized series of first four reflected impulses in a waveguide with a hard elastic bottom

We compared this sequence to the sequence in Fig. 2-22, where there are ideal boundaries [7, 34, 35]:

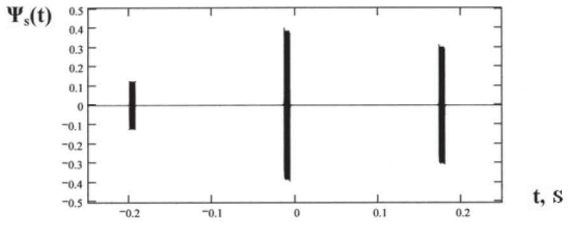

Figure 2-22: The normalized series of the first three reflected impulses with harmonic filling in point Q

The first and fourth pulses of Fig. 2-21 are identical to the first and second pulses of Fig. 2-22. As for the second and third pulses shown in Fig. 2-21, in the case of ideal boundaries and the symmetrical location of a real source and a real scatterer relative to the boundaries of the waveguide, they are compensated (absorb each other) by each of the reflected pulses: i. e., the second and third, pulses (see Fig. 2-21). This shows the difference in the sequences of the reflected pulses when replacing an absolutely hard bottom with that of an elastic hard bottom. Exactly the same result is obtained for the anisotropic (transversely isotropic) bottom, if its isotropy plane coincides with the plane of the impulse incidence.

A similar pattern is observed for an anisotropic bottom, such as one composed of silicon, where there is a quasi-longitudinal wave velocity of about 8300 m/s and a quasi-transverse wave velocity of about 5700 m/s [39]. Due to the high velocities of the quasi-longitudinal and quasi-transverse waves, the total internal reflection effect at the anisotropic bottom manifests itself even more strongly than at the isotropic bottom.

2.4. The Diffraction of a Pulse Sound Signal on a Non-Analytical Elastic Scatterer Put in Planar Waveguide with a Hard Elastic Bottom

Based on the obtained solution, let us consider the more general problem of the pulsed sound signal diffraction that impacts on an elastic scatterer comprised of a finite cylindrical shell supplemented with two hemispherical shells (one on either end) (Fig. 2-23) and placed in a waveguide with a hard elastic bottom (Fig. 2-24). Here, the data was calculated using integral equations [7, 43–47]. We note that a similar problem can be solved with the help of other methods: the boundary element method [46, 48]; the T-matrix method [49]; the method of a potential [50]; the finite element method [51]; and the Green's function method [52].

The first stage will solve the problem of the diffraction of a harmonic wave on such a shell.

The density of the material of the shell is ρ_1 and the Lame's coefficients are λ and μ. The shell was internally filled with the internal liquid medium with a density of ρ_2 and a sound velocity of C_3. It was placed in an external liquid medium with a density of ρ_0 and a sound velocity of C_0. As the shell falls, the plane harmonic wave has the pressure p_i under the angle Θ_0 and with the wave vector $\vec{k}$.

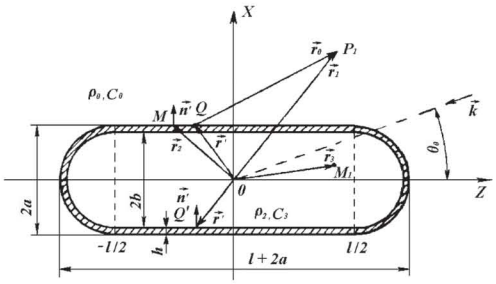

Figure 2-23: The elastic shell in the form of a terminal cylinder ending with semi-spheres

As was shown in [7] and [43–47], the initial equation is an integral equation having the sense of the generalized Huygen's principle for the displacement vector $\vec{u}(\vec{r})$ of the elastic shell:

$$\vec{u}(\vec{r}) = \iint_S \left\{ \vec{t}(\vec{r}')G(\vec{r}';\vec{r}) - \vec{u}(\vec{r}')\left[\hat{n}'\sum(\vec{r}';\vec{r})\right] \right\} dS(\vec{r}'), \quad \vec{r} \in V, \qquad (2.19)$$

where $\vec{t}(\vec{r}') = \hat{n}'T(\vec{r}')$ is the stress vector; $\hat{n}' \equiv \hat{n}'(\vec{r}') = \vec{n}'(\vec{r}')$ is the single vector of the external along the relation to S normal; $T(\vec{r}')$ is the stress tensor of the isotropic material; $G(\vec{r}';\vec{r})$ is the Green's displacement tensor; and $\sum(\vec{r}';\vec{r})$ is the Green's stress tensor. Additionally, if $\vec{r}$ is the point of surface S, then the left part of equation (2.19) will be $\vec{u}(\vec{r}')/2$.

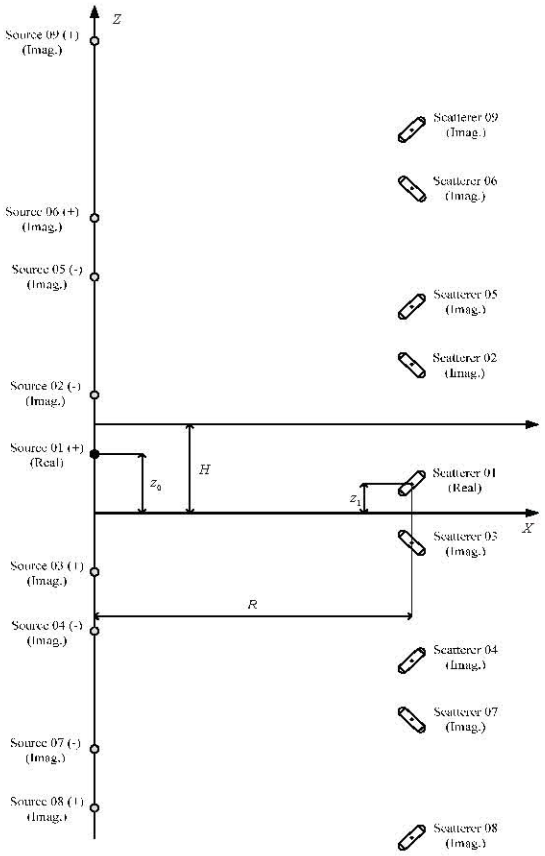

Figure 2-24: The mutual disposition of the impulse point sources and scatterers in the planar waveguide

The displacement vector $\vec{u}(\vec{r})$, the stress tensor$T(\vec{r})$, the Green's displacement tensor $G(\vec{r}';\vec{r})$, and the Green's stress tensor $\Sigma(\vec{r}';\vec{r})$ were connected by the following correlations [7, 47]:

$$T(\vec{r}) = \lambda I \nabla \vec{u}(\vec{r}) + \mu(\nabla \vec{u} + \vec{u}\nabla) \ , \qquad (2.20)$$

$I = I_L + I_T$; $I_L = (\nabla\nabla)/\nabla^2$; $I_L \cdot I_T = 0$; and $I_T = -[\nabla(\nabla I)]/\nabla^2$, where I_L and I_T are the longitudinal and transverse single tensors for the Hamilton's operator ∇:

$$\sum(\vec{r}';\vec{r}) = \lambda I \nabla G(\vec{r}';\vec{r}) + \mu\left[\nabla G(\vec{r}';\vec{r}) + G(\vec{r}';\vec{r})\nabla\right] \ ; \qquad (2.21)$$

$$G(\vec{r}';\vec{r}) = (1/4\pi\rho_t\omega^2)\{k_2 I g(k_2|\vec{r}' - \vec{r}|) +$$
$$+\nabla'[g(k_1|\vec{r}' - \vec{r}|) - g(k_2|\vec{r}' - \vec{r}|)]\nabla\} \ , \qquad (2.22)$$

where k_1 and k_2 are the wave numbers of the longitudinal and transverse waves in the material of the shell.

The second integral equation presents the Kirchhoff integral for the diffracted pressure $p_\Sigma(P_1)$ in the external medium:

$$C(P_1)p_\Sigma(P_1) = -\iint_{S_a}\{p_\Sigma(Q)(\partial/\partial n')[exp(ikr_0/r_0)] -$$
$$-[exp(ikr_0/r_0)]\rho_0\omega^2(\vec{u}\vec{n}')\}dS_a + 4\pi p_i(P_1) \ , \qquad (2.23)$$

where $p_\Sigma(P_1) = p_i(P_1) + p_s(P_1)$; $p_s(P_1)$ is the scattered pressure at point P_1; $C(P_1)$ is the numerical coefficient, equal to 2π if $P_1 \in S_a$ or 4π, if P_1 is outside of S_a; S_a is the external surface of the shell; and Q is the point located on the external surface of the shell.

For the pressure $p_2(M_1)$ in the internal liquid medium at point M_1, the third integral equation is derived:

$$C(M_1)p_2(M_1) = \iint_{S_b}\{p_2(Q')(\partial/\partial n')[exp\,(ikr_3)/r_3] -$$

$$-[exp\,(ikr_3)/r_3]\rho_0\omega^2(\vec{u}\vec{n}')\}dS_b, \qquad (2.24)$$

where Q' is the point of the internal surface of the shell, and S_b is the internal surface of the shell.

$$C(M_1)=\begin{cases}4\pi, & if \quad M_1 \quad out \quad S_b\ ;\\ 2\pi & if \quad M_1 \in S_b\ ;\end{cases}$$

The boundary conditions of the external (S_a) and internal (S_b) surfaces of the shell are added to the integral equations (2.19), (2.23), and (2.24):

$$\tau_i|_{S_a}=0\ ; \quad \tau_i|_{S_b}=0\ ; \quad i=1,\ 2\ ; \qquad (2.25)$$

where 1 signifies that, at both surfaces of the shell, the tangential stresses are equally null and 2 signifies that the normal stress $\sigma_{n'}$, at the external surface of the shell, is equal to the diffracted pressure p_Σ, but at the internal surface it is equal to the pressure p_2:

$$\sigma_{n'}\big|_{S_a}=p_\Sigma\ ; \quad \sigma_{n'}\big|_{S_b}=p_2\ ; \qquad (2.26)$$

In conformity with the conditions outlined in (2.25) and (2.26), the stress vector $\vec{t}(\vec{r}')$ in equation (2.19) is equal to

$$\vec{t}(\vec{r}')=p_\Sigma\vec{n}'\big|_{S_a}\ ; \quad \vec{t}(\vec{r}')=p_2\vec{n}'\big|_{S_b}\ ; \qquad (2.27)$$

Condition 3: the continuity of the normal component of the displacement of both boundaries of the shell, in accordance with the relations of the theory of elasticity for an isotropic body. Condition 3 will have the form:

$$\left.\begin{aligned}u_{n'}&=(1/\rho_0\omega^2)(\partial p_\Sigma/\partial n')\big|_{S_a}\ ;\\ u_{n'}&=(1/\rho_2\omega^2)(\partial p_2/\partial n')\big|_{S_b}\ .\end{aligned}\right\} \qquad (2.28)$$

The substitution of the integral equations, (2.19), (2.23), and (2.24), in the boundary conditions yields the system of equations in terms of unknown functions, p_Σ, p_2, and the components of the displacement vector, $\vec{u}$, at both surfaces of the shell. To obtain the numerical solution to this system, the integral equations are replaced by the quadrature formulas and the grid of the nodal points is chosen at both surfaces of the shell, as has been done for ideal non-analytical scatterers [8, 43].

When choosing the boundary conditions, we will have two types of integrals: (1) integrals with an especially isolated point, and (2) integrals that are considered the principal meaning. The method of calculating integrals of the second type was described in [7].

When calculated, the reflection characteristics of the harmonic signal with frequency ν can enable us to determine the spectral reflectance function $S_S(2\pi\nu)$. Additionally, it can be helpful when applying a Fourier transformation by which we obtain a temporary function of the reflected pulse $\Psi_S(t')$ [53]:

$$\Psi_S(t')=\frac{1}{\pi}Re\int_0^\infty S_S(2\pi\nu)e^{+i2\pi\nu t}d\,(2\pi\nu) \qquad (2.29)$$

Similarly using spectral reflectance characteristics of elastic bodies of spheroidal form [7, 54–57], we can compute the sequences of pulses reflected in the waveguide with a hard elastic bottom.

In the first part of this section, we investigated the interaction of sound impacting a scatterer at the interface between media. It was shown that interference plays a main role in this. The second part of the chapter has been devoted to the study of the spectrum of the scattered field of an ideal prolate spheroid placed in an underwater sound channel with non-reflective boundaries. Lastly, in the third part of the review, the effect of the influence of the parameters of a bottom on a series of pulses, which are reflected from a spheroidal body located in a planar waveguide, has been determined.

As a result of this research, we can draw three conclusions:

1) When studying the propagation and diffraction of pulse signals in a planar waveguide, it is necessary to use imaginary sources as pulse-like bundles of energy, which are spread in any direction (including along the axis of the waveguide) at a group velocity that does not exceed the sound (based on imaginary sources).
2) Replacing the hard elastic bottom with an absolutely hard bottom is acceptable for those sources (both real and imaginary) where waves fall to the hard elastic bottom and test the total internal reflection.
3) We have adopted a model of image sources and image scatterers, which (following internal reflection) is quite acceptable, at least for the first five calculated reflected pulses in a planar waveguide with a hard elastic bottom.

CHAPTER 3

THE GREEN'S FUNCTIONS METHOD FOR PROBLEMS OF SOUND DIFFRACTION

3.1. The Sound Scattering of Bodies with a Simple Form (Sphere; Spheroid) with Mixed Boundary Conditions

Initially, the Green's function method was used to solve the problem of the sound scattering from ideal scatterers in mixed boundary conditions. It was later applied to the sound diffraction studies of ideal and elastic bodies of a non-analytical form. The first part of section 3 sets out a detailed illustration for the use of the Green's function method to solve diffraction problems regarding simple bodies (sphere; spheroid) in mixed boundary conditions. Analytical solutions are complemented by the results of calculations of similar bodies in the Fresnel and Fraunhofer zones of the scattered sound field. In future, the Green's function method will be extended to ideal and elastic scatterers of a non-analytical form.

Ideal scatterers, ones that have dissimilar boundary conditions on different parts of the surface area (Dirichlet or Neumann conditions) refer to bodies with mixed boundary conditions. Sound diffraction problems regarding such scatterers are solved by means of one or two methods. The first method, which was proposed by A. Sommerfeld [29], is called the variational method (or the method of least squares) [29, 58, 59]. The second method, the Green's function method [45, 59–61], is based on the use of the corresponding Green's function for each part of the surface of the scatterer. We will now look at the use and characteristics of both methods and an example of a sphere, with radius R, in mixed boundary conditions (one half of a sphere is ideally soft; another is ideally hard $S_2\left(\theta = 90 \div 180^\circ\right)$). On the surface area of a sphere $S_1\left(\theta = 0 \div 90^\circ\right)$, the Dirichlet condition is perfomed and in the area , the Neumann condition is perfomed (Fig. 3-1). In accordance with the given boundary conditions, and by using the variational method, a functional G^N of the following form [29] is made:

$$G^N = k^2 \int_{S_1} \left| \Phi_i + \Phi_s \right|^2 dS + \int_{S_2} \left| \frac{\partial \Phi_i}{\partial n} + \frac{\partial \Phi_s}{\partial n} \right|^2 dS . \qquad (3.1)$$

where k represents the wave number of the incident plane wave.

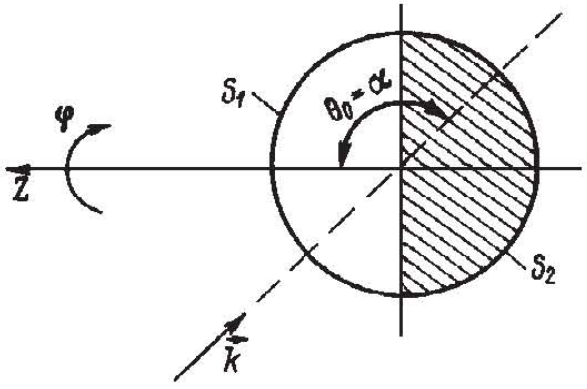

Figure 3-1: The sphere with mixed boundary conditions

In general, ($\theta_0 = \alpha \neq 0^\circ$ or $\theta_0 = \alpha \neq 180^\circ$) the problem is three-dimensional and the potentials of incident (Φ_i) and scattered (Φ_s) waves are found in the following form:

$$\Phi_i(r;\theta;\varphi) = \sum_{m=0}^{\infty}\sum_{n=0}^{m} i^n (2n+1)\varepsilon_m [(n-m)!/(n+m)!] \times \\ \times P_n^m(\cos\alpha) P_n^m(\cos\theta) j_n(kr)\cos m\varphi ; \tag{3.2}$$

$$\Phi_s(r;\theta;\varphi) = \sum_{v=0}^{N}\sum_{q=0}^{v} A_q^v P_q^v(\cos\theta) h_q^{(1)}(kr)\cos v\varphi , \tag{3.3}$$

where A_q^v represents the unknown coefficients of expansions, $\varepsilon_m = \begin{cases} 1, & m = 0; \\ 2, & m \neq 0. \end{cases}$

In expanded form, a functional is G^N [45, 59]:

$$G^N = k^2 R^2 \times$$
$$\times \int_0^{2\pi}\int_0^{\pi/2} \left\{ \sum_{m=0}^{\infty}\sum_{n=0}^{m} i^n (2n+1)\varepsilon_m P_n^m(\cos\alpha)[(n-m)!/(n+m)!] P_n^m(\cos\theta) j_n(kR) \times \right.$$
$$\left. \times \cos m\varphi + \sum_{v=0}^{N}\sum_{q=0}^{v} A_q^v P_q^v(\cos\theta) h_q^{(1)}(kr)\cos v\varphi \right\} \times$$
$$\times \left\{ \sum_{m_1=0}^{\infty}\sum_{n_1=0}^{m_1} i^{n_1} (2n_1+1)\varepsilon_{m_1} [(n_1-m_1)!/(n_1+m_1)!] P_{n_1}^{m_1}(\cos\alpha) P_{n_1}^{m_1}(\cos\theta) j_{n_1}(kR) \times \right.$$
$$\left. \times \cos m_1\varphi + \sum_{v_1=0}^{N}\sum_{q_1=0}^{v_1} \overline{A}_{q_1}^{v_1} P_{q_1}^{v_1}(\cos\theta) h_{q_1}^{(2)}(kR)\cos v_1\varphi \right\} \sin\theta\, d\theta\, d\varphi +$$
$$+ R^2 \int_0^{2\pi}\int_{\pi/2}^{\pi} \left\{ \sum_{m=0}^{\infty}\sum_{n=0}^{m} i^n (2n+1)\varepsilon_m P_n^m(\cos\alpha)[(n-m)!/(n+m)!] P_n^m(\cos\theta) j_n'(kR) k \times \right.$$
$$\left. \times \cos m\varphi + \sum_{v=0}^{N}\sum_{q=0}^{v} A_q^v P_q^v(\cos\theta) h_q^{(1)'}(kR) k \cos v\varphi \right\} \times$$
$$\times \left\{ \sum_{m_1=0}^{\infty}\sum_{n_1=0}^{m_1} i^{n_1} (2n_1+1)\varepsilon_{m_1} [(n_1-m_1)!/(n_1+m_1)!] P_{n_1}^{m_1}(\cos\alpha) P_{n_1}^{m_1}(\cos\theta) j_{n_1}'(kR) k \times \right. \tag{3.4}$$
$$\left. \times \cos m_1\varphi + \sum_{v_1=0}^{N}\sum_{q_1=0}^{v_1} \overline{A}_{q_1}^{v_1} P_{q_1}^{v_1}(\cos\theta) h_{q_1}^{(2)'}(kR) k \cos v_1\varphi \right\} \sin\theta\, d\theta\, d\varphi ,$$

where a line written over unknown coefficients is a sign of a complex conjugation.

The minimization condition of a functional G^N ensures the best satisfaction of boundary conditions on the surface of a scatterer:

$$\partial G^N / \partial \overline{A}_i^i = 0. \tag{3.5}$$

Substituting (3.4) in (3.5), we obtain equations for the determination of unknown coefficients A_q^v:

$$\sum_{v=0}^{N}\sum_{q=0}^{M} A_q^v C_{qq_1}^{vv} = -\sum_{n=0}^{N}\sum_{q=0}^{M} d_{nq_1}^{vv},$$

where M represents the integer index whose value depends on the size of the wave kR;

$$C_{qq_1}^{vv} = h_q^{(1)}(kR)\Delta v \int_0^{\pi/2} P_q^v(\cos\theta) P_{q_1}^v(\cos\theta)\sin\theta\, d\theta +$$

$$+ h_q^{(1)'}(kR) h_{q_1}^{(2)'}(kR)\Delta v \int_{\pi/2}^{\pi} P_q^v(\cos\theta) P_{q_1}^v(\cos\theta)\sin\theta\, d\theta;$$

$$d_{nq_1}^{vv} = 2i^n(2n+1)[(n-v)!/(n+v)!] P_n^v(\cos\alpha)\times$$

$$\times j_n(kR) h_{q_1}^{(2)}(kR) \int_0^{\pi/2} P_n^v(\cos\theta) P_{q_1}^v(\cos\theta)\sin\theta\, d\theta +$$

$$+ j_n'(kR) h_{q_1}^{(2)'}(kR) \int_{\pi/2}^{\pi} P_n^v(\cos\theta) P_{q_1}^v(\cos\theta)\sin\theta\, d\theta;$$

$$\Delta v = \begin{cases} 2, & v = 0; \\ 1, & v \neq 0, \end{cases}$$

In accordance with the Green's function method [6], the potential of a scattered wave Φ_S from a sphere with mixed boundary conditions can be represented by the one-term Huygens integral as follows:

$$\begin{aligned} \Phi_s(P) &= \Phi_s(r;\theta;\varphi) = \\ &= (1/4\pi)\left\{ -\int_{S_1} \Phi_i(Q)\left[\partial G_1(P,Q)/\partial r'\right] dS_1 + \right. \\ &\left. + \int_{S_2} \left[\partial \Phi_i(Q)/\partial r'\right] G_2(P,Q)\, dS_2 \right\}, \end{aligned} \tag{3.6}$$

where P represents the point observation, with the spherical coordinates r, θ, φ; Q represents the surface point with angular coordinates φ'', θ'' and a radial coordinate $r' = R$; G_1 represents the Green's function which vanishes on the surface of a scatterer; and G_2 represents the Green's function which has a zero derivative along the normal of this surface [16, 62]:

$$\begin{aligned} G_1(r;\theta;\varphi;r';\theta';\varphi') &= ik\sum_{m=0}^{\infty}\sum_{n=0}^{m} \varepsilon_m(2n+1) P_n^m(\cos\theta')\times \\ &\times P_n^m(\cos\theta)[(n-m)!/(n+m)!]\cos[m(\varphi-\varphi')]\times \\ &\times \left[j_n(kr') h_n^{(1)}(kr) - h_n^{(1)}(kr')(kr)\, j_n(kR)/h_n^{(1)}(kR)\right]; \end{aligned} \tag{3.7}$$

$$\begin{aligned} G_2(r;\theta;\varphi;r';\theta';\varphi') &= ik\sum_{m=0}^{\infty}\sum_{n=0}^{m} \varepsilon_m(2n+1) P_n^m(\cos\theta'')\times \\ &\times P_n^m(\cos\theta)[(n-m)!/(n+m)!]\cos[m(\varphi-\varphi')]\times \\ &\times \left[j_n(kr') h_n^{(1)}(kr) - h_n^{(1)}(kr') h_n^{(1)}(kr)\, j_n'(kR)/h_n^{(1)'}(kR)\right]. \end{aligned} \tag{3.8}$$

The formula (3.6) for the potential $\Phi_s(r;\theta;\varphi)$ of a scattered wave is approximated as a formula (3.4) of the variational method. However, there are special cases in which the Green's function method can be used because it gives accurate results. We will consider these special cases using the example of the homogene-

ous (soft) sphere, visualizing it being broken into two halves by a plane XOZ (Fig. 3-1). The wave vector $\vec{k}$ of the incident plane wave is put in a plane XOZ ($\theta_0 = 90^\circ$) in the same as the observation point P (on a contour of the border of hemispheres S_1 and S_2). We will find $\Phi_s(P)$ in this point by using Green's function G_1 for the left hemisphere (S_1) and using Green's function G_2 for the right hemisphere (S_2).

For a homogeneous soft sphere, formula (3.6) is converted to the following form:

$$\Phi_s(P) = -(1/4\pi)\left\{\int_{S_1} \Phi_i(Q)[\partial G_1(P,Q)/\partial r']dS_1 + \int_{S_2} [\partial \Phi_s(Q)/\partial r']G_2(P,Q)dS_2\right\}, \quad (3.9)$$

where

$$\Phi_s(Q) = -\sum_{m=0}^{\infty}\sum_{n=0}^{m} i^{n}(2n+1)\varepsilon_m[(n-m)!/(n+m)!]P_n^m(\cos\alpha)P_n^m(\cos\theta')\cos m\varphi' h_n^{(1)}(kr')\times$$
$$\times j_n'(kR)/h_n^{(1)}(kR).$$

Using $\Phi_s(Q)$ and G_1, G_2 from (3.7) and (3.8), we find that the potential of a scattered wave on the surface of a sphere at a point where the contour of the border between the two hemispheres is equal:

$$\Phi_s(P) = -(1/2)\Phi_i(P) - (1/2)\Phi_i(P) = -\Phi_i(P),$$

That is, a boundary condition is fulfilled and the solution is accurate.

If a sphere, θ_0 and $\theta = 90^\circ$, consists of soft and hard hemispheres (Fig. 3-1), the contribution of the ideal soft hemisphere in the potential Φ_s at the point of a contour of the border is equal to $\Phi_i(P)/2$, but the contribution of the ideally hard hemisphere $\partial\Phi_s/\partial r$ to a contour of the border is equal to $2^{-1}(\partial\Phi_1(P)/\partial r)$. The potential Φ_s in plane XOZ will be equal to half a sum of the potentials generated by the soft and hard spheres in the same plane.

The arbitrary orientation of a wave vector $\vec{k}$ of the incident wave with respect to our sphere with mixed boundary conditions the potential of a scattered wave $\Phi_s(r;\theta;\varphi)$ will equal approximately by substituting (3.2) in (3.7) and (3.8) in (3.6) [61]:

$$\Phi_s(r;\theta;\varphi) = (1/2)\sum_{m=0}^{\infty}\sum_{n=0}^{m} i^{-n}(2n+1)\left[(n-m)!/(n+m)!\right]\varepsilon_m P_n^m(\cos\theta)\cos m\varphi P_n^m(\cos\alpha)\times$$
$$\times h_n^{(1)}(kr)\left\{\left[j_n(kR)/h_n^{(1)}(kR)\right] + \left[j_n'(kR)/h_n^{(1)'}(kR)\right]\right\} + (1/2)\sum_{m=0}^{\infty}\sum_{n=0}^{m}\sum_{n_1=0}^{m}(-1)^m\varepsilon_m i^{-n_1}(2n+1)\times$$
$$\times(2n_1+1)\left[(n_1-m)!/(n_1+m)!\right]\left[(n-m)!/(n+m)!\right]\cos m\varphi P_n^m(\cos\theta)P_n^m(\cos\alpha)h_n^{(1)}(kr)\times$$
$$\times\left\{\left[P_{n_1}^{m'}(0)P_n^m(0) - P_n^{m'}(0)P_{n_1}^m(0)\right]/\left[n_1(n_1+1) - n(n+1)\right]\right\}\times$$
$$\times\left\{\left[-j_{n_1}(kR)/h_n^{(1)}(kR)\right] + \left[j_{n_1}'(kR)/h_n^{(1)'}(kR)\right]\right\}, \quad (3.10)$$

where $n \neq n_1$, $n - n_1$ odd.

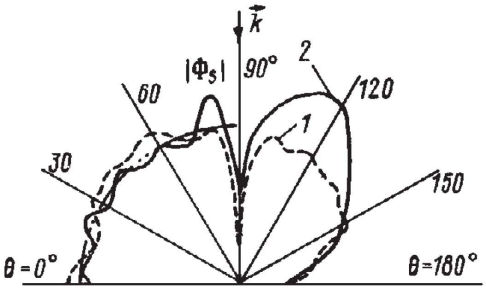

Figure 3-2: The distribution of the module of the scattered wave on the surface of the sphere with mixed boundary conditions: 1, the variational method; 2, the Green's functions method

In contrast to the variational method, the Green's functions method does not require looking for unknown coefficients of expansions and the computation of the potential Φ_s is a very simple problem, since all quantities in (3.10) are known. Fig. 3-2 shows distributions of $|\Phi_s|$ on the surface of a sphere (a half-soft S_1, and a half-hard S_2) by $kR = 5$ and $\alpha = 90^o$. The ideally soft half of a sphere corresponds to the change of angle θ within a range of $0°$ to $90°$. The single value of the potential of a module is shown as a dash-dotted arc; it complies with the strict implementation of a boundary condition on the surface of a sphere; a condition, which is approximately satisfied, although the difference is small between the methods themselves.

Figures 3-3 and 3-4 show modules with angular characteristics of soft (Fig. 3-3, see curve 1) and hard (Fig. 3-4, see curve 3) spheroids and the angular characteristic of a spheroid with mixed boundary conditions (Figs. 3-3 and 3-4, see curve 2).

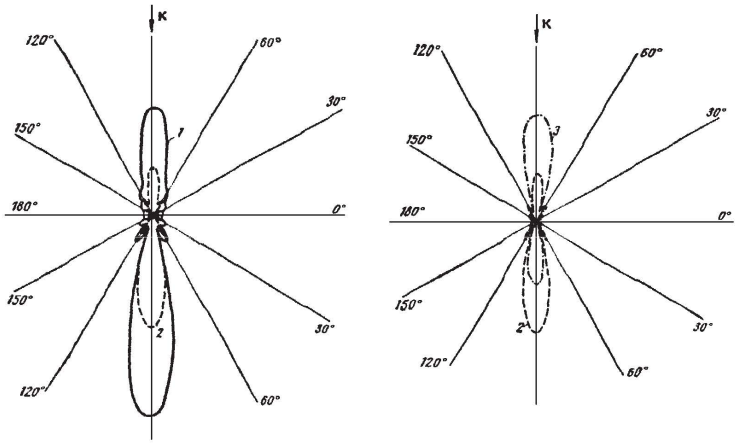

Figure 3-3 (left): Modules angular characteristics

Figure 3-4 (right): Modules angular characteristics of a soft spheroid (curve 1), a hard spheroid (curve 3) and a spheroid with mixed boundary conditions (curve 2)

If, for example, it is decided to introduce a prolate spheroid consisting of two identical halves making contact with each other in a plane ($\eta = 0 \Leftrightarrow \theta = 90^\circ$) and if it is also decided to place a sound source in the same plane ($\eta_0 = 0$) then the total potential Φ_s of a scattered field for an observation point located in the same plane ($\eta = 0$) will be determined by means of expressions (3.11) ($\varphi = 0$) and (3.12)

$$\Phi_s(\xi;\eta;0) = \sum_{n\geq m}^{\infty}\sum_{m=0}^{\infty} i^{-n} \in_m \overline{S}_{m,n}(c,\eta_1)\overline{S}_{m,n}(c,\eta)R^{(3)}_{m,n}(c,\xi)\times \times\left[\frac{R^{(1)}_{m,n}(c,\xi_0)}{R^{(3)}_{m,n}(c,\xi_0)} + \frac{R^{(1)'}_{m,n}(c,\xi_0)}{R^{(3)'}_{m,n}(c,\xi_0)}\right], \tag{3.11}$$

$$\Phi_s(\xi;\eta;\pi)=\sum_{n\geq m}^{\infty}\sum_{m=0}^{\infty} i^{2m-n}\in_m \overline{S}_{m,n}(c,\eta_1)\overline{S}_{m,n}(c,\eta)R^{(3)}_{m,n}(c,\xi)\times \times\left[\frac{R^{(1)}_{m,n}(c,\xi_0)}{R^{(3)}_{m,n}(c,\xi_0)}+\frac{R^{(1)'}_{m,n}(c,\xi_0)}{R^{(3)'}_{m,n}(c,\xi_0)}\right]. \quad (3.12)$$

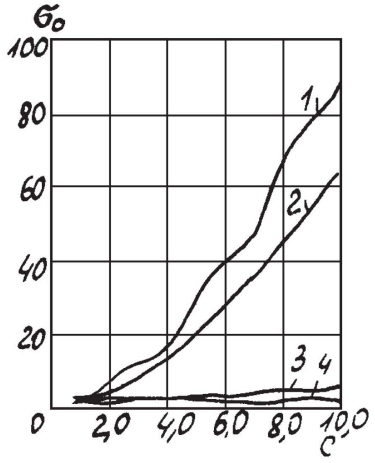

Figure 3-5: Relative backscattering of sound reflected off oblate spheroid cross-sections irradiated along their axis of rotation

Fig. 3-5 presents the given values σ_0 of oblate spheroids (ξ_0 = *0,1005*), which are irradiated along the *Z*-axis of rotation ($\theta_0 = 0^0$). Curve *1* relates to an ideal hard spheroid, while curve *2* relates to an ideal soft spheroid. Curve *3* relates to a spheroid where *1/3* of the surface corresponds to a Neumann condition and *2/3* of the surface corresponds to a Dirichlet condition. Curve *4* relates to a spheroid where one hemispheroid is hard and the other hemispheroid is soft.

Fig. 3-6 shows a module with the angular characteriestics $|\Psi_S(\eta)|$ of the oblate spheroid with a radial coordinate ξ_0 = *0,1005*. Half of the spheroid is hard, while the other half is soft (see curve *1*). A wave falls along the *Z*-axis ($\theta_0 = 0^0 \Leftrightarrow \eta_0 = 1{,}0$) and the wave size *C=10*. Fig. 3-6 presents the modules $|\Psi_S(\eta)|$ for a soft spheroid (see curve *2*) and a hard spheroid (see curve *3*). A comparison of the three curves shows that for a body comprised of combined regions of softness and hardness, the amplitude of the pressure in a wave reflected back from the scatterer is approximately one order of magnitude smaller than for reflections from homogeneous ideal spheroids.

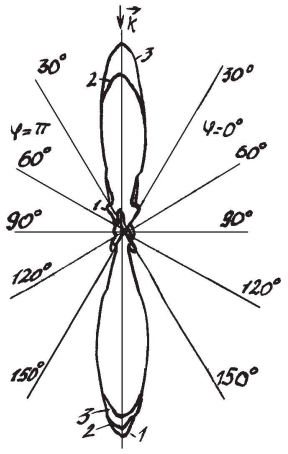

Figure 3-6: A comparison of the modules of the angular scattering characteristics of combined and homogeneous oblate spheroids

3.2. The Green's Functions Method for the Ideal Scatterer with a Non-Analytical Form

We will consider a non-analytical body, the surface of which does not apply to coordinate system with divided variables in the scalar Helmholtz equation. We will examine this non-analytical scatterer, which is in the form of a finite circular cylinder bounded on both ends by hemispheres (Fig. 3-7).

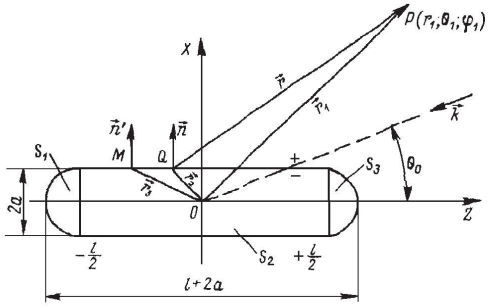

Figure 3-7: The non-analytical smooth scatterer in the form of a cylinder bounded by semi-spheres

Sound pressure, scattered by this body, can be found using one of the numerical methods for the solution of diffraction problems [7, 60, 61, 63–65]. The Green's functions method [60, 61], which is based on the use of the mathematical formulation of the Helmholtz-Huygens (Kirchhoff integral) principle, is one of the most convenient methods. The algorithm of the calculation requires knowledge of the amplitude-phase distribution of the sound pressure and the normal component of oscillatory velocity on some closed surface, as well as the integration of S that includes the lateral surface of cylinder S_2 and the surface of hemispheres S_1 and S_3 (Fig. 3-7).

$$p_S(P) = (1/4\pi)\int_S [p_S(Q)\frac{\partial}{\partial n}G(P,Q) - \frac{\partial p_S(Q)}{\partial n}G(P,Q)]dS, \quad (3.13)$$

where $p_s\ (P)$ represents the sound pressure scattered by the body and P represents the point of observation, which has the spherical coordinates, r, θ, φ; Q represents the observation point on surface S; $p_s(Q)$ represents the sound pressure at point Q; and $G(P,Q)$ represents the Green function of the free space, thereby satisfying the inhomogeneous Helmholtz equation.

In (3.13), the Green function is selected as being a potential point source:

$$G(P,Q) = \frac{e^{ikR}}{R}, \quad (3.14)$$

where $k = 2\pi/\lambda$ represents the wave number, λ represents the length of a sound wave in the liquid environment, and R represents the distance between points P and Q.

Using the relative arbitrariness of the choice of Green's functions, you can get the Kirchhoff formula options, consisting of a single member:

$$p_S(P) = (1/4\pi)\int_S [p_S(Q)\frac{\partial}{\partial n}G^{(1)}(P,Q)]dS, \quad (3.15)$$

$$p_S(P) = -(1/4\pi)\int_S [\frac{\partial p_S}{\partial n}G^{(2)}(P,Q)]dS, \quad (3.16)$$

By using formulas (3.15) and (3.16), the computational procedure is considerably simplified, as you only want to define one of the parameter,s ($p_s(Q)$ or $dp_s(Q)/dn$), on surface S. However, it is necessary to match surface S with a coordinate of the surface of one of coordinate systems in which the separation of variables is possible. Thus, the application of the Green's function method for the faces of the analytical surfaces an interconnected infinite cylinder and a hemisphere on either end is its main feature.

The possibility of the efficacy of using such a method and test calculations of the scattered field have been considered in [44], [55], and [66]. For example, an experiment regarding the solution of test problem [55] for the direct calculation of the far field of a point source [67] and [68] has shown that, with magnification of wave size C, the results of calculations σ_0 for both methods are getting closer to each other. When solving the problem of diffraction to determine the values of $p_s(Q)$ and $dp_s(Q)/dn$ on surface S, you can use the following expression:

For the homogeneous Dirichlet conditions (for an ideally soft body), pressure scattered waves on surface S has the following form:

$$p_s(Q) = -p_i(Q), \quad (3.17)$$

For the homogeneous Neumann conditions (for an ideally rigid body):

$$\frac{\partial p_i(Q)}{\partial n} = \frac{\partial p_S(Q)}{\partial n}, \quad (3.18)$$

where $p_i(Q)$ represents the sound pressure of the incident wave at point Q. When determining the $p_t(Q)$ values, you can use the expression for the scalar potential of the plane monochromatic wave as determined with relation to a single amplitude of an impact on the body of a sound wave emanating from a source located at infinity.This potential for a perfectly reflective sphere is reflected in natural functions in solving the Helmholtz equation in a spherical coordinate system, which has the following form [43]:

$$p_i(r,\theta,\varphi) = \sum_{n=0}^{\infty}\sum_{m=0}^{\infty}\varepsilon_n i^n (2n+1)\frac{(n-m)!}{(n+m)!}\cos m\varphi P_n^m(\cos\theta) j_n(kr); \quad (3.19)$$

$\varepsilon_n = 1(n=0);\ \varepsilon_n = 2(n \neq 0);$

and the expression (3.19) is simplified when considering the axis-symmetric problem (dependent on the coordinate φ)

$$p_i(r,\theta) = \sum_{m=0}^{\infty} i^m (2m+1) P_m(\cos\theta) j_m(kr) \quad (3.20)$$

for a scatterer in the form of a perfectly reflective cylindrical scalar potential incident plane harmonic wave, as assessed in relation to the unit amplitude of the wave vector $\vec{k}$ aimed at angle θ_0 of the Z-axis of the cylinder. This connects the natural functions' solutions to the Helmholtz equation in a circular cylindrical coordinate system:

$$p_i(r,\varphi,z) = -\exp(ik\cos\theta_0 z)\sum_{m=0}^{\infty}\varepsilon_m(-1)^m H_m^{(1)}(kr)\cos m\varphi\frac{\Omega I_m(kr_0\sin\theta_0)}{\Omega H_m^{(1)}(kr_0\sin\theta_0)}, \quad (3.21)$$

when the plane wave vector $\vec{k}$ is perpendicular to the z axis of the cylinder. This expression (3.21) is simplified as [43]

$$p_i(r,\varphi) = -\sum_{m=0}^{\infty}\varepsilon_m(-1)^m H_m^{(1)}(kr)\cos m\varphi\frac{\Omega I_m(kr_0)}{\Omega H_m^{(1)}(kr_0)} \quad (3.22)$$

3.3. Results of the Numerical Experiment

To calculate the integral (3.15) and (3.16) on surface S, the quadrature formulas were used. A step of integration surface S in the axial and circumferential directions $(dz_0, d\varphi_0, d\theta_0)$ in the system of nodal points must not exceed 0,5 λ (Figs. 3-8, 3-9).

Using the Green's functions method, the equivalent radius R_{eq} of the ideal non-analytical body was calculated for several values of wave size ka (where a is the radius of the cylinder and adjacent hemispheres

of the non-analytical scatterer) and was likewise calculated for different angles of irradiation (Figs. 3-10–3-12)

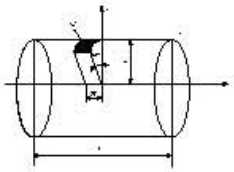

Figure 3-8: The coordinate system, connected with the cylinder

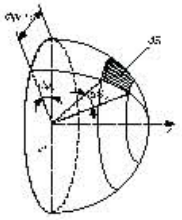

Figure 3-9: The coordinate system, connected with the hemispheres

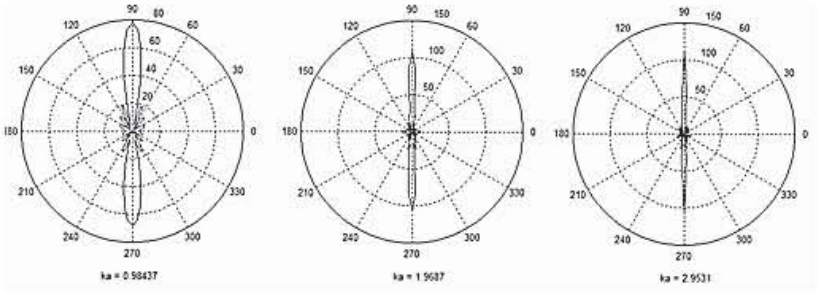

Figure 3-10: Angular diagrams of equivalent radiuses R_{eq} at the angle of the incident $\theta_0 - 90^0$.

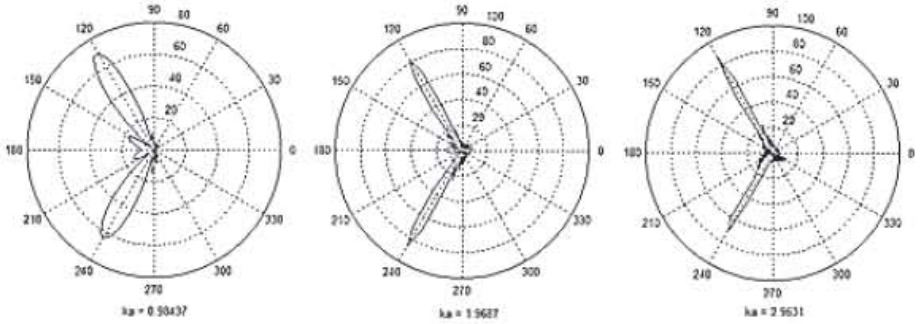

Figure 3-11: Angular diagrams of equivalent radiuses R_{eq} at the angle of the incident $\theta_0 - 60^0$.

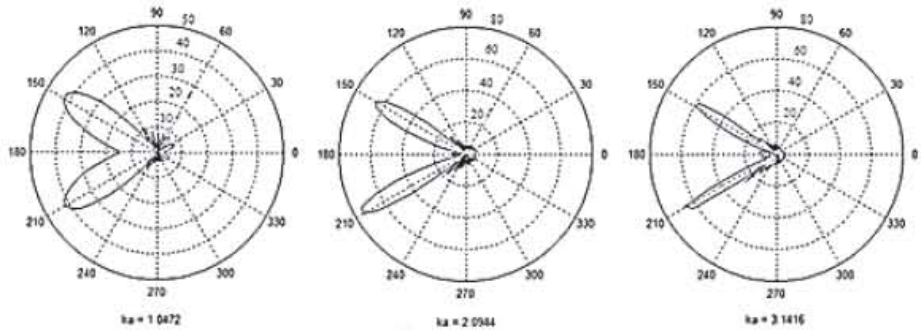

Figure 3-12: Angular diagrams of equivalent radiuses R_{eq} at the angle of the incident $\theta_0 - 30^0$.

The analysis of equivalent radiuses R_{eq} presented in these pictures permits the following conclusions to be made:

1) The angular position corresponds to the reflecting and diffraction lobes and totally corresponds to their physical representations.
2) The angular characteristics of a non-analytical submarine object are rather similar to the angular diagrams of spheroid bodies [7, 45].

In all figures, a diffraction (shadow) petal can be clearly observed and it grows and shrinks with increasing frequency. In Figures 3-10–3-12, the mirror petal is shown. This is, with an increasing frequency, similar to the shadow petal but, in contrast, it is limited asymptotically. You may notice that the angular diagrams of the non-analytical scatterer are very similar to the angular characteristics of the scattering elongated spheroids (the ideal and elastic ones) with a 1:10 ratio of the semi-axes [7, 55, 64, and 67]. In contrast to another work [18] that used a method of integral equations and presented calculations for a non-analytical body with a short cylindrical insert, the cylindrical insert in this study was much longer. The values of other equivalent radiuses at other angles of incidence are given in works [68] and [69].

3.4. The Green's Functions Method for Elastic Scatterers with a Non-Analytical Form

The solution of the problem of sound scattering by an elastic shell of the non-analytical form is based on an article [52]. The Green's function method is approximate because it does not take account the interaction between individual elements forming a compound body of the non-analytical form. The interaction between scatterers shaped as spheroids and elliptical cylinders is shown in [7] and this interaction was negligibly small. In addition, the sound scattering characteristics for bodies with mixed boundary conditions calculated using the Green's function method, namely, the Sommerfeld method (a method for undetermined coefficients [7, 55]); the agreement between the results was fairly good.

For the non-analytical bodies, two structures were considered:

1) A finite-length circular cylindrical elastic shell, limited at each end by the two halves of a prolate spheroidal shell (Fig. 3-13);

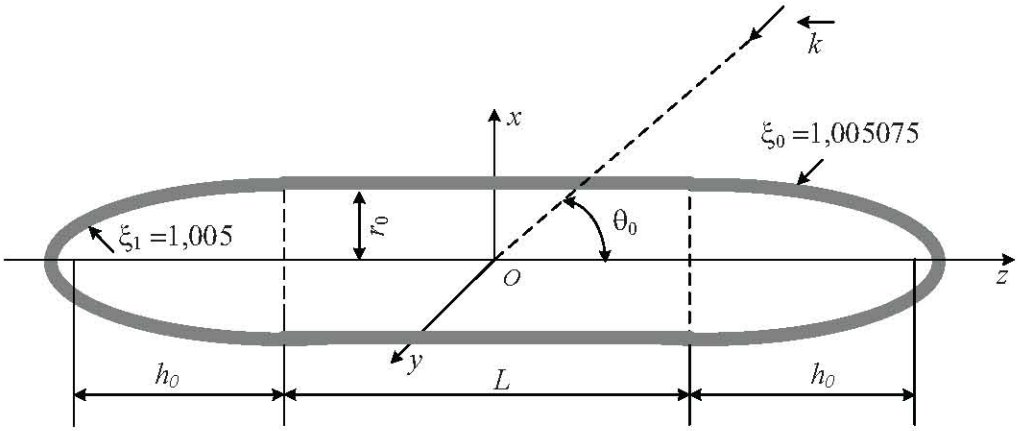

Figure 3-13: The cylindrical shell with the semi-spheroidal shells

2) A cylindrical shell bounded at each end by two halves of a spherical shell (Fig. 3-14).

In article [52] a solution is given for acoustic scattering problems in relation to the constituent parts of non-analytical bodies. For cylindrical and spheroidal shells, Debye and Debye-type potentials are used. In [52], the angular scattering characteristics of such compound bodies are calculated for waves of different sizes.

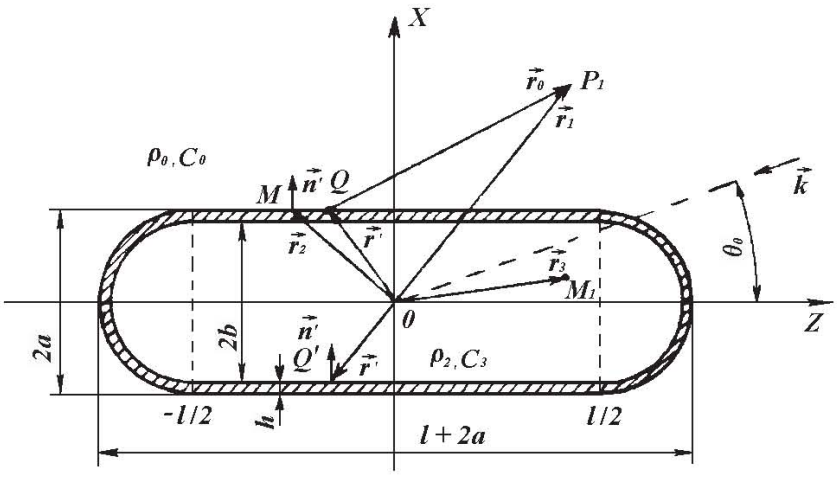

Figure 3-14: The elastic shell, in the form of a cylinder, terminating with a semi-sphere at each end

We will consider a compound elastic shell, which is formed by a finite cylindrical shell whose ends are closed by two hemispherical shells of the same diameter (Fig. 3-14). To apply the Green's functions method, it is necessary to take the solution to the axisymmetric problem of plane wave diffraction by an elastic spherical shell in terms of dynamic elasticity theory [70] and transform this solution into the three-dimensional version. The resulting solution differs little from that obtained above for the three-dimensional problem of diffraction by a spheroidal elastic shell [7, 55, 67, 71].

Figures 3-15 and 3-16 show the absolute values of the angular characteristics $|D(\varphi)|$ (in the *XOY* plane, $\theta_0=90^0$) for a non-analytical elastic scatterer in the form of a cylindrical shell connected to the spherical half-shells (Fig. 3-10).

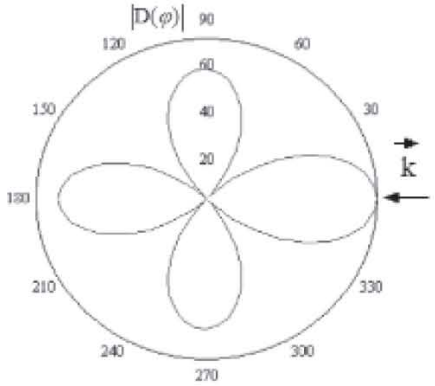

Figure 3-15: The modulus of an angular characteristic

The Green's function method can, in combination with analytical methods, be used for the solution of tasks concerned with the diffraction of a plane sound wave on an elastic isotropic scatter of a non-analytical form—one that consists of a circular cylindrical shell of terminated length L and radius r_0, bounded at each end by the halves of each elongated spheroidal shell [69] (Fig. 3-13).

The internal surface of the spheroidal shell is given by coordinate $\xi_1 = 1{,}005$ (with the proportion of the axes of the inner spheroid 10:1 and the inter-focal distance $2h_0$ and externally by coordinate $\xi_0 = 1{,}005075$.

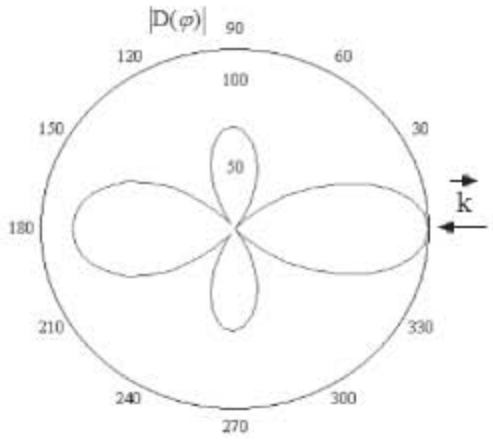

Figure 3-16: The modulus of an angular characteristic

The shell material is isotropic, with a density of ρ_1, modules of elasticity, coefficients Lame λ_1 and μ_1, and Young's modulus E. Inside the shell, there is a gas with a density of ρ_2, a coefficient of volumetric compression K_2, a modulus of compression, and sound velocity c_2.

The scatterer is submerged within an ideal compressed liquid with a density of ρ_0 and a coefficient of volumetric compression K_0. The potential of the sound wave is submitted to to mathematical analysis by means of the scalar Helmholtz equation.

The amplitude-phase distribution of the sound pressure and normal component of the vibrating velocity at the points of this non-analytical surface is a distribution, which is found from the strict solution of the three-dimensional boundary tasks. These are concerned with the dynamic theory of elasticity on the endless elastic cylindrical surface and the elastic spheroidal surfaces, respectively.

The main result of this study is the calculation of the angular characteristics of bodies with a non-analytical form using the Green's functions method, which had previously been developed and used to solve problems of sound diffraction by bodies with mixed boundary conditions. The advantage of the Green's functions method is its simplicity (it is much simpler than the Sommerfeld method), while a drawback is its approximate nature, as it does not take into account the individual elements forming the scatterer of non-analytical form.

In future studies, we intend to compare the above calculations with experimental data on sound scattering by an elastic cylindrical shell [7, 18], calculations of scattered fields formed by spheroidal elastic shells [56], and the resonance characteristics of prolate and oblate spheroidal elastic shells [57].

CHAPTER 4

SOME METHODS OF SOLVING PROBLEMS OF SOUND DIFFRACTION ON BODIES THAT HAVE A NON-ANALYTICAL FORM

4.1. Integral Equations Method

This section analyzes the following numerical methods of solving problems of sound diffraction on ideal and elastic scatterers of a non-analytical form: the integral equations method, the Green's function method, the finite elements method, the boundary elements method, the Kupradze method, the T-matrix method, and the geometrical theory of diffraction method. There are a large number of numerical methods for conducting sound-scattering studies on ideal and elastic bodies of a non-analytical form. Section 4 presents the theoretical bases of seven such methods, along with their numerical experimentation.

We can discern the ideal non-analytical scatterer to be in the form of a terminal cylinder with semi-spheres on each end (see Fig. 4-1).

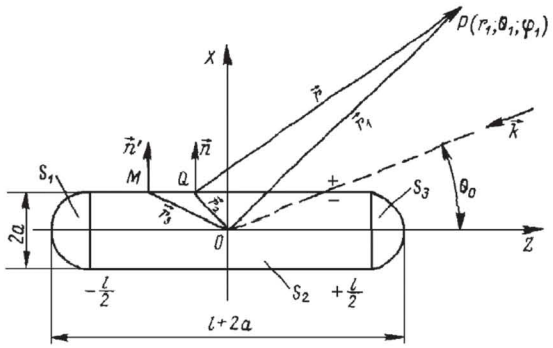

Figure 4-1: The non-analytical smooth scatterer in the form of a cylinder with semi-spheres on each end

The pressure $p_s\ (r_1; \theta_1; \phi_1)$ in the scattered wave at observation point

$P\ (r_1; \theta_1; \phi_1)$ is equal to [7, 16, 45, 63, 72]:

$$p_s(r_1; \theta_1; \phi_1) = (1/4\pi) \int_S \int \{[\partial p_s(Q)/\partial n]\, exp\ (ikr)/r - p_s(Q)(\partial/\partial n)[exp(ikr)/r]\}\, dS, \quad (4.1)$$

where Q represents a point on the surface of the scatterer.

Then, (4.1) the Dirichlet condition at the surface assumes the following:

$$p_s^D(r_1; \theta_1; \phi_1) = (1/4\pi) \int_S \int \{[\partial p_s^D(Q)/\partial n]\, exp\ (ikr)/r + p_i(Q)(\partial/\partial n)[exp(ikr)/r]\}\, dS \quad (4.2)$$

The Neumann condition:

$$p_s^N(r_1; \theta_1; \phi_1) = -(1/4\pi) \int_S \int \{[\partial p_i(Q)/\partial n]\, exp\ (ikr)/r + p_s^N(Q)(\partial/\partial n)[exp(ikr)/r]\}\, dS\ . \quad (4.3)$$

We can find the function $\Psi = \left(\partial p_\Sigma/\partial n'\right)$ from the solution to the non-homogeneous Fredholm equation of the second kind [7, 16, 45, 63, 72]:

$$\left(\frac{1}{2}\right)\Psi(r_3; \theta_3; \phi_3) - \left(\frac{1}{4\pi}\right)\int_S \int \Psi(Q)\left(\frac{\partial}{\partial n'}\right)\left[exp\frac{(ikr_3')}{r_3'}\right] dS =$$

$$\left(\frac{\partial}{\partial n'}\right) exp\left(i\vec{k}\vec{r}_3\right)\ . \quad (4.4)$$

The integral to the left of (4.4) must be understood.

With the help of Ψ, we can find the scattered pressurep_s^D at any point in the medium $P(r_1;\theta_1;\phi_1)$:

$$p_s^D(r_1;\theta_1;\phi_1) = (1/4\pi)\int_S\int \Psi(Q)[exp\,(ikr)/r]dS\ . \qquad (4.5)$$

The Neumann condition uses the function, $\Phi = p_\Sigma$, which represents the solution to the Fredholm equation of the second kind [7, 16, 45, 63, 72]:

$$(1/2)\Phi(r_3;\theta_3;\phi_3) + (1/4\pi)\int_S\int \Phi(Q)\big(\partial/\partial n'\big)\big[exp\,\big(ikr_3'\big)/r_3'\big]dS = exp\big(i\vec{k}\vec{r}_3\big)\ . \quad (4.6)$$

The scattered pressure at point $P(r_1;\theta_1;\phi_1)$ can be expressed through function Φ:

$$p_s^N(r_1;\theta_1;\phi_1) = -(1/4\pi)\int_S\int \Phi(Q)(\partial/\partial n)[exp\,(ikr)/r]dS\ . \qquad (4.7)$$

The scattered pressure $p_s^D(r_1;\theta_1;\phi_1)$ can be found either with the help of the integral (4.2) ((4.3), for the Fredholm equation of the first kind), or with the help of equation (5) ((6) for the Fredholm equation of the second kind).

Surface S consists of S_2 and the surfaces S_1 and S_3 (see Fig. 4-1).

To calculate the integrals (4.2), (4.3), and (4.5): (4.6) on surface $S = S_1 + S_2 + S_3$, we will use the grid of the nodal points [7, 45, 63, 72] (Figures 4-2 and 4-3).

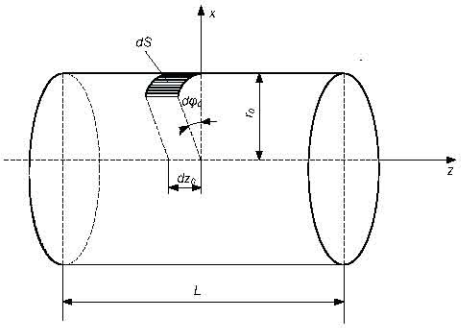

Figure 4-2: The coordinate system connected with the cylinder

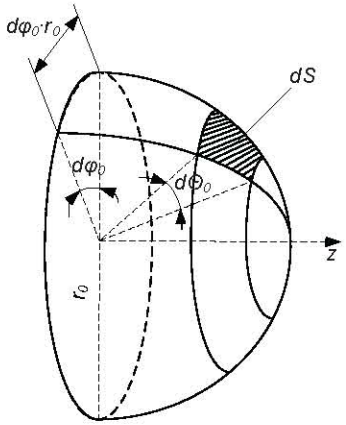

Figure 4-3: The coordinate system, connected with the hemispheres

Fig. 4-4 presents $|p_s(r_1,\theta_1,\phi_1)|$ for the chosen parameters by $\theta_0 = 90^0$ (curve 1 corresponds to the T-matrixes method, but curve 2 represents the integral equations method).

We are going to apply the integral equations method, which is also used in [2-5] for ideal non-analytical scatterers, to the elastic shell of the non-analytical form.

To find the quality of this type of scatterer, we are going to consider the terminal isotropic elastic

cylindrical shell with the semi-spheres on each end (see Fig. 4-5). The density of the material of the shell is ρ_1, and the Lame's coefficients are λ and μ. The shell was filled with the internal liquid medium with density ρ_2 and sound velocity C_3, and it was placed in the external liquid medium with density ρ_0 and sound velocity C_0.

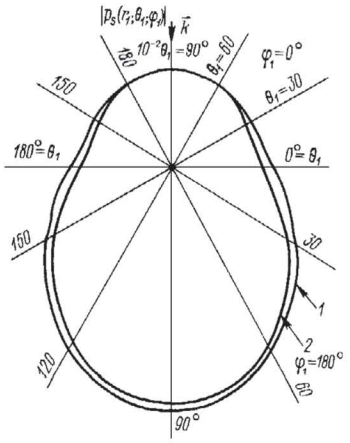

Figure 4-4: The modulus of the angular distribution of the scattered pressure

The shell is irradiated by the plane harmonic wave with pressure p_i under the angle Θ_0 and with the wave vector $\vec{k}$

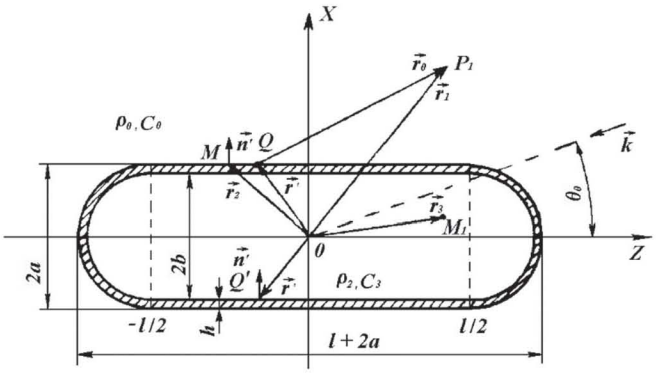

Figure 4-5: The elastic shell is in the form of a terminal cylinder with semi-spherical ends

As shown in [7, 72], the initial equation is the integral equation, which uses the generalized Huygen's principle for the displacement vector $\vec{u}(\vec{r})$ of the elastic shell:

$$\vec{u}(\vec{r}) = \iint_S \left\{ \vec{t}(\vec{r}')G(\vec{r}';\vec{r}) - \vec{u}(\vec{r}')\left[\hat{n}'\sum(\vec{r}';\vec{r})\right]\right\} dS(\vec{r}'), \quad \vec{r} \in V, \tag{4.8}$$

where $\vec{t}(\vec{r}') = \hat{n}'T(\vec{r}')$ is the stress vector; $\hat{n}' \equiv \hat{n}'(\vec{r}') = \vec{n}'(\vec{r}')$ is the single vector of the external along the relation to S normal; $T(\vec{r}')$ is the stress tensor of the isotropic material; $G(\vec{r}';\vec{r})$ is the displacement Green's tensor; $\sum(\vec{r}';\vec{r})$ is the stress Green's tensor. If $\vec{r}$ concerns the point of the surface S, then the left part of equation (4.8) $\vec{u}(\vec{r}')/2$ will stand.

The second integral equation presents the Kirchhoff integral for diffracted pressure $p_\Sigma(P_1)$ in the external medium [7, 73]:

$$C(P_1)p_\Sigma(P_1) = -\iint_{S_a}\left\{p_\Sigma(Q)\left(\frac{\partial}{\partial n'}\right)\left[exp\left(\frac{ikr_0}{r_0}\right)\right] - \left[exp\left(\frac{ikr_0}{r_0}\right)\right]\rho_0\omega^2(\vec{u}\vec{n}')\right\} dS_a + 4\pi p_i(P_1), \tag{4.9}$$

where $p_\Sigma(P_1) = p_i(P_1) + p_s(P_1)$; $p_s(P_1)$ is the scattered pressure at point P_1; $C(P_1)$ is the numerical coefficient equal to 2π. If $P_1 \in S_a$ is equal to 4π, and if P_1 does not belong to S_a, then S_a is the external surface of the shell and Q is a point on the external surface of the shell.

For pressure $p_2(M_1)$ in the internal liquid medium at point M_1, the third integral equation is derived as follows:

$$C(M_1)p_2(M_1) = \iint_{S_b} \left\{ p_2(Q') \left(\frac{\partial}{\partial n'}\right) \left[exp \frac{(ikr_3)}{r_3} \right] - \left[exp \frac{(ikr_3)}{r_3} \right] \rho_0 \omega^2 (\vec{u}\vec{n}') \right\} dS_b, \quad (4.10)$$

where Q' is the point of the internal surface of the shell;

$$C(M_1) = \begin{cases} 4\pi, & if \quad M_1 \quad out \quad S_b; \\ 2\pi & if \quad M_1 \in S_b; \end{cases}$$

and S_b is the internal surface of the shell.

The boundary conditions on the external (S_a) and internal (S_b) surfaces of the shell [7, 43, 45, 63, 72] are added to the integral equations (4.8), (4.9), and (4.10). In order to chose the boundary conditions, we will consider two types of integrals: ones with an isolated special point, and others that are considered to form the sense of the principal meaning. The method to calculate the second type is described in [7].

Applying the normal modes and image sources methods for a harmonic signal in the plane waveguide is equivalent to [74]. Harmonic signals in the plane waveguide have previously been studied sufficiently [7, 75, 76]. On the basis of the imaginary sources and imaginary scatterers method, the problem of the scattering of the pulse signals on elastic spheroidal bodies is solved, as it is accommodated in the plane waveguide by the ideal boundary conditions. The pulse signals are bunches of energy [7]; therefore, their propagation along the axis of the plane waveguide is in a group velocity, which lies in the principles of the imaginary sources and scatterers method (the method of normal waves in the waveguide is not applicable in this case). The temporal and spectral characteristics of the pulse signals reflected and diffracted from the spheroidal-shape elastic bodies are obtained, for the first time, in this work.

The spectrum $S_0(2\pi\nu)$ of the sound pulse of the source with the harmonic filling has the following appearance [53]:

$$S_0(2\pi\nu) = \frac{i\nu_0}{\pi(\nu_0^2 - \nu^2)} (-1)^n \, sin(\pi n \frac{\nu}{\nu_0}), \quad (4.11)$$

where ν_0 represents the frequency of the filling of the impulse; n represents the number of the oscillation periods of the harmonic signal in the pulse; and ν represents the circular frequency.

The spectrum $S_0(2\pi\nu)$ is connected with $\Psi_i(t)$ of the source by the return Fourier transformation:

$$\Psi_i(t) = (\pi)^{-1} \, Re \int_0^\infty S_0(2\pi\nu) \, exp(+i2\pi\nu) d(2\pi\nu) \quad (4.12)$$

The spectrum of the scattered (reflected or transmitted) signal $S_s(2\pi\nu)$ is the product of the spectrum $S_0(2\pi\nu)$ and the corresponding meanings of the angular characteristic of the scattering of the spheroidal shell $D(\eta, \varphi, \nu)$, whereη and φ represent the angular coordinates at the point of the observation. The spectrum-diffracted signal $S_\Sigma(2\pi\nu)$ depends on $S_0(2\pi\nu)$ and $S_S(2\pi\nu)$.

In $S_S(2\pi\nu)$ and $S_\Sigma(2\pi\nu)$, the images $\Psi_S(t')$ and $\Psi_\Sigma(t')$ represent scattered and diffracted pulses, respectively [7]:

$$\Psi_S(t') = \frac{1}{\pi} Re \int_0^\infty S_S(2\pi\nu) e^{+i2\pi\nu t} d\,(2\pi\nu) \quad (4.13)$$

$$\Psi_\Sigma(t') = \frac{1}{\pi} Re \int_0^\infty S_\Sigma(2\pi\nu) e^{+i2\pi\nu t} d\,(2\pi\nu) \quad (4.14)$$

4.2. Finite Elements Method

The finite elements (MFE) method, and its variations, calculates the solutions for the sound radiation of elastic bodies in nearly all forms. Here, we have considered the possibility of using MFE with the Green's functions method to calculate the numerical solution for the distant field of sound radiation by an extended spheroid shell, under the influence of the point sources on its surface (Fig. 4-6):

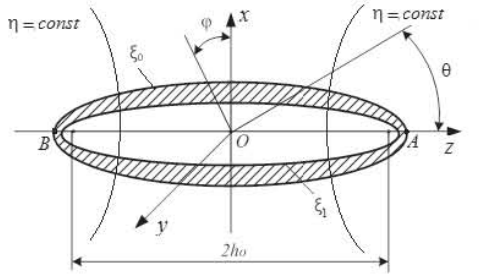

Figure 4-6: Extended spheroid shell, under the influence of the point sources on its surface

The choice of body is caused by the definite solution to the task of identifying the effect of the sound radiation from the spheroid shell under the influence of point sources on its surface. This solution was found using the reciprocity theorem from the three-dimensional boundary task for the diffraction of a monochromatic plane wave on this shell. The solution is presented in [51, 77]. This task can be interpreted as the sound radiation of an elastic body under the influence of turbulent pulsations of liquid flow and the calculation based on the focused force that is stipulated by this pulsation if of interest. In this case, it is useful to compare the results of the numerical solution with the analytical solution results to validate its accuracy.

The geometrical and physical parameters of the shell are similar to those presented in Fig. 4-8. The point sources of the harmonic signal are situated at the ends of the shell at points A and B; these sources imitate the turbulent pulsation and produce some amplitude-phase distribution (AFD) of the sound wave potential on the external surface ξ_0 and in the liquid surrounding the shell.

The numerical solution comprised two stages [51]:

1) First, the values of sound wave potential and its gradient on the closed test area in the nearest field in the Fresnel zone created by the point sources are calculated
2) Second, the results regarding the distant field in the Fraunhofer zone are to be re-calculated.

1) In the first stage, it is necessary to conjugate the MFE solutions on the surface of area S in the sphere V_1, adjoining the shell, with the exact analytical solution to the Helmholtz equation relative to the external surface of an endless sphere V_2 with an infinitely large radius (Fig. 4-7).

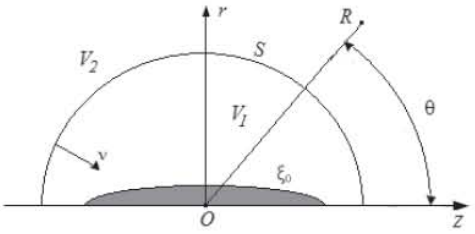

Figure 4-7: The conjugation of FEM with its exact analytical solution

2) The functional of the full energy, if the system is "shell-fluid", will have the form:

3) $$E(w,\Phi_1,\Phi_2) = P + T - \iint_s i\omega\rho_0\Phi_1 w dS + \iint_s \frac{\rho_0}{2}\Phi_1\frac{\partial\Phi_\Sigma}{\partial v}dS + \iint_s \rho_0(\Phi_1-\Phi_2)\frac{\partial\Phi_\Sigma}{\partial v}dS, \quad (4.15)$$

where P and T are the potential and kinetic energies of the shell; w represents normal displacement of the shell; the surface ξ_0; Φ_1и Φ_2 correspondingly represents the potentials of the velocity of liquid volumes V_1 and V_2 that meet the Helmholtz equation parameters and radiation continuing for infinity in volume V_2.

The condition of the stationary state of E functionally leads to the fulfillment of the shell movement equation and the Helmholtz equation in the sphere V_1, as well as the equality of the normal speeds $\frac{\partial \Phi_1}{\partial \nu}$ and $\frac{\partial \Phi_2}{\partial \nu}$ and the potentials Φ_1 andΦ_2 on surface S.

The axial symmetry of the shell and the sources of radiation leads to the displacement of the shell and the potential of the liquid's velocity will not be subject to the azimuthal coordinate φ.

The substitution of the forms that approximate the shell displacements and potentials Φ_1 and Φ_2 in the stationary state of E functionally leads to the linear algebraic system to solve equations.

To solve this task, it is necessary to use the circular finite elements for the shell, the liquid, and the filling gas for the conjugation of these elements, as well as the finite elements for the sphere V_2. Using these elements, it is possible to calculate the nearest field for the arbitrary sources in the form of the shells, if they are spinning. In this case, the numerical calculations are made for a finite-elementary net that consists of 131 elements and 410 focal points (Fig. 4-8).

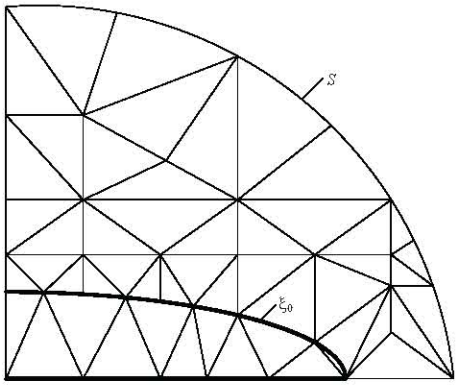

Figure 4-8: The finite-elementary net in the nearest shell field

The AFD of the sound pressure and the normal component of vibrational speed in the focal points of the control surface in the nearest field is the initial for the second stage of the task solution. The sound pressure in the distant field is found with Kirchhoff's integral, which is also used in (4.15).

The following two variants of the forms of the control surface were used in the calculations: a non-analytical body in the form of a cylinder with half-spheres on either end (from a measuring process organization point of view, this particular variant is the most useful; see Fig. 4-9a) and an analytical solution (a sphere; see Fig. 4-9b).

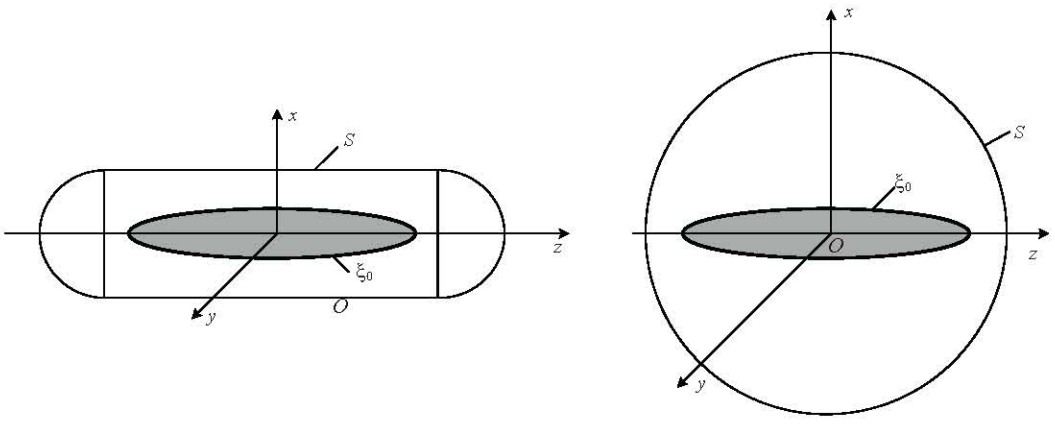

Figure 4-9: The control surface in the form of (*a*) an enclosed cylinder (one with half-spheres at either end) and (*b*) a sphere

On the basis of the proposed algorithms in [51], we calculated the angled distribution of sound pressure levels, due to the sound radiated by the elastic spheroid shell. These calculations demonstrated a rather satisfactory correspondence to the results of the analytical and numerical methods.

4.3. The Boundary Elements Method

To solve tasks concerning radiation and diffraction for the bodies of non-analytical surfaces, the boundary element method (BEM) has been successfully used during recent years. Numerous scientific works are published in this research area, which state the theoretical basis of the method (as well as the different aspects of the application) [47, 48, 77]. The bibliographic analysis shows that BEM is one of the most relevant and widely used methods, among the other numerical methods, to solve boundary tasks. The following advantages of BEM (in comparison with MFE, for example) are present when solving boundary tasks:

1) The task of sampling the boundary, sphere, and scatterer, rather than the whole sphere, as a result of which additional measures to find the condition of radiation at infinity are not required
2) The task of reducing the initial differential equation to the boundary integral equation, which presents the exact formulation of the stated task. Here, the accumulation of error occurs during processing a numerical solution to the integral equations by sampling, approximation, and calculation
3) The use of the analytical method, which is valid for the whole sphere, provides a potentially higher accuracy than FEM. Where the approximation is commited in every area, for scatterers of a general geometric form, the boundary surface is presented in the form of a collection of elementary areas [7, 51, 77].

The formation of isoparameter elements allows for the key coordinates of every initial element x_{i_α} to be converted to the corresponding curvilinear coordinates x_i $(i = 1,2,3)$. Here, the element's geometry (global coordinates) and the main variables (of displacement) are stated using the following similarly interpolative relations (functions of the form) [51, 77] (see Figures 4-10a and 4-10b):

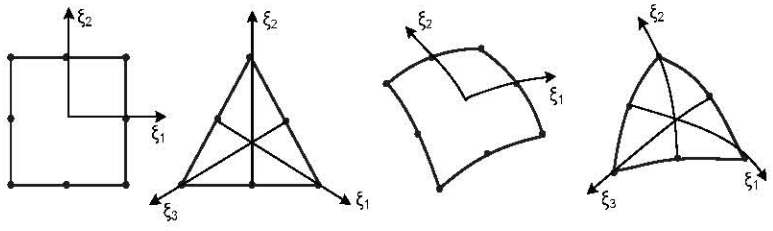

a) *b)*

Figure 4-10: The (a) initial boundary elements and (b) the corresponding curvilinear isoparameter boundary elements

The curvilinear coordinates of every point of the element x_i $(i = 1,2,3)$ will be connected by the key coordinates x_{i_α} in the expressions [7, 51, 77]:

$$x_i(\xi) = \sum_\alpha N_\alpha(\xi) x_{i\alpha},\ \alpha = 1,2,\ldots,6\text{or } 8 \qquad (4.16)$$

The functions of the local coordinates are described as follows:

a) Quadrangular elements

$N_1(\xi) = (1/4)(\xi_1+)(\xi_2+1)(\xi_1+\xi_2-1); N_2(\xi) = (1/4)(\xi_1-1)(\xi_2+1)(\xi_1-\xi_2+1);$ $N_3(\xi) = (1/4)(1-\xi_1)(\xi_2-1)(\xi_1+\xi_2+1); N_4(\xi) = (1/4)(\xi_1+1)(\xi_2-1)(\xi_2-\xi_1+1);$

$$N_5(\xi) = (1/2)(\xi_1+1)(1-\xi_2^2); N_6(\xi) = (1/2)(\xi_2+1)(1-\xi_1^2);$$

$$N_7(\xi) = (1/2)(\xi_1-1)(\xi_2^2-1); N_8(\xi) = (1/2)(1-\xi_2)(1-\xi_1^2);$$

b) Triangular elements

$$N_1(\xi) = \xi_1(2\xi_1-1); N_2(\xi) = \xi_2(2\xi_2-1); N_3(\xi) = \xi_3(2\xi_3-1);$$

$$N_4(\xi) = 4\xi_1\xi_3; N_5(\xi) = 4\xi_1\xi_2; N_6(\xi) = 4\xi_2\xi_3.$$

These correlations present the implicit conversion of the surface element to the planar square or to the equilateral planar triangle in Fig. 4-10.

The correlations for the interpolation of displacements and stresses are expressed similarly with regard to each element [78]:

$$u_i(\xi) = \sum_\alpha N_\alpha(\xi)u_{i\alpha}; \quad (4.17)$$

$$t_i(\xi) = \sum_\alpha N_\alpha(\xi)t_{i\alpha}, \quad (4.18)$$

When submitting (4.17) and (4.18) in the equation and using the rule of numerical integration, we get

$$[H]\{u\} = [\tilde{G}]\{t\}, \quad (4.19)$$

where H and G are the matrix of coefficients used in the result of numerical integration. Here, we form the integral equation for diffracted pressure by basing it on the viewpoint at [7, 64]:

$$C(P_1)p_\Sigma(P_1) = -\iint_S\{p_\Sigma(Q)(\partial/\partial n')[exp(ikr)/r] - [exp(ikr)/r]\rho\omega^2(\vec{u}\,\vec{n}')\}dS + 4\pi p_i(P_1), \quad (4.20)$$

Now, we interpolate the components of the vector on each boundary element and, similar to that of (4.17) and (4.18), the sound pressure on each element is presented as follows:

$$p_\Sigma(\xi) = \sum_\alpha N_\alpha(\xi)p_{\Sigma_\alpha}. \quad (4.21)$$

When we substitute (4.17), (4.18), and (4.19) into (4.20) and complete the numerical integration, we receive

$$[T]\{u\} = [D]\{p_\Sigma\} + 4\pi\{p_i\}, \quad (4.22)$$

where T and D they each are "matrices" of the coefficients.

At the next stage, we can then solve the (4.19) and (4.22) system of equations using the boundary conditions. According to one of the boundary conditions, the number of indeterminate stresses in the equation (4.19) can be expressed through pressure:

$$[H]\{u\} = [G]\{t\} + [F]\{p_\Sigma\}, \quad (4.23)$$

where G and F they each are "matrices" of the coefficients received from matrix G in equation (4.19).

In each of these particular cases, it is possible to use the principle of the net of nodal points for the scatterers with axially symmetrical bodies. (This principle was used before, in [68].) Thus, it is possible to implement the cylindrical coordinate system (r, φ, z), connected with the cylinder, and the spherical coordinate systems (r, θ, φ), connected with the half-spheres, for bodies with surfaces consisting of fragments.

In the process of numerical integration, the element of the cylinder's surface with radius r_0 will be equal to $r_0 d\varphi_0 dz_0$; for the half-sphere, the element of the surface in the spherical coordinates is equal to $dS = r_0{}^2 sin\theta_0 d\theta_0 d\varphi_0$ (Fig. 4-2, 4-3).

In the process of forming the net of the boundary elements for this task, the discretization step for the boundary surface in the direction of every coordinate should not also exceed $0.5\lambda_0$.

According to the Helmholtz theorem, the displacement vector $\vec{u}$ can be presented in the following form:

$$\vec{u} = -grad\Phi + rot\vec{\Psi}, \quad (4.24)$$

where Φ is the scalar, $\vec{\Psi}$ is the vector potentials that obey the scalar Helmholtz equation and the vector Helmholtz equation, respectively:

$$\Delta\Phi + k_1^2\Phi = 0; \quad (4.25)$$

$$\Delta\vec{\Psi} + k_2^2\vec{\Psi} = 0, \quad (4.26)$$

where $k_1 = \omega/c_1$; $k_2 = \omega/c_2$; c_1 and c_2 are velocities of linear and transverse waves, respectively, in the scatterer's material.

For the cylinder surface, the vector $\vec{\Psi}$ is parallel to the axis of cylinder.

Due to the axis of symmetry in the spherical surfaces, the vector potential $\vec{\Psi}$ will also have only one component Ψ_φ, which is different from zero, $\Psi = \Psi_\varphi$, in the spherical coordinate system. Thus, the Helmholtz vector equation transfers into a scalar equation for the only component of a vector potential, which is different from zero:

$$\Delta\Psi + k_2^2\Psi = 0. \qquad (4.27)$$

The potential of the diffused wave, as well as the potentials Φ и and Ψ, have forms corresponding to the planar wave and containing the voluntary constants that are determined from the boundary conditions. When all the main physical variables are functions of only two coordinates, the displacement vector will also possess two components.

Using the correlations for the generalized law of Hooke for an isotropic sphere, which is not dependent on the choice of coordinate systems, it is possible to present the elastic stresses on the finite surface through the deformation components and through potentials Φ and Ψ [7, 55]:

a) for a cylindrical surface:

$$\sigma_r = \lambda_1 k_1^2 \Phi + 2\mu\left(-\frac{\partial^2\Phi}{\partial r^2} - r^{-2}\frac{\partial\Phi}{\partial\varphi}r^{-1}\frac{\partial^2\Phi}{\partial r\partial\varphi}\right); \qquad (4.28)$$

$$\tau_{r\varphi} = \mu\left(-2r^{-1}\frac{\partial^2\Phi}{\partial r\partial\varphi} + 2r^{-2}\frac{\partial\Phi}{\partial\varphi} - k_2^2\Psi - 2\frac{\partial^2\Psi}{\partial r^2}\right), \qquad (4.29)$$

where $\vartheta = \varepsilon_r + \varepsilon_\varphi = div\vec{u}$;

b) for a spherical surface:

$$u_r = -\frac{\partial\Phi}{\partial r} + r^{-1}\Psi ctg\theta + r^{-1}\frac{\partial\Psi}{\partial\theta}; \qquad (4.30)$$

$$\sigma_r = \lambda k_1^2\Phi + 2\mu\left(-\frac{\partial^2\Phi}{\partial r^2} + r^{-1}ctg\theta\frac{\partial\Psi}{\partial r} - r^{-2}\Psi ctg\theta + r^{-1}\frac{\partial^2\Psi}{\partial r\partial\theta} - r^{-2}\frac{\partial\Psi}{\partial r}\right); \qquad (4.31)$$

$$\tau_{r\theta} = \mu\left(r^{-2}ctg\theta\frac{\partial\Psi}{\partial\theta} + r^{-2}\frac{\partial^2\Psi}{\partial\theta^2} - \frac{\partial^2\Psi}{\partial r^2} - 2r^{-2}\frac{\partial\Phi}{\partial\theta} - r^{-2}\Psi\, sin^{-2}\theta\right), \qquad (4.32)$$

where $\vartheta = \varepsilon_r + \varepsilon_\varphi = div\vec{u}$.

The following boundary conditions are to be executed at the points of the boundary surface where the normal (radial) component of the displacement vector u_r is continuous and connected with the normal derivative of diffracted pressure. Normal stress is equal to the diffracted pressure:

$$u_r = \rho_0^{-1}\omega^{-2}\frac{\partial p_\Sigma}{\partial n} \text{ by } r{=}a \qquad (4.33)$$

where p_i, p_s are the sound pressures of the falling and dispersed waves, respectively. The normal stress σ_r is equal to the acoustic pressure in the liquid:

$$\sigma_r = p_\Sigma \text{ by } r{=}a. \qquad (4.34)$$

The tangential stresses are zero:

$$\tau_{r\varphi} = \tau_{r\theta} = 0 \text{ by } r{=}a. \qquad (4.35)$$

When submitting the component of the displacement vector and elastic stress to the boundary conditions (4.33)–(4.35), we will receive the algebraic systems for the equations at every point on the surface in order to find out the indeterminate coefficients in the equations of potentials Φ and Ψ.

The indeterminate coefficients are received using the ratio of determinants from the Cramer rule that allows for the distribution of $p_{\Sigma}(Q)$ and u_r at the nodes of the boundary elements.

The calculation for the diffracted sound pressure $p_s(P)$ in a liquid sphere is processed based on (4.26) using the numerical integration of quadrature formulas.

The task solution to the problem of calculating the diffraction of the elastic isotropic surface does not differ in principle from the examined solution for a constant elastic body: the internal boundary (with a liquid or gas filler or a vacuum inside the shell) is added and, therefore, the number of indeterminate coefficients and boundary conditions in (4.28) through (4.35) will increase.

The additional boundary conditions are formed the following way:

c) The normal stress on the internal surface of the shell is either missing (as in the case of a hollow shell) or is equal to the sound gas pressure (as in the case of a gas-filled shell);

d) There is an absence of tangential stress on the internal surface of the shell.

As with the diffraction task to estimate the accuracy of the numerical solution derived using BEM in [77], the modules for the angular characteristics in the diffusion of an elastic sphere and spheroid were calculated. These modules were compared to the analogical characteristics of the same bodies using the analytical solution and were shown to have a rather satisfactory correspondence (Figs. 4-11, 4-12). Also, the results of the MFE calculations for the scattering characteristics of an elastic scatterer with a non-analytical surface form (a cylinder with a hemisphere at each end) have also been presented. The results were approximate to the corresponding results of the precise solution for spheroids; this solution was obtained from [7, 55].

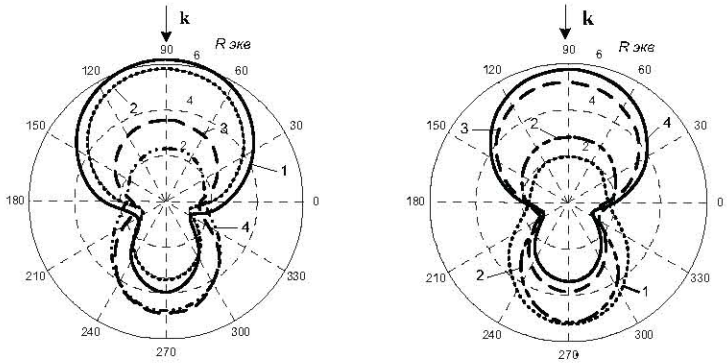

Figure 4-11: Modules of the angular characteristics of spherical scatterers (BEM) when ka=1, R_{eq}: *a)* solid sphere: 1, hard; 2, steel; 3, aluminum; 4, rubber; *b*) spherical shell thickness h: 1, kh = 0.01; 2, kh = 0.03; 3, kh = 0.05; 4, kh = 0.1

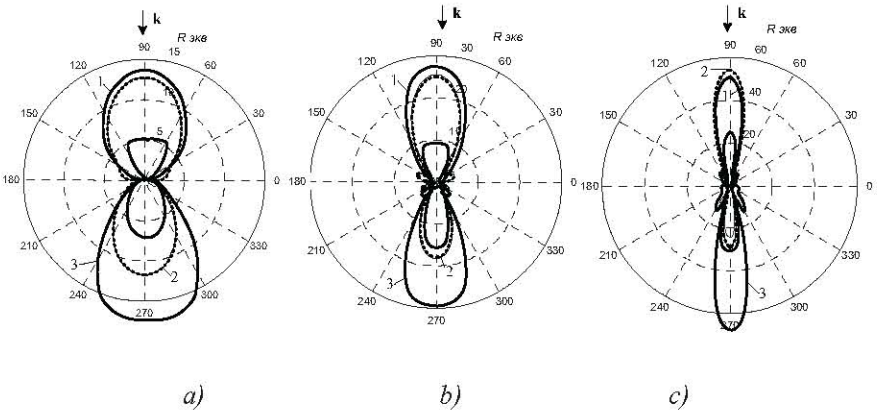

Figure 4-12: Modules of the angular characteristics of spheroids, R_{eq}: 1—steel (exact solution); 2—steel (BEM); 3—rubber (BEM); (a) for C=3; b) for C=5; C) for C=10; (where $C = kh_0$)

CHAPTER 5

MEASURING THE CHARACTERISTICS OF SOUND REFLECTION AND SCATTERING USING ELASTIC CYLINDRICAL SHELLS IN HYDROACOUSTIC BASIN CONDITIONS

5.1. The Criteria Needed to Make Acoustical Diffracted Measurements

A method and an experimental setup intended for measuring the amplitude and phase of the acoustic field in the near zone of a scatterer are described. The results from measuring the scattering characteristics of low-frequency sound signals emitted by elastic cylindrical shells are analyzed.

The following two problems regard the amplitude phase characteristics of the scattered sound field in the near zone of a scatterer made in the form of an elastic finite cylindrical shell. Both problems are solved on the basis of experimental data [7, 18]:

1) The determination of the nature of sound scattering by the shell at low-sounding frequencies;
2) The calculation of the angular scattering of sound in the Fraunhofer zone from the measurement of both the amplitude and phase of the scattered field in the Fresnel zone.

The measurement of the characteristics of the sound reflection and scattering is (in general) very often conducted on the models in the hydroacoustic basins, the shallow ponds, and any other areas used for such research intentions [79, 80]. A principal difference in the diffracted experiment (DE) between the conditions of the shallow water area (SWA) and that of the hydroacoustic basin (HB), with a comparison based on the natural conditions of deep sea, consists of the reflective boundaries near to the source and the scatterer (such as a free surface; a bottom; or the walls of the basin). As a rule, the experimenters are interested in the characteristics of the sound reflection of a Fraunhofer zone (of a distant field) corresponding to an infinite medium where a sound plane wave falls down and irradiates from the sound source, which is infinitely removed from the scatterer.

Therefore, in the DE, and according to the conditions of the HB or the SWA by the principal problem, there is an exception with regard to the influence of the reflective boundaries from the division of the mediums in the characteristics of the scatterer. The solution to this problem is begun with a choice as to the form of the sound signal. The optimum properties with this point of view have a pulse signal with a harmonic or frequency-modulated filling. The application of this type of signal allows us to distinguish when the signal is reflected on a body or background that prevents this from happening. Therefore, in future, we should give our attention to pulse type signals.

We will choose a distance between the source of the pulse signal and the scatterer so that the wave, when falling on the body (at least within the limits of the scatterer), could be received by the plane wave without much difference. We will place a hydrophone, as a receiver of the reflected signal, in the Fraunhofer zone. The criterion for the minimum distance between the combined antenna and the scatterer, which corresponds to the above two requirements is founded on a known formula: $R_{\min} >> \frac{D^2}{\lambda}$ (where D is the maximum dimension of the scatterer, and λ is the length of the sound wave in the medium) [79, 81]. However, in the diffracted measurements, the criterion of the minimum distance can be found with the help of the radial wave functions that appearing through the fundamental solutions to the scalar Helmholtz equation [55, 82]. For example, in the simplest form of bodies (a sphere, an infinite cylinder, or prolate and oblate spheroids) we will first determine a difference in the angular characteristics of the sound scattering through plane and spherical sound waves. (Later, we will compare plane and cylindrical waves). In order to do this, we need to know the potential of expansion in the spherical (or cylindrical) wave by using the Helmholtz equation [83]:

1) In the spherical coordinate system, an expansion has the form

$$exp\frac{(ikR)}{R} = ik\sum_{n=0}^{\infty}(2n+1)P_n(cos\,\theta)j_n^{(1)}(kr_1)\ ,\quad r_1 > r > 0\ , \tag{5.1}$$

where R represents the distance between the source and the point of an observation; r represents the radial coordinate of the point of an observation; r_1 represents the radial coordinate of the source; and θ represents the angular coordinate of the point of the observation relative to a polar axis;

2) In the circular cylindrical coordinate system, an expansion has the form

$$H_0^{(1)}(kR) = \sum_{n=0}^{\infty}\varepsilon_n J_n(kr)H_n^{(1)}(kr_1)\cos n\,\phi\ ,\quad r_1 > r > 0\ , \tag{5.2}$$

where r_1, r, and R form a triangle so that angle φ is concluded between sides r and r_1;

$$\varepsilon_n = \begin{cases} 1 & by \quad n = 0\ ; \\ 2 & by \quad n \neq 0\ ; \end{cases}$$

3) In the prolate spheroidal coordinate system an expansion has the form

$$exp\frac{(ikR)}{R} = 2ik\sum_{m=0}^{\infty}\sum_{n\geq m}^{\infty}\varepsilon_m\bar{S}_{m,n}(C,\eta_1)\bar{S}_{m,n}(C,\eta')\times$$
$$\times R_{m,n}^{(3)}(C,\xi_1)R_{m,n}^{(1)}(C,\xi')\cos m\,\phi\ ,\quad \xi_1 > \xi'\ , \tag{5.3}$$

where ξ_1, $\eta_1(\eta_1 = cos\ \theta_1)$, $\varphi_1 = 0$ represents the spheroidal coordinates of the source, while ξ' η' $(\eta' = cos\,\theta')$ and φ represent the spheroidal coordinates of the point of the observation.

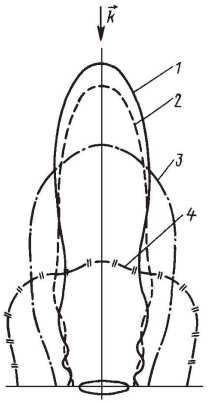

1 - the plane wave ; 2 - $\xi_1 = 10$;
3 - $\xi_1 = 2{,}4$; 4 - $\xi_1 = 1{,}1$

Figure 5-1: Modules of the angular characteristics of the soft spheroid

Analogously, (5.3) will look the expansion of the potential of the spherical wave and, in the oblate spheroidal coordinate system only C must substitute into iC; ξ_1 must substitute into $i\xi_1$ and ξ' must substitute into $i\xi'$.

So, in future, we are limited by the prolate spheroidal coordinate system, remembering what we can cross over to the oblate coordinates by means of a simple substitution of the wave dimension and the radial coordinate.

The formulas for the potential of the plane wave are derived from (5.1) – (5.3), if r_1 and ξ_1 direct us toward infinity, instead of the radial functions of the third type and the Hankel functions, then their asymptotical meanings are used [7, 55]. We have written these asymptotics for the radial functions in our chosen coordinate systems [7, 55]:

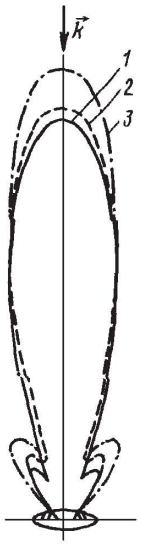

Figure 5-2: Modules of characteristics of the sound scattering of the hard spheroid

1) The asymptotic from a Hankel function has the following form in the spherical coordinate system:

$$h_n^{(1)}(kr_1) \underset{kr_1\to\infty}{\cong} \left(\frac{1}{kr_1}\right) i^{1-n}\, exp(ikr_1)\ ; \qquad (5.4)$$

2) The asymptotic in a Hankel function has the following form in the cylindrical coordinate system:

$$H_n^{(1)}(kr_1) \underset{kr_1\to\infty}{\cong} \sqrt{\frac{2}{\pi kr_1}}\, exp\left[ikr_1 - i\left(\frac{\pi}{2}\right)\left(n+\frac{1}{2}\right)\right]\ ; \qquad (5.5)$$

3) The asymptotic of a third-kind radial function has the following form in the prolate spheroidal coordinate system:

$$R_{m,n}^{(3)}(C,\xi_1) \underset{C\xi_1\to\infty}{\cong} \left(\frac{i^{-n-1}}{C\xi_1}\right) exp(iC\xi_1)\ . \qquad (5.6)$$

In these real situations, we have the terminal meanings, r_1 and ξ_1. In this case, however, we can correctly accomplish a passage from the spherical (or cylindrical) wave to the plane wave (the field of the falling wave) or from the Fresnel zone in the Fraunhofer zone (the field of the scattered wave field, which is the area where we explore the wave). We will apply the expansions, (5.1)–(5.3).

The convergence of the series located in the right parts of these formulas (5.1)–(5.3) depends on this as they are quickly diminished (over the modulus) along with a growth of the indexes from the summing up of the products from the radial functions of the first and third kinds. The numbers of the members of the series (n_{lim}, m_{lim}) on which the summation must be broken can be established from tables of radial functions. This procedure is shown and explained below. It can be determined from the tables of the radial functions and it will be defined by the function of the wave dimension kr_0 (the sphere and the cylinder); or the C (the spheroid) of the coordinate r or ξ (in the given case, it corresponds to the coordinate of the external surface of the scatterer (r_0 or ξ_0); or it is circumscribed round the coordinate surface and it corresponds to this with the requisite degree of precision. Practically, and for all intents and purposes, we can be limited by the members in that the modulus of the product of the radial functions of the first and third kinds are 3–4 orders of magnitude smaller than the largest module representing the product of these functions and the lesser meanings of the indexes. As well as this, it can be placed on the boundary of the Fraunhofer zone for ideal scatterers in the form of a sphere, cylinder, or spheroid (or similar forms). However, in this case, the indexes n_{lim} (the sphere, and the cylinder) or n_{lim} and m_{lim} (the spheroid) of the radial functions of the third kind must be fulfilled. The asymptotical formulas (5.4)–(5.6) are determined by the more complicated combination of the radial functions of the first and third kinds (the hard scatterer and the derivatives of these functions), and by entering the coefficients of the expansion of the pressure in the scattered wave over the functions of the Helmholtz equation. The concrete formula for these coefficients has been settled as it has proceeded both from the shade of the boundary conditions and from the type of source which generates the falling wave. For

the ideal scatterer in the form of a prolate spheroid, the combination of the radial functions has the following form:

The point source

a) the soft spheroid

$$R_{m,n}^{(3)}(C,\xi_1)R_{m,n}^{(3)}(C,\xi)\frac{R_{m,n}^{(1)}(C,\xi_0)}{R_{m,n}^{(3)}(C,\xi_0)}\ ; \qquad (5.7)$$

b) the hard spheroid

$$R_{m,n}^{(3)}(C,\xi_1)R_{m,n}^{(3)}(C,\xi)\frac{R_{m,n}^{(1)'}(C,\xi_0)}{R_{m,n}^{(3)'}(C,\xi_0)}\ ; \qquad (5.8)$$

The plane wave

a) the soft spheroid

$$R_{m,n}^{(3)}(C,\xi_1)\frac{R_{m,n}^{(1)}(C,\xi_0)}{R_{m,n}^{(3)}(C,\xi_0)}\ ; \qquad (5.9)$$

b) the hard spheroid

$$R_{m,n}^{(3)}(C,\xi)R_{m,n}^{(1)'}(C,\xi_0)/R_{m,n}^{(3)'}(C,\xi_0). \qquad (5.10)$$

If we use the formulas (5.9) and (5.10), we will find the boundary ξ of the Fresnel zone and the Fraunhofer zone of the scattered pressure for the plane falling wave and can then place the point source ($\xi_1=\xi$) on this boundary. That is, as seen from the comparison of (5.7) and (5.8) with (5.9) and (5.10), this boundary will, in general, show the irradiation for both types. Figs. 5-1, 5-2 confirm these through the angular characteristics of the scattered pressure by the soft and hard spheroids in the Fraunhofer zone from the plane and spherical waves. In Fig. 5-2, curve 1 corresponds to the modulus of the angular characteristic of the sound scattering by the hard spheroid and the plane falling wave. Curve 2 corresponds to the point source with the coordinate $\xi_1=10,0$ and the distribution of the modulus of the scattered pressure on the radial coordinate $\xi_1=10,0$ by the falling plane wave. Curve 3 characterises the distribution of the modulus of the scattered pressure for the radial coordinate $\xi_1=10,0$ (this is the coordinate of the source).

The numerical estimations shown include the minimal distance $R_{\min}$ from the scatterer to the boundaries of the Fresnel and Fraunhofer zones. This was found to be the following inequality $R_{\min}\geq 2(D^2/\lambda)$.

We see that, for spheroidal form scatterers, the linear distance from the surface of the scatterer ξ_0 to the boundary line, ξ_2, depends on the angle of the observation. Θ is the greatest distance to the border for the angle $\theta=0^\circ$ and the shortest distance for $\theta=90^o$ (the oblate spheroid, as with the prolate spheroid the situation will be opposite and the maximum distance will be $\theta = 90^0$, while the minimum is $\theta = 0^0$). We can also notice that for the angle $\theta=0^\circ$ (the axially symmetric problem), the index m in all the formulas has one meaning: $m=0$.

When taking the measurements of diffracted acoustics in natural ponds, one must remember the following principal demands [79]:

1) To have large enough dimensions so as to minimize unintended interference evoked by the sound reflections from the way the pulse regime is administered.
2) To have a low level of surrounding noise.
3) To have a liquid medium, which must be free from all sorts of factors that could potentially evoke a refraction or scattering of the sound (such as different flows, temperature gradients, sea creatures, bubbles, and soil).

Protection from rainy weather must be ensured in order to secure a low level of background noise; the stability, and thus the accuracy, of the monitoring platform; and convenience when taking measurements.

Sources of extraneous noise audible from the basin include ships, industrial plants (especially their associated water pumps), freight transport, railroads, rain, and waves. Sources of extraneous noise audible from the auxiliary platforms are different as they include piers, bridges, and barges, as well as ships. Piers and bridges offer the most convenient and stable working conditions. If the basin is large and deep, one must use a sailing construction; however, stability and convenience must be secured by including a weighted vertical dimension of the construction and by securing it in place by means of service lines running under the water to posts leading to the shore.

The frequency range of the reflective body does not determine the simple criterion for the minimal acceptable depth when gathering measurements in the basin.

The quality of the hydroacoustic basin depends on the degree to which it can remove the sound reflections or the elimination of the interference resulting from the reflections. If the sound reflections are destroyed or attenuated by absorbing the boundaries of the basin, then the basin will be submerged.

A big part of the problem when conducting measurements in hydroacoustic basins is that they are not closed and are similar to natural ones, but not terms of their dimensions. However, an exception is the reserved submerged basin, as it can imitate the conditions of the measurements of the deep ocean, given the high static pressures and the low temperature of the water within it.

As shown by the results of the pulse regime, the shape of the basin does not play an important role. A limiting factor is the distance to the reflective boundaries of the surfaces closest to the path that propagates the straight acoustic signal from the source to the scatterer and receiver.

5.2. The Structural Schema of the Experiment and its Methodology

A block diagram of the plant used to generate the pulse regime and gather the amplitude phase measurements of the reflected (scattered) signal is presented in Figure 5-3.

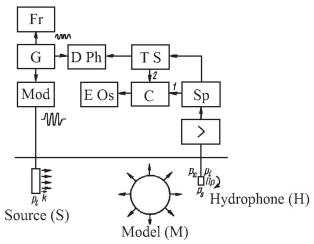

Figure 5-3: A block diagram of the plant used to measure the sound scattering

The block diagram includes the radiating section, the scatterer (model), and the liquid medium. We will explain principles of how it works using time diagrams of the voltages in the radiating section (Fig. 5-4).

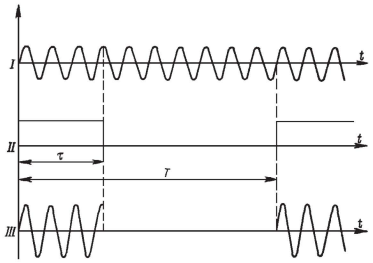

Figure 5-4: The time diagrams of the voltages in the plant's radiating section

The harmonic oscillations generator (G) creates the harmonic signal with the frequency, ω (see diagram I in Fig. 5-4). The crystal-controlled digital frequency meter (Fr) controls the frequency. When it is entered into the modulator (Mod), it creates a rectangular video pulse over the duration τ (see diagram II in Fig. 5-4). The harmonic signal is turned into the pulse signal by the pulse's rectangular envelope and the harmonic filling on frequency ω (see diagram III in Fig. 5-4). This pulse signal, with the help of source S, exposes the liquid medium from either the basin or the water area to the sound. Hydrophone H (the receiver in Fig. 5-3) is able to receive different signals, which are independent from the situation. If it turns out well, then it will divide the signal p_s, which is reflected from the model and the hindrance, p_p, thereby creating the sound reflection from the boundaries of the divided medium. The receiver will fix the signal p_s towards the model's scatter. If the model is absent, then the hydrophone will only receive the straight signal p_i. If the receiver is placed near the model, then the straight and scattered signals cannot be divided. In addition, the hydrophone is able to fix the diffracted pulse signal.

At low frequencies, the interference of sound reflections can only be avoided when they are near the model. In this case, it is almost impossible to separate the direct signals from the reflected signals when both are measured.

The receiver detects the total (diffracted) signal. If the undistorted signal (obtained without the model) is known at the same points, then the scattered signal can be determined using the difference between the diffracted and straight signals when the amplitudes and phases of these signals are measured simultaneously. From the distributions of the scattered or diffracted signals, it is possible to calculate the angular characteristics of the far field of the scatterer using the Kirchhoff integral [82–85]. In acoustics, this method of extrapolating the near-field data to the far field was first applied to hydroacoustic arrays. This is known as the DRL method in the literature [79, 81, 83, 86].

The sound pulse (p_s, p_i, or p_Σ) is turned by the hydrophone using an electric signal. This first occurs at the preliminary amplifier (>) and then when the spectrometer's (Sp) ultrasonic frequencies are turned towards the frequency of the filling in pulse ω. Further, the signal propagates the two channels. Over the first channel, the signal that is filtered out by the spectrometer (Sp) is given a time selector (TS) that cuts out 1–2 periods in the placement part of the pulse. The pulse signal with the time selector and the harmonic signal with the harmonic oscillations generator (G) use the digital phase-meter's (DPh) two entrances, which then measures the phase of the signal received by the hydrophone relative to the signal from the generator (G). Simultaneously, the signal with spectrometer (Sp) arrives at the commutator's (C) first entrance. The second entrance receives the signal with the time selector (TS), which is dependent on the position of the commutator's relay. This is displayed on the cathode-ray oscilloscope's (Eos) screen. We can then observe either the total time of the pulse's linear sweep picture in the liquid medium. This is either based on the time or the placement of the time selector (TS).

This example uses the DRL method [7, 9]. If we know the distribution of the scattered p_s or diffracted $p_\Sigma = p_i + p_s$ pressures on the surface S surrounding the scatterer, then with the help of the Kirchhoff integral, we can determine $p_s(P)$ or $p_\Sigma(P)$ at any arbitrary point of observation P [7, 18, 79–81]:

$$p_s(P) = \left(\frac{1}{4\pi}\right) \iint_S \left\{ \left[\frac{\partial p_d(Q)}{\partial n}\right] G(P;Q) - p_d(Q) \left[\frac{\partial G(P;Q)}{\partial n}\right] \right\} dS \ , \qquad (5.11)$$

where index d is s or Σ; Q represents the point of the surface S; and $G\ (P;\ Q)$ represents the Green function, according to the non-homogeneous Helmholtz equation [2].

The values of $G\ (P;\ Q)$ are chosen so that surface S disappears (G_1) or turns into zero. Its normal derivative is G_2, and so we get the following two integral formulas:

$$p_s(P) = -\left(\frac{1}{4\pi}\right) \iint p_d(Q) \left[\frac{\partial G_1(P;Q)}{\partial n}\right] dS \ ; \qquad (5.12)$$

$$p_s(P) = \left(\frac{1}{4\pi}\right) \iint \left[\frac{\partial p_d(Q)}{\partial n}\right] G_2(P;Q) dS \ . \qquad (5.13)$$

For the surface S of spheroidal or spherical forms, the formulas for G_1 and G_2 have the following form [7]:

$$G_1(\xi,\eta,\phi;\xi',\eta',\phi') = 2ik\sum_{n=0}^{\infty}\sum_{m=-n}^{n}\bar{S}_{m,n}(C,\eta)\bar{S}_{m,n}(C,\eta')\times$$
$$\times exp[im(\phi-\phi')]\left[R_{m,n}^{(1)}(C,\xi')R_{m,n}^{(1)}(C,\xi) - R_{m,n}^{(3)}(C,\xi')R_{m,n}^{(3)}(C,\xi)\times\right.$$
$$\left.\times R_{m,n}^{(1)}(C,\xi_0)\frac{R_{m,n}^{(3)}(C,\xi')}{R_{m,n}^{(3)}(C,\xi_0)}\right], \quad \xi > \xi' ; (5.14)$$

$$G_2(\xi,\eta,\phi;\xi',\eta',\phi') = 2ik\sum_{n=0}^{\infty}\sum_{m=-n}^{n}\bar{S}_{m,n}(C,\eta)\bar{S}_{m,n}(C,\eta')\times$$
$$\times exp[im(\phi-\phi')]\left[R_{m,n}^{(1)}(C,\xi')R_{m,n}^{(3)}(C,\xi) - R_{m,n}^{(3)}(C,\xi')R_{m,n}^{(1)'}(C,\xi_0)\times\right.$$
$$\left.\times\frac{R_{m,n}^{(3)}(C,\xi')}{R_{m,n}^{(3)'}(C,\xi_0)}\right], \quad \xi > \xi' ; (5.15)$$

$$G_1(r,\theta,\phi,r',\theta',\phi') = ik\sum_{n=0}^{\infty}(2n+1)\sum_{m=-n}^{n}\left[\frac{(n-m)!}{(n+m)!}\right]\times$$
$$\times P_n^m(cos\,\theta)P_n^m(cos\,\theta')\,exp[im(\phi-\phi')]\left[j_n(kr')h_n^{(1)}(kr) -\right.$$
$$\left.- j_n(kr_0)h_n^{(1)}(kr)\frac{h_n^{(1)}(kr')}{h_n^{(1)}(kr_0)}\right], \quad r > r' ; (5.16)$$

$$G_2(r,\theta,\phi,r',\theta',\phi') = ik\sum_{n=0}^{\infty}(2n+1)\sum_{m=-n}^{n}\left[\frac{(n-m)!}{(n+m)!}\right]\times$$
$$\times P_n^m(cos\,\theta)P_n^m(cos\,\theta')\,exp[im(\phi-\phi')]\left[j_n(kr')h_n^{(1)}(kr) -\right.$$
$$\left.- j_n'(kr_0)h_n^{(1)}(kr)\frac{h_n^{(1)}(kr')}{h_n^{(1)'}(kr_0)}\right], \quad r > r' , (5.17)$$

where ξ, η, φ; r, θ, and φ represent the spheroidal and spherical coordinates of the point of the observation P; ξ',η',ϕ' and r',θ',ϕ' represent the spheroidal and spherical coordinates of point Q on surface S in which $\xi=\xi_0$ and $r' = r_0$.

An advantage of the monomial integrals (5.12) and (5.13) in comparison with the two integrals (5.11) is that, in order to define the pressure in the distant field, it is enough to only know the distribution of the pressure $p_d(Q)$ or its normal derivative $\frac{dp_d(Q)}{dn}$ along surface S. The formulas (5.14)–(5.17) are simplified [88] due to the substitution of the radial functions $R_{m,n}^{(3)}(C,\xi)$ and $h_n^{(1)}(kr)$ with their asymptotical meanings. This is a fair statement for the distant field in the Fraunhofer zone.

With regard to the binominal integral (5.11) as the Green function $G(P;Q)$, we used

$$G(P;Q)=exp(ikr)/r, \quad (5.18)$$

where r represents the distance between points P and Q. Additionally, due to the absence of miniature receivers from the oscillating velocity sound wave, we can use one to two approximations:

1) For the scattered wave near surface S, we can account for its movement by spreading it within a plane. Measuring the normal derivative $\frac{dp_s(Q)}{dn}$ is unnecessary, as $\frac{dp_s(Q)}{dn} = ikp_s(Q)$.

2) To measure the derivative $\frac{dp_s(Q)}{dn}$, we can substitute the relationship between the terminal differences of the pressures $[\Delta p_s(Q)]$ and the distances Δq with the measurements of the surfaces, S_1 and S_2:

$$\frac{dp_s(Q)}{dn} \approx \frac{\Delta p_s(Q)}{\Delta q}.$$

In the Fraunhofer zone (r is big), then the usual approximations are fair [6]:

$$p_s(P) = D(\theta,\phi)\,exp\frac{(ikR)}{R}, \quad (5.19),$$

where R is the distance from the beginning of system O's coordinates to the point of the observation; $D(\theta,\varphi)$ is the angular characteristic of the scattering of sound in the spherical coordinates θ, φ; and

$$\left(\frac{\partial}{\partial n}\right)\left[exp\frac{(ikr)}{r}\right] \approx \left(\frac{\partial}{\partial n}\right)\left[exp\frac{(ikR)}{R}\right] \approx$$
$$\approx ikR^{-1}\,exp(ikR)\left(\frac{\partial R}{\partial n}\right) = ikR^{-1}\,cos\,\theta'\,exp(ikR)\ , \qquad (5.20).$$

In the distant zone, the single vector from Q through P can be substituted with the single vector $\vec{m}$ from point O through point P, so that

$$cos\,\theta' = m_x n_x + m_y n_y + m_z n_z\ .$$

In practice, the continuous distributions of both the pressure $p_s(Q)$ and the normal derivative $\frac{dp_s(Q)}{dn}$ are substituted for discrete distributions. From the integrals, we can find the numerical quadraturs for both of the following approximations [7, 18, 82, 84]:

$$D(\theta,\phi) = \left(\frac{ih_0C}{4\pi}\right)(\xi_0^2-1)^{\frac{1}{2}}\int_0^{2\pi}d\phi'\int_{-1}^{+1}\left[-p_d(Q)\,cos\,\theta' + p_d(Q)\right]\times$$
$$\times\left(\xi'^2-\eta'^2\right)^{\frac{1}{2}}exp(iB)\,d\eta' = \left(\frac{ih_0C}{4\pi}\right)(\xi_0^2-1)^{\frac{1}{2}}\sum_{m=1}^{M}D_m\sum_{l=1}^{L}A_l\times$$
$$\times\,\Phi_1\left(\eta_l',\phi_m'\right)\ ,\quad \xi' = \xi_0\ ;\quad d = S\quad or\quad \Sigma\ ;(5.21)$$

$$D(\theta,\phi) = \left(\frac{h_0^2}{4\pi}\right)(\xi_0^2-1)^{\frac{1}{2}}\int_0^{2\pi}d\phi'\int_{-1}^{+1}\left[-p_d(Q)ik\,cos\,\theta'' + \left[\frac{\Delta p_d(Q)}{\Delta q}\right]\right]\times$$
$$\times\left(\xi'^2-\eta'^2\right)^{\frac{1}{2}}exp(iB)\,d\eta' = \left(\frac{h_0^2}{4\pi}\right)(\xi_0^2-1)^{\frac{1}{2}}\sum_{m=1}^{M}D_m\sum_{l=1}^{L}A_l\times$$
$$\times\,\Phi_2\left(\eta_l',\phi_m'\right)\ ,\quad \xi' = \xi_0\ ;\quad d = S\quad or\quad \Sigma\ ;(5.22)$$

where $\Phi_1(\eta_l',\phi_m')$ and $\Phi_2(\eta_l',\phi_m')$ represent the meanings of the corresponding integrand functions in the nodes of the numerical quadratures; L and M represent the number of the nodes following the coordinates η' and ϕ', respectively; A_l and D_m represent the main coefficients; and the formulas for $cos\,\theta'$ and B are given in [8]. By using (5.22) for the calculation $\frac{\Delta p_d(Q)}{\Delta q}$, we can measure the pressures exerted on the two disposed confocal surfaces, as the distance between them is much smaller than the length of the sound wave λ in the liquid. An exception is the non-homogeneous flexural waves in the scatterers, which occur in the form of elastic shells. Here, the distance from the surface of each scatterer to the nearest (main) point must not be $\lambda/2$ the distance between the main points. Also, in order to avoid false maximums, the distance must be less than $\lambda/2$.

The measurements of the diffracted pressure's distributions near the model can be scattered pressure with the help of the construction presented in Figure 5-5.

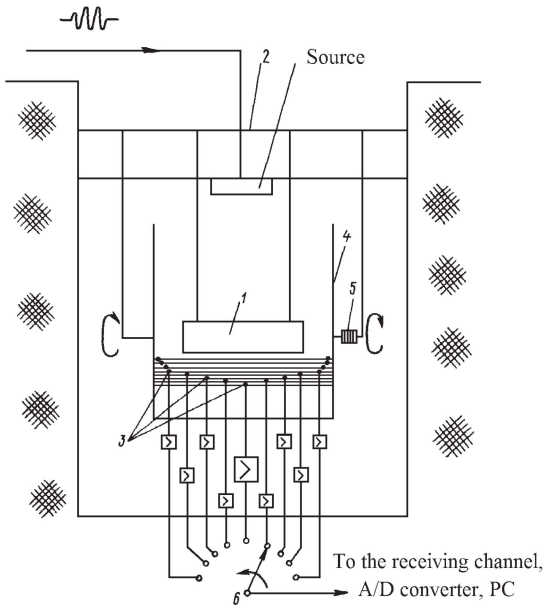

Figure 5-5: The angular gear used to measure the distributions in the near zone

The model (1) was suspended in the construction (2) with the help of metallic strings. The miniature hydrophones (3) were fixed to the angular gear strings (4), which were made from hollow (water-filled) metal tubes. In order to obtain the correct phase measurements, the hydrophone size needs to be small in comparison to the sound's wavelength. The low-speed electric motor (5) rotated the angular gear around the model at the required time and on an assigned angle. At each of the system's fixed positions, the amplitude-phase distribution of the diffracted pressure was measured using a switch (6) and the receiving channel of the experimental setup (see Fig. 5-5). The distribution was sent to the PC via an A/D converter, and this was used to calculate the angular characteristic was calculated. The sound pressure, which was scattered by the elastic shell, was measured in the Fresnel zone using the setup in Figure 5-5 and the structure in Figure 5-6.

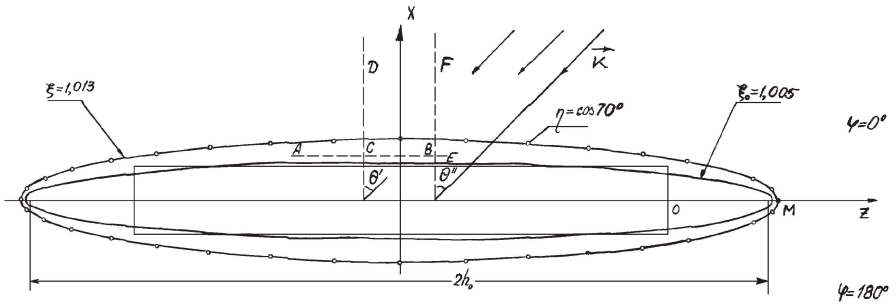

Figure 5-6: The directions of the measurements, AB, CD, EF, and OM; the measuring points; and the cylindrical shell's contour on the measuring template

The latter (Fig. 5-6) consisted of a rigid template, which was fixed above the water's surface. The paper sheet was glued to the upper surface of the template. The cylindrical shell's contour with flat ends; the approximating contour in an elliptical shape; the elliptical contour; and the measurements of AB, CD, EF, and OM were drawn. Along the shell contour, the elliptical contour and the AB, CD, EF, and OM suspended the miniature spherical hydrophones with a diameter of d=5 mm. The strings were strained with the load, which was positioned near the bottom of the tank in order to eliminate its effect on the scattered sound field measurements [85].

In both types of experimental setup, changing the source's position with respect to the scatterer varied the angle at which the model was insonified. The insonifying pulse length was always greater than the maximal size of the model.

As in the setup shown in Figure 5-5, the measurements were performed twice. First, the magnitude of the diffracted pressure and its phase were measured in the presence of the shell. Then, the shell was lifted to the surface, and then the pressure magnitude and the phase of the incident wave were measured at the same points as before.

5.3. The Analysis of the Results

The measured amplitude-phase distributions of the diffracted or scattered fields near the scatterer allow for the determination of the factors that govern the formation of the scattered field. Figure 5-7 shows the magnitude and the phase of the scattered pressure for the finite cylindrical shell, which is insonified along its rotational axis.

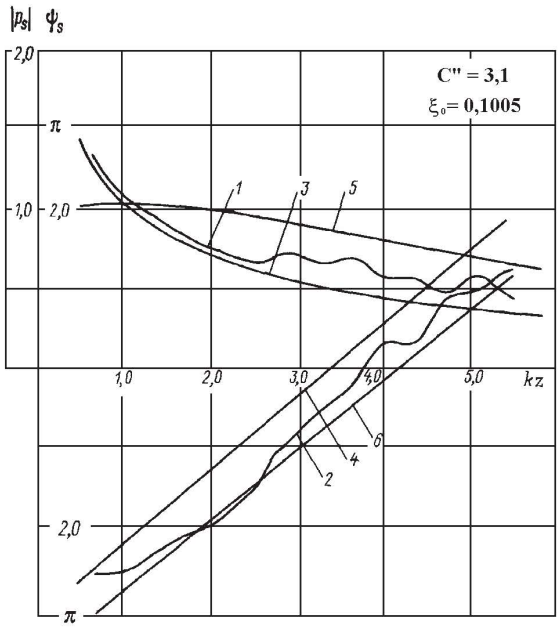

Figure 5-7: The magnitude-phase distributions of the scattered field

At this axis (the OM direction in Fig. 5-6), the distributions of the magnitude and the phase were measured at different wave distances kz from the end of the shell with radius a. Curves 1 and 2 represent the experimental values of the magnitude and the phase of the scattered pressure, respectively. Curves 3 and 4 represent the corresponding distributions for the elastic hollow oblate spheroidal shell with a major semiaxis a and insonification along the OM direction [89]. Distributions 5 and 6 characterize the magnitude and the phase of the scattered pressure soft oblate spheroid. The wave size of the body was $C = ka = 3{,}1$.

Figure 5-8 shows similar distributions for the magnitude and phase of the scattered pressure for the aforementioned spheroidal shell along the OM direction with another wave size of $C = 1{,}0$.

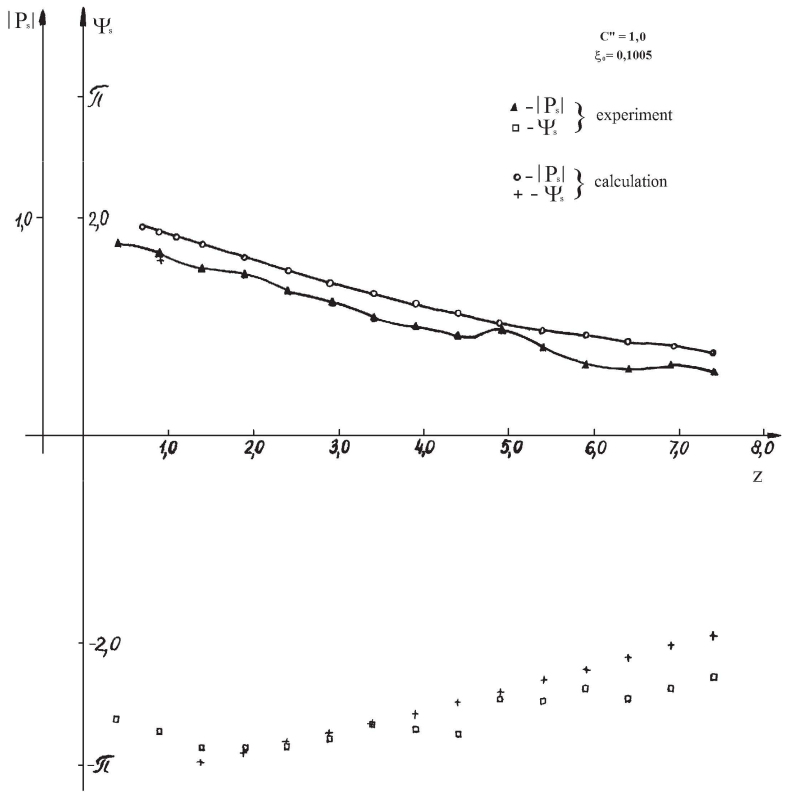

Figure 5-8: The calculated and experimental distributions for the magnitude and phase of the diffracted pressure

Figures 5-9 and 5-10 compare the experimental and, for the acoustically soft infinite cylinder, the calculated distributions of the magnitude and phase of the diffracted pressure.

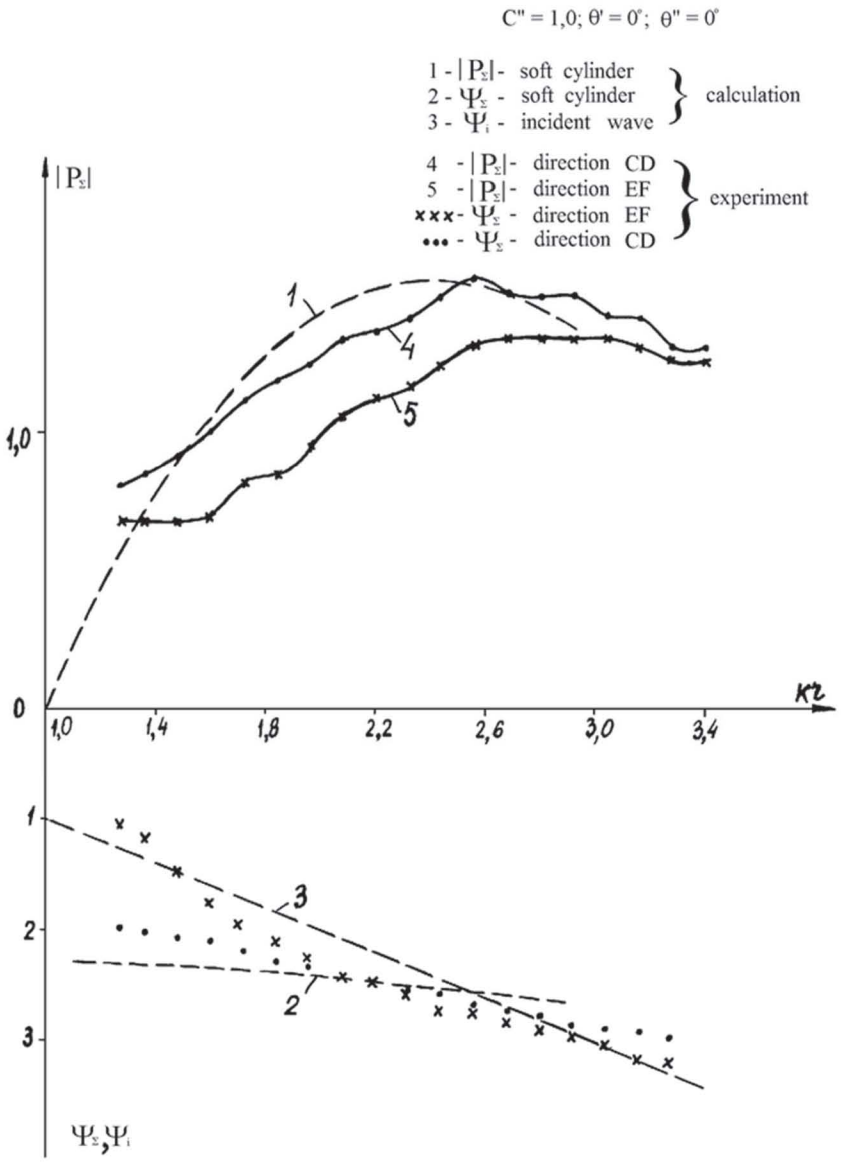

Figure 5-9: Calculated and experimental distributions for the magnitude and phase of the diffracted field

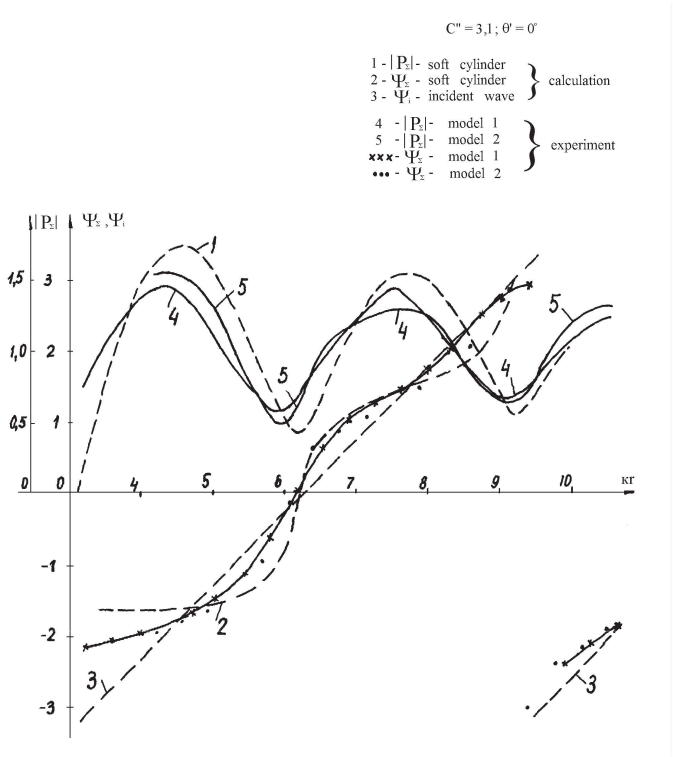

Figure 5-10: The calculated and experimental distributions for the magnitude and phase of the diffracted field

Distributions were measured along the EF direction and the data was obtained for bounded cylinders with the wave size $C = ka = 1{,}0$ (Fig. 5-9) and $C = ka = 3{,}1$ (Fig. 5-10). In addition, Figure 5-9 compares the distributions of the magnitude and phase of the diffracted pressure obtained for two shells (model 1 and model 2) with identical lengths and diameters but with ends of different thicknesses. In both cases, the shells were irradiated along the EF direction.

The structure represented in Figure 5-6 makes it possible to obtain the angular sound-scattering characteristic $D(\theta)$ for axisymmetric models insonified along their axis of rotation by recalculating the relation of the near field to the far field. This is because it is not necessary to measure $|p_s|$ and d ψ_s for the different values of the angle φ. Figure 5-11 displays the results of the measurements of the magnitude of the angular characteristic $|D(\theta)|$. This is completed for the aforementioned cylindrical shell by using the setup and method of measurement described above.

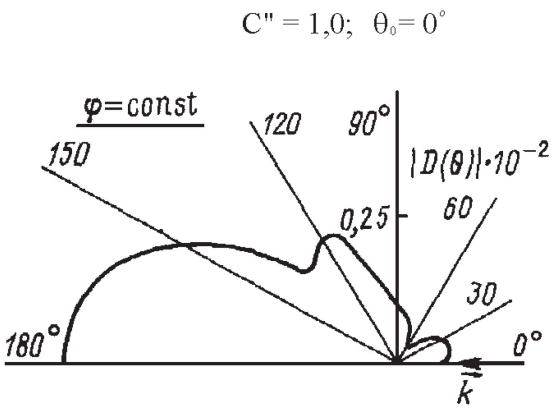

Figure 5-11: A module of the angular sound-scattering characteristic of the hollow cylindrical shell

CHAPTER 6

THE PROPAGATION OF ELASTIC WAVES IN ISOTROPIC AND ANISOTROPIC BODIES

6.1. Calculating the Phase Velocities of Three-Dimensional Flexural Waves in Isotropic Cylindrical Bars and Shells Using Debye and Debye-Type Potentials

The mathematical models of elastic wave propagation in an elastic bar and an elastic shell are very close to each other. The contact boundary value problem formulated for a shell differs from the one formulated for a bar in that it contains an additional boundary surface, which leads to an additional number of unknown coefficients determined by the additional boundary conditions. By contrast, at high frequencies, the wave processes in a shell differ little from those in a layer; therefore, a simultaneous study of these structures is justified. We begin with the more simple of the two structures: namely, the bar.

Wave motion in an isotropic elastic layer was described in [90]. As in [91–95], in our work, we analyze the phase velocities of elastic waves in an isotropic cylindrical bar with an arbitrary radius, a. Unlike [2–6], we consider a rigorous solution to the problem of the phase velocity of a three-dimensional flexural wave in such a bar [96–99]. The novelty of this study lies in calculating the phase velocities of three-dimensional flexural waves propagating in isotropic bars and shells with the use of a rigorous method based on equations of dynamic theory and Sebye- and Debye-type potentials.

We denote the density of the bar material by ρ and Lame coefficients, λ and μ; the isotropic bar under consideration is assumed to be in a vacuum. The bar displacement vector $\vec{U}$obeys the Lame equation:

$$(\lambda + 2\mu) graddiv\vec{U} - \mu curlcurl\vec{U} = -\rho\omega^2\vec{U} \ , - (6.1)$$

where ω represents the circular frequency of the harmonic vibrations.

According to the Helmholtz theorem, the displacement vector $\vec{U}$ of an elastic bar is represented as the combination of a scalar function Φ and a vector function $\vec{A}$:

$$\vec{U} = -grad\Phi + curl\vec{A} \ . \qquad (6.2)$$

The vector function $\vec{A}$ is expressed through Debye-type potentials, χ and Ψ [100, 56], which are close to Debye potentials, U and V [96], but which differ in that they are more convenient for calculations of the cylindrical coordinate system:

$$\vec{A} = \chi\vec{e}_z + acurl(\Psi\vec{e}_z) \ , \qquad (6.3)$$

where $\vec{e}_z$ represents the unit vector.

We introduce the circular cylindrical coordinates r, φ, and z. Cylindrical components of the displacements vector $\vec{U}(U_r, U_\phi, U_z)$are represented in terms of the potential Φ and the cylindrical components of the f function $\vec{A}(A_r, A_\phi, A_z)$ [96, 97]:

$$\left.\begin{aligned} U_r &= -\frac{\partial\Phi}{\partial r} + \frac{1}{r}\frac{\partial A_z}{\partial\phi} - \frac{\partial A_\phi}{\partial z} \ ; \\ U_\phi &= -\frac{1}{r}\frac{\partial\Phi}{\partial\phi} + \frac{\partial A_r}{\partial z} - \frac{\partial A_z}{\partial r} \ ; \\ U_r &= -\frac{\partial\Phi}{\partial z} + \frac{1}{r}A_\phi + \frac{\partial A_\phi}{\partial r} - \frac{1}{r}\frac{\partial A_r}{\partial\phi} \ . \end{aligned}\right\} \qquad (6.4)$$

Cylindrical components (A_r, A_φ, A) of the function $\vec{A}$ are expressed through potentials χ and Ψ and take the form

$$A_r = \frac{a}{r}\frac{\partial \Psi}{\partial \phi} \; ; (6.5)$$

$$A_\phi = -a\frac{\partial \Psi}{\partial r} \; ; (6.6)$$

$$A_z = \chi \; . (6.7)$$

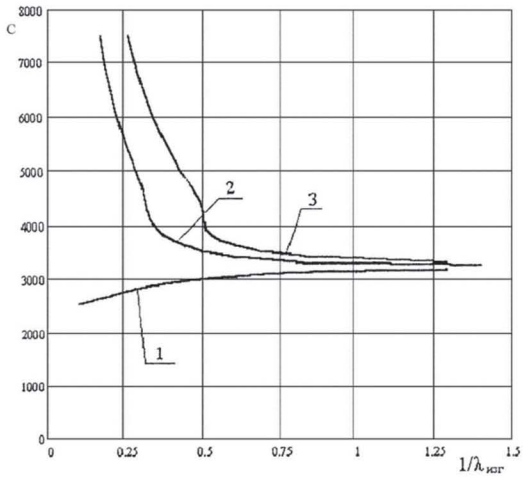

Figure 6-1: Phase velocities of first three modes of a flexural wave

Potentials Φ, χ, and Ψ can be expanded in the eigen-functions of the scalar Helmholtz equation:

$$\left.\begin{aligned} \Phi &= e^{ikz}\sum_{m=0}^{\infty} A_m J_m(h'r)\cos(m\phi) \; ; \\ \Psi &= e^{ikz}\sum_{m=0}^{\infty} B_m J_m(\kappa' r)\cos(m\phi) \; ; \\ \chi &= e^{ikz}\sum_{m=1}^{\infty} C_m J_m(\kappa' r)\sin(m\phi) \; , \end{aligned}\right\} \quad (6.8)$$

where $h' = \left(h^2 - k^2\right)^{1/2}$; $\kappa' = (\kappa^2 - k^2)^{1/2}$; h represents the wave number of the longitudinal wave in the bar material; k represents the desired wave number of the three-dimensional flexural wave; $J_m(h'r)$ represents the cylindrical Bessel function; and A_m, B_m, C_m represents unknown coefficients, which are determined from boundary conditions at the bar surface—namely, the absence of normal and tangential stresses:

$$(\lambda + 2\mu)\frac{\partial U_r}{\partial r} + \lambda\left(\frac{1}{r}\frac{\partial U_\phi}{\partial \phi} + \frac{1}{r}U_r + \frac{\partial U_z}{\partial z}\right)\Big|_{r=a} = 0 \quad ; \quad (6.9)$$

$$\frac{\partial U_\phi}{\partial r} - \frac{1}{r}U_\phi + \frac{1}{r}\frac{\partial U_r}{\partial \phi}\Big|_{r=a} = 0 \; ; \quad (6.10)$$

$$\frac{\partial U_r}{\partial z} + \frac{\partial U_z}{\partial r}\Big|_{r=a} = 0 \; . \quad (6.11)$$

Substituting expansions (6.8) in boundary conditions (6.9) through (6.11), we arrive at the third-order determinant

$$\Delta = \begin{vmatrix} a_{11} & a_{12} & a_{13} \\ a_{21} & a_{22} & a_{23} \\ a_{31} & a_{32} & a_{33} \end{vmatrix}, \quad (6.12)$$

where

$$a_{11} = -(\lambda + 2\mu)J_m''(h'a) + \lambda\left[(a^{-2}m^2 + k^2)J_m(h'a) - a^{-1}J_m'(h'a)\right] \; ;$$

$$a_{12} = 2\mu aikJ_m''(\kappa' a) \; ;$$

$$a_{13} = 2\mu a^{-1} m\left(J_m'(\kappa' a) - a^{-1} J_m(\kappa' a)\right) ;$$

$$a_{21} = 2\mu a^{-1}\left[J_m'(h' a) - a^{-1} J_m(h' a)\right] ;$$

$$a_{22} = 2i\kappa m a^{-1} J_m(\kappa' a) - 2ikm J_m'(\kappa' a) ;$$

$$a_{23} = -J_m''(\kappa' a) - m^2 a^{-2} J_m(\kappa' a) + a^{-1} J_m'(\kappa' a) ;$$

$$a_{31} = -2ikJ_m'(h' a) ;$$

$$a_{32} = a^{-1} J_m'(\kappa' a)[m^2 - a^{-2}k^2 + 1] - 2m^2 a^{-2} J_m(\kappa' a) - J_m''(\kappa' a) - aJ_m'''(\kappa' a) ;$$

$$a_{33} = ikma^{-1} J_m(\kappa' a) .$$

Determinant (6.12) proves to be the same for cases that use Debye potentials and Debye-type potentials. This result indirectly confirms the correctness of the method chosen to solve the problem. Setting the determinant (6.12) equal to zero (which ensures a nontrivial solution), and assuming that the bar radius is a=1,0, we obtain a characteristic equation for determining the wavenumbers of three-dimensional flexural waves.

To estimate the response of a liquid to the phase velocities in the bar, the latter was placed in water. In this case, boundary conditions (6.9) through (6.11) complement the continuity condition for the normal components of the displacement vector in both the bar and the liquid:

$$U_r = -\frac{\partial \Phi_1}{\partial r}\Big|_{r=a} \quad (6.13)$$

where

$$\Phi_1 = e^{ikz} \sum_{m=0}^{\infty} D_m H_m^{(1)}(\gamma' r) \cos(m\phi) \ ; (6.14)$$

$\gamma' = (\gamma^2 - k^2)^{1/2}$;γ represents the wave number of a three-dimensional wave in the liquid; $H_m^{(1)}(\gamma' r)$ represents the Hankel function; and D_m represent unknown coefficients determined from boundary conditions.

Condition (6.9) becomes inhomogeneous:

$$(\lambda + 2\mu)\frac{\partial U_r}{\partial r} + \lambda\left(\frac{1}{r}\frac{\partial U_\phi}{\partial \phi} + \frac{1}{r}U_r + \frac{\partial U_z}{\partial z}\right)\Big|_{r=a} = \rho_0 \omega^2 \Phi_1 \quad , \qquad (6.15)$$

where ρ_0 represents the density of the liquid medium. Substituting expansions (6.8) and (6.14) in the boundary conditions (6.10), (6.11), (6.13) and (6.15), we arrive at the fourth-order determinant

$$\Delta = \begin{vmatrix} a_{11} & a_{12} & a_{13} & a_{14} \\ a_{21} & a_{22} & a_{23} & a_{24} \\ a_{31} & a_{32} & a_{33} & a_{34} \\ a_{41} & a_{42} & a_{43} & a_{44} \end{vmatrix} , (6.16)$$

where elements $a_{11} \div a_{33}$ coincide with those appearing in equation (6.12):

$$a_{14} = \rho_0 \omega^2 H_m(\gamma' a) ;$$

$$a_{24} = 0 ;$$

$$a_{34} = 0 ;$$

$$a_{41} = -J_m'(h' a) ;$$

$$a_{42} = aikJ_m'(\kappa' a) ;$$

$$a_{43} = a^{-1} m J_m'(\kappa' a) ;$$

$$a_{44} = -H_m'(\gamma' a)\ .$$

In the presence of the liquid, wave numbers k that make the determinant (6.16) equal to zero become complex because of the bar radiation causing irreversible losses. Unlike the bar, a flexural wave propagating in a cylindrical shell can be three-dimensional or two-dimensional (axisymmetric). The result reported in [101] was used in [102] and [103] to study phase velocities of elastic waves in an isotropic cylindrical shell.

To study a three-dimensional flexural wave propagating in an isotropic cylindrical shell, we applied the same mathematical device used to study flexural waves in a bar. However, in this case, the inclusion of the second (inner) boundary surface leads to a greater number of unknowns and a greater number of boundary conditions. Now, expansions of potentials Φ, V, and U take the following form [71, 104, 105]:

$$\left.\begin{aligned} \Phi &= e^{ikz}\sum_{m=0}^{\infty} \cos m\phi \left[A_m J_m(h'r) + B_m N_m(h'r)\right]; \\ V &= e^{ikz}\sum_{m=0}^{\infty} \cos m\phi \left[C_m J_m(\kappa'r) + D_m N_m(\kappa'r)\right]; \\ U &= e^{ikz}\sum_{m=1}^{\infty} \sin m\phi \left[E_m J_m(\kappa'r) + F_m N_m(\kappa'r)\right], \end{aligned}\right\} \qquad (6.17)$$

where $h' = (k_1^2 - k^2)^{1/2}$; $\kappa' = (k_2^2 - k^2)^{1/2}$; $N_m(h'r)$ represents the cylindrical Neumann function; and $A_m, B_m, C_m, D_m, E_m, F_m$ represent unknown coefficients determined from the boundary conditions, which are set at the outer $(r = a)$ and the inner $(r = b)$ surfaces of the shell.

Boundary conditions exist, in the absence of stresses, on the two surfaces of the shell:

(r=a and r=b)

$$(\lambda + 2\mu)\left(\frac{\partial U_r}{\partial r}\right) + \lambda\left[\frac{1}{r}\left(\frac{\partial U_\phi}{\partial \phi}\right) + \frac{1}{r}U_r + \left(\frac{\partial U_z}{\partial z}\right)\right]\Big|_{r=a;r=b} = 0 \qquad (6.18)$$

$$\left(\frac{\partial U_\phi}{\partial r}\right) + \frac{1}{r}U_\phi + \frac{1}{r}\left(\frac{\partial U_r}{\partial \phi}\right)\Big|_{r=a,r=b} = 0 \qquad (6.19)$$

$$\left(\frac{\partial U_r}{\partial r}\right) + \left(\frac{\partial U_z}{\partial z}\right)\Big|_{r=a,r=b} = 0 \qquad (6.20)$$

Substituting expansions (6.17) in boundary conditions (6.18 through 6.20) (using the orthogonality functions $\cos m\phi$ and $\sin m\phi$), we arrive at the following sixth-order determinant for the mth mode of three-dimensional flexural waves [71, 104, 105]:

$$\Delta = \begin{vmatrix} a_{11} & a_{12} & a_{13} & a_{14} & a_{15} & a_{16} \\ a_{21} & a_{22} & a_{23} & a_{24} & a_{25} & a_{26} \\ a_{31} & a_{32} & a_{33} & a_{34} & a_{35} & a_{36} \\ a_{41} & a_{42} & a_{43} & a_{44} & a_{45} & a_{46} \\ a_{51} & a_{52} & a_{53} & a_{54} & a_{55} & a_{56} \\ a_{61} & a_{62} & a_{63} & a_{64} & a_{65} & a_{66} \end{vmatrix}, \qquad (6.21)$$

where

$$\begin{aligned} a_{11} &= -(\lambda + 2\mu)J_m''(h'a) + \\ &\quad + \lambda\left[a^{-2}m^2 J_m(h'a) - a^{-1}J_m'(h'a) + k^2 J_m(h'a)\right]; \end{aligned}$$

$$\begin{aligned} a_{12} &= -(\lambda + 2\mu)N_m''(h'a) + \\ &\quad + \lambda\left[a^{-2}m^2 N_m(h'a) - a^{-1}N_m'(h'a) + k^2 N_m(h'a)\right]; \end{aligned}$$

$$\begin{aligned} a_{13} &= (\lambda + 2\mu)\left\{-ik_2 m^2\left[J_m(\kappa'a) - J_m'(\kappa'a)\right] + \right. \\ &\quad + ik_2 J_m''(\kappa'a) + ik_2 k^2\left[J_m(\kappa'a) + aJ_m'(\kappa'a)\right]\left.\right\} + \\ &\quad + \lambda\left\{ik_2 a^{-2}J_m(\kappa'a)(k^2 + m^2) - ik_2 a^{-1}J_m'(\kappa'a)(m^2 + k^2) - \right. \\ &\quad \left. - 2ik_2 k^2 J_m(\kappa'a) - ik_2 J_m''(\kappa'a)\right\}; \end{aligned}$$

$$a_{14} = (\lambda + 2\mu)\{-ik_2 m^2[N_m(\kappa' a) - N'_m(\kappa' a)] +$$
$$+ ik_2 N''_m(\kappa' a) + ik_2 k^2[N_m(\kappa' a) + aN'_m(\kappa' a)]\} +$$
$$+ \lambda\{ik_2 a^{-2} N_m(\kappa' a)(k^2 + m^2) - ik_2 a^{-1} N'_m(\kappa' a) \times$$
$$\times(m^2 + k^2) - 2ik_2 k^2 N_m(\kappa' a) - ik_2 N''_m(\kappa' a)\};$$

$$a_{15} = 2(\lambda + 2\mu)(a^{-2} - 1)ikmJ_m(\kappa' a);$$

$$a_{16} = 2(\lambda + 2\mu)(a^{-2} - 1)ikmN_m(\kappa' a);$$

$$a_{21} = -(\lambda + 2\mu)J''_m(h'b) +$$
$$+ \lambda[b^{-2} m^2 J_m(h'b) - b^{-1} J'_m(h'b) + k^2 J_m(h'b)];$$

$$a_{22} = -(\lambda + 2\mu)N''_m(h'b) +$$
$$+ \lambda[b^{-2} m^2 N_m(h'b) - b^{-1} N'_m(h'b) + k^2 N_m(h'b)];$$

$$a_{23} = (\lambda + 2\mu)\{-ik_2 m^2[J_m(\kappa' b) - J'_m(\kappa' b)] +$$
$$+ ik_2 J''_m(\kappa' b) + ik_2 k^2[J_m(\kappa' b) + bJ'_m(\kappa' b)]\} +$$
$$+ \lambda\{ik_2 b^{-2} J_m(\kappa' b)(k^2 + m^2) - ik_2 b^{-1} J'_m(\kappa' b)(m^2 + k^2) -$$
$$- 2ik_2 k^2 J_m(\kappa' b) - ik_2 J''_m(\kappa' b)\};$$

$$a_{24} = (\lambda + 2\mu)\{-ik_2 m^2[N_m(\kappa' b) - N'_m(\kappa' b)] +$$
$$+ ik_2 N''_m(\kappa' b) + ik_2 k^2[N_m(\kappa' b) + bN'_m(\kappa' b)]\} +$$
$$+ \lambda\{ik_2 b^{-2} N_m(\kappa' b)(k^2 + m^2) - ik_2 b^{-1} N'_m(\kappa' b) \times$$
$$\times(m^2 + k^2) - 2ik_2 k^2 N_m(\kappa' b) - ik_2 N''_m(\kappa' b)\};$$

$$a_{25} = 2(\lambda + 2\mu)(b^{-2} - 1)ikmJ_m(\kappa' b);$$

$$a_{26} = 2(\lambda + 2\mu)(b^{-2} - 1)ikmN_m(\kappa' b);$$

$$a_{31} = 2ma^{-1}[J'_m(h'a) - a^{-1} J_m(h'a)];$$

$$a_{32} = 2ma^{-1}[N'_m(h'a) - a^{-1} N_m(h'a)];$$

$$a_{33} = ik_2 m\{J_m(\kappa' a)[a^{-2}(2 - m^2) - k^2] - J''_m(\kappa' a) - a^{-1} J'_m(\kappa' a)\};$$

$$a_{34} = ik_2 m\{N_m(\kappa' a)[a^{-2}(2 - m^2) - k^2] - N''_m(\kappa' a) - a^{-1} N'_m(\kappa' a)\};$$

$$a_{35} = ikJ'_m(\kappa' a)ak_2^2;$$

$$a_{36} = ikN'_m(\kappa' a)ak_2^2;$$

$$a_{41} = 2mb^{-1}[J'_m(h'b) - b^{-1} J_m(h'b)];$$

$$a_{42} = 2mb^{-1}[N'_m(h'b) - b^{-1} N_m(h'b)];$$

$$a_{43} = ik_2 m\{J_m(\kappa' b)[b^{-2}(2 - m^2) - k^2] - J''_m(\kappa' b) - b^{-1} J'_m(\kappa' b)\};$$

$$a_{44} = ik_2 m\{N_m(\kappa' b)[b^{-2}(2 - m^2) - k^2] - N''_m(\kappa' b) - b^{-1} N'_m(\kappa' b)\};$$

$$a_{45} = ikJ'_m(\kappa' b)bk_2^2;$$

$$a_{46} = ikN'_m(\kappa' b)bk_2^2;$$

$$a_{51} = -2ikJ'_m(h'a);$$

$$a_{52} = -2ikN_m'(h'a);$$

$$a_{53} = -kk_2\{J_m(\kappa'a)(m^2 + a^{-1}k^2) + 5J_m'(\kappa'a) + aJ_m''(\kappa'a)\};$$

$$a_{54} = -kk_2\{N_m(\kappa'a)(m^2 + a^{-1}k^2) + 5N_m'(\kappa'a) + aN_m''(\kappa'a)\};$$

$$a_{55} = k_2^2 m[a^{-1}J_m(\kappa'a) - J_m'(\kappa'a)];$$

$$a_{56} = k_2^2 m[a^{-1}N_m(\kappa'a) - N_m'(\kappa'a)];$$

$$a_{61} = -2ikJ_m'(h'b);$$

$$a_{62} = -2ikN_m'(h'b);$$

$$a_{63} = -kk_2\{J_m(\kappa'b)(m^2 + b^{-1}k^2) + 5J_m'(\kappa'b) + bJ_m''(\kappa'b)\};$$

$$a_{64} = -kk_2\{N_m(\kappa'b)(m^2 + b^{-1}k^2) + 5N_m'(\kappa'b) + bN_m''(\kappa'b)\};$$

$$a_{65} = k_2^2 m[b^{-1}J_m(\kappa'b) - J_m'(\kappa'b)];$$

$$. a_{66} = k_2^2 m[b^{-1}N_m(\kappa'b) - N_m'(\kappa'b)];$$

Setting the determinant (6.21) equal to zero, we obtain the characteristic equation for wave numbers of the *m*th mode of three-dimensional flexural waves in an isotropic cylindrical shell with an arbitrary (but constant) thickness.

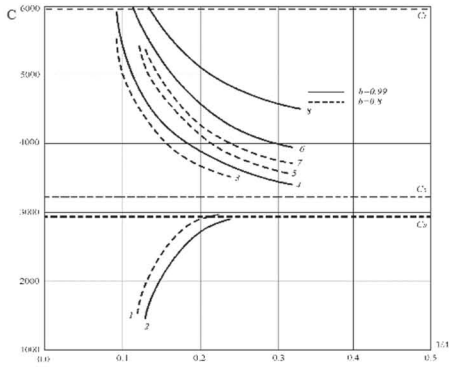

Figure 6-2: Phase velocities of three-dimensional flexural waves in steel shells

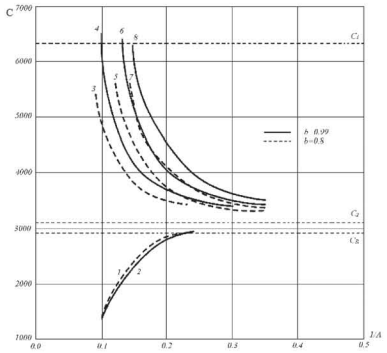

Figure 6-3: Phase velocities of three-dimensional flexural waves in aluminum shells

Figures 6-2 and 6-3 represent the solution to the characteristic equation for steel and aluminum shells of different thickness. In calculations, the outer radius a was assumed to be identical to 1,0 and the inner radius b had been given two values: b = 0,99 (indicated by a solid line) and 0,8 (indicated by a dashed line). The plots show velocity values for longitudinal (c_1), transverse (c_2) and Rayleigh (c_R) waves. The value of m=1 corresponds to the 0th mode of the flexural wave with its velocity asymptotically tending to the Rayleigh wave velocity c_R; $\Lambda = c_1/f$ is the wave length of the longitudinal wave propagating in the shell material;

and f is the wave frequency in hertz. Fig. 6-2 shows the phase velocities of three-dimensional flexural waves in steel shells, and Fig. 6-3 corresponds to aluminum shells.

Now, we will consider flexural and longitudinal axisymmetric waves. According to [71, 104], in the axisymmetric case, boundary conditions (6.18) through (6.20) are simplified; condition (6.19) vanishes; and condition (6.18) takes the form of

$$(\lambda + 2\mu)\left(\frac{\partial U_r}{\partial r}\right) + \lambda\left[\frac{1}{r}U_r + \left(\frac{\partial U_z}{\partial z}\right)\right]\Big|_{r=a,r=b} = 0 \quad (6.22)$$

The fourth-order determinant obtained from the boundary conditions takes the following form [71, 104, 105]:

$$\Delta = \begin{vmatrix} a_{11} & a_{12} & a_{13} & a_{14} \\ a_{21} & a_{22} & a_{23} & a_{24} \\ a_{31} & a_{32} & a_{33} & a_{34} \\ a_{41} & a_{42} & a_{34} & a_{44} \end{vmatrix}; \quad (6.23)$$

where

$$a_{11} = -(\lambda + 2\mu)J_0''(h'a) + \lambda\left[k^2 J_0(h'a) - a^{-1}J_0'(h'a)\right];$$

$$a_{12} = -(\lambda + 2\mu)N_0''(h'a) + \lambda\left[k^2 N_0(h'a) - a^{-1}N_0'(h'a)\right];$$

$$a_{13} = -2i\mu k J_1'(\kappa'a);$$

$$a_{14} = -2i\mu k N_1'(\kappa'a);$$

$$a_{21} = -(\lambda + 2\mu)J_0''(h'b) + \lambda\left[k^2 J_0(h'b) - b^{-1}J_0'(h'b)\right];$$

$$a_{22} = -(\lambda + 2\mu)N_0''(h'b) + \lambda\left[k^2 N_0(h'b) - b^{-1}N_0'(h'b)\right];$$

$$a_{23} = -2i\mu k J_1'(\kappa'b);$$

$$a_{24} = -2i\mu k N_1'(\kappa'b);$$

$$a_{31} = -2ikJ_0'(h'a);$$

$$a_{32} = -2ikN_0'(h'a);$$

$$a_{33} = k^2 J_1(\kappa'a) - J_1(\kappa'a) + J_1'(\kappa'a) + J_1''(\kappa'a);$$

$$a_{34} = k^2 N_1(\kappa'a) - N_1(\kappa'a) + N_1'(\kappa'a) + N_1''(\kappa'a);$$

$$a_{41} = -2ikJ_0'(h'b);$$

$$a_{42} = -2ikN_0'(h'b);$$

$$a_{43} = k^2 J_1(\kappa'b) - J_1(\kappa'b) + J_1'(\kappa'b) + J_1''(\kappa'b);$$

$$a_{44} = k^2 N_1(\kappa'b) - N_1(\kappa'b) + N_1'(\kappa'b) + N_1''(\kappa'b). \text{ EE}$$

Expanding the determinant (6.23) and setting it equal to zero, we obtain the characteristic equation for wave numbers of flexural and longitudinal axisymmetric waves.

For torsional axisymmetric waves, the determinant is given in [71]:

$$\Delta = \begin{vmatrix} a^{-1}J_1'(\kappa_1 a) - J_1(\kappa_1 a)a^{-2} & a^{-1}N_1'(\kappa_1 a) - N_1(\kappa_1 a)a^{-2} \\ b^{-1}J_1'(\kappa_1 b) - b^{-2}J_1(\kappa_1 b) & b^{-1}N_1'(\kappa_1 b) - b^{-2}N_1(\kappa_1 b) \end{vmatrix}, \quad (6.24)$$

where $\kappa_1 = (k_2^2 - k^2)^{1/2}$ in which k is the desired wave number of the torsional axisymmetric wave in the shell. Setting determinant (6.24) equal to zero, we obtain the characteristic equation for wave numbers of torsional axisymmetric waves.

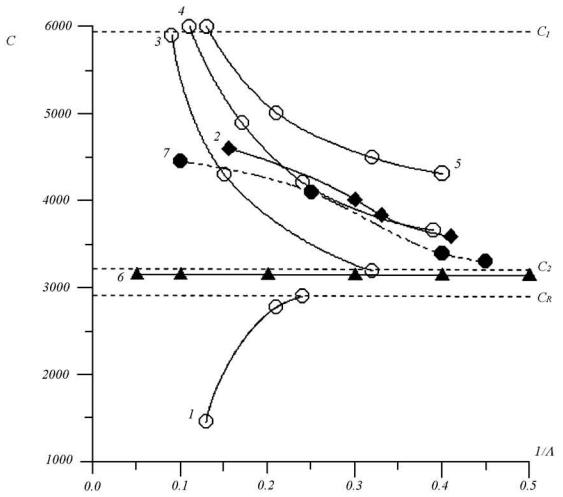

Figure 6-4: Phase velocities of flexural, longitudinal, and torsional axisymmetric waves in the shell

Fig. 6-4 shows the phase velocities of flexural, longitudinal, and torsional axisymmetric waves. Curve *1* characterizes the phase velocity of the 0th mode of the flexural wave; curve *2* corresponds to the 0th mode of the longitudinal wave; curves *3, 4,* and *5* correspond to nonzero modes of longitudinal and flexural waves; straight line *6* is for the 0th mode of the torsional wave; curve *7* is for the first mode of the torsional wave; and Φ_1.

To determine the influence of both the external and the internal liquid media on the dispersion curves of phase velocities in the shell, we add two columns and two rows to the sixth-order determinant (6.21). Therefore, it is transformed into an eighth-order determinant, while the fourth-order determinant is transformed into a sixth-order one. Sound wave potentials Φ_1 (in the external medium) and Φ_2 (in the shell filler) are expanded in cylindrical functions according to the following formulas:

$$\Phi_1 = \sum_{m=0}^{\infty} G_m H_m^{(1)}(\gamma_1 r)\cos m\phi e^{ikz}, \qquad (6.25)$$

$$\Phi_2 = \sum_{m=0}^{\infty} K_m J_m(\gamma_2 r)\cos m\phi e^{ikz}, \qquad (6.26)$$

where $\gamma_1 = \sqrt{(\omega/c_3)^2 - k^2}$; $\gamma_2 = \sqrt{(\omega/c_4)^2 - k^2}$; c_3 and c_4 are velocities of sound in external and internal media, respectively.

The surface wave vector component along the Z-axis, $z \Rightarrow k$ is the same as in shell due to Snell's law. The boundary condition (6.18) set for normal stresses at two surfaces of the shell is transformed as follows:

$$(\lambda + 2\mu)(\partial U_r/\partial r) + \\ +\lambda\left[\frac{1}{r}\left(\frac{\partial U_\phi}{\partial \phi}\right) + \frac{1}{r}U_r + (\partial U_z/\partial z)\right] + i\omega\rho_1\Phi_1 = 0, \quad |_{r=a} \qquad (6.27)$$

where ρ_1 represents the density of the external medium and

$$(\lambda + 2\mu)(\partial U_r/\partial r) + \\ +\lambda\left[\frac{1}{r}\left(\frac{\partial U_\phi}{\partial \phi}\right) + \frac{1}{r}U_r + (\partial U_z/\partial z)\right] + i\omega\rho_2\Phi_2 = 0, \quad |_{r=b} \qquad (6.28)$$

where ρ_2 represents the density of the internal medium. In addition, two other boundary conditions, which consist of the continuity of normal components in the displacement vector at the two boundaries, are necessary:

$$\frac{\partial \Phi}{\partial r} + \frac{1}{r}\frac{\partial A_z}{\partial \phi} - \frac{\partial A_\phi}{\partial z} - \frac{\partial \Phi_1}{\partial r}\Big|_{r=a} = 0 \qquad (6.29)$$

$$\frac{\partial \Phi}{\partial r}+\frac{1}{r}\frac{\partial A_z}{\partial \phi}-\frac{\partial A_\phi}{\partial z}-\frac{\partial \Phi_2}{\partial r}\Big|_{r=b}=0 \tag{6.30}$$

In the axisymmetric case, condition (6.22) is transformed as follows:

$$(\lambda+2\mu)\left(\frac{\partial U_r}{\partial r}\right)+\lambda\left[\frac{1}{r}U_r+\left(\frac{\partial U_z}{\partial z}\right)\right]+i\omega\rho_1\Phi_1\Big|_{r=a}=0 \tag{6.31}$$

$$(\lambda+2\mu)\left(\frac{\partial U_r}{\partial r}\right)+\lambda\left[\frac{1}{r}U_r+\left(\frac{\partial U_z}{\partial z}\right)\right]+i\omega\rho_2\Phi_2\Big|_{r=b}=0 \tag{6.32}$$

In the axisymmetric case, the added boundary conditions are expressed as follows:

$$\frac{\partial \Phi}{\partial r}-\frac{\partial A}{\partial z}-\frac{\partial \Phi_1}{\partial r}=0\Big|_{r=a} \tag{6.33}$$

$$\frac{\partial \Phi}{\partial r}-\frac{\partial A}{\partial z}-\frac{\partial \Phi_2}{\partial r}=0\Big|_{r=b} \tag{6.34}$$

Here,

$$\Phi_1=G_0H_0^{(1)}(\gamma_1 r)e^{ikz}; \tag{6.35}$$

$$\Phi_2=K_0J_0(\gamma_2 r)e^{ikz}. \tag{6.36}$$

Boundary conditions (6.27), (6.28), (6.33), and (6.34) add two rows to the determinant, and factors multiplying unknown coefficients G_m, K_m или G_0, K_0 (the axisymmetric problem) add two columns. In each of these two columns, only two rows are not zero. If the shell is in contact with the liquid on one side only (while the other side is in contact with the vacuum), the determinant used for finding wave numbers will be of seventh order in the three-dimensional problem and of fifth order in the axisymmetric case: i. e., the corresponding determinants (6.21) and (6.23) will each acquire one additional row and column.

6.2. The Dynamic Theory of the Elasticity of the Transversely Isotropic Medium

Based on the use of the dynamic theory of the elasticity of the anisotropic medium and with the help of the hypothesis of the shells being thin, the characteristic equation for wave numbers of elastic waves in the thin transversely isotropic cylindrical shell is determined.

Let us consider the infinite thin transversely isotropic cylindrical shell. The elastic wave is spread along the axis Z that is orthogonal to the plane of the isotropy. The transversely isotropic elastic medium is characterized by the five elastic moduli [19]: $A_{11}, A_{12}, A_{13}, A_{33}, A_{44}$ or by the technical modules $E_1, E_3, \mu_1, \mu_3, \nu_1, \nu_3$. In the chosen orientation of the axis, $Z-E_1$, is the Young's modulus; $\mu_1$is the shear modulus; $\nu_1$is the Poisson's ratio in the plane of the isotropy; and$E_3, \mu_3$and ν_3 are the same values in the transverse plane. These modules are connected with each other by the relationship [39, 67, 71, 106]:

$$\left.\begin{aligned} &A_{11}=\frac{E_1}{(1+\nu_1)m}\left(1-\nu_3^2\frac{E_1}{E_3}\right)\ ;\quad A_{33}=E_3(1-\nu_3)/m\ ;\\ &A_{44}=\mu_3\ ;\quad A_{12}=\frac{E_1}{(1+\nu_1)m}\left(\nu_1+\nu_3^2\frac{E_1}{E_3}\right)\ ;\quad A_{13}=E_1\nu_3/m\ ;\\ &\frac{A_{11}-A_{12}}{2}=\mu_1\ ;\quad m=1-\nu_1-2\nu_3^2\frac{E_1}{E_3}\ . \end{aligned}\right\} \tag{6.37}$$

Hooke's law for the transversely isotropic elastic medium is written in the next form [39]:

$$\left.\begin{aligned}
&\sigma_r = A_{11}\varepsilon_r + A_{12}\varepsilon_\phi + A_{13}\varepsilon_z \ ;\\
&\sigma_\phi = A_{12}\varepsilon_r + A_{11}\varepsilon_\phi + A_{13}\varepsilon_z \ ;\\
&\sigma_z = A_{13}\left(\varepsilon_r + \varepsilon_\phi\right) + A_{33}\varepsilon_z \ ;\\
&\tau_{\phi z} = A_{44}\gamma_{\phi z} \ ;\\
&\tau_{rz} = A_{44}\gamma_{rz} \ ;\\
&\tau_{r\phi} = \frac{1}{2}(A_{11} - A_{12})\gamma r_z \ ,
\end{aligned}\right\} (6.38)$$

where $\varepsilon_r, \varepsilon_\varphi, \varepsilon_z, \gamma_{rz}, \gamma_{\varphi z}, \gamma_{r\varphi}$ are components of the tensor of deformations, which are equal to each other [19]:

$$\left.\begin{aligned}
&\varepsilon_r = \partial U_r/\partial r \ ; \quad \varepsilon_z = \partial U_z/\partial z \ ;\\
&\varepsilon_\phi = r^{-1}\left(\partial U_\phi/\partial\phi\right) + U_r/r \ ;\\
&\gamma_{\phi z} = r^{-1}(\partial U_z/\partial\phi) + \partial U_\phi/\partial z \ ;\\
&\gamma_{rz} = (\partial U_r/\partial z) + \partial U_z/\partial r \ ;\\
&\gamma_{r\phi} = \left(\partial U_\phi/\partial r\right) - r^{-1}U_\phi + r^{-1}(\partial U_r/\partial\phi) \ .
\end{aligned}\right\} (6.39)$$

where U_r, U_φ, U_z are components of the displacement vector $\vec{U}$.

Equations of the dynamic balance in the circular cylindrical system of coordinates with the harmonic dependence starting from the time of $exp(i\omega t)$ have the following appearance [39, 67, 71, 106]:

$$\left.\begin{aligned}
&(\partial\sigma_r/\partial r) + r^{-1}\left(\partial\tau_{r\phi}/\partial\phi\right) + (\partial\tau_{rz}/\partial z) + r^{-1}\left(\sigma_r - \sigma_\phi\right) + \rho\omega^2 U_r = 0 \ ;\\
&\left(\partial\tau_{r\phi}/\partial r\right) + r^{-1}\left(\partial\sigma_\phi/\partial\phi\right) + \left(\partial\tau_{\phi z}/\partial z\right) + r^{-1}2\tau_{r\phi} + \rho\omega^2 U_\phi = 0 \ ;\\
&(\partial\tau_{rz}/\partial r) + r^{-1}\left(\partial\tau_{\phi z}/\partial\phi\right) + (\partial\sigma_z/\partial z) + r^{-1}\tau_{rz} + \rho\omega^2 U_z = 0 \ ,
\end{aligned}\right\} (6.40)$$

where

$$\left.\begin{aligned}
&\sigma_r = A_{11}\frac{\partial U_r}{\partial r} + \frac{A_{12}}{r}\frac{\partial U_\phi}{\partial\phi} + \frac{A_{12}}{r}U_r + A_{13}\frac{\partial U_z}{\partial z} \ ;\\
&\sigma_\phi = A_{12}\frac{\partial U_r}{\partial r} + \frac{A_{11}}{r}\frac{\partial U_\phi}{\partial\phi} + \frac{A_{11}}{r}U_r + A_{13}\frac{\partial U_z}{\partial z} \ ;\\
&\sigma_z = A_{13}\frac{\partial U_r}{\partial r} + \frac{A_{13}}{r}\frac{\partial U_\phi}{\partial\phi} + \frac{A_{13}}{r}U_r + A_{33}\frac{\partial U_z}{\partial z} \ ;\\
&\tau_{\phi z} = \frac{A_{44}}{r}\frac{\partial U_z}{\partial\phi} + A_{44}\frac{\partial U_\phi}{\partial z} \ ; \qquad \tau_{rz} = A_{44}\frac{\partial U_r}{\partial z} + A_{44}\frac{\partial U_z}{\partial r} \ ;\\
&\tau_{r\phi} = \frac{A_{11}}{2}\frac{\partial U_\phi}{\partial r} - \frac{A_{11}}{2r}U_\phi + \frac{A_{11}}{2r}\frac{\partial U_r}{\partial\phi} - \frac{A_{12}}{2}\frac{\partial U_\phi}{\partial z} + \frac{A_{12}}{2r}U_\phi - \frac{A_{12}}{2r}\frac{\partial U_r}{\partial\phi} \ .
\end{aligned}\right\} (6.41)$$

Components of the displacement vector U_r, U_φ, U_z can be presented in the following series form [67, 71, 106]:

$$\left.\begin{aligned}
&U_r = e^{ikz}\textstyle\sum_{m=0}^{\infty}\cos m\,\phi\cdot U_m(r) \ ;\\
&U_\phi = e^{ikz}\textstyle\sum_{m=1}^{\infty}\cos m\,\phi\cdot V_m(r) \ ;\\
&U_z = e^{ikz}\textstyle\sum_{m=0}^{\infty}\cos m\,\phi\cdot W_m(r) \ ,
\end{aligned}\right\} (6.42)$$

where k is the wave number of the elastic wave.

Then, substituting (6.41) into (6.40), we receive equations of the dynamic balance in displacements [67, 71, 106]:

$$\frac{\partial^2 U_r}{\partial r^2} - r^{-2}a_1\frac{\partial U_\phi}{\partial\phi} + r^{-1}a_2\frac{\partial^2 U_\phi}{\partial r\partial\phi} - r^{-2}U_r + r^{-1}\frac{\partial U_r}{\partial r} +$$
$$+a_3\frac{\partial^2 U_z}{\partial r\partial z} + r^{-2}a_1\frac{\partial^2 U_r}{\partial\phi^2} + a_4\frac{\partial^2 U_r}{\partial z^2} - r^{-2}\frac{\partial U_\phi}{\partial\phi} + a_5 U_r = 0 \ , (6.43)$$

$$r^{-2}\frac{\partial^2 U_\phi}{\partial\phi^2} + a_1\frac{\partial^2 U_\phi}{\partial r^2} - a_1 r^{-2}U_\phi + a_1 r^{-1}\frac{\partial U_\phi}{\partial\phi} +$$
$$+(1+a_1)r^{-2}\frac{\partial U_r}{\partial\phi} + a_2\frac{\partial^2 U_r}{\partial r\partial\phi} + r^{-1}a_3\frac{\partial^2 U_z}{\partial z\partial\phi} +$$

$$+a_4\frac{\partial^2 U_\phi}{\partial z^2}+a_5U_\phi=0\ ;(6.44)$$

$$\frac{\partial^2 U_z}{\partial r^2}+a_6\frac{\partial^2 U_z}{\partial z^2}+a_7\frac{\partial^2 U_r}{\partial r\partial z}+r^{-1}a_7\frac{\partial^2 U_\phi}{\partial z\partial\phi}+r^{-2}\frac{\partial^2 U_z}{\partial\phi^2}+$$
$$+r^{-1}a_7\frac{\partial U_r}{\partial z}+r^{-1}\frac{\partial U_z}{\partial r}+a_8U_z=0\ ,(6.45)$$

where $a_1=\frac{A_{11}-A_{12}}{2A_{11}}$; $a_2=\frac{A_{11}+A_{12}}{2A_{11}}$; $a_3=\frac{A_{13}+A_{44}}{A_{11}}$; $a_4=\frac{A_{44}}{A_{11}}$; $a_5=\frac{\rho\omega^2}{A_{11}}$; $a_6=\frac{A_{33}}{A_{44}}$; $a_7=\frac{A_{44}+A_{13}}{A_{44}}$; $a_8=\frac{\rho\omega^2}{A_{44}}$.

Now if components of the displacement vector U_r, U_φ, U_z taken from (6.42) are substituted into (6.43) through (6.45), then we receive the following equations for the radial functions $U_m(r), V_m(r), W_m(r)$ [67, 71, 106]:

$$\frac{\partial^2 U_m}{\partial r^2}-r^{-2}a_1mV_m+r^{-1}a_2m\frac{\partial V_m}{\partial r}-r^{-2}U_m+r^{-1}\frac{\partial U_m}{\partial r}+$$
$$+a_3ik\frac{\partial W_m}{\partial r}-r^{-2}a_1m^2U_m-a_4k^2U_m-r^{-2}mV_m+a_5U_m=0\ ,(6.46)$$

$$r^{-2}m^2V_m+a_1\frac{\partial^2 V_m}{\partial r^2}-a_1r^{-2}V_m+a_1r^{-1}\frac{\partial V_m}{\partial r}-$$
$$-(a_1+1)r^{-2}mU_m-a_2m\frac{\partial U_m}{\partial r}-r^{-1}a_3mikW_m-$$
$$-a_4k^2V_m+a_5V_m=0\ ;(6.47)$$

$$\frac{\partial U_m}{\partial r}+a_9r^{-1}mV_m+a_9r^{-1}U_m+a_{10}ikW_m\Big|_{\substack{r=a\\r=b}}=0\ .(6.48)$$

The boundary conditions are as follows: normal (σ_r) and tangent ($\tau_{r\varphi}, \tau_{rz}$) stresses on both the external ($r=a$) and internal ($r=b$) surfaces of the elastic shell are equal to zero. These values are added to equations (6.46) through (6.48) [67, 71, 106]:

$$\frac{\partial U_m}{\partial r}+a_9r^{-1}mV_m+a_9r^{-1}U_m+a_{10}ikW_m\Big|_{\substack{r=a\\r=b}}=0\ ;(6.49)$$

$$\frac{\partial V_m}{\partial r}-r^{-1}V_m-r^{-1}mU_m\Big|_{\substack{r=a\\r=b}}=0\ ;(6.50)$$

$$ikU_m+\frac{\partial W_m}{\partial r}\Big|_{\substack{r=a\\r=b}}=0\ .(6.51)$$

where

$$a_9=\frac{A_{12}}{A_{11}}\ ;\ a_{10}=\frac{A_{13}}{A_{11}}\ .$$

6.3. Hypothesis of Thin Shells

The fellow parameter $\xi=\frac{z}{R_0}$ can be used for thin shells, where $R_0=\frac{a+b}{2}$ is the middle radius and $z=r-R_0$ is the coordinate taken from the middle surface [67, 71, 106, 107]:

$$\left.\begin{aligned} U_m(r) &= \sum_{n=0}^{N_1} x_n \xi^n \ ; \\ V_m(r) &= \sum_{n=0}^{N_1} y_n \xi^n \ ; \\ W_m(r) &= \sum_{n=0}^{N_1} z_n \xi^n \ . \end{aligned}\right\} (6.52)$$

We substitute decompositions (6.52) in the boundary conditions (6.49) through (6.51) and in six equations relative to $3(N_1 + 1)$ unknown coefficients x_n, y_n, z_n [91–93]:

$$R_0^{-1} \sum_{n=0}^{N_1} x_n n(\xi_1)^{n-1} + a_9 m(R_0 + h/2)^{-1} \sum_{n=0}^{N_1} y_n(\xi_1)^n +$$
$$+a_9(R_0 + h/2)^{-1} \sum_{n=0}^{N_1} x_n(\xi_1)^n + a_{10} ik \sum_{n=0}^{N_1} z_n(\xi_1)^n = 0 \ , (6.53)$$

$$R_0^{-1} \sum_{n=0}^{N_1} x_n n(-\xi_1)^{n-1} + a_9 m(R_0 - h/2)^{-1} \sum_{n=0}^{N_1} y_n(-\xi_1)^n +$$
$$+a_9(R_0 - h/2)^{-1} \sum_{n=0}^{N_1} x_n(-\xi_1)^n + a_{10} ik \sum_{n=0}^{N_1} z_n(-\xi_1)^n = 0 \ ; (6.54)$$

$$R_0^{-1} \sum_{n=0}^{N_1} y_n n(\xi_1)^{n-1} - (R_0 + h/2)^{-1} \sum_{n=0}^{N_1} y_n(\xi_1)^n -$$
$$-m(R_0 + h/2)^{-1} \sum_{n=0}^{N_1} x_n(\xi_1)^n = 0 \ ; (6.55)$$

$$R_0^{-1} \sum_{n=0}^{N_1} y_n n(-\xi_1)^{n-1} - (R_0 + h/2)^{-1} \sum_{n=0}^{N_1} y_n(-\xi_1)^n -$$
$$-m(R_0 + h/2)^{-1} \sum_{n=0}^{N_1} x_n(-\xi_1)^n = 0 \ ; (6.56)$$

$$ik \sum_{n=0}^{N_1} x_n(\xi_1)^n + R_0^{-1} \sum_{n=0}^{N_1} z_n n(\xi_1)^{n-1} = 0 \ ; (6.57)$$

$$ik \sum_{n=0}^{N_1} x_n(-\xi_1)^n + R_0^{-1} \sum_{n=0}^{N_1} z_n n(-\xi_1)^{n-1} = 0 \ . (6.58)$$

The rest of the equations can be derived, by means of the substitution of the decompositions (6.52) into equations (6.46) through (6.48) and by the equating of coefficients of identical powers ξ_1 [91–93]:

$$\begin{aligned} &x_{n+2}(n+2)(n+1) + x_{n+1}(n+1)(2n+1) + \\ &+x_n(n^2 - 1 - a_1 m^2 - a_4 k^2 R_0^2 + a_5 R_0^2) + \\ &+x_{n-1} 2R_0^2(a_5 - k^2 a_4) + x_{n-2} R_0^2(a_5 - k^2 a_4) + \\ &+y_{n+1}(n+1) a_2 m + y_n[a_2 mn - a_1(m+1)] + \\ &+z_{n+1} ikR_0(n+1)a_3 + z_n 2ikR_0 n a_3 + z_{n-1} ikR_0(n-1)a_3 = 0 \ ; (6.59) \end{aligned}$$

$$\begin{aligned} &-x_{n+1} a_2 mR_0(n+1) - x_n m(a_1 + 1 + 2a_2 R_0 n) - x_{n-1} a_2 mR_0(n-1) + \\ &+y_{n+2} a_1(n+2)(n+1) + y_{n+1}(n+1)a_1(1+2n) - \\ &-y_n[a_1(n^2 - 1) - m^2 - a_4 k^2 R_0^2 + a_5 R_0^2] - y_{n-1} 2R_0^2(a_4 k^2 - a_5) - \\ &-y_{n-2} R_0^2(a_4 k^2 - a_5) - z_n a_3 mikR_0 - z_{n-1} a_3 mikR_0 = 0 \ ; (6.60) \end{aligned}$$

$$\begin{aligned} &x_{n+1}(n+1)a_7 ikR_0 + x_n ikR_0 a_7(2n+1) + x_{n-1} a_7 ikR_0 n + \\ &+y_n a_7 mikR_0 + y_{n-1} a_7 mikR_0 + z_{n+2}(n+2)(n+1) + \\ &+z_{n+1}(n+1)(2n+1) + z_n(n^2 - m^2 - a_6 k^2 R_0^2 + a_8 R_0^2) - \\ &-z_{n-1} 2R_0^2(a_6 k^2 - a_6) - z_{n-2} R_0^2(a_6 k^2 - a_6) = 0 \ , (6.61) \end{aligned}$$

where $n = 0,1,2,\ldots$

It is necessary to use $3(N_1 + 1) - 6$ in equations (6.59) through (6.61) and to use $n = 0$ and $n = 1$ coefficients with negative indexes are equal to zero. Then, in common with equations through (6.58), the

homogeneous system of $3(N_1+1)$ equations relative to the coefficients x_n, y_n, z_n is formed. Afterwards, we expand the determinant of this system and let this determinant be equal to zero. We receive the characteristic equation for wave numbers k in the elastic waves of the mode m in the transversely isotropic cylindrical shell.

Now we turn to elastic waves, which have axial symmetry, where the dependence on the angle φ disappears. If the vector of the shell displacement $\vec{U}$does not have the component U_φ, then we have waves with vertical polarization. In this case, the components of the strains $\gamma_{r\varphi}, \gamma_{\varphi z}$ and tangent stresses $\tau_{r\varphi}, \tau_{\varphi z}$ are equal to zero, but stresses $\sigma_r, \sigma_\varphi, \sigma_z$ and τ_{rz} are equal to [67, 71, 106]:

$$\left.\begin{aligned}
\sigma_r &= A_{11}\frac{\partial U_r}{\partial r}+\frac{A_{12}}{r}U_r+A_{13}\frac{\partial U_z}{\partial z}\ ;\\
\sigma_\phi &= A_{12}\frac{\partial U_r}{\partial r}+\frac{A_{11}}{r}U_r+A_{13}\frac{\partial U_z}{\partial z}\ ;\\
\sigma_z &= A_{13}\frac{\partial U_r}{\partial r}+\frac{A_{13}}{r}U_r+A_{33}\frac{\partial U_z}{\partial z}\ ;\\
\tau_{rz} &= A_{44}\frac{\partial U_r}{\partial z}+A_{44}\frac{\partial U_z}{\partial r}\ .
\end{aligned}\right\} \quad (6.62)$$

Dynamic balance equations, where two take the following form [67, 71, 106]:

$$\left.\begin{aligned}
&A_{11}\left(\frac{\partial^2 U_r}{\partial r^2}+\frac{1}{r}\frac{\partial U_r}{\partial r}-\frac{U_r}{r^2}\right)+A_{44}\left(\frac{\partial^2 U_r}{\partial z^2}+\frac{\partial^2 U_z}{\partial r^2}\right)+\\
&+A_{13}\frac{\partial^2 U_z}{\partial z\partial r}+\rho\omega^2 U_r=0\ ;\\
&A_{44}\left(\frac{\partial^2 U_r}{\partial r\partial z}+\frac{\partial^2 U_z}{\partial r^2}+\frac{1}{r}\frac{\partial U_r}{\partial z}+\frac{1}{r}\frac{\partial U_z}{\partial r}\right)+\\
&+A_{13}\left(\frac{\partial^2 U_r}{\partial r\partial z}+\frac{1}{r}\frac{\partial U_r}{\partial z}\right)+A_{33}\frac{\partial^2 U_z}{\partial z^2}+\rho\omega^2 U_z=0\ .
\end{aligned}\right\} \quad (6.63)$$

Displacements U_r and U_z can be introduced in the following form [67, 71, 106]:

$$\left.\begin{aligned}
U_r &= e^{ikz}U(r)\ ;\\
U_z &= e^{ikz}W(r)\ .
\end{aligned}\right\} \quad (6.64)$$

For the thin shell the components, $U(r)$ and $W(r)$ can be expanded in the following series:

$$\left.\begin{aligned}
U(r) &= \sum_{n=0}^{N_1} x_n\xi^n\ ;\\
W(r) &= \sum_{n=0}^{N_1} z_n\xi^n\ .
\end{aligned}\right\} \quad (6.65)$$

Boundary conditions can be expressed as [91–93]

$$\left.\begin{aligned}
&\frac{\partial V}{\partial r}+a_9 r^{-1}V+a_{10}ikW\Big|_{\substack{r=a\\r=b}}=0\ ;\\
&ikV+\frac{\partial W}{\partial r}\Big|_{\substack{r=a\\r=b}}=0\ .
\end{aligned}\right\} \quad (6.66)$$

When (6.64) and (6.65) are not inserted into boundary conditions (6.66) and are inserted into dynamic balance equations instead then (6.63) results in the system of $2(N_1+1)$ equations in order to calculate unknown coefficients x_n, z_n. The characteristic equation for wave numbers k of elastic axisymmetrical waves in the transversely isotropic cylindrical shell are received by expanding the determinant, which is equal to zero. The axisymmetrical wave of the horizontal polarization (torsional wave) has only one component (U_φ) of the displacement vector $\vec{U}$. The problem, in this case, has an analytical solution. Components of strains $\varepsilon_r, \varepsilon_\varphi, \varepsilon_z, \gamma_{rz}$ are equal to zero, but components of strains $\gamma_{\varphi z}$ and $\gamma_{r\varphi}$ are equal to the following: $\gamma_{\varphi z}=\frac{\partial U_\varphi}{\partial z}; \gamma_{r\varphi}=\frac{\partial U_\varphi}{\partial r}-\frac{U_\varphi}{r}$.

The equation of the dynamic balance has the following form:

$$\frac{\partial \tau_{r\phi}}{\partial r} + \frac{\partial \tau_{\phi z}}{\partial z} + \frac{2\tau_{r\phi}}{r} + \rho\omega^2 U_\phi = 0 \text{ (6.67)}$$

Using (6.38) and (6.39), we can describe (6.67) in the following form:

$$\mu_1 \frac{\partial^2 U_\phi}{\partial r^2} + \mu_3 \frac{\partial^2 U_\phi}{\partial z^2} - \frac{\mu_1}{r^2} U_\phi + \frac{\mu_1}{r} \frac{\partial U_\phi}{\partial r} + \rho\omega^2 U_\phi = 0 \text{ . (6.68)}$$

The component U_φ can be presented as:

$$U_\phi = V(r) \cdot e^{i(k_t z - \omega t)} \text{ , (6.69)}$$

where k_t is the torsional wave number.

We substitute (6.68) in) (6.69) and, as a result have

$$\frac{d^2V}{dr^2} + \frac{1}{r}\frac{dV}{dr} + \left(\frac{\rho\omega^2}{\mu_1} - k_t^2 \frac{\mu_3}{\mu_1} - \frac{1}{r^2}\right) V = 0 \text{ . (6.70)}$$

The equation (6.70) is the Bessel equation for Bessel $J_1(\chi_1 r)$ and Neumann $N_1(\chi_1 r)$ functions of the first order:

$$V(r) = BJ_1(\chi_1 r) + CN_1(\chi_1 r) \text{ , (6.71)}$$

where $B$and C are arbitrary constants; $\chi_1 = \left(\kappa^2 - k_t^2 \frac{\mu_3}{\mu_1}\right)^{1/2}$; $\chi = \left(\sqrt{\mu_1/\rho}\right)^{-1} \omega$.

From the boundary condition $\tau_{r_\varphi} = 0$ [r=a;r=b], we receive a determinant for torsional wave numbers k_t:

$$\Delta = \begin{vmatrix} J_1'(\chi_1 a) - \frac{1}{a} J_1(\chi_1 a) & N_1'(\chi_1 a) - \frac{1}{a} N_1(\chi_1 a) \\ J_1'(\chi_1 b) - \frac{1}{b} J_1(\chi_1 b) & N_1'(\chi_1 b) - \frac{1}{b} N_1(\chi_1 b) \end{vmatrix} = 0, \text{ (6.72)}$$

where $J_1'(\chi_1 a) = \left.\frac{\partial J_1(\chi_1 r)}{\partial r}\right|_{r=a}$

CHAPTER 7

DIFFRACTION OF SOUND ON BODIES IN THE FORM OF SPHEROIDS AND ELLIPTICAL CYLINDERS

7.1. The Characteristics of the Reflectivity of Scatterers and Types of Boundary Conditions

In this section, the resonances of prolate and oblate spheroidal bodies are investigated. Hydroacoustics, as a rule, studies the distant scattered fields of various bodies. Pressure in a scattered wavep_s (scattered pressure) of the circular frequency ω in the Fraunhofer zone (far field) in an unbounded liquid for the final body can be represented in the form [7, 55, 108]:

$$p_s(r,\theta,\phi) = (A/r)D(\theta,\phi)\, exp[-i(\omega t - kr)], (7.1)$$

where r, θ, φ represent spherical coordinates of the observation point; $D\ (\theta;\ \varphi)$ represents the angular characteristic of the scatterer; $k=2\pi/\lambda$ represents the number of waves in a liquid; λ represents the length of a sound wave in a liquid medium; and A represents the amplitude factor. In other words, it is possible to separate the characteristics of a scattering body, the wave size of the scatterer, and its shape, material, and orientation relative to the source and the observer, thereby determining $D\ (\theta;\ \varphi) = 1$ the characteristics of the source (amplitude A of the wave created at the location of the scatterer) and the distance r to the observation point.

We assume that the distance r from the source (the irradiating antenna) to the scatterer is such that, in the incident wave, the pressure p_i obeys a relation of the type (7.1) [7, 55, 108]:

$$. p_i(r_1;\theta_1;\phi_1) = (B/r_1)D(\theta_1;\phi_1)\, exp[-i(\omega t - kr_1)], (7.2),$$

where r, θ, and φ represent the scatter's coordinates in a system of the source's spherical coordinates; $D\ (\theta;\ \varphi)$ represents the angular characteristic of a radiation system; B represents the amplitude of the pressure of the wave created by the source at a distance of 1m from $A=B/r$.

For the intensity I_s of the reflected signal at the observation point, we can write the following [7, 55, 108]:

$$I_s = (A^2|D(\theta;\phi)|^2)/(r^2 2\rho_0 c) = K(I_0/r^2), \quad (7.3)$$

where $K = |D(\theta;\phi)|^2; I_0 = A^2/2\rho_0 c$ represents the intensity of the wave incident on the reflecting object (the source is non-directed $D\ (\theta;\ \varphi) = 1$).

As a rule, the distance from the source to the scatterer is such that the wave incident on the body, at least within its geometric dimensions, can be considered to be flat.

For the logarithm (7.3), we obtain the following:

$$10\, lg\, I_s = 10\, lg\, K + 10\, lg\, I_0 - 20\, lg\, r. (7.4)$$

In real conditions, the intensity $I_s$of the reflected wave decreases more rapidly than r^2does, due to the sound attenuation in the marine environment. Therefore, the total attenuation, due to the spacing of the front of the spherical wave, is denoted by $2H$.

The quantity, $10lgK$, is called the strength of the target. To calculate it, one can write that it proceeds from (7.4) [7, 55, 108]: $T = E - S + 2H, (7.5)$

where $E = 10\,lg\,I_s$; $S = 10\,lg\,I_0$.

However, since $K = |D(\theta;\phi)|^2$, then [7, 55, 108]: $T = 10\,lg\,K = 20\,lg|D(\theta;\phi)|$. (7.6)

For an ideally reflective sphere with a radius R and large wave dimensions kR we can, with a good approximation, use θ and φ for all angles except for the shadow direction: $|D(\theta;\phi)| = const = R/2$. (7.7)

But for a scatterer with arbitrary parameters, we need to introduce the concept of the equivalent radius $Re\,q$ in accordance with the formula [7, 55, 108]: $Re\,q = 2|D(\theta;\phi)|$. (7.8)

When the radiating antenna is the same as the receiving antenna, the system is called a combined or single-position. We can only measure one value of the scattered pressure corresponding to the coordinates of the combined system. Since the total diagram of the scattering of the sound is not considered and is usually unknown, it is convenient to assume that the obstacle acts as an isotropic scatterer which creates, in all directions, the same scattered pressure as in the combined system. Under this assumption, one can introduce a new characteristic for the reflectivity of bodies. This is a relative backscattering cross-section σ_0, which is the ratio of the total power P_s dissipated by the fictitious isotropic scatterer to the power P_i incident on the reflecting object of the wave from the source [7, 55, 108]:

$$\begin{aligned}\sigma_0 &= Ps/P_i = \lim_{r\to\infty}\left[\left(4\pi r^2/A_0\right)I_s/I_0\right] = \\ &= \lim_{r\to\infty}\left[\left(4\pi r^2/A_0\right)\left|p_s\right|^2 2\rho_0 c/2\rho_0 c\left|p_i\right|^2\right] = \\ &= \lim_{r\to\infty}\left[4\pi r^2 A^2\left|D(\theta;\varphi)\right|^2/A_0 r^2 A^2\right] = \left(4\pi/A_0\right)\left|D(\theta;\varphi)\right|^2,\end{aligned} \quad (7.9)$$

where A_0 represents the area of the geometrical shadow of a scatterer (its projection on a plane of a wave front) for a given direction of incidence of the wave from a source.

In so-called spaced (two-position) systems, a receiving antenna is located in an arbitrary direction with respect to a radiating antenna. For such a system, we introduce the concept of a two-position scattering cross-section, which is determined by the said formula (7.9). In this case, I_s represents the intensity of a sound in the direction of a receiving antenna. The total scattering cross-section σ can be calculated only based on the known angular characteristic $D(\theta;\varphi)$ of a reflecting object. It is defined as the ratio of a total scattering power P_s in a solid angle 4π in relation to the intensity I_0 of a wave irradiating on an obstacle from a source [7, 55, 108].

$$\begin{aligned}\sigma = P_s/I_0 = \\ = \lim_{r\to\infty}\left[\left(A^2 2\rho_0 c/r^2 2\rho_0 c A^2\right)\int_S\int|D(\theta;\phi)|^2 dS\right] = \\ = \int_0^{2\pi}\int_0^{\pi}|D(\theta;\phi)|^2\,sin\,\theta\,d\theta d\phi,\end{aligned} \quad (7.10)$$

where $dS = r^2\,sin\,\theta\,d\theta d\phi$ represents the surface element of a sphere of radius r.

The relative cross-section of the scattering σ_r is expressed in terms of a total cross-section σ and an area of the geometric shadow A_0: $\sigma_r = \sigma/2A_0$.

With the help of formulas (7.6), (7.8), and (7.9), one can establish relations between the named characteristics of the reflectivity of scatterers [7, 55, 108]:

$$\left.\begin{array}{ll}\sigma_0 = \pi\,Re\,q/A_0\,; & Re\,q = 2|D(\theta;\phi)|; \\ T = 20\,lg(Re\,q/2)\,; & T = 10\,lg(\sigma_0 A_0/4\pi)\,; \\ T = 20\,lg|D(\theta;\phi)|\,. & \end{array}\right\} (7.11)$$

To calculate the scattered field and the characteristics of a sound reflection by bodies in the liquid, an important role is played by the boundary conditions on their surface. We can formulate them in connection with the following three-dimensional problem [7, 55, 107, 108]:

On the boundary ξ_0 of a liquid body with a vacuum (absolutely soft medium) or an elastic body with a vacuum, the homogeneous Dirichlet condition must be satisfied:

1. For a liquid body

$$\Phi_0|_{\xi_0} = 0, (7.12)$$

where Φ_0 represents the potential of a displacement in a liquid medium

a) For an elastic body

$$\sigma_n|_{\xi_0} = 0; \qquad \tau_{n\alpha}|_{\xi_0} = \tau_{n\beta}\big|_{\xi_0} = 0, (7.13)$$

where $\sigma_n$and $\tau_{n\alpha}$, $\tau_{n\beta}$ represent normal and tangential stresses within an elastic body.

2. On the boundary of a liquid body with an absolutely hard medium or elastic bodies with an absolutely hard medium, the homogeneous Neumann condition must be satisfied:

a) For a liquid body

$$(\partial\Phi_0/\partial n)|_{\xi_0} = 0, (7.14)$$

where *n* represents a normal border

b) For an elastic body

$$\vec{u}|_{\xi_0} = 0, (7.15)$$

where $\vec{u}$represents the displacement vector of elastic body particles.

3. At an interface between an elastic body and a medium (rigidly connected/fused), the continuity of normal and tangential stresses and displacements must be observed.

4. At the liquid-elastic interface, normal displacements are continuous; normal stresses in an elastic body are equal to the boundary pressures in a liquid medium; and tangential stresses in an elastic body at the boundary with a liquid are absent.

5. At the interface between two liquid media pressures, where normal displacements are continuous.

In most books and articles on wave processes, the problems presented are generally concerned with the diffraction of electromagnetic waves rather than acoustic waves. Therefore, it is necessary to be able to interpret the results of the solutions to electromagnetic problems with respect to acoustic waves [14, 15, 16, 40, 53, 107]. Methods for the mathematical description of electromagnetic and acoustic waves are, formally, very close, as both are subject to the wave equation [14, 15, 16, 40, 53, 107]. Therefore, many, although by no means all, of the results obtained for electromagnetic waves are valid for sound waves.

7.2. The Acoustic Model of an Agitated Sea Surface

The model for a sound field in a shallow sea with an agitated surface presupposes an approximation of sea waves generated by soft elliptical cylinders. In the first approximation, ellipses (cross-sections of wind) waves can be considered to be equal at a constant wind velocity, which allows the train of wind waves to be transformed into a grate of elliptical cylinders (Fig. 7-1).

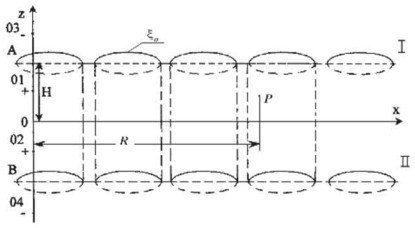

Figure 7-1: Diagram of real and imaginary sources and scatterers

When using the imaginary sources method for a waveguide with an uneven upper boundary caused by wind waves and by a constant sound velocity, the problem is reducible to finding the diffraction fields (p_Σ) of the real and imaginary sources separated from each other by elliptical cylinders. The diffracted pressure p_Σ at the observation point P is found through the following [109]:

$$p_\Sigma(P) = \sum_{m=1}^{\infty} p_{i,om}(P) + \sum_{q=1}^{\infty}\sum_{t=1}^{\infty} p_{s,ot}^{q}(P) \quad (7.16)$$

where $p_{i,om}$represents the pressure within an irradiating wave from the real *(m=1)* and imaginary *(m>1)* sources creating a radially symmetric cylindrical wave; $p_{s,ot}^{q}(P)$ represents the scattered pressure from a cylinder with number l from a grate with a number q. Due to the velocity of wind waves $V<<c$ (where c represents sound velocity in a waveguide) the Doppler effect will not be taken into account. Between the depth of waveguide H and the height h of the waves, the inequality, $H >> h$, is satisfied; this makes it impossible to take into account an interaction between grates of elliptical cylinders. The distance from the sources to observation point P is assumed to be such that a wave incident in the neighborhood of point P can be assumed to be plane with an amplitude that varies in accordance with the cylindrical law. The cylindrical scatterer with number t pounds of pressure

$p_{s,ot}(\xi_t, \eta_t, z_t)$ in the coordinates $\xi_t, \eta_t, z_t$of the same cylinder will be sought in the following form [109]:

$$p_{s,ot}(\xi_t, \eta_t, z_t) = 2e^{ihz_t}\sum_{l=0}^{\infty}\left[a_l^t c_l^t Me_l^{(1)}(\xi_t, q_t)ce_l(\eta_t, q_t) + b_l^t d_l^t Ne_l^{(1)}(\xi_t, q_t)se_l(\eta_t, q_t)\right], \quad (7.17)$$

where $Me_l^{(1)}(\xi_t, q_t)$ and - $Ne_l^{(1)}(\xi_t, q_t)$ are modified even and odd Mathieu functions of the 3rd kind; a_l^t and b_l^trepresent the unknown coefficients of decompositions, which are determined from the boundary conditions. The boundary conditions on the surface of soft-sound elliptical cylinders of each of q grates are equal to zero in the diffracted pressures:

$$\sum_{m=1}^{\infty} p_{i,om} + \sum_{t=1}^{\infty} p_{s,ot}^{q} = 0|_{\xi=\xi_{ot}} \quad (7.18)$$

where the first sum refers to incident waves, and the second sum refers to scattered waves.

High-Frequency Asymptotics

Using $\lambda << h_{min}$, where h_{min}represents the minimum height of wind waves, the calculation of diffracted sound pressure is greatly simplified due to the following factors:

1) The sound-insulating capacity of gratings increases for real and imaginary sources, especially at oblique angles of incidence;
2) The dominant role in a formation of a scattered sound field begins to play out in a mirror-reflection of a petal-like shape;
3) Taking into account the intense absorption and scattering of sound by air bubbles (especially resonant), by saturating near-surface layers of water, we can limit ourselves to the consideration of a single reflection of sound from or coming through the cylinder gratings.

In the deep sea, a single mapping of the source 01, with respect to the upper boundary, and its identical elliptical half-cylinders is presented in Fig. 7-2.

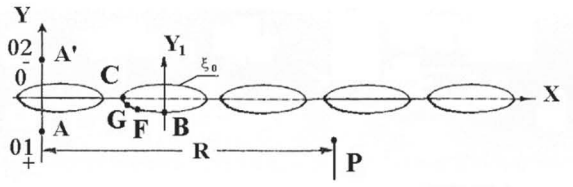

Figure 7-2: Circuit of sources and scatterers in the deep sea

The problem of the diffraction of sound is reducible to calculating the scattered field of the elliptical cylinders, which are irradiated by real (01) and imaginary (02) sources (Fig. 7-2). The scattered signal is received either at point *A* (a combined system), or at point *P* (spaced or two-position system). Primary attention will be paid to the real source "(01)", since the contribution of an imaginary source "(02)" in the sound scattered field is negligible (especially at high frequencies) because of the screening effect of the grate of the elliptical cylinders. We solve the problem using a plane formulation, assuming the source of the second field is in the form of an infinitely thin cylindrical radiator with an axis parallel to the elliptical cylinders' axes (Fig. 7-2).

At high frequencies, as it well known, a small part of the scatterer's surface is equal to half of the first Fresnel zone and this plays a decisive role in the formation of the scattered field. This allows us to exclude the interaction of scatterers (elliptical cylinders) with each other.

For the spaced system, the maximum scattered pressure will correspond to the angles of the mirror reflection of the sound by elliptical cylinders. At other angles of incidence, the reflected signal at point *P* will be noticeably smaller (assuming that the velocity of the wind is constant and all the elliptical cylinders have the same shape and sized sections). For a combined system, the maximum reflected signal corresponds to the moment of the sound's passage through the center of an elliptical cylinder through point *O* (Fig. 7-2).

To determine the mirror component reflection that contributes the most to the equally spaced system, let us compare the modules angular scattering characteristics, where$|D(\theta;\phi)|$ represents a sound-soft prolate spheroid with a semi-axes ratio of 1 : 10 for three angles of irradiation $\theta_0 = 30°$, $\theta_0 = 60°$, and $\theta_0 = 90°$ at high frequencies (the wave size of the spheroid is 65 units). A comparison between these three characteristics makes it possible to arrive at the important conclusion that the maxima of the mirror lobes irradiation ($\theta_0 = 30°$ and $\theta_0 = 60°$) at high frequencies almost coincides with the maximum of the inverse reflection at $\theta_0 = 90°$. In figures, it looks like this: $|D(30°, 0°)| = 0{,}15386$, $|D(60°, 0°)| = 0{,}15231$, and $|D(90°, 0°)| = 0{,}15163$.

In view of the plane formulation, a calculation of the inverse reflection of sound by an elliptic cylinder will be performed according to the well-known formula:

$$p_s = \frac{p_0}{\sqrt{2r}} R^{1/2} \quad (7.19)$$

where p_0 represents the pressure of an incident wave; R represents the radius of a curvature; and r represents the distance from a central axis of the cylinder to a point of an observation. The shapes and sizes of an elliptic section of a cylinder can be found with the help of the following expressions:

$$\lambda = 2\pi V^2/g; \quad (7.20)$$

$$h = 0{,}2V^2/g; \quad (7.21)$$

where λ represents the characteristic length of the wind wave; h represents its height; and g represents its acceleration due to gravity.

In our model, λ is a major axis of an ellipse and h represents a minor semi-axis. Using formulas (7.20) and (7.21), we calculated the λ and h values for three velocities of the wind: V = 10 m/s; 20 m/s; 30 m/s. The values obtained are presented in Table 7.1.

Table 7.1

V, m/s	λ, m	h, m	$\nu_{кр}$, Hz
10,0	62,8	2,0	495,
20,0	252,2	8,0	123,
30,0	565,2	18,0	55,1

Calculations of the radius of curvature R were performed by the following formulas:

$$\left.\begin{array}{l} R = \frac{1}{k}\ ;\ k = \left|\frac{d^2y}{dx^2}\right| : \left|1 + \left(\frac{dy}{dx}\right)^2\right|^{3/2}; \\ \frac{x^2}{a^2} + \frac{y^2}{b^2} = 1, \end{array}\right\} \quad (7.22)$$

where k represents curvature.

The values of R were calculated for points B and C (Fig. 7-2). It can be shown that R is proportional to V^2. The values of R for the velocity V=*10* m/s at points B and C are presented in Table 7.2.

Table 7.2

Points	B	C
R, m.	492,98	0,127

The performed calculations make it possible to estimate fluctuations in the reflected signals for the combined and spaced systems at different wind velocities.

Point C, which gives the minimum value of R in our model, cannot be a point of contact of the plane at the wave front and the elliptical contour of a cylinder, since it is always in the zone of the sound shadow. The proposed schema of calculation can be extended to elliptic sections with a different semi-axis ratio (i.e., ellipses with different radial coordinate values).

In [110–112], a lattice formed by elliptic cylinders was used as a model of the rough sea surface. The difficulty of calculating the reflection of sound from such a model sea surface depends on the strength of the interactions between neighboring elliptic cylinders. In [31, 113], the scattering characteristics were calculated for sound scattering by interacting bodies irradiated with a plane harmonic wave. In [113], the diffraction of a low-frequency stationary sound by a lattice of elliptic cylinders was considered in the Fresnel zone. In [31], the scattering of a sound signal by a spheroid placed at the boundary between two media was studied. Both of these studies were carried out using, first, the summation theorem for the eigen functions of the Helmholtz equation in the elliptic cylindrical and spheroidal coordinates and, second, the corresponding coupling functions proposed by Ivanov [30]. A solution to the problem of sound scattering by two interacting elliptic cylinders was found in [114]. Based on the results obtained in [31, 114, 115], we can calculate the interaction of two elliptical cylinders under irradiation from a plane harmonic wave in the far field (the Fraunhofer zone) in a wide-frequency band.

We introduce two elliptical cylindrical coordinate systems ξ_g, η_g, z_g ($g = 0, -1$), which are related to the cylinders $g = 0$ and $g = -1$, respectively (see Fig. 7-3). The $Y0$ and $Y1$ axes, as well as the $Z0$ and $Z1$ axes, are parallel to each other; and the X_g axis is the same for both coordinate systems. The cylinders have identical half-focal lengths $h0 = h1$, and the radial coordinates of the elliptical cylinders are also identical: $\xi 0 = \xi$ (see Fig. 7-3). The distance $l0,1$ between the centers of the cylinders is

$l_{0,-1} = 2a + \Delta$ (Fig. 7-3), where a is the major semi-axis of any of the cylinders. The aforementioned system of two elliptic elliptical cylinders is irradiated by a plane harmonic wave with a frequency ν and a wave vector k lying in the XOY plane (a planar $\eta_{0,0} = \eta_{0,-1}$ axis). At the surfaces of the two cylinders, the homogeneous Dirichlet condition is satisfied. For a cylinder marked by the index g, its angular characteristic $A_g(\eta)$ has the form [30, 113–115]

$$A_g(\eta) = 2^{3/2}(\pi k)^{-1/2}e^{-i\pi/4}\sum_{n=0}^{\infty} a_n^g\, c_n Ce_n(\xi_{0,g}; g_g)ce_n(\eta; g_g) + b_n^g d_n Se_n(\xi_{0,g}; g_g)se_n(\eta_g; g_g) \quad (7.23)$$

where c_n, d_n are the expansion coefficients, $ce_n(\eta_g; q_g)$ is the even Mathieu function of the first kind; $se_n(\eta_g; q_g)$ is the odd Mathieu function of the first kind; $Ce_n(\xi_{0,g}; q_g)$ is the modified even Mathieu function of the first kind; $Se_n(\xi_{0,g}; q_g)$ is the modified odd Mathieu function of the first kind; $q_g = h_g^2\kappa^2/4$; a_n^g and b_n^g are unknown expansion coefficients determined from the boundary conditions. The method of finding these coefficients with the use of the coupling function and the summation theorem for the wave functions of an elliptic cylinder was described in detail in [30, 113–115]. For a single cylinder (with the number g=0), the unknown expansion coefficients are determined by the following formulas [115]:

$$a_n^0 = -ce_n(\eta_{0,0}; q_0)\frac{Ce_n(\xi_{0,0};q_0)}{Me_n^{(1)}(\xi_{0,0};q_0)};$$

$$b_n^0 = -se_n(\eta_{0,0}; q_0)\frac{Se_n(\xi_{0,0};q_0)}{Ne_n^{(1)}(\xi_{0,0};q_0)}.$$

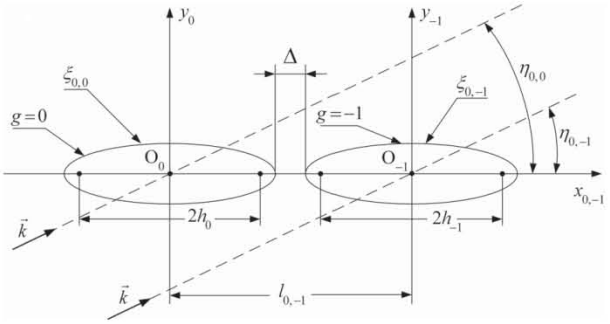

Figure 7-3: The relative positions of elliptical cylinders

The presence or absence of interaction between the scatterers can be determined from the difference between the angular scattering characteristic of a single cylinder and the corresponding characteristic of the same cylinder positioned near the other identical cylinder. For this purpose, we performed the calculations for a single cylinder and an interacting cylinder in a wide range of variations using the following parameters: the wave size q_g (the cyclic frequency ν), the angle of incidence $\eta_{0,g}$, and the distance between the cylinders. In the presence of the second cylinder, the unknown expansion coefficients a_n^g and b_n^g ($g = 0, -1$) are determined from the infinite algebraic system [31, 113]:

$$a_n^g + \sum_{m=0}^{\infty}(\alpha_{nm}^t a_m^t + \beta_{nm}^t b_m^t) = v_n^g; \quad (7.24)$$

$$b_n^g + \sum_{m=0}^{\infty}(\gamma_{nm}^t a_m^t + \delta_{nm}^t b_m^t) = w_n^g, \quad (7.25)$$

where

$$\alpha_{nm}^{-1} = 2\frac{c_m Ce_m(\xi_{0,-1};q_{-1})}{c_n Me_n^{(1)}(\xi_{0,-1};q_{-1})}Q_{mn}^{(1)}(-1; 0; 0);$$

$$\beta_{nm}^{-1} = 2\frac{d_m Se_m(\xi_{0,-1};q_{-1})}{c_n Me_n^{(1)}(\xi_{0,-1};q_{-1})}\overline{Q}_{mn}^{(1)}(-1;0;0);$$

$$\gamma_{nm}^{-1} = 2\frac{c_m Ce_m(\xi_{0,-1};q_{-1})}{d_n Ne_n^{(1)}(\xi_{0,-1};q_{-1})}R_{mn}^{(1)}(-1;0;0);$$

$$\delta_{nm}^{-1} = 2\frac{d_m Se_m(\xi_{0,-1};q_{-1})}{d_n Ne_n^{(1)}(\xi_{0,-1};q_{-1})}\overline{R}_{mn}^{(1)}(-1;0;0);$$

$$v_n^0 = -\frac{ce_n(\eta_{0,0};q_0)}{c_n Me_n^{(1)}(\xi_{0,0};q_0)};$$

$$w_n^0 = -\frac{se_n(\eta_{0,0};q_0)}{d_n Ne_n^{(1)}(\xi_{0,0};q_0)},$$

The results of our calculations are shown in Figures 7-4 to 7-9, which represent the magnitudes of the angular characteristics of a single cylinder (curves 1) and an interacting cylinder (curves 2). For the calculations, we used the following cylindrical dimensions and variations in the parameters listed above: $2a$ = 63m and $2h_0$ = 62.8m (Figs. 7-4–7-9).

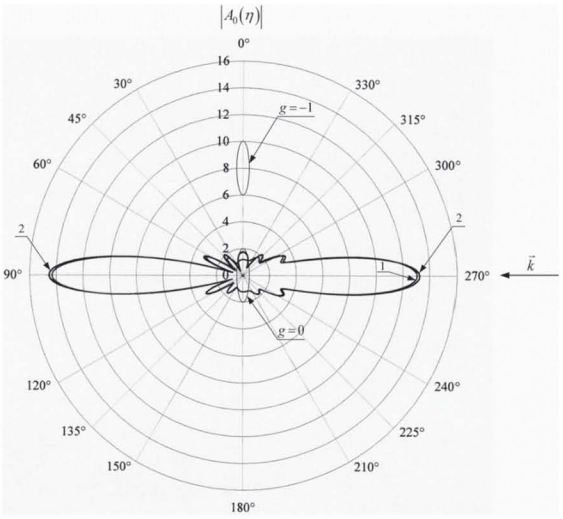

Figure 7-4: The magnitudes of the angular characteristics ($q^{1/2} = 5$; $\eta_{0,0} = 90^0$; $\Lambda_1 = 0{,}2$m.)

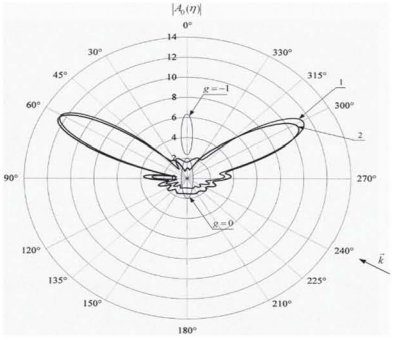

Figure 7-5: The magnitudes of the angular characteristics ($q^{1/2} = 5$; $\eta_{0,0} = 60^0$; $\Lambda_1 = 0{,}2$m.)

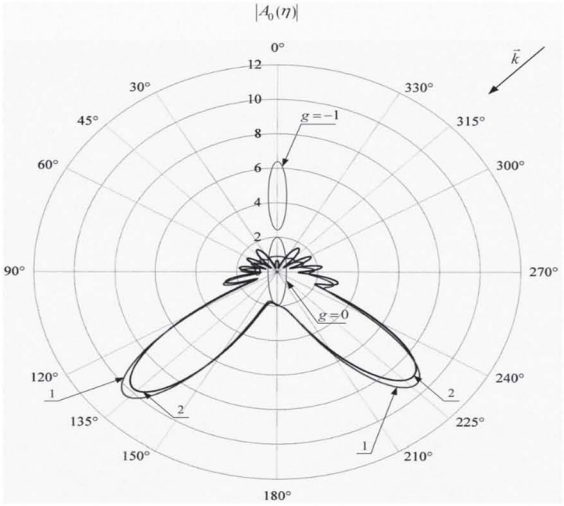

Figure 7-6: The magnitudes of the angular characteristics ($q^{1/2}=5$; $\eta_{0,0}=135^0$; $\Lambda_1=0{,}2\text{m}.$)

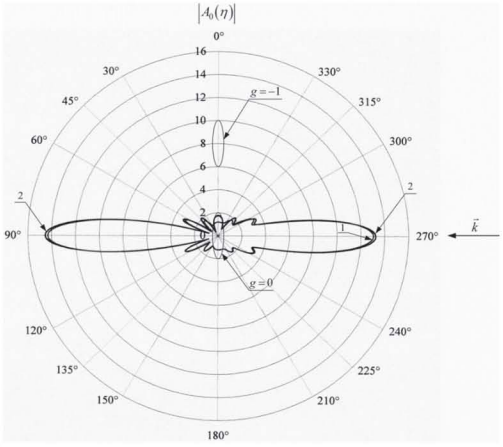

Figure 7-7: The magnitudes of the angular characteristics ($q^{1/2}=5$; $\eta_{0,0}=90^0$; $\Lambda_1=63\text{m}.$)

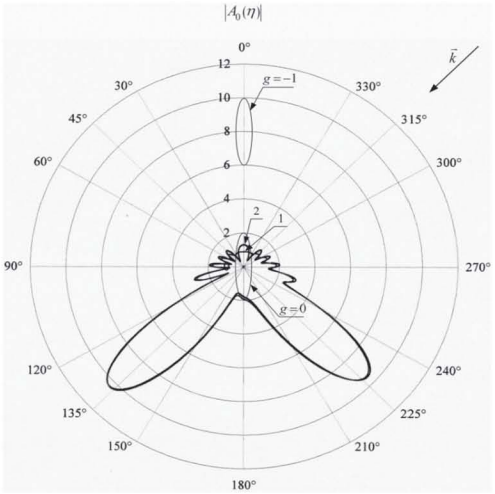

Figure 7-8: The magnitudes of the angular characteristics ($q^{1/2}=5$; $\eta_{0,0}=135^0$; $\Lambda_1=63\text{m}.$)

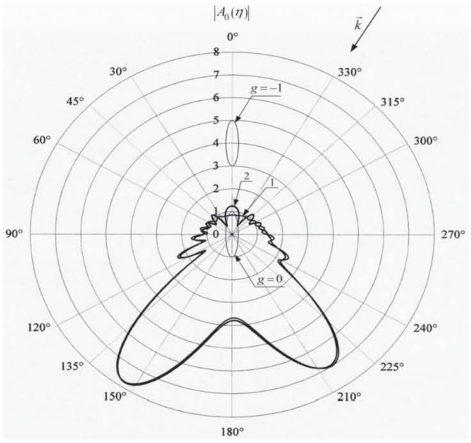

Figure. 7-9: The magnitudes of the angular characteristics ($q^{1/2} = 5$; $\eta_{0,0} = 150^0$; $\Lambda_1 = 63$m.)

By analyzing the numerical experiment for determining the strength of the interactions between two scatterers (in the form of elliptic cylinders), we found that, for the chosen cylinder parameters (the wave size, the distance between the cylinders, the shape and size of the scatterers, and the type of the boundary conditions), the interaction is rather weak (Figs. 7-4 through 7-9). Therefore, in its application to wind waves on the sea surface, this conclusion makes it possible to calculate the scattered field of each single wave without considering its interaction with neighboring waves and to take the simple sum of the complex contributions of individual wind waves at the observation point.

The interaction between the scatterers was tested in an actual experiment on low-frequency sound scattering by elastic cylindrical shells [18].

7.3. The Characteristics of the Diffraction in Ideal Spheroids and the Watson Transformation

Prolate and oblate (flattened) spheroids are scatterers with analytic surfaces in systems of prolate and oblate (flattened) spheroidal coordinates (Fig. 7-10). Prolate and oblate systems of coordinates can be obtained by rotating a two-dimensional elliptic elliptical coordinate system consisting of confocal ellipses and hyperboloids around large and small axes of ellipses, respectively [116].

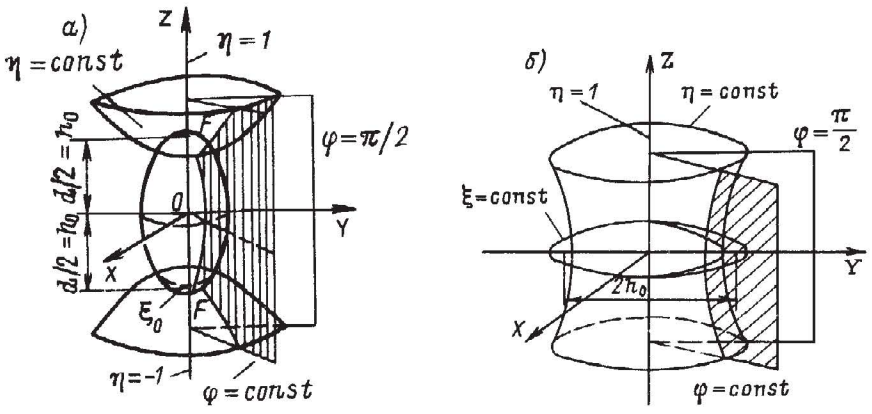

a) b)

Figure 7-10: The systems for prolate (a) and oblate (b) spheroidal coordinates

We have denoted the interfocus distance as $2h_0$. The prolate coordinates, ξ, η, φ, shown in Fig. 7-10a, are expressed in terms of the Cartesian coordinates x, y, z as follows [116]:

$$\left.\begin{array}{l} x = h_0(1-\eta^2)^{1/2}(\xi^2-1)^{1/2}\cos\phi \ ; \\ (y = h_0(1-\eta^2)^{1/2}(\xi^2-1)^{1/2}\sin\phi \ ; \\ z = h_0\xi\eta \ . \end{array}\right\} (7.26)$$

The radial coordinate ξ and two angle coordinates, η and φ, change within the following limits $1 \le \xi < \infty$; $0 \le \phi \le 2\pi$. For oblate spheroidal coordinates ξ, η, and φ, this conversion is as follows:

$$\left.\begin{array}{l} x = h_0(1-\eta^2)^{1/2}(\xi^2+1)^{1/2}\cos\phi \ ; \\ y = h_0(1-\eta^2)^{1/2}(\xi^2+1)^{1/2}\sin\phi \ ; \\ z = h_0\xi\eta \ . \end{array}\right\} (7.27)$$

where $-1 \le \eta \le 1$; $0 \le \xi < \infty$; $0 \le \phi \le 2\pi$.

Expressions for scale factors $h_1=h_\xi$, $h_2=h_\eta$, $h_3=h_\varphi$ have the following form:

For the prolate system

$$\left.\begin{array}{l} h_\xi = h_0(\xi^2-\eta^2)^{1/2}(\xi^2-1)^{-1/2} \ ; \\ h_\eta = h_0(\xi^2-\eta^2)^{1/2}(1-\eta^2)^{-1/2} \ ; \\ h_\phi = h_0(1-\eta^2)^{1/2}(\xi^2-1)^{1/2} \ . \end{array}\right\} (7.28)$$

For the oblate system [116]

$$\left.\begin{array}{l} h_\xi = h_0(\xi^2+\eta^2)^{1/2}(\xi^2+1)^{-1/2} \ ; \\ h_\eta = h_0(\xi^2+\eta^2)^{1/2}(1-\eta^2)^{-1/2} \ ; \\ h_\phi = h_0(1-\eta^2)^{1/2}(\xi^2+1)^{1/2} \ . \end{array}\right\} \quad (7.29)$$

The scattered wave potential $\Phi_s(\xi,\ \eta,\ \phi)$ for an ideal prolate spheroid has the following form [7, 55, 108, 117]:

$$\Phi_s(\xi,\ \eta,\ \phi) = \sum_{m=0}^{\infty}\sum_{n\ge m}^{\infty} B_{m,n}R_{m,n}^{(3)}(C,\xi)\bar{S}_{m,n}(C,\eta)\ \cos m\phi \ , (7.30)$$

where $B_{m,n}$ represents the unknown coefficients, which are determined by the boundary conditions

$$B_{m,n} = -2\varepsilon_m i^{-n}\bar{S}_{m,n}(C,\eta_0)\frac{\Omega R_{m,n}^{(1)}(C,\xi_0)}{\Omega R_{m,n}^{(3)}}(C,\xi_0) \ , (7.31);$$

ξ_0 represents radial coordinate of the prolate spheroid $\Omega=1$ for the ideal soft spheroid; and $\Omega = (\partial/\partial\xi)|_{\xi=\xi_0}$ for the ideal hard spheroid.

The angular diagram of the scattering of sound is found using the asymptotes of radial functions of the third kind [7, 55, 108, 117]:

For the prolate spheroid

$$D(\eta,\phi) = -\left(\frac{2}{ik_1}\right)\sum_{m=0}^{\infty}\sum_{n\ge m}^{\infty}(-1)^n\varepsilon_m i^{-n}\bar{S}_{m,n}(C,\eta_0)\cos m\phi \times$$
$$\times\frac{\bar{S}_{m,n}(C,\eta)\Omega R_{m,n}^{(1)}(C,\xi_0)}{\Omega R_{m,n}^{(3)}(C,\xi_0)} \ ; \quad (7.32)$$

For the oblate spheroid

$$D(\eta,\phi) = -\left(\frac{2}{ik_1}\right)\sum_{m=0}^{\infty}\sum_{n\ge m}^{\infty}(-1)^n\varepsilon_m i^{-n}\bar{S}_{m,n}(-iC,\eta_0)\cos m\phi \times$$
$$\times\frac{\bar{S}_{m,n}(-iC,\eta)\Omega R_{m,n}^{(1)}(-iC,i\xi_0)}{\Omega R_{m,n}^{(3)}(-iC,i\xi_0)} \ . (7.33)$$

Figures (7-11)–(7-14) show the different characteristics of sound scattering by ideal spheroids (prolate and oblate ones).

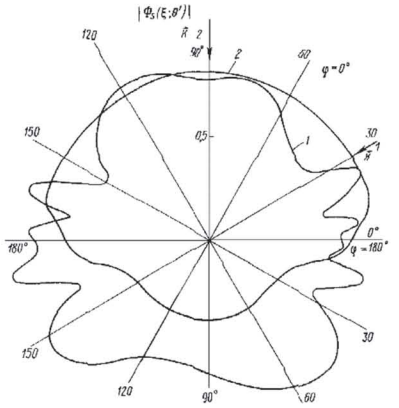

Figure 7-11: The distribution of the module $|\Phi_s(\xi, \theta')|$ in the Fresnel zone

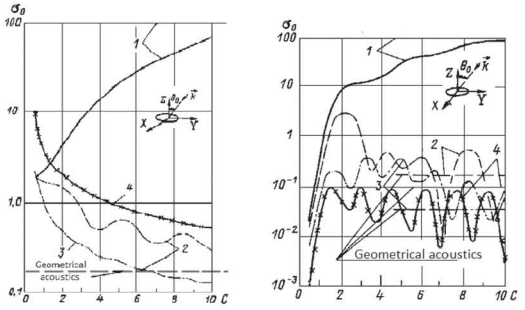

a) b)

Figure 7-12: The relative cross-sections for the backscattering of oblate spheroids: a) a soft spheroid b) a hard spheroid

When using the Watson transformation for ideal scatterers of a spheroidal form, it is expedient to use the spheroidal wave functions proposed in [118]. $\Phi_\Sigma = \Phi_i + \Phi_s$

$$\Phi_\Sigma(\xi, \eta, \phi) = (1/2) \sum_{m=0}^{\infty} \sum_{n \geq m}^{\infty} exp(-in\pi/2)\, \varepsilon_m (2n+1) \Gamma(n+1-m) \times$$
$$\times [\Gamma(n+1+m)]^{-1} PS_n^m(\eta; \gamma^2) PS_n^m(\eta_0; \gamma^2) \cos m\phi \times$$
$$\times \left[\Omega S_n^{m(3)}(\xi_0; \gamma)\right]^{-1} \left[\Omega S_n^{m(3)}(\xi_0; \gamma) S_n^{m(4)}(\xi; \gamma) - \Omega S_n^{m(4)}(\xi_0; \gamma) S_n^{m(3)}(\xi; \gamma)\right], \quad (7.34)$$

where $PS_n^m(\eta; \gamma^2)$ represents an angular spheroidal function; $S_n^{m(3)}(\xi; \gamma)$ and

$S_n^{m(4)}(\xi; \gamma)$ represent the radial spheroidal functions of the third and fourth kinds, respectively; $\gamma = 2\pi h_0/\lambda$ represents the wave dimension of the spheroid; and $\Gamma(n+1-m) = (n-m)!$ represents the gamma function.

We use the Watson transformation and represent the series (7.34) as an infinite sum of contour integrals on the complex plane ν of one the indices [119]

$$\Phi_\Sigma(\xi,\eta,\phi) = (4)\sum_{m=0}^{\infty}\varepsilon_m \cos m\phi \oint exp\left(\frac{iv\pi}{2}\right)(2v+1)\times$$
$$\times\left[\Omega S_n^{m(3)}(\xi_0;\gamma)S_n^{m(4)}(\xi;\gamma) - \Omega S_n^{m(4)}(\xi_0;\gamma)S_n^{m(3)}(\xi;\gamma)\right]\times$$
$$\times\Gamma(v+1-m)PS_v^m(-\eta;\gamma^2)PS_v^m(\eta_0;\gamma^2)[\Gamma(v+1+m)(-1)^m\times$$
$$\times sin\,\pi v\Omega S_n^{m(3)}(\xi_0;\gamma)(\xi_0;\gamma)]^{-1}dv\ . (7.35)$$

We assign all contours to the corresponding index m. The value of each of the integrals of the series is equal to the sum of the residues of the integrand with respect to simple poles at points $v = n$, where n is an integer. In the case of a sphere, the contours of integrations embrace the positive part of the real axis of the complex plane v. Therefore, the contour with the index of $m=0$ is practically the same as the contour for the ideal sphere. This contour $m=0$ is shown in Fig. 7-13. As for the other contours ($m>0$), we shall deal with them in the following way:

1) Contours with index $m \leq$ entire ($\gamma\xi_0$) (integer part $\gamma\xi_0$) will encompass all points $n \geq 0$, where n represents an integer and so they will not differ in any way from the contour described by m=0.
2) At $m >$, the entire ($\gamma\xi_0$) contours will include only the integer, $n \geq m$.

Artificial stretching of integration contours to the left of the point $v = -1/2$ ($m \leq$ entire ($\gamma\xi_0$)) (Fig. 7-13) does not affect the magnitude of the integral in any way, if we recall that $PS_n^m(\eta;\gamma^2) = 0$ by $n < m$. By making a change to the independent variable $v = t - (1/2)$, based on the properties of the gamma function and the spheroidal wave functions, we find that the that the integrand is odd$t = v + 1/2$.

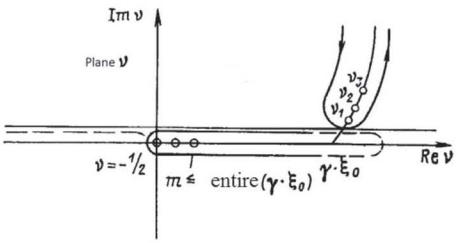

Figure 7-13: The integration contour $m=0$ for an ideal spheroid

The oddness of the integrand allows us to modify the integration contours as follows:

1) Contours with indices $m \leq$ entire ($\gamma\xi_0$) are transformed into straight lines parallel to the real axis and lie in the upper half-plane v, then they turn into semicircles of an infinitely large radius and loops that cover the poles v_s (Fig. 7-13). They are defined as the roots of the following equation:

$$\Omega S_{v_s}^{m(3)}(\xi_0;\gamma) = 0\ ; (7.36)$$

2) Roots with indices $m >$ entire ($\gamma\xi_0$) are formed into two half-lines bonded by points $v = \pm m$ (Fig. 7-14).

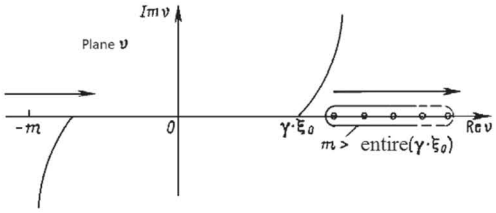

Figure 7-14: The integration contour $m >$ entire ($\gamma\xi_0$) for an ideal spheroid

Asymptotic formulas for radial spheroidal functions of the third and fourth kinds with one complex index and one real index for $\gamma >> 1$ have the form [118, 119]:

$$S_v^{m(3)}(\xi_0,\gamma) \underset{\gamma\to\infty}{\approx} (\xi_0^2-1)^{-m/2}\xi_0^m[(1+B)/\gamma\xi_0]\,exp[i\gamma\xi_0 - i(v+1)\pi/2]\ ;$$
$$S_v^{m(4)}(\xi_0,\gamma) \underset{\gamma\to\infty}{\approx} (\xi_0^2-1)^{-m/2}\xi_0^m[(1+B)/\gamma\xi_0]\,exp[-i\gamma\xi_0 + i(v+1)\pi/2]\ , (7.37)$$

where B has the order ξ_0^{-q}.

Therefore, functions $S_v^{m(3)}(\xi_0,\gamma)$ and $S_v^{m(4)}(\xi_0,\gamma)$ can be represented as the product of following functions [118, 119]:

$$S_v^{m(3)}(\xi_0,\gamma) \underset{\gamma\to\infty}{\approx} F_3(\xi_0)h_v^{(1)}(\xi_0,\gamma)\ ;$$
$$S_v^{m(4)}(\xi_0,\gamma) \underset{\gamma\to\infty}{\approx} F_4(\xi_0)h_v^{(2)}(\xi_0,\gamma)\ . (7.38)$$

Since functions $F_3(\xi_0)$ and $F_4(\xi_0)$ do not vanish on the complex plane v, the zeros of the function $\Omega S_v^{m(3)}(\xi_0;\gamma)$ coincide asymptotically ($\gamma >> 1$) with the zeros of the function $\Omega h_v^{(1)}(\gamma\xi_0)$, and consequently, with the zeros of the cylindrical function $\Omega H_v^{(1)}(\gamma\xi_0)$. The contour integrals of the first type ($m \le$ entire ($\gamma\xi_0$)) can be replaced by the sum of residues or the sum of the poles v, and the infinite sum of the integrals (7.35) is then represented as two terms (see 119):

$$\Phi_\Sigma(\xi,\eta,\phi) = (\pi/2)\sum_{m=0}^{\text{entire }(\gamma\xi_0)}\varepsilon_m\cos m\phi \sum_s 2v_s(-1)^{-m}\times$$
$$\times(\sin\pi v_s)^{-1}[\Gamma(v_s+1-m)/\Gamma(v_s+1+m)]PS_{v_s}^m(-\eta;\gamma^2)\times$$
$$\times PS_{v_s}^m(\eta_0;\gamma^2)\,exp(-i\pi v_s/2)\,S_{v_s}^{m(3)}(\xi;\gamma)\times$$
$$\times\left[\Omega S_v^{m(4)}(\xi_0;\gamma)/(\partial/\partial v)\Omega S_v^{m(3)}(\xi_0;\gamma)\right]\Big|_{v_s} +$$
$$+(i/4)\sum_{m=\text{entire }(\gamma\xi_0)+1}^{\infty\sum\phi\, exp(-iv\pi/2)(2v+1)[\Gamma(v+1-m)/\Gamma(v+1+m)]} 2cos$$
$$\times PS_v^m(-\eta;\gamma^2)PS_v^m(\eta_0;\gamma^2)[(-1)^m\sin\pi v\Omega S_v^{m(3)}(\xi_0;\gamma)]^{-1}\times$$
$$\times\left[\Omega S_v^{m(3)}(\xi_0;\gamma)\Omega S_v^{m(4)}(\xi;\gamma) - \Omega S_v^{m(4)}(\xi_0;\gamma)\Omega S_v^{m(3)}(\xi;\gamma)\right]dv\ . (7.39)$$

As an analogy, with the spherical and cylindrical Hankel functions of the third kind, the module varies slowly until $|v| < \gamma\xi_0$ and $|v| > \gamma\xi_0$ increase (for $m=0$). Considering this, we come to the conclusion that the second term in (7.39) is negligibly smaller than the first. As with the first term, it is sufficient to leave it as $m \le$ entire ($\gamma\xi_0/2$). As a result, the relation (7.39) takes the following form [119]:

$$\Phi_\Sigma(\xi,\eta,\phi) = (\pi/2)\sum_{m=0}^{\text{entire }(\gamma\xi_0/2)}\varepsilon_m\cos m\phi\sum_s(2v_s+1)\times$$
$$\times exp(-i\pi v_s/2)\,[(-1)^m\sin\pi v]^{-1}[\Gamma(v+1-m)/\Gamma(v+1+m)]\times$$
$$\times PS_{v_s}^m(-\eta;\gamma^2)PS_{v_s}^m(\eta_0;\gamma^2)\left[\Omega S_v^{m(4)}(\xi_0;\gamma)/(\partial/\partial v)\,\Omega S_v^{m(3)}(\xi_0;\gamma)\right]\Big|_{v_s}\times$$
$$\times S_{v_s}^{m(3)}(\xi;\gamma)\ . (7.40)$$

This Watson transformation allows us to move from the summation $\gamma^2/2$ in the terms of the double series on undamped waves to the sum $\approx \gamma$ in the terms of the double series (7.40).

When solving the axisymmetric diffraction problem with regard to an ideal spheroid, the index m assumes only one value for m: $m=0$ and, in its expression (7.40), there only remains a series of wave residues [119]:

$$\Phi_{\Sigma}(\xi,\eta,\phi) = (\pi/2)\sum_{s}(2v_s+1)(sin\,\pi\,v_s)^{-1}\times$$
$$\times PS^{0}_{v_s}(-\eta;\gamma^2)PS^{0}_{v_s}(1;\gamma^2)\,exp(-i\pi v_s/2)\,S^{0}_{v_s}(\xi;\gamma)\times$$
$$\times\left[\Omega S_v^{0(4)}(\xi_0;\gamma)/(\partial/\partial v)\,\Omega S_v^{0(3)}(\xi_0;\gamma)\right]\Big|_{v_s}.$$

CHAPTER 8

THE APPLICATION OF EQUATIONS AND METHODS FOR SOUND DIFFRACTION IN THE SYNTHESIS OF HYDROACOUSTIC ANTENNAS

8.1. The Synthesis of a Spheroidal Surface Antenna According to a Predetermined Radiation Pattern

Antennas used in hydroacoustics have a variety of directional patterns, depending on their purpose. In particular, they can be directed to one plane rather than another in order to have a narrow main lobe, to keep the width of the main maximum in a wide frequency range, and so on. Requirements for antenna directivity characteristics play an initial data-related role when solving antenna synthesis problems. This is calculated using the amplitude-phase distribution of the pressure of vibrational velocity on its surface, provided there is a given directional characteristic. The synthesis of an antenna will be considered. Our example is a solid (continuous) cloistered form system with a curved spheroidal surface (the revolving body). The choice of surface form is not accidental because, with the help of coordinate systems, prolate and oblate spheroids can be described (approximately or strictly) due to their large number of surfaces for revolution.

For example, a sphere and an infinite cylinder can be considered to be particular cases of bodies of a spheroidal form. An infinitely thin bar of finite length is a degenerate prolate spheroid. However, an infinitely thin disk is a degenerate oblate spheroid. We will take an antenna in the form of a prolate spheroid and look for the distribution of pressure $p_s(Q)$ or its derivative along the normal $\partial p_s(Q)/\partial n$ on this surface, providing there is the given angular characteristic $R_1(\theta, \phi)$. We will introduce prolate spheroidal coordinates ξ, η, ϕ with the interfocus $d = 2h_0$. Pressure in the far field of an antenna$p_1(\theta, \phi, r)$ can be represented as a product of the angular characteristic$R_1(\theta, \phi)$ by the potential of a point source $(exp\ i\ kr)/r$.

Using single term integral formulas, we can obtain Fredholm integral equations of the first kind relative to the pressure $p_S(Q)$ or $\partial p_S(Q)/\partial n_0$exerted onto the surface of an antenna [7, 55, 97, 120–124].

$$\left.\begin{aligned} R_1(\theta,\varphi) &= \frac{r}{e^{ikr}}\frac{1}{4\pi}\int_S p_S(Q)\frac{\partial G_1}{\partial n_0}dS; \\ R_1(\theta,\varphi) &= -\frac{r}{e^{ikr}}\frac{1}{4\pi}\int_S \frac{\partial p_S(Q)}{\partial n_0}G_2 dS \end{aligned}\right\}, \quad (8.1)$$

where r represents distance to an observation point and Q represents an antenna point.

The directional diagram $R(\theta, \phi)$ is, in essence, a normalized angular characteristic $R_1(\theta, \phi)$:

$$R(\theta,\varphi) = R_1(\theta,\varphi) / R_1(\theta_0,\varphi_0), \quad (8.2)$$

where$R_1(\theta, \phi)$ represents the normalizing value of the angular characteristic, usually in the direction of its maximum. Therefore, in the future, the synthesis problem can be solved for the angular characteristic $R_1(\theta, \phi)$ and then, (8.2) can be used to go to the directional diagram $R(\theta, \phi)$. Therefore, the surface of the antenna is given by coordinate ξ_0. Green's functions $G_1$and G_2can be expended in spheroidal functions [7, 55, 97, 120–124]:

$$G_1(\xi,\eta,\varphi;\xi',\eta',\varphi') = 2ik\sum_{m=0}^{\infty}\sum_{n\geq m}^{\infty}\bar{S}_{mn}(C,\eta)\,exp\,i\,m(\varphi-\varphi')\times$$

$$\times\left[R_{mn}^{(1)}(C,\xi')R_{mn}^{(3)}(C,\xi) - \frac{R_{mn}^{(1)}(C,\xi_0)}{R_{mn}^{(3)}(C,\xi_0)}R_{mn}^{(3)}(C,\xi)R_{mn}^{(3)}(C,\xi')\right]\times$$

$$\times\bar{S}_{mn}(C,\eta');\ (8.3)$$

$$G_2(\xi,\eta,\varphi;\xi',\eta',\varphi') = 2ik\sum_{m=0}^{\infty}\sum_{n\geq m}^{\infty}\bar{S}_{mn}(C,\eta)\,exp\,i\,m(\varphi-\varphi')\times$$

$$\times\left[R_{mn}^{(1)}(C,\xi')R_{mn}^{(3)}(C,\xi) - \frac{R_{mn}^{(1)}{}'(C,\xi_0)}{R_{mn}^{(3)}{}'(C,\xi_0)}R_{mn}^{(3)}(C,\xi)R_{mn}^{(3)}(C,\xi')\right]\times$$

$$\times\bar{S}_{mn}(C,\eta');\ (8.4)$$

where ξ, η, and φ represent the spheroidal coordinates of the observation point and the coordinates of a point source. In the far field, expressions for Green's functions can be simplified, taking into account the asymptote of radial functions of the third kind

$$\left.\begin{array}{l} R_{mn}^{(3)}(C,\xi_0) \\ R_{mn}^{(3)}(C,\xi) \underset{C\xi\to\infty}{\approx} \dfrac{i^{-n-1}}{C\xi}e^{iC\xi}; \\ \dfrac{e^{iC\xi}}{C\xi} \approx \dfrac{e^{ikr}}{kr} \end{array}\right\}.\ (8.5)$$

The antenna surface element can be described in terms of $dS = h_\eta h_\phi d\eta d\phi$ (h_η and h_ϕ representing scale factors for coordinates η and φ, respectively) and $dn_0 = h_\xi d\xi$ (h_ξ representing the scale factor for the coordinate ξ).

Substituting values dS and dn_0 in (8.1) with an allowance for (8.5), we obtain [7, 55, 97]:

$$R_1(\eta,\varphi) = \int_1^1\int_0^{2\pi}\Phi^{(1),(2)}(\eta',\varphi')K^{(1),(2)}(\eta,\varphi;\eta',\varphi')d\eta' d\varphi',\ (8.6)$$

where $\Phi^{(1)}(\eta',\varphi') = p_s(Q); \Phi^{(2)}(\eta',\varphi') = \partial p_s(Q)/\partial\xi';$

$K^{(1),(2)}(\eta,\phi;\eta',\phi')$ represents kernels of the Fredholm integral equations of the first kind equal to:

$$K^{(1)}(\eta,\varphi;\eta',\varphi') = \frac{1}{2\pi ik}\sum_{m=0}^{\infty}\sum_{n\geq m}^{\infty}\frac{i^{-n}}{R_{mn}^{(3)}(C,\xi_0)}\bar{S}_{mn}(C,\eta)\times$$

$$\times\bar{S}_{mn}(C,\eta')\,exp\,i\,m(\varphi-\varphi');$$

$$K^{(2)}(\eta,\varphi;\eta',\varphi') = \frac{1}{2\pi ik}\sum_{m=0}^{\infty}\sum_{n\geq m}^{\infty}\frac{i^{-n}}{R_{mn}^{(3)}(C,\xi_0)}\bar{S}_{mn}(C,\eta)\times$$

$$\times\bar{S}_{mn}(C,\eta')\,exp\,i\,m(\varphi-\varphi').$$

Eigen values $\Lambda^{(1),(2)}$ of kernels $K^{(1),(2)}(\eta,\phi;\eta',\phi')$ are found from the solution to the Fredholm integral equation of the second kind:

$$\Phi^{(1),(2)}(\eta,\varphi) - \Lambda^{(1),(2)}\int_{-1}^{1}\int_0^{2\pi}\Phi^{(1),(2)}(\eta',\varphi')\times$$

$$\times K^{(1),(2)}(\eta,\varphi;\eta',\varphi')d\eta' d\varphi' = R_1(\eta,\varphi).\ (8.7)$$

The solution of equation (8.7) has the form:

$$\Phi^{(1),(2)}(\eta,\varphi)=R_1(\eta,\varphi)+\sum_{m=0}^{\infty}\sum_{n\geq m}^{\infty}B^{(1),(2)}\overline{S}_{mn}(C,\eta)\exp im\varphi. \quad (8.8)$$

Substituting (8.8) for (8.7), and integrating η' and ϕ', as well as using the orthogonality of the exponential and angular spheroidal functions, we can find the eigen values of the kernels [7, 55, 97]:

$$\Lambda_{mn}^{(1)}=i^{1+n}kR_{mn}^{(3)}(C,\xi_0); \quad (8.9)$$

$$\Lambda_{mn}^{(2)}=i^{1+n}kR_{mn}^{(3)\prime}(C,\xi_0). \quad (8.10)$$

By means of the known eigen functions of the kernel's $K^{(1),(2)}(\eta,\phi;\eta',\phi')$ functions

$\bar{S}_{mn}(C,\eta)$ and $exp\, i\, m\phi$, the generalized Fourier coefficients of the characteristic [7, 55, 97] can be found:

$$a_{mn}=\frac{1}{2\pi}\int_1^1\int_0^{2\pi}R_1(\eta,\varphi)\overline{S}_{mn}(C,\eta)\exp(-im\varphi)\,d\eta d\varphi. \quad (8.11)$$

The solution to the integral equation (8.1) will be physically realizable if the series $\sum_m\sum_n a_{mn}^2\left(\Lambda_{mn}^{(1),(2)}\right)^2$ converges. When this condition is satisfied, one function (since the kernel eigen functions are complete) satisfies the equation (8.1) and it can be calculated as the average limit [7, 55, 97]:

$$\Phi^{(1),(2)}(\eta,\varphi)=\sum_{m=0}^{\infty}\sum_{n\geq m}^{\infty}a_{mn}\Lambda_{mn}^{(1),(2)}\overline{S}_{mn}(C,\eta)\exp im\varphi. \quad (8.12)$$

The same eigenvalues are obtained by considering the diffraction problem of sound scattering by an ideal spheroid (whether soft or hard). In reality, the angular characteristic of a soft spheroid (in the field of a plane incident wave) has the form [7, 55, 97]:

$$R_1(\eta,\varphi)=-\frac{2}{ik}\sum_{m=0}^{\infty}\sum_{n\geq m}^{\infty}(-1)^n\bar{S}_{mn}(C,\eta_1)\bar{S}_{mn}(C,\eta)\frac{R_{mn}^{(1)}(C,\xi_0)}{R_{mn}^{(3)}(C,\xi_0)}e^{im\varphi},$$

where$\eta_1$represents the angular coordinate of the wave vector of a plane incident wave, and ξ_0 represents the radial coordinate of a scattering surface. The Fourier coefficients $a_{mn}$of the angular characteristic in accordance with (8.11) are equal:

$$a_{mn}=-\frac{(-1)^n 2}{ik}\overline{S}_{mn}(C,\eta_1)\frac{R_{mn}^{(1)}(C,\xi_0)}{R_{mn}^{(3)}(C,\xi_0)}. \quad (8.13)$$

In view of the homogeneous Dirichlet boundary condition on the surface of the scatterer $(\xi=\xi_0)$, the function $\Phi^{(1)}(\eta,\phi)$is equal (with the opposite sign) to the distribution pressure in the plane incident wave of the unit amplitude along surface of the scatterer ξ_0 [7, 55, 97]:

$$\Phi^{(1)}(\eta,\varphi)=-2\sum_{m=0}^{\infty}\sum_{n\geq m}^{\infty}i^{-n}\bar{S}_{mn}(C,\eta_1)\bar{S}_{mn}(C,\eta)R_{mn}^{(1)}(C,\xi_0)\, exp\, i\, m\, \varphi$$

Comparing expressions for $\Phi^{(1)}(\eta,\phi)$with (8.12) and taking into account (8.13), we are able to find the eigen values of $\Lambda_{mn}^{(1)}$ [7, 55, 97]:

$$\Lambda_{mn}^{(1)}=i^{1+n}kR_{mn}^{(3)}(C,\xi_0), \quad (8.14)$$

which coincides with (8.9).

Similarly, referring to the hard spheroid, we obtain [7, 55, 97]:

$$\Lambda_{mn}^{(2)}=i^{1+n}kR_{mn}^{(3)\prime}(C,\xi_0), \quad (8.15)$$

Analysis of the eigen values $\Lambda_{mn}^{(1),(2)}$ shows that the physically realizable solution $\Phi^{(1),(2)}(\eta,\phi)$ will be provided by the Fourier coefficients a_{mn}, which decrease with the increasing indices *m* and *n* faster than the radial functions of the first kind $R_{mn}^{(1)}(C,\xi_0)$ for $\Phi^{(1)}(\eta,\phi)$, or their first derivatives along the radial coordinate $R_{mn}^{(1)\prime}(C,\xi_0)$ for $\Phi^{(2)}(\eta,\phi)$. If, in all formulas, the obtained wave size *C* is replaced with *-iC* and the radial coordinate *ξ is* replaced with *iξ*, we will obtain a solution to the problem of synthesis of the oblate spheroidal antenna. By fixing the interfocus distance *d* to zero, we can pass from spheroidal coordinates to spherical coordinates.

In the case of an antenna with the size $C >> 1{,}0$, then the Watson transformation can be used to solve the problem [124].

8.2. The Synthesis of a Linear Radiator Using Prolate Spheroid Functions and the Synthesis of the Volume of a Spheroidal Antenna

A linear antenna in the form of a segment of an infinitely thin bar is a degenerate prolate spheroid ($\xi_0 = 1$). The synthesis of such an antenna can be performed according to the same schema. These will not only depend on the angle φ but, in addition, Fredholm integral equations of the first kind, thereby linking the angular characteristic $R_1(\eta)$ with the required distributions $p_S(Q)$ or $\partial p_S(Q)/\partial\xi'|_{\xi'=1}$, which are given in [55, 97, 121–125]:

$$\left.\begin{aligned} R_1(\eta) &= \int_1^1 p_S^*(Q)K^{(1)}(\eta,\eta')d\eta'; \\ R_1(\eta) &= \int_1^1 \frac{\partial p_S^*(Q)}{\partial\xi'}K^{(2)}(\eta,\eta')d\eta' \end{aligned}\right\}, \quad (8.16)$$

where

$$K^{(1)}(\eta,\eta') = h_0\sum_{n=0}^{\infty} i^{-n}\bar{S}_{on}(C,\eta)\bar{S}(C,\eta')R_{0n}^{(1)\prime}(C,\xi')|_{\xi'=1};$$

$$K^{(2)}(\eta,\eta') = -h_0\sum_{n=0}^{\infty} i^{-n}\bar{S}_{on}(C,\eta)\bar{S}(C,\eta')R_{0n}^{(1)\prime}(C,\xi')|_{\xi'=1}.$$

Factor $\xi_0^2 - 1$ vanishes when $\xi_0 - 1$is in expressions for $p_S^*(Q)$and $\partial p_S^*(Q)/\partial\xi'|_{\xi'=1}$. This emphasizes that as soon as the antenna degenerates into an infinitely thin bar, it cannot be ensured to have $R_1(\eta)$ finite values of distributions $p_S(Q)$ or $\partial p_S(Q)/\partial\xi'|_{\xi'=1}$; only distributions $p_S^*(Q)$and$\partial p_S^*(Q)/\partial\xi'|_{\xi'=1}$ will be finite.

The eigen values of nuclei $K^{(1)}(\eta,\eta')$ and $K^{(2)}(\eta,\eta')$will be equal [55, 97, 116, 123, 124]:

$$\left.\begin{aligned} \Lambda_{0n}^{(1)} &= \frac{i^n}{h_0}\left[R_{0n}^{(1)\prime}(C,1)\right]^{-1}; \\ \Lambda_{0n}^{(2)} &= \frac{i^n}{h_0}\left[R_{0n}^{(1)\prime}(C,1)\right]^{-1} \end{aligned}\right\}. \quad (8.17)$$

The distributions of $p_S^*(Q)$and $\partial p_S^*(Q)/\partial\xi'|_{\xi'=1}$are sought in the following series:

$$\left.\begin{aligned} p_S^*(Q) &= \sum_{n=0}^{\infty} a_{0n}\Lambda_{0n}^{(1)}\overline{S}_{0n}(C,\eta) \\ \left.\frac{dp_S^*(Q)}{d\xi'}\right|_{\xi'=0} &= \sum_{n=0}^{\infty} a_{0n}\Lambda_{0n}^{(2)}\overline{S}_{0n}(C,\eta) \end{aligned}\right\}. \quad (8.18)$$

Distributions (8.33) will be finite if series $\sum_n a_{0n}^2 \left(\Lambda_{0n}^{(1)}\right)^2$ and $\sum_n a_{0n}^2 \left(\Lambda_{0n}^{(2)}\right)^2$ coincide.

There are other methods to synthesize a linear antenna [122, 127]. In particular, A. A. Pistol'kors [130] applied eigen functions to the synthesis of a linear antenna, using a system of elliptic cylindrical coordinates and the eigen functions of an elliptic cylinder (Mathieu functions). The antenna appeared in the form of a hole with a width d of infinite length. But since the antenna distribution along the length of the antenna remains constant, it appears to be recruited from an infinite number of identical linear antennas. This is because its tranverse distribution is nothing more than the distribution of the field in the linear antenna. Another method for synthesizing a linear antenna—the partial diagram method—is based on the representation of a desired field distribution in the form of a convergent series of exponential functions. Then, the role of partial diagrams (angular characteristics) is played by the function $S_n(z) = [sin\,\pi\,(n-z)/\pi(n-z)]$. In another version of this method, the partial diagrams are Bessel functions. When using the Fourier integral method with reference to the synthesis of a linear antenna, the antenna is assumed to be infinitely long, but the field distribution behind its physical wire is assumed to be close to zero. In practice, very often the angular characteristic $R_1(\eta)$is given in tabular form. On the basis of the characteristic Fourier coefficients a_{mn} may not satisfy the necessary conditions for physical realization. In this case, one must resort to approximate solutions, which provide physically realizable angular characteristics. Fig 8-1 shows two angular characteristics: (1) The solid curve shows the modulus $|R_1(\eta)|$ for a soft prolate spheroid with a radial coordinate $\xi_0 = 1{,}005$, where the wave size of the body us $C=10{,}0$; (2) the characteristic $R_1(\eta)$ was given in tabular form with Step 5°. The dashed curve refers to the modulus of the angular characteristic $|R_1^*(\eta)|$of the synthesized antenna, with the form of an oblate spheroid with a radial coordinate of $\xi_0 = 0{,}1005$ at wave size $C=10{,}0$. When the given function $R_1(\eta)$is approximated with any degree of accuracy by a function possesses the required properties, the criterion for their proximity will be the smallness of the value $max|R_1(\eta,\phi) - R_1^*(\eta,\phi)|$.

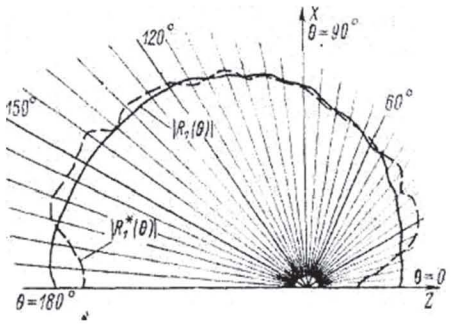

Figure 8-1: Modules of a given $|R_1(\theta)|$ and its synthesized $|R_1^*(\theta)|$ angular characteristic

Another approximate method for the synthesis of an antenna, is called approximate-on synthesis. In this method, the predetermined angular characteristic or a directivity diagram is represented as a polynomial and well-known methods of the theory of interpolation are used to determine its coefficients so that an obtained polynomial, in a sense, constitutes the best approach was for approaching a given characteristic. The degree of approximation of the obtained angular characteristic relative to a given factor is estimated by means of the norm:

$$Q(A) = \left\| R_1(\eta,\varphi) - R_1^*(\eta,\varphi) \right\|, \quad (8.19)$$

where A represents coefficients of the approximating polynomial.

A solution to the synthesis problem involves a set of coefficients A_{opt}, which minimize the functional (8.19).

A method for the synthesis of surface and linear antennas using eigen functions can be found in volume V_0 of the spheroidal form with the external surface $\xi_0$using the angular characteristic $R_1(\eta,\phi)$. These functions are related by an integral equation [120, 126–129]:

$$R_1(\eta,\varphi) = \int_{V_0} F(\xi',\eta',\varphi') K(\eta,\varphi;\xi',\eta',\varphi') d\xi' d\eta' d\varphi', \quad (8.20)$$

where

$F(\xi',\eta',\varphi') = h_0^3(\xi'^2 - \eta'^2)\Phi(\xi',\eta',\varphi');$

The solution to the equation (8. 20) represents a series:

$$F(\xi',\eta',\varphi') = \sum_{m=0}^{\infty}\sum_{n\geq m}^{\infty} b_{mn}\overline{S}_{mn}(C,\eta')\exp im\varphi' R_{mn}^{(1)}(C,\xi'), \quad (8.21)$$

where this represents the Fourier coefficients of given angular characteristic.

The distribution $F(\xi',\eta',\phi')$ is physically realizable if the series $\sum_n\sum_m b_{mn}^2\left[R_{mn}^{(1)}(C,\xi_0)\right]^2$ converges. Because of the zero-point scale factors, the density of sources has a singularity in the coordinate system: $\xi' = 1;\ \eta' = 1.$

8.3. Evaluation of Antenna Efficiency Using a Reactivity Parameter

The efficiency of a surface and active (radiating) antenna is determined, on the one hand, by the ratio between the active $(r_S)$and reactive (x_S)components of the radiation resistance z but, on the other hand, the reactivity parameter Q can also be used, if the antenna power W is represented in the form $W = Re\,W + i\,Im\,W$. In the latter case, the reactivity parameter Q curvilinear surface antenna of a spheroidal form providing the directivity characteristic of $R_1(\eta,\phi)$is equal to $Q = |Im\,W|/|Re\,W|$. The pressure distribution on the surface antenna in accordance with (8.27) has the form [7, 55, 121]:

$$p_1(\eta,\varphi) = \sum_{m=0}^{\infty}\sum_{n\geq m}^{\infty} a_{mn}\Lambda_{mn}^{(1)}\overline{S}_{mn}(C,\eta)\exp im\varphi, \quad (8.22)$$

where

$\Lambda_{mn}^{(1)} = i^{1+n}kR_{mn}^{(3)}(C,\xi')|_{\xi'=\xi_0}.$

The normal component [of the vibrational velocity of antenna points $v_n(\eta,\phi)$, in turn, will be

$$v_n(\eta,\varphi) = -\frac{1}{i\omega\rho_0}\frac{1}{h_{\xi_0}}\left.\frac{dp_1(\eta,\varphi)}{d\xi'}\right|_{\xi'=\xi_0}. \quad (8.23)$$

The total power of the synthesized antenna, providing a given angular characteristic, can be found to be [7, 55, 121]

$$W = \frac{1}{2\omega\rho_0}\int_S \frac{i}{h_{\xi_0}} p_1(\eta,\varphi)\left.\frac{dp_1^*(\eta,\varphi)}{d\xi'}\right|_{\xi'=\xi_0} dS =$$

$$= \frac{\pi h_0\left(\xi_0^2-1\right)}{\omega\rho_0}k^2 i\sum_{m=0}^{\infty}\sum_{n\geq m}^{\infty}|a_{mn}|^2 R_{mn}^{(3)}(C,\xi_0)R_{mn}^{(4)'}(C,\xi_0), \quad (8.24)$$

where

$R_{mn}^{(4)}(C,\xi_0) = R_{mn}^{(1)}(C,\xi_0) - iR_{mn}^{(2)}(C,\xi_0);$

$p_1^*(\eta,\phi)$ – complex conjugate $p_1(\eta,\phi)$.

The radiated power is determined by the real part (8.24) and the reactive imaginary part (8.24). We will now consider the special case of the angular characteristic $R_1(\eta,\phi)$, which is represented as the product of the following eigen function:

$$R_1(\eta,\varphi) = \overline{S}_{mn}(C,\eta)\exp im\varphi. \quad (8.25)$$

In view of the orthogonality of the eigen function, only one Fourier coefficient is different from the zero of the characteristic $R_1(\eta,\phi)$ with indices m and n : $a_{mn}=1$. The pressure distribution

$p_1(\eta,\phi)$ along the antenna surface repeats the given characteristic $R_1(\eta,\phi)$ and the total power

of the antenna W will be equal to {7, 55, 121]

$$W=\frac{k^2h_0\pi}{\omega\rho_0}(\xi_0^2-1)i\left\{R_{mn}^{(1)}(C,\xi_0)R_{mn}^{(1)'}(C,\xi_0)+R_{mn}^{(2)}(C,\xi_0)R_{mn}^{(2)'}(C,\xi_0)+\right.$$

$$\left.+i\left[R_{mn}^{(1)}(C,\xi_0)R_{mn}^{(2)'}(C,\xi_0)-R_{mn}^{(2)}(C,\xi_0)R_{mn}^{(1)'}(C,\xi_0)\right]\right\}$$

The reactivity parameter Q in this case is calculated from formulae [7, 55, 121].

$$Q=\frac{\left|R_{mn}^{(1)}(C,\xi_0)R_{mn}^{(1)'}(C,\xi_0)+R_{mn}^{(2)}(C,\xi_0)R_{mn}^{(2)'}(C,\xi_0)\right|}{\left|R_{mn}^{(1)}(C,\xi_0)R_{mn}^{(2)'}(C,\xi_0)-R_{mn}^{(2)}(C,\xi_0)R_{mn}^{(1)'}(C,\xi_0)\right|}. \quad (8.26)$$

Figure 8-2: shows the comparison function values *Q(n)* for antennas with a radial coordinate

$\xi_0=1{,}005$ and $\xi_0=1{,}6$ at *m=0* and wave size *C=10,0.* The higher the reactivity, the greater the number of mode *n*; the antenna of smaller dimensions ($\xi_0=1{,}005$) has a higher reactivity. Figure 8-3 shows the reactivity parameter Q of the pulsating mode *(m=0, n=0)* is the range of the radial coordinate ξ_0 from *1,005* to *10,0.*, while the wave size C is still equal to *10,0.* With a further increase in the radial coordinate ξ_0, the function $Q(\xi_0)$ will tend asymptotically towards zero.

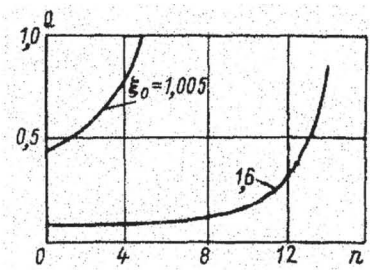

Figure 8-2: Dependence of the reactivity parameter on the mode number

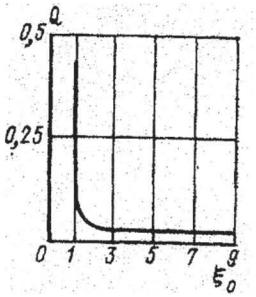

Figure 8-3: Dependence of the reactivity parameter on the radial coordinate

We will find the partial acoustic resistance z on which the antenna with the angular characteristic (8.25) is loaded [7, 55, 121]:

$$z=x+iy=\left.\frac{p_1(\eta,\varphi)}{v_n(\eta,\varphi)}\right|_{\xi=\xi_0}=-i\omega\rho_0h_{\xi_0}\frac{R_{mn}^{(3)}(C,\xi_0)\left[R_{mn}^{(4)'}(C,\xi_0)\right]}{\left[R_{mn}^{(1)'}(C,\xi_0)\right]^2+\left[R_{mn}^{(2)'}(C,\xi_0)\right]^2};$$

$$x=-i\omega\rho_0h_{\xi_0}\frac{R_{mn}^{(1)}(C,\xi_0)R_{mn}^{(2)'}(C,\xi_0)-R_{mn}^{(2)}(C,\xi_0)R_{mn}^{(1)'}(C,\xi_0)}{\left[R_{mn}^{(1)'}(C,\xi_0)\right]^2+\left[R_{mn}^{(2)'}(C,\xi_0)\right]^2}=$$

$$=\frac{\omega\rho_0h_{\xi_0}W^{(1),(2)}}{\left[R_{mn}^{(1)'}(C,\xi_0)\right]^2+\left[R_{mn}^{(2)'}(C,\xi_0)\right]^2}. \quad (8.27)$$

where $W^{(1),(2)}$ represents the Wronskian of the 1st and 2nd kinds of functions

$$y = -i\omega\rho_0 h_{\xi_0} \frac{R_{mn}^{(1)}(C,\xi_0)R_{mn}^{(1)'}(C,\xi_0) - R_{mn}^{(2)}(C,\xi_0)R_{mn}^{(2)'}(C,\xi_0)}{\left[R_{mn}^{(1)'}(C,\xi_0)\right]^2 + \left[R_{mn}^{(2)'}(C,\xi_0)\right]^2}. \quad (8.28)$$

Comparing (8.27) and (8.28) with (8.26), we find that the reactivity parameter Q of the acoustic

(8.25) is equal to the ratio of the modules of the active and reactive parts of the full acoustic resistance:

$Q = |y|/|x|$.

8.4. The synthesis of a Compensating Antenna

Along with passive methods to compensate for pressure in a reflector or scattered waves [130 132], one can achieve the same goal and active means, based on the application of a compensating radiating system which creates, at the point of reception, the opposite pressure on the sign. In the expression for the pressure in the scattered field $p_s(P)$ (where P represents the observation point), we separate, as usual, the radial and angular function

$$p_s(P) = \frac{e^{ik\sigma r}}{r} R_0(\alpha, \phi),$$

where r represents the distance between the point P and the center of the scatterer O ((Fig. 8-4); $k = \frac{2\pi}{\lambda}$;

the wave number $R_0(\alpha, \phi) = |R_0(\alpha, \phi)|\, exp[i\Phi_0(\alpha, \phi)]$ represents a scattering characteristic; λ represents the length of a sound wave in a medium; $\Phi_0(\alpha, \phi)$ represents the phase characteristic; and α, φ represents angular coordinates of the observation point (Fig. 8-4).

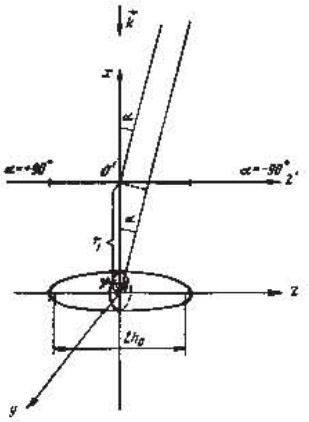

Figure 8-4: The mutual arrangement of the scatterer and the compensating antenna

On the basis of $R_0(\alpha, \phi)$ we synthesize the radiating system using the amplitude angular characteristic of which $|R_0(\alpha, \phi)|$ will be close to the selected sectors of angles α and φ. The phase angular characteristic of an antenna $= \Phi_1(\alpha, \phi)$ will shifted by π relative to the angular phase characteristic $\Phi_0(\alpha, \phi)$.

The accurate reproduction of the directivity characteristic $R_1(\alpha, \phi) = |R_1(\alpha, \phi)|\, exp[i\Phi_1(\alpha, \phi)]$ is only possible if it belongs to functions of the class $W_{\sigma,\sigma'}$ [122]. Otherwise, we can only talk about the approximate directional characteristic, $R_1^*(\alpha, \phi)$. Since the compensating antenna is intended to compensate for the pressure created by an ideal soft spheroid scattered wave in the Fraunhofer zone, we use the expression $R_0(\alpha, \phi)$ for spheroidal functions. The wave incident on the body is assumed to be plane [7, 55, 117, 126]

$$R_0(\alpha, \phi) = -\frac{2}{ik}\sum_{m=0}^{\infty}\sum_{n\geq m}^{\infty}(-1)^n \in_m \overline{S}_{m,n}\left[C, cos\left(\alpha - \frac{\pi}{2}\right)\right] \times$$

$$\times \overline{S}_{m,n}[C, cos(\alpha_0 - \frac{\pi}{2})] \frac{R^{(1)}_{m,n}(C, \xi_0)}{R^{(3)}_{m,n}(C, \xi_0)} cos\, m\, \phi$$

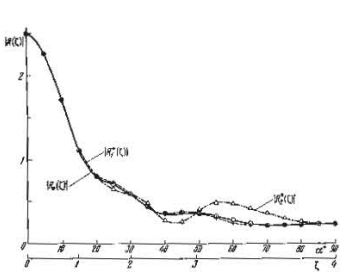

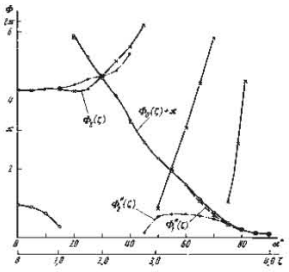

Figure 8-5 (left): Modules of the angular characteristics of the scatterer and synthesized antenna

Figure 8-6 (right): Phase angular characteristics of the scatterer and synthesized antenna

We will consider a linear antenna that must compensate for the scattered field of the soft spheroid for the angles $\alpha = -90° \div +90°$, $\phi = 0 - 5°, 355° - 360°$. We note that, in this sector, along the azimuthal angle φ, the radius-vectors of the initial diagrams only vary a little. At the first stage, the natural path difference between the antenna and the scatterer is not taken into account. It is assumed that the antenna and the scatterer are in the same region of the medium. Alternately, the longitudinal axis of the antenna coincides with the Z axis, and its center is at point O (Fig. 8-4). Since the initial amplitude and phase characteristics of the scatterer were specified in tabular form, the method of synthesis will be approximate. When calculating the sensitivity

$f_1(\gamma) = |F_1(\gamma)|\, exp[i\psi_1(\gamma)]$ $\left(\gamma = \frac{2\pi z'}{l}\right)$, ($l$ represents the length of the radiating system; z' represents the distance along the antenna, as measured from its center) and for the directional characteristics we used expansions [122, 126]:

$$f_1(\gamma) = \sum_{n=-entiera}^{n=entiera} R_1(n) e^{-in\gamma};$$

$$R_1^*(\zeta) = \sum_{n=-entiera}^{n=entiera} R_1(n) S_n(\zeta).$$

Expansion coefficients $R_1(n)$ (partial characteristics) are equal to values $R_1(\xi)$ in integer points.

The module with the largest integer is $|n_{max}|||a$ because the symmetry of the scattering diagram and the partial characteristics are identical pairs $R(+n) = R(-n)$).

The found partial characteristics enabled us to calculate the amplitude $|E_1(\gamma)|$ and phase - $\psi_1(\gamma)$ characteristics of the sensitivity distribution along the linear antenna (Fig. 8-7), as well as its amplitude and phase directional characteristics (as previously shown in Figures 8-5 and 8-6).

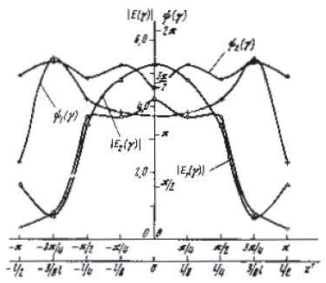

Figure 8-7: Amplitude and phase distribution of the synthesized linear antenna's sensitivity

The above method, with the help of function $S_n(\xi)$ was used to calculate the sensitivity of $f_2(\gamma)$ and the directional characteristic of the compensating antenna $R_2^*(\xi)$ (Figs. 8-5, 8-6, and 8-7). As we see, compensation is only observed within the limits of the main maximum of the scattering ($\alpha = 0° \pm 40°$). To achieve compensation in the remaining field of the angle change, α, it is necessary to increase the dimensions of the antenna (that is, to increase the parameter a). As a result of this, the number of nodal points n will grow, in which the initial and calculated directional characteristics coincide. Due to the natural difference between the paths taken, the relative amplitude compensation

$$\frac{|R_\Sigma|}{|R_0(\alpha,\phi)|} = \frac{|R_0(\alpha,\phi) + R_2{}^*(\alpha,\phi)|}{|R_0(\alpha.\phi)|}$$

at angle φ in the selected range of the variation will not exceed 8%.

CHAPTER 9

THE CHARACTERISTICS OF SOUND SCATTERING FROM INFINITE CYLINDERS

9.1. The Solution for Three-Dimensional Problems of Sound Diffraction on Elastic Bodies with a Cylindrical Form Using Debye Potentials

We will now turn to the oblique incidence of the plane wave on the elastic hollow cylindrical shell. The geometry of the problem is shown in Fig. 9-1.

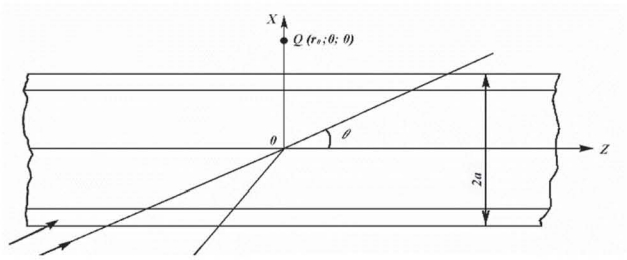

Figure 9-1: Hollow elastic cylindrical shell in the field of the plane sound wave

The scalar potential of an incident wave $\Phi_i(r,\phi,z)$ for a unit amplitude with a wave vector$\vec{k}$tilted at an angle of θ the axis Z. We can expand this in terms of eigen functions of the scalar Helmholtz equation in a circular cylindrical coordinate system:

$$\Phi_i(r,\phi,z) = e^{i\gamma z}\sum_{m=0}^{\infty}\varepsilon_m(-i)^m J_m(k_\gamma r)\ \cos m\,\phi, \qquad (9.1)$$

where$\gamma = k\cos\theta$; $k_\gamma = k\sin\theta$; $\varepsilon_m = \begin{cases}1 \text{ by } m = 0;\\ 2 \text{ by } m \neq 0.\end{cases}$

We can now transform the representation for the vector function, $\vec{A}$generated in [100], by introducing an additional operator *rot* in order that$\vec{A}$automatically obeys the gauge condition ($div\vec{A} = 0$):

$$\vec{A} = curl(\chi\vec{e}_z) + curlcurl(\psi\vec{e}_z), \qquad (9.2)$$

where $\vec{e}_z$ represents the unit vector in the direction of the Z axis and χ and ψ represent scalar potentials which satisfy the scalar Helmholtz equation [7, 67, 71, 100, 108]:

$$\left.\begin{aligned}\Delta\chi + k_2^2\chi = 0\\ \Delta\psi + k_2^2\psi = 0\end{aligned}\right\} \qquad (9.3)$$

Components of vector function$\vec{A}$, in accordance with (9.2), will accept the following:

$$\left.\begin{aligned}A_r &= \frac{1}{r}\frac{\partial\chi}{\partial\phi} + \frac{\partial^2\psi}{\partial r\partial z}\ ;\\ A_\phi &= -\frac{\partial\chi}{\partial r} + \frac{1}{r}\frac{\partial^2\psi}{\partial\phi\partial z}\ ;\\ A_z &= -\frac{1}{r}\frac{\partial\psi}{\partial r} - \frac{\partial^2\psi}{\partial r^2} - \frac{1}{r^2}\frac{\partial^2\psi}{\partial\phi^2}\ ,\end{aligned}\right\} \qquad (9.4)$$

Components of the displacement vector $\vec{u}$ will be equal to:

$$\left.\begin{aligned} U_r &= \frac{\partial \Phi}{\partial r} - \frac{1}{r^2}\frac{\partial^2 \psi}{\partial r \partial \phi} - \frac{1}{r}\frac{\partial^3 \psi}{\partial r^2 \partial \phi} - \frac{1}{r^3}\frac{\partial^3 \psi}{\partial \phi^3} + \\ &\quad + \frac{\partial^2 \chi}{\partial r \partial z} - \frac{1}{r}\frac{\partial^3 \psi}{\partial \phi \partial z^2}\ ; \\ U_\phi &= \frac{1}{r}\frac{\partial \Phi}{\partial \phi} + \frac{1}{r}\frac{\partial^2 \chi}{\partial \phi \partial z} + \frac{\partial^3 \psi}{\partial r \partial z^2} + \frac{1}{r^2}\frac{\partial \psi}{\partial r} - \\ &\quad - \frac{1}{r}\frac{\partial^2 \psi}{\partial r^2} - \frac{\partial^3 \psi}{\partial r^3} + \frac{2}{r^3}\frac{\partial^2 \psi}{\partial \phi^2} - \frac{1}{r^2}\frac{\partial^3 \psi}{\partial r \partial \phi^2}\ ; \\ U_z &= \frac{\partial \Phi}{\partial z} - \frac{1}{r}\frac{\partial \chi}{\partial r} + \frac{1}{r^2}\frac{\partial^2 \psi}{\partial \phi \partial z} - \frac{\partial^2 \chi}{\partial r^2} - \frac{1}{r^2}\frac{\partial^2 \psi}{\partial \phi \partial z} + \\ &\quad - \frac{1}{r^2}\frac{\partial^2 \chi}{\partial \phi^2}. \end{aligned}\right\} \quad (9.5)$$

Potentials Φ, χ, Ψ and the potential of the scattering wave $\Phi_s$expand in terms of the eigen functions of the scalar Helmholtz equation in a circular cylindrical system:

$$\left.\begin{aligned} \Phi &= e^{i\gamma z}\sum_{m=0}\left[A_m J_m\left(h' r\right) + B_m N_m\left(h' r\right)\right] \cos m\,\phi\ ; \\ \chi &= e^{i\gamma z}\sum_{m=0}^{\infty}\left[C_m J_m\left(æ' r\right) + D_m N_m\left(æ' r\right)\right] \cos m\,\phi\ ; \\ \Psi &= e^{i\gamma z}\sum_{m=1}^{\infty}\left[E_m J_m\left(æ' r\right) + F_m N_m\left(æ' r\right)\right] \sin m\,\phi\ ; \\ \Phi_s &= e^{i\gamma z}\sum_{m=0}^{\infty} G_m H_m^{(1)}\left(k_\gamma r\right) \cos m\,\phi\ , \end{aligned}\right\} \quad (9.6)$$

where$h' = (k_1^2 - k^2)^{1/2}$; $æ' = (k_2^2 - k^2)^{1/2}$; and$A_m, B_m, C_m, D_m, E_m, F_m, G_m$represent unknown coefficients. We will find these from the following boundary conditions:

1) The continuity of the normal components from the displacement vector in an elastic shell and a liquid medium at the outer boundary *(r=a)*:

$$\frac{\partial \Phi}{\partial r} - \frac{1}{r^2}\frac{\partial^2 \Psi}{\partial r \partial \phi} - \frac{1}{r}\frac{\partial^3 \Psi}{\partial r^2 \partial \phi} - \frac{1}{r^3}\frac{\partial^3 \Psi}{\partial \phi^3} + \frac{\partial^2 \chi}{\partial r \partial z} - \\ - \frac{1}{r}\frac{\partial^3 \Psi}{\partial \phi \partial z^2} = \frac{\partial}{\partial r}(\Phi_i + \Phi_s)\Big|_{r=a} \quad (9.7)$$

2) The equality between the normal stress in the elastic shell at the outer boundary to the pressure in a liquid medium:

$$(\lambda + 2\mu)\frac{\partial U_r}{\partial r} + \lambda\left(r^{-1}\frac{\partial U_\phi}{\partial \phi} + r^{-1}U_r + \frac{\partial U_z}{\partial z}\right) = \\ = -\rho_0 \omega^2 (\Phi_i + \Phi_s)|_{r=a}\ , \quad (9.8)$$

where$\rho_0$represents the density of the liquid medium.

3) The absence of the normal stress from the hollow shell's inside boundary:

$$(\lambda + 2\mu)\frac{\partial U_r}{\partial r} + \lambda\left(r^{-1}\frac{\partial U_\phi}{\partial \phi} + r^{-1}U_r + \frac{\partial U_z}{\partial z}\right) = 0|_{r=b} \quad (9.9)$$

4) The absence of tangential stresses on both boundaries of the shell:

$$\left.\begin{aligned} &\frac{\partial U_\phi}{\partial r} + r^{-1}\frac{\partial U_r}{\partial \phi} - r^{-1}U_\phi = 0\Big|_{\substack{r=a;\\ r=b}}\ ; \\ &\frac{\partial U_r}{\partial z} + \frac{\partial U_z}{\partial r} = 0\Big|_{\substack{r=a.\\ r=b}} \end{aligned}\right\} \quad (9.10)$$

Substituting expansions (9.1) and (9.6) in (9.5) and then the boundary conditions in (9.7)–(9.10), we obtain the heterogeneous system of seven equations with respect to an infinite number of unknown coefficients for the expansions of potentials. Using the orthogonality of trigonometric functions *cos mφ* and *sin mφ,* we can reduce the problem to that of finding seven unknown coefficients with a fixed index m: $A_m, B_m, C_m, D_m, E_m, F_m, G_m$of the seven equations boundary conditions) from heterogeneous system. Coefficients $G_m$of the potential of the scattered wave Φ_s that is of interest in the first place will be found using Cramer's rule from the ratio of two determinants from the seventh order [7, 67, 71, 108]:

$$G_m = \Delta'/\Delta \,, \qquad (9.11)$$

where Δ' represents the minor of the system and Δ represents its determinant, which is equal to [7, 67, 71,108]:

$$a_{12} = N_m'(h'a) \,;$$

$$a_{13} = ikJ_m'(æ'a) \,;$$

$$a_{11} = J_m'(h'a) \,;$$

$$a_{12} = N_m'(h'a) \,;$$

$$a_{13} = ikJ_m'(æ'a) \,;$$

$$a_{14} = ikN_m'(æ'a) \,;$$

$$a_{15} = a^{-1}mJ_m(æ'a)\left(a^{-2}m^2 + k^2\right) - a^{-2}mJ_m'(æ'a) - \\ - a^{-1}mJ_m''(æ'a) \,;$$

$$a_{16} = a^{-1}mN_m(æ'a)\left(a^{-2}m^2 + k^2\right) - a^{-2}mN_m'(æ'a) - \\ - a^{-1}mN_m''(æ'a) \,;$$

$$a_{17} = -H_m^{(1)'}(k_\gamma a) \,;$$

$$a_{21} = (\lambda + 2\mu)J_m''(h'a) + \lambda\left[a^{-1}J_m'(h'a) - \right. \\ \left. - \left(m^2a^{-2} + k^2\right)J_m(h'a)\right] \,;$$

$$a_{23} = 2\mu ikJ_m''(æ'a) \,;$$

$$a_{24} = 2\mu ikN_m''(æ'a) \,;$$

$$a_{25} = (\lambda + 2\mu)a^{-1}\left\{ma^{-1}J_m(æ'a)\left(a^{-1}m^2 - k^2 - 3a^{-2}m^2\right) + \right. \\ + mJ_m'(æ'a)\left(2a^{-2} + k^2\right) - mJ_m'''(æ'a)\Big\} + \\ + \lambda a^{-1}\left\{a^{-1}mJ_m(æ'a)\left(k^2 - a^{-2}m^2\right) + \right. \\ \left. + mJ_m'(æ'a)\left(a^{-2}m^2 - k^2\right) - 2a^{-1}mJ_m''(æ'a) - mJ_m'''(æ'a)\right\} \,;$$

$$a_{26} = (\lambda + 2\mu)a^{-1}\left\{ma^{-1}N_m(æ'a)\left(a^{-1}m^2 - k^2 - 3a^{-2}m^2\right) + \right. \\ + mN_m'(æ'a)\left(2a^{-2} + k^2\right) - mN_m'''(æ'a)\Big\} + \\ + \lambda a^{-1}\left\{a^{-1}mN_m(æ'a)\left(k^2 - a^{-2}m^2\right) + \right. \\ \left. + mN_m'(æ'a)\left(a^{-2}m^2 - k^2\right) - 2a^{-1}mN_m''(æ'a) - mN_m'''(æ'a)\right\} \,;$$

$$a_{27} = \rho_0\omega^2 H_m^{(1)}(k_\gamma a) \,;$$

$$a_{31} = (\lambda + 2\mu)J_m''(h'b) + \lambda\left[b^{-1}J_m'(h'b) - \right. \\ \left. - \left(m^2b^{-2} + k^2\right)J_m(h'b)\right] \,;$$

$$a_{32} = (\lambda + 2\mu)N_m''(h'b) + \lambda\left[b^{-1}N_m'(h'b) - \right. \\ \left. - \left(m^2b^{-2} + k^2\right)N_m(h'b)\right] \,;$$

$$a_{33} = 2\mu ikJ_m''(æ'b) \,;$$

$$a_{34} = 2\mu ikN_m''(\text{æ}'b) ;$$

$$\begin{aligned} a_{35} = {} & (\lambda + 2\mu)b^{-1}\{mb^{-1}J_m(\text{æ}'b)(b^{-1}m^2 - k^2 - 3b^{-2}m^2) + \\ & + mJ_m'(\text{æ}'b)(2b^{-2} + k^2) - mJ_m''(\text{æ}'b)\} + \\ & + \lambda b^{-1}\{b^{-1}mJ_m(\text{æ}'b)(k^2 - b^{-2}m^2) + \\ & + mJ_m'(\text{æ}'b)(b^{-2}m^2 - k^2) - 2b^{-1}mJ_m''(\text{æ}'b) - mJ_m'''(\text{æ}'b)\}; \end{aligned}$$

$$\begin{aligned} a_{36} = {} & (\lambda + 2\mu)b^{-1}\{mb^{-1}N_m(\text{æ}'b)(b^{-1}m^2 - k^2 - 3b^{-2}m^2) + \\ & + mN_m'(\text{æ}'b)(2b^{-2} + k^2) - mN_m'''(\text{æ}'b)\} + \\ & + \lambda\, b^{-1}\{b^{-1}mN_m(\text{æ}'b)(k^2 - b^{-2}m^2) + \\ & + mN_m'(\text{æ}'b)(b^{-2}m^2 - k^2) - 2b^{-1}mN_m''(\text{æ}'b) - mN_m'''(\text{æ}'b)\}; \end{aligned}$$

$$a_{37} = 0 ;$$

$$a_{41} = 2ma^{-1}\left[a^{-1}J_m(h'a) - J_m'(h'a)\right] ;$$

$$a_{42} = 2ma^{-1}\left[a^{-1}N_m(h'a) - N_m'(h'a)\right] ;$$

$$a_{43} = 2mika^{-1}\left[a^{-1}J_m(\text{æ}'a) - J_m'(\text{æ}'a)\right] ;$$

$$a_{44} = 2mika^{-1}\left[a^{-1}N_m(\text{æ}'a) - N_m'(\text{æ}'a)\right] ;$$

$$\begin{aligned} a_{45} = {} & a^{-1}m^2J_m(\text{æ}'a)(8a^{-3} - a^{-2}m^2 - k^2) + \\ & + a^{-3}J_m'(\text{æ}'a)(3k^2 - 3 - 4m^2) + \\ & + a^{-2}J_m''(\text{æ}'a)(3 - k^2 + 2m^2) + \\ & + a^{-1}J_m'''(\text{æ}'a) - J_m^{IV}(\text{æ}'a); \end{aligned}$$

$$\begin{aligned} a_{46} = {} & a^{-1}m^2N_m(\text{æ}'a)(8a^{-3} - a^{-2}m^2 - k^2) + \\ & + a^{-3}N_m'(\text{æ}'a)(3k^2 - 3 - 4m^2) + \\ & + a^{-2}N_m''(\text{æ}'a)(3 - k^2 + 2m^2) + \\ & + a^{-1}N_m'''(\text{æ}'a) - N_m^{IV}(\text{æ}'a); \end{aligned}$$

$$a_{47} = 0 ;$$

$$a_{51} = 2mb^{-1}\left[b^{-1}J_m(h'b) - J_m'(h'b)\right] ;$$

$$a_{52} = 2mb^{-1}\left[b^{-1}N_m(h'b) - N_m'(h'b)\right] ;$$

$$a_{53} = 2mikb^{-1}\left[b^{-1}J_m(\text{æ}'b) - J_m'(\text{æ}'b)\right] ;$$

$$a_{54} = 2mikb^{-1}\left[b^{-1}N_m(\text{æ}'b) - N_m'(\text{æ}'b)\right] ;$$

$$\begin{aligned} a_{55} = {} & b^{-1}m^2J_m(\text{æ}'b)(8b^{-3} - b^{-2}m^2 - k^2) + \\ & + b^{-3}J_m'(\text{æ}'b)(3k^2 - 3 - 4m^2) + \\ & + b^{-2}J_m''(\text{æ}'b)(3 - k^2 + 2m^2) + \\ & + b^{-1}J_m'''(\text{æ}'b) - J_m^{IV}(\text{æ}'b); \end{aligned}$$

$$a_{56} = b^{1}m^{2}N_m(æ'b)\left(8b^{3} - b^{2}m^{2} - k^{2}\right) +$$
$$+ b^{3}N'_m(æ'b)\left(3k^{2} - 3 - 4m^{2}\right) +$$
$$+ b^{2}N''_m(æ'b)\left(3 - k^{2} + 2m^{2}\right) +$$
$$+ b^{1}N'''_m(æ'b) - N_m^{IV}(æ'b);$$

$$a_{57} = 0;$$

$$a_{61} = 2ikJ'_m(h'a);$$

$$a_{62} = 2ikN'_m(h'a);$$

$$a_{63} = -2a^{-3}m^{2}J_m(æ'a) +$$
$$+ J'_m(æ'a)\left(a^{-2} + a^{-2}m^{2} - k^{2}\right) - J''_m(æ'a);$$

$$a_{64} = -2a^{-3}m^{2}N_m(æ'a) +$$
$$+ N'_m(æ'a)\left(a^{-2} + a^{-2}m^{2} - k^{2}\right) - N''_m(æ'a);$$

$$a_{65} = a^{1}mikJ_m(æ'a)\left(a^{2}m^{2} + k^{2}\right) +$$
$$+ a^{2}mikJ'_m(æ'a)\left(3a^{2} - 2\right) -$$
$$- a^{3}mikJ''_m(æ'a);$$

$$a_{66} = a^{1}mikN_m(æ'a)\left(a^{2}m^{2} + k^{2}\right) +$$
$$+ a^{2}mikN'_m(æ'a)\left(3a^{2} - 2\right) -$$
$$- a^{3}mikN''_m(æ'a);$$

$$a_{67} = 0;$$

$$a_{71} = 2ikJ'_m(h'b);$$

$$a_{72} = 2ikN'_m(h'b);$$

$$a_{73} = -2b^{3}m^{2}J_m(æ'b) +$$
$$+ J'_m(æ'b)\left(b^{2} + b^{2}m^{2} - k^{2}\right) - J''_m(æ'b);$$

$$a_{74} = -2b^{3}m^{2}N_m(æ'b) +$$
$$+ N'_m(æ'b)\left(b^{2} + b^{2}m^{2} - k^{2}\right) - N''_m(æ'b);$$

$$a_{75} = b^{1}mikJ_m(æ'b)\left(b^{2}m^{2} + k^{2}\right) +$$
$$+ b^{2}mikJ'_m(æ'b)\left(3b^{2} - 2\right) -$$
$$- b^{3}mikJ''_m(æ'b);$$

$$a_{76} = b^{1}mikN_m(æ'b)\left(b^{2}m^{2} + k^{2}\right) +$$
$$+ b^{2}mikN'_m(æ'b)\left(3b^{2} - 2\right) -$$
$$- b^{3}mikN''_m(æ'b);$$

$$a_{77} = 0;$$

$$b_{17} = \varepsilon_m(-i)^m J'_m(k_\gamma a);$$

$$b_{27} = -\rho_0 \omega^2 \varepsilon_m (-i)^m J_m(k_\gamma a) \ .$$

Now we will turn to the problem of the diffraction of a harmonic wave from the frequency ω from the point source Q on the elastic cylindrical shell. The source is at a distance of r_0 from the shell axis Z. The shell is placed in an external liquid medium with a density of ρ_0 and the velocity of a sound c_0.

The potential Φ_i of the harmonic point source is determined by series [7, 87, 71. 108, 133]:

$$\Phi_i(r,\phi,z) = \frac{i}{2}\sum_{n=0}^{\infty} cos(n\phi) \cdot \varepsilon_n \int_{-\infty}^{+\infty} exp(i\gamma z) \cdot H_n^{(1)}(k_\gamma r_0) \cdot J_n(k_\gamma r) d\gamma \ , (9.12)$$

where $k_\gamma = (k^2 - \gamma^2)^{1/2}$; $k = \omega/c_0$; γ and k_γ represent components of the wave vector $\vec{k}$axial and radial respectively (Fig. 9-1); $\varepsilon_n = \begin{cases} 1, & n = 0 \\ 2, & n \neq 0. \end{cases}$

The potential of the scattered wave $\Phi_s(r,\phi,z)$can be written in an analogous way:$\Phi_i(r,\phi,z)$

$$\Phi_s(r,\phi,z) = \sum_{n=0}^{\infty} a_n \, cos(n\phi) \cdot \int_{-\infty}^{+\infty} A(\gamma) \, exp(i\gamma z) \cdot H_n^{(1)}(k_\gamma r) \, d\gamma \ , (9.13)$$

where a_n and $A(\gamma)$ are unknown coefficients and functions γ, respectively.

These are found from the boundary conditions. We can write the cylindrical components of the displacement vector $\vec{U}(U_r, U_\phi, U_z)$ through the potential Φ and the cylindrical components of the function $\vec{A}(A_r, A_\phi, A_z)$ [133]:

$$\left.\begin{aligned} U_r &= \frac{\partial \Phi}{\partial r} + \frac{1}{r}\frac{\partial A_z}{\partial \phi} - \frac{\partial A_\phi}{\partial z} \ ; \\ U_\phi &= \frac{1}{r}\frac{\partial \Phi}{\partial \phi} + \frac{\partial A_r}{\partial z} - \frac{\partial A_z}{\partial r} \ ; \\ U_z &= \frac{\partial \Phi}{\partial z} + \frac{1}{r}A_\phi + \frac{\partial A_\phi}{\partial r} - \frac{1}{r}\frac{\partial A_r}{\partial \phi}. \end{aligned}\right\} \quad (9.14)$$

The cylindrical components $A_r, A_\phi, A_z$of the function $\vec{A}$are expressed through the Debye potential U and V [133]:

$$A_r = k_2^2 r U + r\frac{\partial^2 U}{\partial r^2} + z\frac{\partial^2 U}{\partial r \partial z} + 2\frac{\partial U}{\partial r} + i\frac{1}{r}k_2 z\frac{\partial V}{\partial \phi} \ ; \quad (9.15)$$

$$A_\phi = -ik_2\left[z\frac{\partial V}{\partial r} - r\frac{\partial V}{\partial z}\right] + \frac{1}{r}\frac{\partial U}{\partial \phi} + \frac{\partial^2 U}{\partial r \partial \phi} + \frac{1}{r}z\frac{\partial^2 U}{\partial z \partial \phi} \ ; (9.16)$$

$$A_z = k_2^2 z U + z\frac{\partial^2 U}{\partial z^2} - ik_2^2\frac{\partial V}{\partial \phi} + r\frac{\partial^2 U}{\partial r \partial z} + 2\frac{\partial U}{\partial z}, \quad (9.17)$$

where k_2 represents the wave number of the transverse wave in the material of the shell.

The potentials Φ, U, and V also decompose into series on own functions of the scalar Helmholtz equation [7, 67, 71, 108, 133]:

$$\Phi(r,\varphi,z) = \sum_{n=0}^{\infty} cos(n\varphi)\left[b_n \int_{\infty}^{+\infty} B(\gamma) exp(i\gamma z) J_n(h_\gamma r) d\gamma + \right.$$
$$\left. + b_n' \int_{\infty}^{+\infty} B'(\gamma) exp(i\gamma z) N_n(h_\gamma r) d\gamma \right]; \quad (9.18)$$

$$U(r,\varphi,z)=\sum_{n=1}^{\infty} sin(n\varphi)\left[c_n\int_{\infty}^{+\infty}C(\gamma)exp(i\gamma z)J_n(æ_\gamma r)d\gamma + c_n'\int_{\infty}^{+\infty}C'(\gamma)exp(i\gamma z)N_n(æ_\gamma r)d\gamma\right]; \quad (9.19)$$

$$V(r,\varphi,z)=\sum_{n=0}^{\infty} cos(n\varphi)\left[d_n\int_{\infty}^{+\infty}D(\gamma)exp(i\gamma z)J_n(æ_\gamma r)d\gamma + d_n'\int_{\infty}^{+\infty}D'(\gamma)exp(i\gamma z)N_n(æ_\gamma r)d\gamma\right]; \quad (9.20)$$

where $h_\gamma=(k_1^2-\gamma^2)^{1/2}$; $k_1=\omega/c_1$represents the wave number $f$of the longitudinal wave in the material of the shell; c_1 represents the velocity of the longitudinal wave in the material of a shell; $N_n(æ_\gamma r)$ represents the cylindrical Neumann function; $æ_\gamma=(k_2^2-\gamma^2)^{1/2}$;$b_n, b_n'$; c_n, c_n';d_n, d_n' and $B(\gamma)$, $B'(\gamma)$; $C(\gamma)$, $C'(\gamma)$; $D(\gamma)$, $D'(\gamma)$ represent the unknown coefficients and functions, respectively. These are determined from the following boundary conditions:

1) A normal component of displacement vector $U_r$is continuous on the outer boundary of the shell

2) The sound pressure in a liquid is equal to the normal stress exerted on the outer boundary of the shell

3) The normal stress experienced within a shell on an internal boundary is zero

4) Tangential stresses on shell boundaries are zero

In an analytical form, the listed boundary conditions are as follows:

$$\Delta' \quad (9.21)$$

$$\Delta=\begin{vmatrix} a_{11} & a_{12} & a_{13} & a_{14} & a_{15} & a_{16} & a_{17}\\ a_{21} & a_{22} & a_{23} & a_{24} & a_{25} & a_{26} & a_{27}\\ a_{31} & a_{32} & a_{33} & a_{34} & a_{35} & a_{36} & a_{37}\\ a_{41} & a_{42} & a_{43} & a_{44} & a_{45} & a_{46} & a_{47}\\ a_{51} & a_{52} & a_{53} & a_{54} & a_{55} & a_{56} & a_{57}\\ a_{61} & a_{62} & a_{63} & a_{64} & a_{65} & a_{66} & a_{67}\\ a_{71} & a_{72} & a_{73} & a_{74} & a_{75} & a_{76} & a_{77} \end{vmatrix}, \quad (9.22)$$

$$\Delta'=\begin{vmatrix} b_{11} & a_{12} & a_{13} & a_{14} & a_{15} & a_{16} & a_{17}\\ b_{21} & a_{22} & a_{23} & a_{24} & a_{25} & a_{26} & a_{27}\\ 0 & a_{32} & a_{33} & a_{34} & a_{35} & a_{36} & a_{37}\\ 0 & a_{42} & a_{43} & a_{44} & a_{45} & a_{46} & a_{47}\\ 0 & a_{52} & a_{53} & a_{54} & a_{55} & a_{56} & a_{57}\\ 0 & a_{62} & a_{63} & a_{64} & a_{65} & a_{66} & a_{67}\\ 0 & a_{72} & a_{73} & a_{74} & a_{75} & a_{76} & a_{77} \end{vmatrix}. \quad (9.23)$$

$$\frac{\partial U_\phi}{\partial r}-\frac{1}{r}U_\phi+\frac{1}{r}\frac{\partial U_r}{\partial \phi}=0|_{\substack{r=a\\ r=b}}; \quad (9.24)$$

$$\frac{\partial U_r}{\partial z}+\frac{\partial U_z}{\partial r}=0|_{\substack{r=a\\ r=b}}. \quad (9.25)$$

The substitution of series (9.12), (9.13), and (9.18)–(9.20) in the boundary conditions (9.21)–(9.25) yields an infinite system of equations for finding unknown co-efficients and functions $a_nA(\gamma)$; $b_nB(\gamma)$; $b_n'B'(\gamma)$; $c_nC(\gamma)$;$c_n'C'(\gamma)$; $d_nD(\gamma)$;$d_n'D'(\gamma)$. Due to the orthogonality of trigonometric functions *cos(nφ)* and *sin(nφ)*, an infinite system breaks up into seven equations with a fixed index *n* to find the seven combinations for the unknown co-efficients and functions.

$a_n A(\gamma)$for the potential $\Phi_s$of a scattering wave is calculated using the Cramer rule from the ratio of two determinants from the seventh order:

$$a_n A(\gamma) = \Delta'/\Delta\ , \qquad (9.26)$$

where Δ represents the determinant of a system and Δ'represents its minor, which is equal to function [133]

$$\Delta = \begin{vmatrix} a_{11} & a_{12} & a_{13} & a_{14} & a_{15} & a_{16} & a_{17} \\ a_{21} & a_{22} & a_{23} & a_{24} & a_{25} & a_{26} & a_{27} \\ a_{31} & a_{32} & a_{33} & a_{34} & a_{35} & a_{36} & a_{37} \\ a_{41} & a_{42} & a_{43} & a_{44} & a_{45} & a_{46} & a_{47} \\ a_{51} & a_{52} & a_{53} & a_{54} & a_{55} & a_{56} & a_{57} \\ a_{61} & a_{62} & a_{63} & a_{64} & a_{65} & a_{66} & a_{67} \\ a_{71} & a_{72} & a_{73} & a_{74} & a_{75} & a_{76} & a_{77} \end{vmatrix},$$

$$\Delta' = \begin{vmatrix} b_{11} & a_{12} & a_{13} & a_{14} & a_{15} & a_{16} & a_{17} \\ b_{21} & a_{22} & a_{23} & a_{24} & a_{25} & a_{26} & a_{27} \\ 0 & a_{32} & a_{33} & a_{34} & a_{35} & a_{36} & a_{37} \\ 0 & a_{42} & a_{43} & a_{44} & a_{45} & a_{46} & a_{47} \\ 0 & a_{52} & a_{53} & a_{54} & a_{55} & a_{56} & a_{57} \\ 0 & a_{62} & a_{63} & a_{64} & a_{65} & a_{66} & a_{67} \\ 0 & a_{72} & a_{73} & a_{74} & a_{75} & a_{76} & a_{77} \end{vmatrix}.$$

$$a_{11} = -H_n^{(1)\prime}(k_\gamma a)\ ;$$

$$a_{12} = J_n'(h_\gamma a)\ ;$$

$$a_{13} = N_n'(h_\gamma a)\ ;$$

$$a_{14} = ni\gamma\left[aJ_n(æ_\gamma a) + 2J_n'(æ_\gamma a)\right]\ ;$$

$$a_{15} = ni\gamma\left[aN_n(æ_\gamma a) + 2N_n'(æ_\gamma a)\right]\ ;$$

$$a_{16} = iæ\left[(n^2 + a\gamma^2)J_n(æ_\gamma a) + J_n'(æ_\gamma a)\right]\ ;$$

$$a_{17} = iæ\left[(n^2 + a\gamma^2)N_n(æ_\gamma a) + N_n'(æ_\gamma a)\right]\ ;$$

$$a_{21} = \rho_0\omega^2 H_n^{(1)}(k_\gamma a)\ ;$$

$$a_{22} = (\lambda + 2\mu)\left[J_n''(h_\gamma a)\right] - \\ -\lambda\left[a^{-2}n^2 J_n(h_\gamma a) - a^{-1}J_n'(h_\gamma a) + \gamma^2 J_n(h_\gamma a)\right];$$

$$a_{23} = (\lambda + 2\mu)\left[N_n''(h_\gamma a)\right] - \\ -\lambda\left[a^{-2}n^2 N_n(h_\gamma a) - a^{-1}N_n'(h_\gamma a) + \gamma^2 N_n(h_\gamma a)\right];$$

$$a_{24} = 2(\lambda + 2\mu)(a^{-2} - 1)i\gamma n J_n(æ_\gamma a)\ ;$$

$$a_{25} = 2(\lambda + 2\mu)(a^{-2} - 1)i\gamma n N_n(æ_\gamma a)\ ;$$

$$a_{26} = (\lambda + 2\mu)\left\{-iæn^2\left[J_n(æ_\gamma a) - J_n'(æ_\gamma a)\right] + \right. \\ \left. + iæJ_n''(æ_\gamma a) + iæ_\gamma\gamma^2\left[J_n(æ_\gamma a) + aJ_n'(æ_\gamma a)\right]\right\};$$

$$a_{27} = (\lambda + 2\mu)\{-i\text{æ}n^2[N_n(\text{æ}_\gamma a) - N_n'(\text{æ}_\gamma a)] + i\text{æ}N_n''(\text{æ}_\gamma a) + i\text{æ}\gamma^2[N_n(\text{æ}_\gamma a) + aN_n'(\text{æ}_\gamma a)]\};$$

$$a_{31} = 0;$$

$$a_{32} = (\lambda + 2\mu)[J_n''(h_\gamma b)] - \lambda[b^{-2}n^2 J_n(h_\gamma b) - b^{-1}J_n'(h_\gamma b) + \gamma^2 J_n(h_\gamma b)];$$

$$a_{33} = (\lambda + 2\mu)[N_n''(h_\gamma b)] - \lambda[b^{-2}n^2 N_n(h_\gamma b) - b^{-1}N_n'(h_\gamma b) + \gamma^2 N_n(h_\gamma b)];$$

$$a_{34} = 2(\lambda + 2\mu)(b^{-2} - 1)i\gamma n J_n(\text{æ}_\gamma b);$$

$$a_{35} = 2(\lambda + 2\mu)(b^{-2} - 1)i\gamma n N_n(\text{æ}_\gamma b);$$

$$a_{36} = (\lambda + 2\mu)\{-i\text{æ}n^2[J_n(\text{æ}_\gamma b) - J_n'(\text{æ}_\gamma b)] + i\text{æ}J_n''(\text{æ}_\gamma b) + i\text{æ}\gamma^2[J_n(\text{æ}_\gamma b) + bJ_n'(\text{æ}_\gamma b)]\};$$

$$a_{37} = (\lambda + 2\mu)\{-i\text{æ}n^2[N_n(\text{æ}_\gamma b) - N_n'(\text{æ}_\gamma b)] + i\text{æ}N_n''(\text{æ}_\gamma b) + i\text{æ}\gamma^2[N_n(\text{æ}_\gamma b) + bN_n'(\text{æ}_\gamma b)]\};$$

$$a_{41} = 0;$$

$$a_{42} = 2na^{-1}[-J_n'(h_\gamma a) + a^{-1}J_n(h_\gamma a)];$$

$$a_{43} = 2na^{-1}[-N_n'(h_\gamma a) + a^{-1}N_n(h_\gamma a)];$$

$$a_{44} = i\gamma a\text{æ}^2 J_n'(\text{æ}_\gamma a);$$

$$a_{45} = i\gamma a\text{æ}^2 N_n'(\text{æ}_\gamma a);$$

$$a_{46} = i\text{æ}n\{J_n(\text{æ}_\gamma a)[a^{-2}(2 - n^2) - \gamma^2] - J_n''(\text{æ}_\gamma a) - a^{-1}J_n'(\text{æ}_\gamma a)\};$$

$$a_{47} = i\text{æ}n\{N_n(\text{æ}_\gamma a)[a^{-2}(2 - n^2) - \gamma^2] - N_n''(\text{æ}_\gamma a) - a^{-1}N_n'(\text{æ}_\gamma a)\};$$

$$a_{51} = 0;$$

$$a_{52} = 2nb^{-1}[-J_n'(h_\gamma b) + b^{-1}J_n(h_\gamma b)];$$

$$a_{53} = 2nb^{-1}[-N_n'(h_\gamma b) + b^{-1}N_n(h_\gamma b)];$$

$$a_{54} = i\gamma b\text{æ}^2 J_n'(\text{æ}_\gamma b);$$

$$a_{55} = i\gamma b\text{æ}^2 N_n'(\text{æ}_\gamma b);$$

$$a_{56} = ikn\{J_n(\text{æ}_\gamma b)[b^{-2}(2 - n^2) - \gamma^2] - J_n''(\text{æ}_\gamma b) - b^{-1}J_n'(\text{æ}_\gamma b)\};$$

$$a_{57} = i\text{æ}n\{N_n(\text{æ}_\gamma b)[b^{-2}(2-n^2)-\gamma^2]- \\ -N_n''(\text{æ}_\gamma b)-b^{-1}N_n'(\text{æ}_\gamma b)\};$$

$$a_{61} = 0\ ;$$

$$a_{62} = 2i\gamma J_n'(h_\gamma a)\ ;$$

$$a_{63} = 2i\gamma N_n'(h_\gamma a)\ ;$$

$$a_{64} = \text{æ}^2 n[a^{-1}J_n(\text{æ}_\gamma a) - J_n'(\text{æ}_\gamma a)]\ ;$$

$$a_{65} = \text{æ}^2 n[a^{-1}N_n(\text{æ}_\gamma a) - N_n'(\text{æ}_\gamma a)]\ ;$$

$$a_{66} = -\gamma\,\text{æ}\{J_n(\text{æ}_\gamma a)[n^2 + a^{-1}\gamma^2]+ \\ +5J_n'(\text{æ}_\gamma a)+aJ_n''(\text{æ}_\gamma a)\};$$

$$a_{67} = -\gamma\,\text{æ}\{N_n(\text{æ}_\gamma a)[n^2 + a^{-1}\gamma^2]+ \\ +5N_n'(\text{æ}_\gamma a)+aN_n''(\text{æ}_\gamma a)\};$$

$$a_{71} = 0\ ;$$

$$a_{72} = 2i\gamma J_n'(h_\gamma b)\ ;$$

$$a_{73} = 2i\gamma N_n'(h_\gamma b)\ ;$$

$$a_{74} = \text{æ}^2 n[b^{-1}J_n(\text{æ}_\gamma b) - J_n'(\text{æ}_\gamma b)]\ ;$$

$$a_{75} = \text{æ}^2 n[b^{-1}N_n(\text{æ}_\gamma b) - N_n'(\text{æ}_\gamma b)]\ ;$$

$$a_{76} = -\gamma\,\text{æ}\{J_n(\text{æ}_\gamma b)[n^2 + b^{-1}\gamma^2]+ \\ +5J_n'(\text{æ}_\gamma b)+bJ_n''(\text{æ}_\gamma b)\};$$

$$a_{77} = -\gamma\,\text{æ}\{N_n(\text{æ}_\gamma b)[n^2 + b^{-1}\gamma^2]+ \\ +5N_n'(\text{æ}_\gamma b)+bN_n''(\text{æ}_\gamma b)\};$$

$$b_{11} = \frac{i}{2}\varepsilon_n H_n^{(1)}(k_\gamma r_0)J_n'(k_\gamma a)\ ;$$

$$b_{21} = -\rho_0\omega^2\frac{i}{2}\varepsilon_n H_n^{(1)}(k_\gamma r_0)J_n(k_\gamma a)\ .$$

9.2. Sound Scattering Using Layered Viscoelastic Cylindrical Shells

In the second section of this chapter, we will consider the diffraction of sound by cylindrical layers of viscoelastic shell. Let the harmonic continuous sound signal with frequency ω irradiate the system of cylindrical elastic and viscoelastic layers (Fig. 9-2). In other words, we will direct a plane sound wave toward this structure so that a wave vector $\vec{k}$ from the incident wave is perpendicular to the Z axis in a system of cylindrical layers (a plane problem).

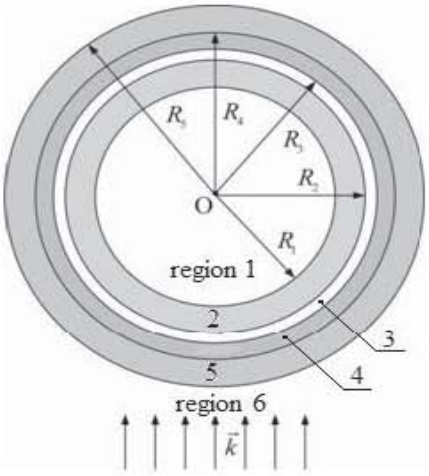

Figure 9-2: The system is comprised of both viscoelastic and elastic cylindrical layers

The system consists of 4 layers: Regions 2, 4 and 5 are the viscoelastic layers; Region 3 is the elastic layer; Region 1 is the vacuum; and Region 6 is the water. All viscoelastic layers differ from each other in terms of the density of the material, elastic modules, and loss factors. Due to the presence of losses in the viscoelastic layers, the wave numbers of transverse (shear) waves will become complex. Therefore, the corresponding arguments based on the cylindrical functions of Bessel and Neumann will likewise be complex.

We have introduced the following designations for the sound pressures and displacement potentials (both scalar and vector ones) for our problem:

1. The inside layer (Region 1) is the vacuum, within which the wave process is absent
2. Layer 2, which is viscoelastic (Fig. 9-2), is characterized by a scalar potential Φ_2 and a vector potential $\vec{\Psi}_2$
3. Layer 3, which is elastic, has potentials Φ_3 and $\vec{\Psi}_3$, respectively
4. Layer 4, which is viscoelastic, has potentials Φ_4 and $\vec{\Psi}_4$
5. Layer 5, which is viscoelastic, has potentials Φ_5 and $\vec{\Psi}_5$
6. In an external liquid medium (Region 6), there is a sound pressure in an incident wave p_i and pressure in a scattered (reflected) wave p_s. p_s

In view of this plain statement of the problem, all vector potentials will have only one component that is different from zero, namely Ψ_2, which we will denote Ψ. We will decompose all potentials and pressures using the fundamental solutions of the Helmholtz equation in the circular cylindrical system for the following coordinates:

$$\Phi_2(r,\varphi) = \sum_{m=0}^{\infty}[I_m J_m(k_2 r) + K_m N_m(k_2 r)]\cos m\varphi\ ;$$

$$\Psi_2(r,\varphi) = \sum_{m=1}^{\infty}[L_m J_m(k_2' r) + Q_m N_m(k_2' r)]\sin m\varphi;$$

$$\Phi_3(r,\varphi) = \sum_{m=0}^{\infty}[P_m J_m(k_3 r) + R_m N_m(k_3 r)]\cos m\varphi;$$

$$\Psi_3(r,\varphi) = \sum_{m=1}^{\infty}[S_m J_m(k_3' r) + T_m N_m(k_3' r)]\sin m\varphi;$$

$$\Phi_4(r,\varphi) = \sum_{m=0}^{\infty}[V_m J_m(k_4 r) + W_m N_m(k_4 r)]\cos m\varphi;$$

$$\Psi_4(r,\varphi) = \sum_{m=1}^{\infty}[X_m J_m(k_4' r) + Y_m N_m(k_4' r)]\sin m\varphi;$$

$$\Phi_5(r,\varphi) = \sum_{m=0}^{\infty}[V_{1m} J_m(k_5 r) + W_{1m} N_m(k_5 r)]\cos m\varphi\ ;$$

$$\Psi_5(r,\varphi) = \sum_{m=1}^{\infty}[X_{1m} J_m(k_5' r) + Y_{1m} N_m(k_5' r)]\sin m\varphi\ ;$$

$$p_i(r,\varphi) = \sum_{m=0}^{\infty}\varepsilon_m(-i)^m J_m(k_6 r)\cos m\varphi;$$

$$p_s(r,\varphi) = \sum_{m=0}^{\infty} A_m H_m^{(1)}(k_6 r)\cos m\varphi;$$

where $k_2 - k_6$and $k_2^{'} - k_5^{'} -$ are wave numbers of longitudinal and transverse waves in the elastic layer, viscoelastic layers, and the external liquid medium. The angular scattering diagram using the layer system takes the following form:

$$D(\varphi) = -exp(-i\pi/4)(\pi k_6)^{-1} \sum_{m=0}^{\infty}(-i)^m A_m \cos m\varphi.$$

Modules of angular scattering diagrams$D(\varphi)$ are presented in Fig. 9-3 for different wave sizes: Fig. 9-3a corresponds to $k_6R_5 \approx 3{,}78$, Fig. 9-3b to $k_6R_5 \approx 7{,}56$, and Fig. 9-3c to $k_6R_5 \approx 11{,}35$.

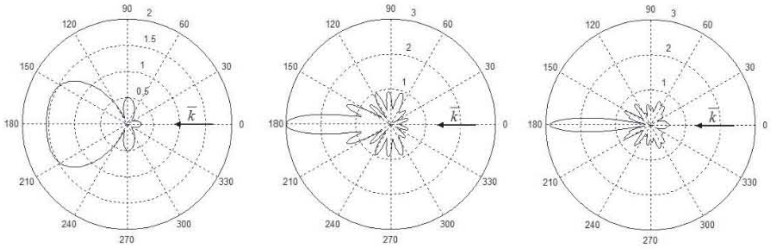

a) b) c)

Figure 9-3: Modules of angular scattering diagrams $|D(\varphi)|$

CONCLUSION

This monograph has presented the author's scientific work on the diffraction, radiation, and propagation of elastic waves in isotropic and anisotropic media and various bodies. It has also shown the results of his research into the synthesis of hydroacoustic antennas.

Using Debye potentials, a solution for the three-dimensional problem of sound diffraction from spheroidal-shaped elastic bodies has been obtained. Based on this approach, the characteristics of sound scattering by spheroidal elastic bodies have been calculated, and the nature of their resonances has been revealed and explained.

The analytical expressions for the three-dimensional characteristics of the sound scattering (the angular scattering characteristic, the relative backscattering cross-section, the total scattering cross-section, and the relative scattering cross-section), the equivalent radius, and its target strength have been obtained and their one-to-one correspondence has been established. These characteristics have been calculated and analyzed up to a wave size of C=100. The Watson transformation has been obtained for the three-dimensional problem of the diffraction of sound from an ideal spheroid.

The characteristics of the sound scattering by the spheroidal bodies located near the media interface have been calculated. Theoretically formulated and physically verified conditions where one can ignore the multiple reflections of sound from the interface between the media have been created.

The sequence of pulses which are reflected by a spheroid placed in a planar waveguide with an elastic bottom has been calculated using a method involving imaginary sources and imaginary scatterers.

The spectral characteristic of the reflected pulsed signal for a spheroid located in an underwater sound channel has been found.

Using the Debye and "Debye-type" potentials, the characteristic equations for the phase velocities of the three-dimensional flexural waves have been both obtained and solved. The equations for calculating the phase velocities of elastic waves in a transversely isotropic elastic shell have been found using the small parameter method.

The author proposes a new method (the Green's function method) for solving problems connected to the diffraction of sound from bodies with mixed boundary conditions and elastic bodies of a non-analytical form. The effectiveness of this method has been demonstrated by calculating the field of sound scattered by similar bodies.

This monograph provides an overview of the methods to solve problems with regard to the sound diffraction from bodies with a non-analytical form (including integral equations, a finite element method, and a boundary element method). The calculation of the scattered fields demonstrates the effectiveness of these methods.

In Chapter 8, using the equations and diffraction theory method, problems related to surface, volume, and linearity regarding the synthesis of the hydroacoustic antennas have been solved using the given pattern of acoustical radiation.

BIBLIOGRAPHY

1. Kleshchev, A. A. *Proc. of LKI Ship Acoust.* 43 (1978).
2. Kleshchev, A. A. *Sov. Phys. Acoust.* 21 (1975): 938.
3. Gaunard, G. C., and M. F. Werby. *J. Acoust. Soc. Am.* 77 (1985): 2081.
4. Werby, M. F., and G. J. Tango. *J. Acoust. Soc. Am.* 79 (1986): 1260.
5. Werby, M. F., and L. H. Green. *J. Acoust. Soc. Am.* 81 (1987): 783.
6. Werby, M. F., and G. C. Gaunaurd. *J. Acoust. Soc. Am.* 82 (1987): 1369.
7. Kleshchev, A. A. *Hydroacoustic Scatterers.* St. Petersburg: Sudostroenie, 1992 (1st ed.); St. Petersburg: Prima, 2012 (2nd ed.) [in Russian].
8. Kleshchev, A. J. *Techn. Acoust.* 2 (1995): 27.
9. Kleshchev, A. A. E. I. Kuznetsova. *Intern. J. Theor. Mathem. Phys.* 3 (2013): 4.
10. Debye, P. *Ann. Phys.* 30 (1909): 775.
11. Frank, P., and R. von Mises. *Differential and Integral Equations of Mechanics and Physics.* Moscow: ONTL, 1937 [in Russian].
12. Franz, W. *Theorie der Beugung Elektromagnetischer Wellen.* Berlin, Germany: Springer, 1957.
13. Meixner, J. J. *Zs. Naturforsch* 3a (1948): 501.
14. Fock, V. A. "Theory of Diffraction by a Paraboloid of Revolution." In *Diffraction of Electromagnetic Waves by Some Bodies of Revolution.* Soviet Radio, Moscow, 1957, 5–56 [in Russian].
15. Fock, V. A. "Electromagnetic Diffraction and Propagation Problems." Soviet Radio, Moscow, 1970 [in Russian].
16. Hoenl, H., Maue, A., and K. Westpfahl. *Theorie der Beugung.* Moscow: World, 1964 [in Russian].
17. Gutman, T. L., and A. A. Kleshchev. *Proc. of LKI* 91 (1974).
18. Kleshchev , A. A. *Acoust. Phys.* 57 (2011): 375.
19. Kleshchev, A. A. *Int. J. Phys.* 1 (2013): 5.
20. Andronov, V. *Acoust. Phys.* 57 (2011): 121.
21. Andronov, V. *Acoust. Phys.* 58 (2012): 521.
22. Andronov, V. *Acoust. Phys.* 59 (2013): 369.
23. Andronov, V. *Acta Acoustica* 99 (2013): 177.
24. Yen, T., and F. Di Maggio, *J. Acoust. Soc. Am.* 41 (1967): 618.
25. Hayek, S., and F. Di Maggio. *Int. J. Sol. Struct.* 6 (1967): 333.
26. Werby, M. F., and L. H. Green. *J. Acoust. Soc. Am.* 74 (1983): 625.
27. Werby, M. F., and L. H. Green. *J. Acoust. Soc. Am.* 76 (1984): 1227.
28. Kleshchev, A. A. *J. Sov. Phys. Acoust.* 23 (1977): 404.
29. Sommerfeld, A. *Differential Equations in Partial Derivatives of Physics.* Moscow: Foreign Literature, 1950 [in Russian].
30. Ivanov, E. A. *Diffraction of Electromagnetic Waves on Two Bodies.* Minsk: Science and Technology, 1968 [in Russian].
31. Kleshchev, A. A. *Sov. Phys. Acoust.* 25 (1979): 143.
32. Tolstoy, I., and K. S. *Kley. Acoust. of Ocean.* Moscow: World, 1969 [in Russian].
33. Kleshchev, A. A., and I. I. Klyukin. *Sov. Phys. Acoust.* 20 (1974): 470.
34. Kleshchev, A. A., and E. I. Kuznetsova. *Proc. of 24th Sess. of Russ. Acoust. Soc.* GEOS, 1 (2011): 743.
35. Kleshchev, A. A., and E. I. Kuznetsova. *Intern. J. Theor. Mathem. Phys.* 2 (2012): 211.
36. Kleshchev, A. A. *J. Advan. Stud. Theor. Phys.* 7 (2013): 697.
37. Kleshchev, A. A. *J. Mor. Int. Techn.* 2 (2015): 77.
38. Kleshchev, A. A. *Amer. Journ. Mod. Phys.* 6 (2017): 51.
39. Lekhnitskiei, S. G. *Theory of Elasticity of Anisotropic Elastic Body.* Moscow: Science, 1977 [in Russian].
40. Brechovakikh, L. M. *Waves in Laminated Mediums.* Moscow: Publ. Acad. Scien. SSSR [or "USSR"?], 1957 [in Russian].
41. Kleshchev, A. A. *J. Zeit. Natur. A.* 70 (2015): 419.

42. Kleshchev, A. A. *J. Advan. Sign. Proc.* 2 (2014): 46.
43. Kleshchev, A. A. *Proc. of LKI Generalship. Syst.* 95 (1989).
44. Kleshchev, A. A. *J. Techn. Acoust.* 2 (1993): 65.
45. Kleshchev, A. A. *J. Mar. Mes.* 2 (2013): 94.
46. Seybert, A. F., Wu, T.W., and X. F. Wu. *J. Acoust. Soc. Am.* 84 (1988): 1906.
47. Podstrigach, J. S., and A. P. Poddubnjak. *Scattering of Sound Beams of Spherical and Cylindrical Form.* Kiev: Naukova Dumka, 1986 [in Russian].
48. Brebbia, C. A., and S. Walker. *Boundary Element Techniques in Engineering.* Moscow: World, 1982 [in Russian].
49. Peterson, B., and S. Strom. *J. Acoust. Soc. Am.* 57 (1975): 2.
50. V. D. Kupradze. *Methods of Potential in Theory of Elasticity.* Moscow: Fizmatgiz, 1963 [in Russian].
51. Dushin, A. Y., Il'menkov, S. L., Kleshchev, A. A., and V. A. Postnov. *Proc. of All-Union Symp. Interaction of Acoustical Waves with Elastic Bodies. Tallinn.* 89 (1989).
52. Il'menkov, S. L., Kleshchev, A. A., and A. S. Klimenkov. *Acoust. Phys.* 60 (2014): 579.
53. Kharcevich, A. A. *Spectrum and Analysis.* Moscow: GITTL, 1957 [in Russian].
54. Kleshchev, A. A. *J. Akust. Zh.* 32 (1986): 268.
55. Kleshchev, A. A., and I. I. Klyukin. (*Principles of Hydroacoustics.* Leningrad: Sudostroenie, 1987 [in Russian].
56. Kleshchev, A. A. *Acoust. Phys.* 58 (2012): 338.
57. Kleshchev, A. A. *Acoust. Phys.* 60 (2014): 253.
58. Karnovskyi, M. I., and V. G. Lozovik. *Sov. Phys. Acoust.* 10 (1964): 313.
59. Karnovskyi, M. I., and V. G. Lozovik. *Sov. Phys. Acoust.* 11 (1965): 176.
60. Kleshchev, A. A. *Sov. Phys. Acoust.* 20 (1974): 632.
61. Kleshchev, A. A. *Proc. of LKI Acoust. of Ships and Oceans.* 19 (1984).
62. Skuchik, E. *Principles of Acoustics.* Moscow: World, 1974 [in Russian].
63. Kleshchev, A. A. *Intern. J. Mech. Appl.* 2 (2012): 124.
64. Su, J.-H., Varadan, V. V., Varadan, V. K., and L. J. Flax. *J. Acoust. Soc.* 68 (1980): 685.
65. Numrich, S. K., Varadan, V. V., and V. K. Varadan. *J. Acoust. Soc. Am.* 70 (1981): 140.
66. Il'menkov, S. L. *Proc. of the 4th Far Eastern Conference on Acoustics.* Vladivostok. 73 (1986).
67. Kleshchev, A. A. *Diffraction and Propagation of Waves in Elastic Mediums and Bodies.* St. Petersburg: Vlas, 2002 [in Russian].
68. Il'menkov, S. L., and A. A. Kleshchev. *Adv. Sign. Roc.* 2 (2014): 50.
69. Il'menkov, S. L., Kleshchev, A. A., Klimenkov, A. S., Legusha, F. F., Mayorov, V. S., Chizhov, G. V., and V. Y. Chizhov. *Proc. of 27th Sess. of RAO.* 1 (2014).
70. Kleshchev, A. A., and S. A. Klimenkov. *Adv. Sign. Proc.* 1 (2013): 68.
71. Kleshchev, A. A. *Diffraction, Radiation, and Propagation of Elastic Waves.* St. Petersburg: Profprint, 2006 [in Russian].
72. Kleshchev, A. A. *J. Techn. Acoust.* 2 (1995): 29.
73. Varadan, V. V., Varadan, V. K., and I. R. Dragonette. *J. Acoust. Soc. Am.* (1982).
74. Grinblat, G. A., Kleshchev, A. A., and K. V. Smirnov. *Acoust. Phys.* 39 (1993): 72.
75. Bostrom, A. "Acoustic, Electromagnetic and Elastic Wave Scattering—on the Matrix Approach." In *Col. Artic*, edited by V. K. Varadan and V. V. Varadan. New York: Pergamon Press, 1980).
76. Grinblat, G. A., and A. A. Kleshchev. *J. Techn. Acoust.* 1 (1994): 3.
77. Il'menkov, S. L. *J. Mar. Intel. Techn.* 1 (2015): 30.
78. Il'menkov, S. L. *J. Mar. Intel. Techn.* 2 (2014): 32.
79. Bobber, R. *Underwater Electroacoustic Measurement.* Moscow: World, 1974 [in Russian].
80. Klyukin, I. I., and A. E. Kolesnikov. *Acoustic Measurements in Shipbuilding.* Leningrad: Sudostroenie, 1982 [in Russian].
81. Horton, C. W. *J. Acoust. Soc. Am.* 34 (1962): 1663.
82. Kleshchev, A. A., and I. I. Klyukin. *Proc. of LKI* 77 (1972): 37.
83. Horton, C. V., and G. S. Innis. *J. Acoust. Soc. Am.* 33 (1961): 877.
84. Kleshchev, A. A., and I. I. Klyukin. *Proc. of 7th All-Union Acoust. Conf.* Leningrad: Nauka, (1973): 123.
85. Kleshchev, A. A. *Proc. of 21st Sess. of Russ. Acoust. Soc.* Moscow: GEOS, (2009): 163.
86. Baker, D. D. *J. Acoust. Soc. Am.* 34 (1962): 1737.
87. Shenderov, E. L. *Wave Problems of Hydroacoustics.* Leningrad: Sudostroenie, 1982 [in Russian].

88. Kleshchev, A. A. *Proc. of 7th All-Union Acoustic Conference.* Leningrad: Nauka, 143 (1973).
89. Kleshchev, A. A. *Sov. Phys. Acoust.* 21 (1975): 57.
90. Achenbach, D., and Y. Xu. *J. Acoust. Soc. Am.* 106 (1999): 84.
91. Bancroft, D. *Phys. Rev.* 59 (1941): 588.
92. Hudson, O. E. *Phys. Rev.* 63. London. A240 (1948): 375.
93. Davis, R. M. *Proc. of Roy. Soc. London.* A240 (1948): 175.
94. Kol'skii, G. *Stress Waves in Solids.* Moscow: IL, 1955).
95. Reiter, R. C. *J. Acoust. Soc. Am.* 46 (1969): 643.
96. Kleshchev, A. A., and I. I. Klyukin. *Proc. of LKI* 109 (1976): 3.
97. Klyukin, I. I., and A. A. Kleshchev. *Ship Acoustics.* Leningrad: Sudostroenie, 1982.
98. Kleshchev, A. A., and K. A. Surgailo. *Proc. of 11th Sess. of Russ. Acoust. Soc.* Moscow: GEOS, 1, (2001): 236.
99. Il'menkov, S. L., and A. A. Kleshchev. *Int. J. Theor. Mathem. Phys.* 2 (2012): 163.
100. Fan, Y., Sinclair, A. N., and F. Honarvar. *J. Acoust. Soc. Am.* 106 (1999): 1229.
101. Cazis, D. C. *J. Acoust. Soc. Am.* 31 (1959): 568.
102. Kumar, R. *Acoustica* 27 (1972): 317.
103. Kumar, R., and R. W. B. Stephens. *Proc. of Roy. Soc. London. A Math. Phys. Eng. Sci.* 329 (1972): 283.
104. Il'menkov, S. L., and A. A. Kleshchev. *Proc. of 11th Sess. Russ. Acoust. Soc.* Moscow: GEOS, (2010): 239.
105. Il'menkov, S. L., and A. A. Kleshchev. *Int. J. Theor. Mathem. Phys* 2(6) (2012): 196.
106. Kleshchev, A. A. *Int. Proc. of 10th Sess. of Russ. Acoust. Soc.* Moscow: GEOS, 1 (2000): 206.
107. Shenderov, E. L. *Radiation and Scattering of Sound.* Sudostroenie, Leningrad, 1989 [in Russian].
108. Kleshchev, A. A. *Diffraction, Radiation and Propagation of Elastic Waves.* Saarbrucken: Lambert Academic Publishing, 2017.
109. Kleshchev, A. A. *Proc. of 16th Sess. of Russ. Acoust. Soc.* GEOS, 2 (2005): 160.
110. Twerski, V. *J. Appl. Phys.* 22 (1951): 825.
111. Twerski, V. *J. Appl. Phys.* 25 (1954): 859.
112. Burke, J. E., and V. Twerski. *J. Acoust. Soc. Am.* 40 (1966): 883.
113. Leiko, A. G., and V. I. Mayatskii. *Sov. Phys. Acoust.* 20 (1974): 256.
114. Kleshchev, A. A. *Proc. of L. K. I.* 97 (1975): 24.
115. Kleshchev, A. A., and E. I. Kuznetsova. *Acoust. Phys.* 57 (2011): 505.
116. Flammer, K. *Tables of Wave Spheroidal Functions.* Moscow: V.C. AN SSSR, 1962 [in Russian].
117. Kleshchev, A. A., and L. S. Sheiba. *Sov. Phys. Acoust.* 16 (1970): 264.
118. Meixner, J., and F. W. Schafke. *Mathieshe Functionen and Spheroidal Functionen.* Berlin: Springer Verlag, 1954).
119. Kleshchev, A. A. *Sov. Phys. Acoust.* 19 (1973): 669.
120. Dymskiy, V. N. *Proc. KAI* 82 (1964): 3.
121. Evstatiev, G. K., Kleshchev, A. A., and I. I. Klyukin. *Principles of Hydroacoustics*, edited by A. A. Kleshchev. Varna: VMEI, 1990.
122. Zelkin, E. G. *Construction of Radiating System from Given Radiation Pattern.* Moscow: Gosenergoizdat, 1963 [in Russian].
123. Kleshchev, A. A. *Proc. of LKI.* 91 (1974): 25.
124. Kleshchev, A. A. *Sov. Phys. Acoust.* 18 (1974): 413.
125. Kleshchev, A. A. *Sov. Phys. Acoust.* 21 (1975): 392.
126. Kleshchev, A. A., and I. I. Klyukin. *Sov. Phys. Acoust.* 20 (1974): 252.
127. Minkovich, E. M., and V. P. Jakovlev. "Antenna synthesis theory." Soviet Radio, Moscow, 1969 [in Russian].
128. Mirovitskiy, D. I. *Proc. of MIREA* 26 (1964): 48.
129. Morse, F., and G. Feshbach. *Methods of Theoretical Physics.* Moscow: IL, 1958 (vol. 1); 1960 (vol. 2) [in Russian].
130. Pistol'kors, A. A. *DAN SSSR.* 39 (1953): 839.
131. Liepa, V. V., and T. B. A. Senior. *Proc. of IEEE* 53 (1965): 1149.
132. Schindler, J. K., Mack, B. B., and P. Blacksmith. *Proc. of IEEE.* 53 (1965): 1137.
133. Kleshchev, A. A. *Acoust. Phys.* 50 (2004): 86.
134. Chizhov, G. V., Chizhov V. Yu., Il'menkov, S. L., Kleshchev, A. A., Kuznetsova, E. I., and F. F. Legusha. *OJMMO* 1 (2013): 1.